Osr1 is a common marker for distinct pre-adipogenic progenitors that mediates a myogenic to adipogenic fate transition

Inaugural Dissertation
to obtain the academic degree
Doctor rerum naturalium (Dr. rer. nat.)

to the Department of Biology, Chemistry, Pharmacy
of the Freie Universität Berlin
by

SOPHIE PÖHLE-KRONAWITTER

Berlin, December 2021

This thesis was carried out during the period of March 2016 and December of 2021 at the **Freie Universität Berlin** and **Max-Planck-Institute for Molecular Genetics** under the supervision of Prof. Dr. Sigmar Stricker.

1st Reviewer: Prof. Dr. Sigmar Stricker

Institute for Biochemistry

Freie Universität Berlin

Thielallee 63, 14195 Berlin

Tel.: +49 30 838 75799

E-Mail: sigmar.stricker@fu-berlin.de

2nd Reviewer: Prof. Dr. Tim J. Schulz

Institute for Biochemistry und Biology

Institute for Nutritional science

Universität Potsdam und DIfE

Arthur-Scheunert-Allee 114-116, 14558 Nuthetal

Tel.: +49 33 200 88 - 2110

E-Mail: tim.Schulz@dife.de

Date of defense: 1st of March 2022

Statutory declaration

I declare that this thesis entitled " Osr1 is a common marker for distinct pre-adipogenic progenitors that mediates a myogenic to adipogenic fate transition" has been composed solely by myself and that it has not been submitted, in whole or in part, in any previous application for a degree. Except where stated otherwise by reference or acknowledgment, the work presented is entirely my own.

Berlin, December 2021

_____

Sophie Pöhle-Kronawitter

TABLE OF CONTENTS

GRAPHICAL SUMMARY

Created with BioRender.com

Key findings:

- Embryos lacking Osr1 expression show a severe reduction of adipose tissue development

- Osr1 interacts with epigenetic remodelers such as CEBPβ, EP300, MLL3 and BRD4 that prime adipogenic identity

- Osr1 marks a novel stem cell with brown adipogenic and myogenic capacity in the dorsal aorta compartment of an E9.5 embryo

- Osr1 labels PAX7+/EBF2+ cells in the dermomyotome that gradually switch from a myogenic to a brown adipogenic identity

- An Osr1+ mesenchymal stromal cell pool (MSC) identifies the earliest committed pre-adipogenic founder population, co-expressing the master regulator of adipogenesis Pparγ at E11.5

- The E11.5 Osr1 lineage contributes to adipogenic tissue organogenesis as well as to the adipogenic niche: the stromal vascular fraction (SVF)

- Osr1+ cells in mature adipose tissue hold an adipogenic potential

ABSTRACT

Adipose depots arise at diverse anatomical locations, at different time points in development, and serve in part complementary functions. While white adipose tissue serves as energy storage, brown adipose tissue is able to dissipate energy to generate heat. This remarkable feature has raised hope for the treatment of metabolic disorders. However, despite extensive work has been done on the identification of brown pre-adipogenic progenitors in late embryogenesis and adult mice, their earliest origin is still obscure. This thesis combines latest techniques as single cell sequencing with classical approaches such as *in vivo* lineage tracing studies using the Osr1$^{CreERt2/+}$;ROSA$^{mTmG/+}$ mouse model to shed light on the very early steps of brown adipose tissue progenitor specification. By analyzing an early embryonic mesenchymal cell pool characterized by the expression of the transcription factor odd-skipped related 1 (Osr1), my work identified two distinct pre-adipogenic progenitor populations. At embryonic day (E)11.5, a pool of Osr1+ cells expressing EBF2 and PAX7 was revealed in the dermomyotome, in line with previous observations that brown adipose tissue traces back to this compartment. Importantly, this work for the first-time localized cells in the dermomyotome that gradually switch from a myogenic to a brown adipogenic identity. In addition, close inspection of OSR1 and adipogenic marker (PPARγ/EBF2/DLK1) expression identified and localized the so far undetected first adipogenic founder population to the peritoneal wall close to the dermomyotome.

Surprisingly, lineage tracing revealed brown adipogenic capacity in the embryo even before E11.5, earlier than previously demonstrated. This was traced back to a novel OSR1+ and PAX7-/EBF2- non-dermomyotomal source that I identified as meso-angioblast stem cells residing in the aorta-gonad-mesonephros (AGM) region.

Loss of Osr1 resulted in a severe reduction of adipose tissue development, demonstrating functional involvement of Osr1 in adipogenesis. Further experiments revealed that Osr1 is required *in vivo* and sufficient *in vitro* to suppress the myogenic potential and promote adipogenesis. An interactome analysis suggested that during this process OSR1 cooperates with an array of epigenetic remodelers like MLL3, EP300, BRD4 as well as the pioneer TF of adipogenesis CEBPβ, to prime and activate the adipogenic fate.

In summary, this research introduces Osr1 as a common marker for two distinct pre-adipogenic progenitors in earliest development and demonstrates that Osr1 is

necessary for a developmental lineage switch required for the establishment of adipose tissue.

ZUSAMMENFASSUNG

Fettdepots entstehen an unterschiedlichen anatomischen Orten, zu unterschiedlichen Zeitpunkten der Entwicklung und erfüllen teilweise komplementäre Funktionen. Während weißes Fettgewebe als Energiespeicher dient, ist braunes Fettgewebe in der Lage, Energie abzubauen, um Wärme zu erzeugen. Diese bemerkenswerte Eigenschaft hat Hoffnung für die Behandlung von Stoffwechselstörungen geweckt. Trotz umfangreicher Arbeiten zur Identifizierung brauner prä-adipogener Vorläufer in der späten Embryogenese und bei erwachsenen Mäusen wurde deren initiale Entstehungsprozess noch nie klar visualisiert. Diese Dissertation kombiniert neueste Techniken wie die Einzel-Zell-mRNA-Sequenzierung mit klassischen Ansätzen, wie *in vivo* Linienverfolgungsstudien mit dem $Osr1^{CreERt2/+}$;$ROSA^{mTmG/+}$ Mausmodell, um die sehr frühen Schritte der Vorläuferspezifikation von braunem Fettgewebe zu beleuchten. Durch die Analyse eines frühen embryonalen mesenchymalen Zellpools, der durch die Expression des Transkriptionsfaktors Odd-Skipped Related 1 (Osr1) gekennzeichnet ist, identifizierte meine Arbeit zwei verschiedene prä-adipogene Vorläuferpopulationen. Am embryonalen Tag (E) 11.5 wurde ein Pool von Osr1+-Zellen, die EBF2 und PAX7 exprimieren, im Dermomyotom entdeckt, in Übereinstimmung mit früheren Beobachtungen, dass braunes Fettgewebe auf dieses Kompartiment zurückgeht. Dadurch lokalisiert diese Arbeit zum ersten Mal Zellen im Dermomyotom, die allmählich von einer myogenen zu einer braunen adipogenen Identität wechseln. Darüber hinaus identifizierte und lokalisierte die genaue Untersuchung der OSR1- und adipogenen Marker (PPARγ/EBF2/DLK1)-Expression die bisher unentdeckte erste adipogene Gründerpopulation an der Peritoneal-Wand in der Nähe des Dermomyotoms.

Überraschenderweise zeigte die Nachverfolgung der Osr1 Abstammungslinie im Embryo bereits vor E11.5 eine braune adipogene Kapazität, wie es zuvor noch nie gezeigt wurde. Der Ursprung wurde auf eine neuartige OSR1+ und PAX7-/EBF2-nicht-dermomyotomale Quelle zurückgeführt, die ich als Mesoangioblasten Stammzellen identifizierte, die sich in der Aorta-Gonaden-Mesonephros (AGM) Region befinden.

Der Verlust von Osr1 führte zu einer starken Reduktion der Fettgewebeentwicklung, was eine funktionelle Beteiligung von Osr1 an der Adipogenese demonstriert. Weitere Experimente zeigten, dass Osr1 *in vivo* erforderlich und *in vitro* ausreichend ist, um

das myogene Potenzial zu unterdrücken und die Adipogenese zu fördern. Eine Protein-Interaktomanalyse legte nahe, dass OSR1 während dieses Prozesses mit einer Reihe epigenetischer Remodeler wie MLL3, EP300, BRD4 sowie dem Pionier-TF der Adipogenese CEBPβ kooperiert, um das adipogene Schicksal zu fördern und zu aktivieren.

Zusammenfassend führt diese Forschung Osr1 als gemeinsamen Marker für zwei verschiedene prä-adipogene Vorläufer in der frühesten Entwicklung ein und zeigt, dass Osr1 für einen Entwicklungslinienwechsel notwendig ist, der für die Entwicklung von Fettgewebe erforderlich ist.

ACKNOWLEDGEMENTS

1 INTRODUCTION

1.1 The Adipose tissue at a glance

1.1.1 The body's rapid response unit

In general terms, the most dominant function of adipose tissue is storing energy in the form of neutral lipids (Harvey et al., 2020, Santoro et al., 2021). Since food supply was not guaranteed in the daily life of an ancient human being, it was mandatory to develop the capacity to store excess energy and to mobilize it at any time to overcome bad living conditions. However, our lifestyle has changed considerably, and the modern world offers convenient sustenance everywhere at any time. However, the human body in terms of energy storing processes has not evolutionarily adapted to the modern lifestyle (Freese et al., 2017). This inevitably leads to many problems by which overnutrition and adipose tissue enlargement affect the body in many aspects of health.

It all starts with food uptake and glucose in the blood, which results in rapid insulin secretion from the pancreatic β-cells (Marchetti et al., 2017). Insulin receptors bind its agonist and regulate glucose translocation into the cells. This is mediated *via* the insulin signaling pathway that activates GLUT4-transporter integration into the plasma membrane. After glucose transfer into the cell -GLUT4 transporters will be recycled to the surface as long as the insulin pathway remains activated (Harvey et al., 2020, Santoro et al., 2021). Of note, GLUT4 is highly abundant in striated muscle (skeletal- and cardiac fibers) and adipocytes, to facilitated prompt glucose uptake for metabolic activation and homeostasis (Mueckler and Thorens, 2013).

In adipocytes 50% of internalized glucose will be converted to triacyl glycerides (TAGs) in lipid droplets (Flatt and Ball, 1964). TAG synthesis is based on glycolysis and gluconeogenesis which both involves free fatty acids (FFAs). While insulin supports TAG storage by actively regulating glucose and FFAs uptake, it inhibits lipolysis on the other hand (Santoro et al., 2021, Choi et al., 2006) (Fig. 1). Thus, over-nutrition results in accumulation of more lipids in adipocytes (hypertrophy) to prevent ectopic lipid accumulation in other tissues (Fig. 1). As soon as the actual maximum of hypertrophy (cells grow in size) is reached pre-adipogenic progenitor cells become activated to generate more adipocytes and store even higher levels of lipids (hyperplasia) (Santoro et al., 2021, Chawla et al., 2011, Makki et al., 2013). Finally, the absolute maximum of

adipose tissue expansion causes lipid accumulation in other organs and pro-inflammatory cytokine secretion recruits immune cells like macrophages to infiltrate adipose tissue (Santoro et al., 2021, Chawla et al., 2011, Makki et al., 2013) (Fig. 1). The dysfunction of adipose tissue leads to insulin resistance and altered insulin and cytokine secretion (Santoro et al., 2021). Therefore, the summary of events generates the metabolic syndrome where obesity (lipotoxicity), high blood pressure and diabetes (↑blood glucose, ↓insulin secretion and sensitivity) represent a greater risk of death (Smith et al., 2001, Harvey et al., 2020, Cornier et al., 2008).
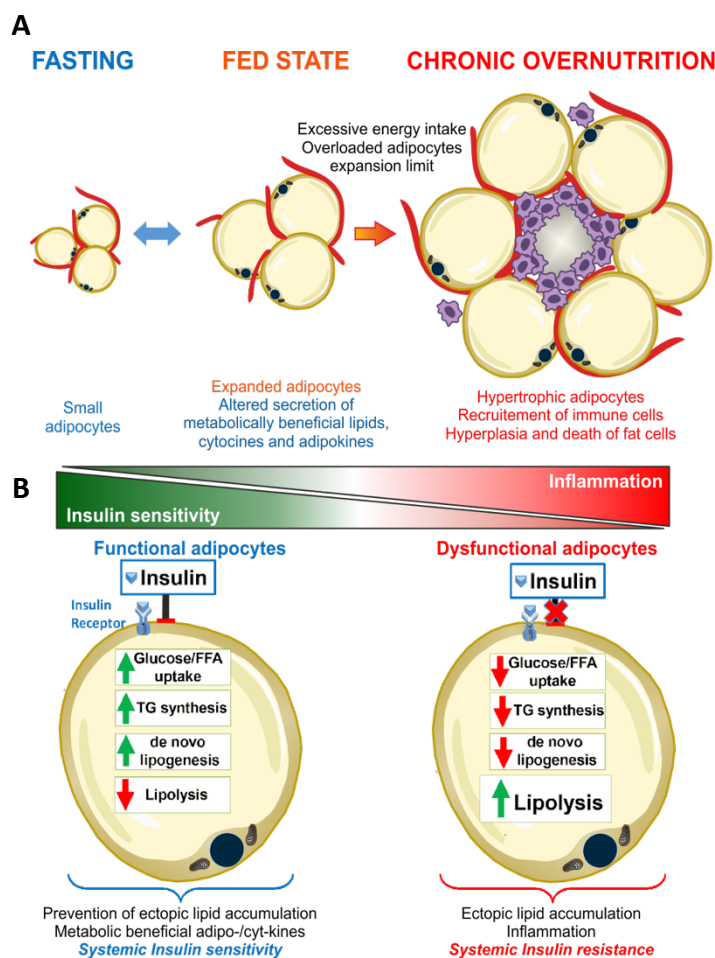
Figure 1. Adipose tissue response to ingestion: A) Adipocytes undergo rapid and reversible morphologic alterations in the conversion between fasting and fed state. Upon food ingestion, adipocytes expand to store excess energy (lipids and glucose) as triacyl glycerides (TGs). Adipocytes can expand in size (hypertrophy) and in number (hyperplasia). As soon as the expansion limit is reached, adipocytes become dysfunctional. Chronic overnutrition causes hypertrophic adipocytes presenting crown-like structures, which contain necrotic cells and macrophages (in purple). Anormal adipose tissue remodeling with chronic overnutrition leads to immune cell recruitment and activation, hypoxia, and fibrosis. B) Insulin effects on glucose and lipid metabolism in functional and dysfunctional adipocytes. Healthy adipocytes are sensitive to metabolic actions of insulin (left) whereas overloaded or dysfunctional adipocytes are resistant to many actions of insulin (right). Altogether, this induces ectopic lipid accumulation in other tissues. (Santoro et al., 2021)

1.1.2 Diversity of adipose tissues and their respective functions

Two main types of adipocytes exist in mammals: the brown fat cell which regulates body thermogenesis a process of energy expenditure and the white adipocyte that is engaged in energy storage as triglycerides (Schulz and Tseng, 2009).
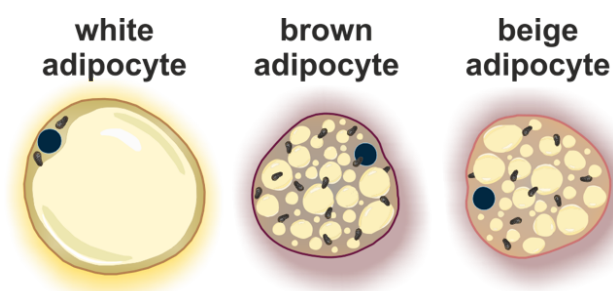
Figure 2. Schematic depiction of adipocyte heterogeneity: Three different types of adipocytes are shown. The white adipocyte on the left carries very few mitochondria and is filled with a single large lipid droplet. The brown (center) as well as the beige adipocyte (right) in contrast hold much higher numbers of mitochondria to drive their metabolic actions. Both beige and brown adipocytes carry multiple small lipid droplets. Brown and white adipocytes form distinct fat depots whereas beige adipocytes arise in white adipose tissue upon stimulation.

The color of a white adipocyte is defined by a single large lipid droplet which occupies most of the cytoplasm. Brown adipocytes instead carry many small lipid droplets and a higher number of mitochondria giving them the typical brown look (Fig. 2). The most important signature gene of brown adipocytes encodes uncoupling protein 1 (UCP1) which locates in the inner membrane of mitochondria. UCP1 uncouples the respiratory chain and thereby diminishes the proton gradient that drives ATP-synthesis. The heat generating translocation of protons is mediated through binding of free fatty acid to UCP1 (Harms and Seale, 2013). To activate the brown adipose tissue (BAT), sufficient supply of oxygen, glucose, FFAs, circulating BAT stimulators and natriuretic peptides or stimuli from the sympathetic nervous system are mandatory (Thoonen et al., 2016). Thus, BAT resides in highly vascularized and innervated locations (Fig. 3). Brown adipose tissue in rodents develop throughout embryogenesis in the subscapular-, interscapular as well as in the cervical – neck region. Interestingly, only subcutaneous (subWAT) and not the visceral white adipose tissue (vWAT) forms during embryogenesis (Fig. 3). Of note, initial embryonic brown and subcutaneous adipose tissue share the same histological features. However, the visceral white adipose tissue that is important to preserve the inner organs and provide an energy reservoir develops

during postnatal life (Kozak, 2011, Kozak and Anunciado-Koza, 2008, Xue et al., 2007).

Nevertheless, a third adipocyte type exists that represents an intermediate state of brown and white fat cell (Fig. 2). The beige adipocyte appears in the white adipose tissue throughout a transdifferentiating process from a white to a brown like adipocyte or from a *de novo* activated perivascular progenitor that upon differentiation carries brown-like characteristics. Different stimuli like cold exposure and β3-adrenergic receptor activation promotes beige fat formation to contribute non-shivering thermogenesis (Jiang et al., 2017, Lee et al., 2014, Cinti, 2012, Cinti, 2009).
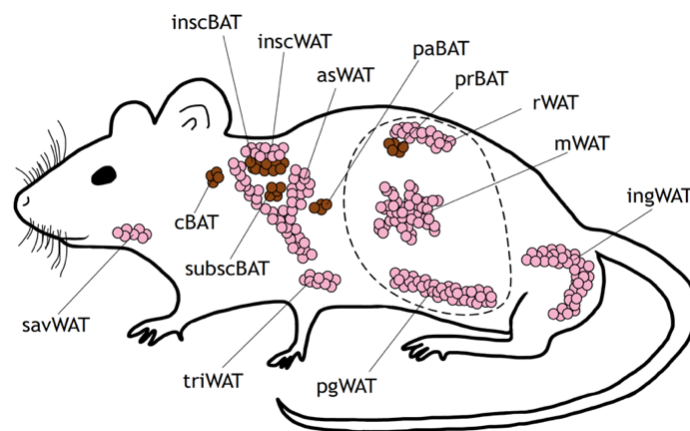
Figure 3: Anatomical location of brown and white adipose tissues
Brown fat depots are depicted in brown and white fat depots are highlighted in pink. The dotted line indicates the visceral cavity which contains the perigonadal white adipose tissue (pgWAT), perirenal brown adipose tissue (prBAT), mesenteric white adipose tissue (mWAT) and retroperitoneal white adipose tissue (rWAT). The most prominent interscapular (inscBAT) and subscapular brown depots (subscBAT) pattern in the shoulder gridle region and appear to be covered by the interscapular white adipose depot (inscWAT) and anterior subcutaneous white adipose depot (asWAT). The cervical brown adipose tissue (cBAT) represents the most cranial BAT. savWAT, salivary gland white adipose tissue; ingWAT, inguinal white adipose tissue; paBAT, peri-aortal brown adipose tissue. (Sebo and Rodeheffer, 2019)

1.2 The developmental origin of adipose tissue

1.2.1 Chronological sequence of adipose tissue organogenesis

As mentioned above the time course of adipose tissue organogenesis is depot dependent. In rodents brown adipose tissue anlagen appear in the interscapular, cervical and subscapular region at E13 (thirteen days after fertilization). Interestingly, around the same stage subcutaneous white adipose tissue forms in the axillary and

inguinal domain (Kozak, 2011, Kozak and Anunciado-Koza, 2008, Xue et al., 2007). The pre-adipogenic cells accumulating in the anlagen already express the adipogenic key regulator peroxisome proliferator-activated receptor γ (PPARγ) but do not recapitulate the typical phenotype of lipid laden adipocytes, since metabolic activation is pending (Mayeuf-Louchart et al., 2019). As embryogenesis proceeds at E15.5 the pre-adipogenic cells gradually change from a fibroblast like appearance to a mature lipid laden adipocyte expressing e.g. perilipin 1, adiponectin and fatty acid binding protein 4. Interestingly, prenatal developing adipose tissue – no matter if brown or white – share the same brown adipocyte phenotype. Also, it has been reported that the inguinal / subcutaneous white adipose tissue holds the highest capacity of browning (Vitali et al., 2012, Wang and Yang, 2017). Postnatally, visceral white adipose tissue appears surrounding its organs showing the classical white adipocyte characteristics (Xue et al., 2007, Kozak, 2011, Kozak and Anunciado-Koza, 2008).

1.2.2 Adipocytes emerge from various lineages

Extensive work has been done to define the ultimate adipogenic progenitor marker. However, tracing experiments have revealed that adipocytes emerge from numerous lineages that are heterogeneously and dynamically distributed during embryogenesis (Sanchez-Gurmaches and Guertin, 2014b, Sanchez-Gurmaches and Guertin, 2014a, Cristancho and Lazar, 2011, Sebo and Rodeheffer, 2019). Therewith, it has become clear that the main source of adipose tissue is from mesodermal origin (Gesta et al., 2007, Cristancho and Lazar, 2011, Sebo and Rodeheffer, 2019, Matsuoka et al., 2005). The only exception are ectodermal derived *Sry-related HMg-Box gene 10 (Sox10)* expressing neural crest progenitors that have been recognized to form cranial white adipose tissue (Billon et al., 2007, Matsuoka et al., 2005) (Fig. 4).

Since cell lineage commitment goes in line with cell specification, it was necessary to pinpoint events during embryogenesis that define the adipogenic trajectory. In the embryo gastrulation represents the first step of lineage segregation. Here, the epiblast stem cells differentiate into the three germ layers: mesoderm, ectoderm and endoderm (Sebo and Rodeheffer, 2019, Lawson et al., 1991). The mesoderm further differentiates into paraxial mesoderm that forms the somites, intermediate mesoderm (IM) and lateral plate mesoderm (LPM) (Sebo and Rodeheffer, 2019). Those three

mesodermal compartments have been identified to express specific markers that define their prospective developmental fate.

The intermediate mesenchyme which forms the urogenital and reproductive system is specified by *odd skipped related gene 1 (Osr1), paired-box genes 2* and *8 (Pax2/8), lim-type homeobox 1 gene (Lhx1)* and *Wilms tumor 1 suppressor gene (Wt1)* expression (Patel and Dressler, 2013). Lineage tracing studies using the Wt1-CreER mouse revealed a notable contribution to visceral - but not subWAT (Chau et al., 2014, Sebo and Rodeheffer, 2019). The Osr1-CreER lineage instead was stated to provide progenitors to subWAT and muscle interstitial adipocytes, exclusively (Vallecillo-Garcia et al., 2017, Stumm et al., 2018). Moreover, *Osr1* and *Wt1* expression has not only been observed in the intermediate mesoderm but also in the lateral plate compartment (Sebo and Rodeheffer, 2019, Chau et al., 2014, Mugford et al., 2008, Prummel et al., 2019). This indicates that complete marker to tissue specificity is not guaranteed and thus supports the fact that adipogenic progenitors are heterogeneously and dynamically distributed during development. However, other markers of the LPM and its derived limb bud mesenchyme were studied whether their lineages hold adipogenic progenitors. The *paired related homeobox 1 (Prx1)* and *homeobox B6 (HoxB6)* lineages were investigated and confirmed adipogenic contribution of LPM to subWAT and ventrolateral white fat depots (Sanchez-Gurmaches et al., 2015, Sebo et al., 2018). In sum, both the LPM (Prx1 and Hoxb6-lineage) and IM (Osr1-lineage) provide progenitors to white adipose tissues (Fig. 4).

Somites arise from the paraxial mesoderm and appear in the dorsal compartment as segmentally organized structures along the rostro-caudal body axis (Tajbakhsh and Spörle, 1998, Sebo and Rodeheffer, 2019). Here, they further specify into three subdomains: sclerotome, myotome and dermomyotome (Tajbakhsh and Spörle, 1998). Each subdomain serves different qualities: the sclerotome harbors cells that generate cartilaginous and osteoid parts of the spinal column and the myotome generates progenitors that form skeletal muscle (Sebo et al., 2018, Sebo and Rodeheffer, 2019, Pang and Thompson, 2011). However, the dermomyotome represents the most heterogenic compartment. It has been demonstrated that the dermomyotome generates the myotome and consequently muscle tissue (Gros et al., 2004, Pu et al., 2013) as well as the dermis of the dorsum (Olivera-Martinez et al., 2004, Ben-Yair et al., 2003, Yusuf and Brand-Saberi, 2006). Finally, various lineage tracing studies targeting the dermomyotome proved adipogenic contribution.

Interestingly with contrasting distribution pattern compared to IM and LPM (Sebo et al., 2018, Sebo and Rodeheffer, 2019). Tracing data of the pan-somite marker *mesenchyme homeobox 1* (*Meox1)* revealed strongest contribution to interscapular-brown and white adipose tissue (iBAT and iWAT) as well as retroperitoneal WAT (rWAT) (Sebo et al., 2018). Furthermore, fate mapping experiments labeling the central dermomyotome have shown that the *paired-box 7* (Pax7) as well as the *engrailed homeobox 1* (En1) lineage play a role in the iBAT formation (Lepper and Fan, 2010, Lepper et al., 2009, Sebo et al., 2018, Keller et al., 2004, Atit et al., 2006, Sgaier et al., 2005). However, tracing *paired-box 3* (Pax3), a marker of the early dermomyotome and myotome, gave comparable results to fate mapping experiments from the *myogenic factor 5* (Myf5) lineage that targets the myotome and myogenic progenitors. Both demonstrate a full coverage of the BATs in the shoulder gridle region and contribution to subWAT and rWAT (Sanchez-Gurmaches and Guertin, 2014b, Sanchez-Gurmaches and Guertin, 2014a, Seale et al., 2008, Engleka et al., 2005, Lang et al., 2005, Tallquist et al., 2000a). In short, the dermomyotomal derivates are the main source of brown pre-adipogenic progenitors (Fig. 4).
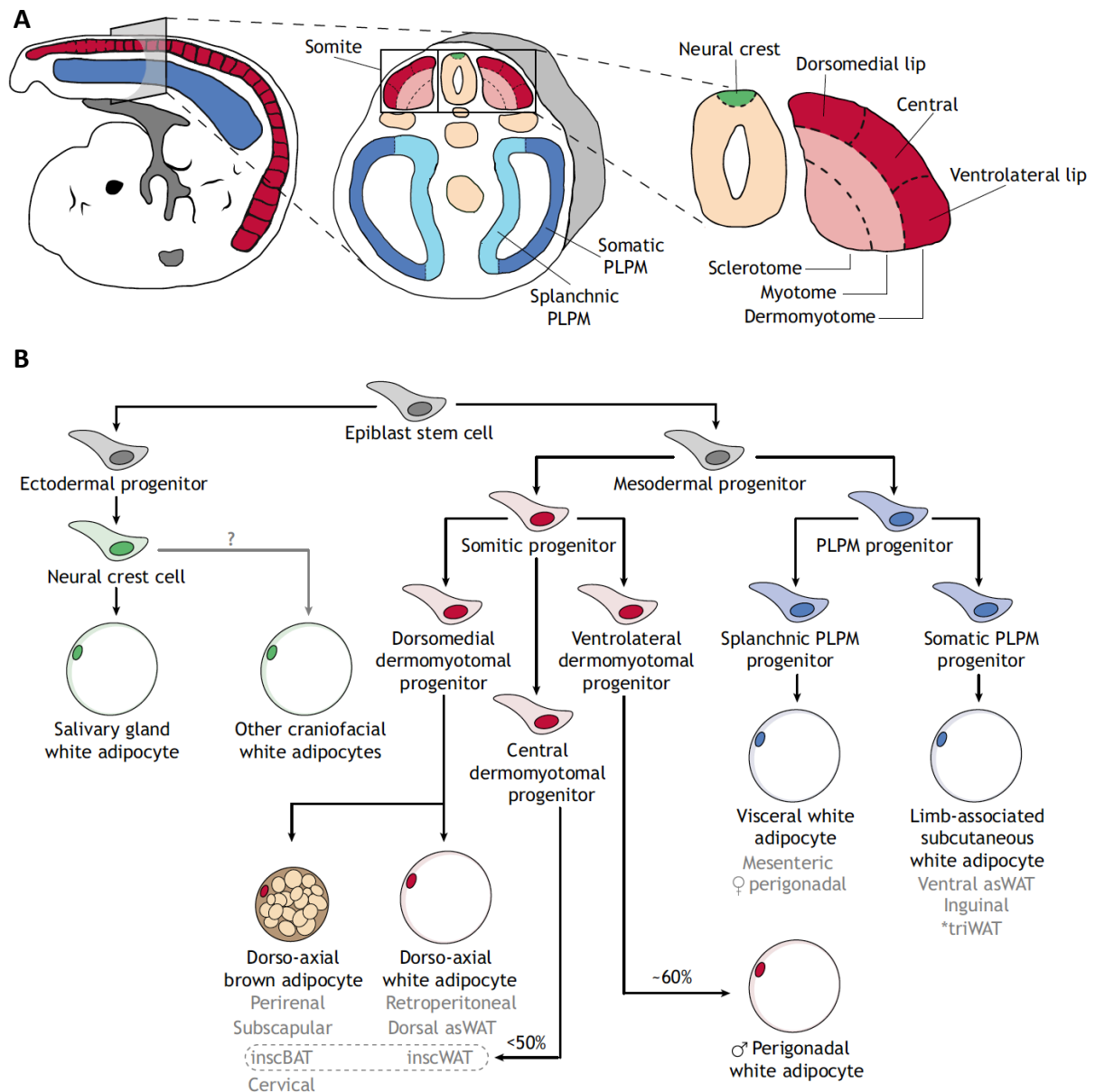
Figure 4: The embryonic adipocyte lineage tree. A) Schematic depiction of an E9.5 mouse embryo. A cross-section highlights important mesodermal and neuro ectodermal sub-compartments. B) summarizes the current lineage-tracing data in mice introducing the posterior lateral plate mesoderm (PLPM) as a source of white adipose tissue, the neural crest cells as a cranial white adipose tissue progenitor and the somites that drive brown and white adipose tissue development. Grey text lists specific adipose depots; arrows describe cell lineage progression; '?' demonstrates an unknown relationship. asWAT, anterior subcutaneous white adipose tissue; inscBAT, interscapular brown adipose tissue; inscWAT, interscapular white adipose tissue;.(Sebo and Rodeheffer, 2019)

1.2.3 Osr1, a potential marker for early adipogenesis

As mentioned above the embryonic Osr1 lineage contributed to subcutaneous WAT at E18.5 (Vallecillo-Garcia et al., 2017). Of note, the Osr1 lineage displayed a huge overlap with the mesenchymal progenitor marker PDGFRα which has been highly

associated with an pre-adipogenic identity and implicates that Osr1 might have a higher relevance in adipose tissue development as previously recognized (Vallecillo-Garcia et al., 2017, Sun et al., 2020).

1.2.3.1 The evolutionary and molecular characteristics of Osr1

The gene *odd-skipped* (odd) was first elaborately described in *Drosophila melanogaster*. In Drosophila the odd gene constitutes a member of the eight pair rule genes and plays a crucial role in the segmentation process during embryogenesis (Nüsslein-Volhard and Wieschaus, 1980, Coulter et al., 1990, Coulter and Wieschaus, 1988). Thus, it is essential for initial developmental processes. Furthermore, the gene is conserved among different classes of the animal systematic, for example between *insecta* (fruit fly), *amphibia* (Xenopus), *aves* (chick) and *mammalia* (human and mouse) (Coulter et al., 1990, So and Danielian, 1999, Debeer et al., 2002, Katoh, 2002, Stricker et al., 2006, Tena et al., 2007, Lan et al., 2011).

The *Odd-skipped related 1* (OSR1) protein consists of 266 amino acids (aa) in mouse (So and Danielian, 1999) and was described as a transcription factor since OSR1 showed capability to bind a specific sequence in the deoxyribonucleic acid (DNA) due to its aa sequence qualities and the architecture of the three identified C2H2 zinc finger domains to regulate activation or repression of downstream targets to promote a mesenchymal precursor state (Goldstein et al., 2005, Saulier-Le Drean et al., 1998, James et al., 2006, James and Schultheiss, 2005, Tena et al., 2007).

1.2.3.2 Osr1 deficiency results in various malformations

As mentioned before Osr1 is detectable in the IM and LPM in early embryogenesis, which indicates its importance in the formation of specific organ systems and tissues (James and Schultheiss, 2005, Prummel et al., 2019, Patel and Dressler, 2013). For instance, the loss of Osr1 in the IM region results in alterations in the urogenital system as kidneys and gonads fail to form (Wang et al., 2005, Mugford et al., 2008, James et al., 2006). Furthermore, data from the Stricker lab described that the lack of Osr1 in the early muscle connective tissue affects the extracellular matrix composition, which than negatively regulates the muscle fiber organization and muscle patterning (Vallecillo-Garcia et al., 2017). Supportingly, in 2012 it was stated that Osr1-knockout

connective tissue cells change identity from a fibroblast-like stromal cell towards a chondrogenic signature (Stricker et al., 2012). Moreover, published data describe that Osr1 has a role to keep cells in a proliferative state, since loss of Osr1 results in decreased numbers of G2/M cells (Zhou et al., 2015). Together, Osr1 influences the identity of mesenchymal cells and cell cycle progression.

However, heart development is a critical and complex process in embryogenesis as a directed blood stream has to be established. On this matter, Osr1-knockout embryos failed to form the primary atrial septum (termed septum primum) in the heart which separates the right atrium from the left (Wang et al., 2005). This defect causes a wrong directed blood flow from the heart into the systemic veins. Moreover, the dilated atria and the hypoplastic venous valves represent further listed heart defects (Wang et al., 2005). The incorrect heart development leads to lethality of Osr1 deficient embryos between the embryonic stage E14 and E15.

1.2.3.3 Embryonically, Osr1 pursues a dynamic expression motif

To understand the general developmental role of Osr1 in vertebrates a detailed expression analysis was obligatory and was first done on chicken. The chick embryo is a common model organism to investigate early developmental processes. The first observation was that Osr1 follows a very dynamic expression throughout embryogenesis and that it is generally overlapping among chicken and mouse embryos (Stricker et al., 2006). In mouse embryos Osr1 expression emerges at the embryonic stage E7.5 specifically in the embryonic mesoderm (seven and a half days after fertilization) (Wang et al., 2005) (Fig. 5A). At stage E8.5, Osr1 expression expands and marks the entire IM from caudal to approximately the cardiac crescent and the dorsal LPM (Wang et al., 2005, Stricker et al., 2006, Mugford et al., 2008) (Fig. 5B and C). As development proceeds, the Osr1+ cell pool continuously spreads and labels various tissues like: fore- and hindgut endoderm, lung bud mesenchyme, a few myocardial cells of the atrial chamber wall and in the caudal IM that expands to the somitic mesoderm at stage E9.5 (Wang et al., 2005) (Fig. 5D-F). Osr1 expression at E10.5 is detectable in the developing branchial arches as well as in the upper trunk, the limb bud mesenchyme and forebrain (Fig. 7 G-H). In the followed stage E11.5, Osr1 expression in the limb buds is shifted to the anterior where a new Osr1 positive domain appears that encloses the proximal limb. Lastly, Osr1+ cells reside in the lateral

mesenchymal layer of the trunk (Wang et al., 2005, Stricker et al., 2006, So and Danielian, 1999). Together, these observations describe Osr1 as a transcription factor that assists organogenesis in a spatial and temporal manner. Of note, Mugford in 2008 investigated the very early Osr1 lineage between E7.5 and E11.5 and stated that "Osr1 expression demarcates a multipotent population (…) that undergoes progressive lineage restriction…"(Mugford et al., 2008). In this study, short pulse lineage tracing data revealed that the Osr1 lineage between E7.5 and E9.5 covers various identities like endothelial, interstitial cell and smooth muscle which disappear at later stages (Mugford et al., 2008).

However, it remains unclear whether Osr1 expressing cells show co-expression with pre-myogenic precursors since it was stated that Osr1+ cells are observed near to the somites in early chicken embryos (Stricker et al., 2006).
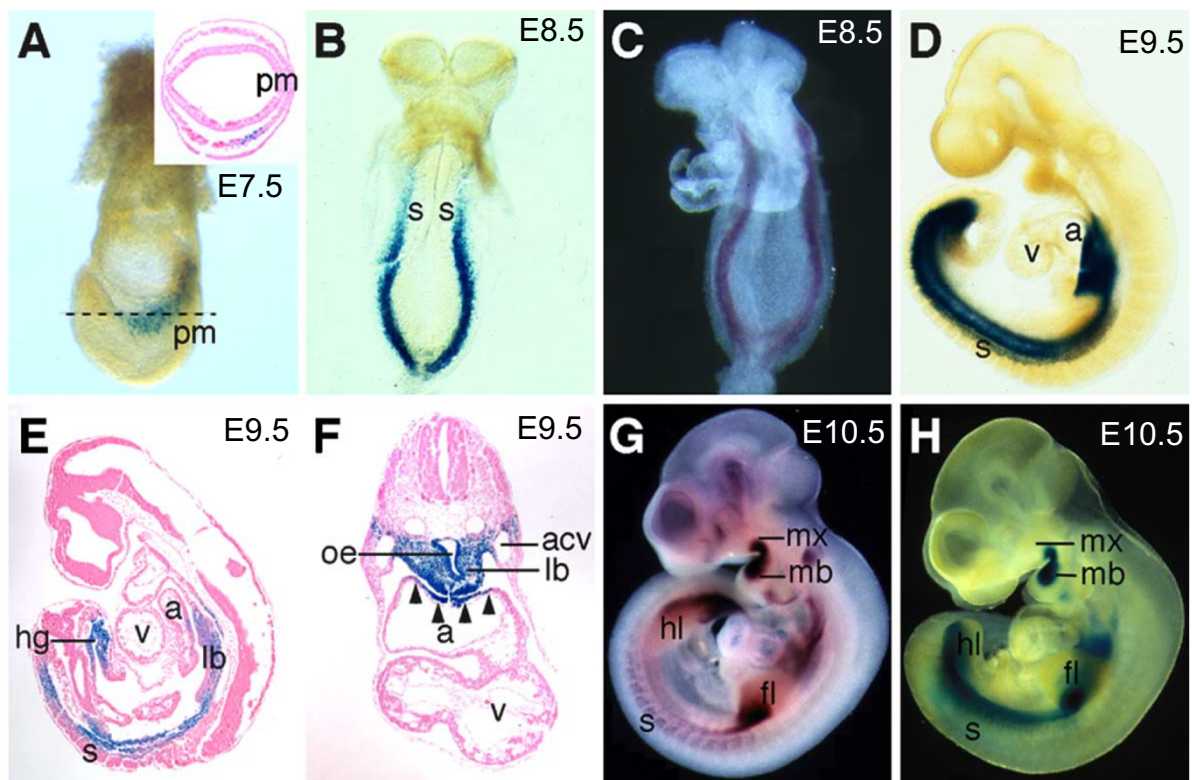
Figure 5: Osr1 expression pattern during early mouse embryogenesis.
A) At E7.5 whole mount β-galactosidase staining (X-GAL) showed Osr1 expression (blue) in the intermediate region of the mesoderm layer but not in the primitive streak (pm). (B and C) At E8.5, Osr1 is detected throughout the intermediate mesoderm caudal to the cardiac crescent. D) By E9.5, Osr1 expression is observed not only in the intermediate mesoderm but also recognized at the dorsal region of the atrium and in the caudal somites. E, F) Sagittal and transverse sections, respectively, depict Osr1 expression in the lung bud mesenchyme, the fore- and hindgut endoderm, and in the dorsal atrial wall. (G, H) By E10.5, the Osr1 expression pattern expands and labeled the first branchial arches, limb buds, and somites. a, atrium; acv, anterior cardinal vein; fl, forelimb bud; hg, hindgut; hl, hindlimb bud; lb, lung bud; mb, mandibular process; mx, maxillary process; oe, esophagus; pm, primitive streak; s, somite; v, ventricle.(Wang et al., 2005)

1.3 The stromal vascular fraction

1.3.1 Perivascular niche design

As described before the adipose tissue has a high remodeling capacity to adapt rapidly to stressors that result in energy expenditure or storage. To adjust to new conditions the adipose tissue is controlled by its niche: the stroma vascular fraction (SVF). Two-third of adipose tissue mass is comprised by the SVF that embeds mature adipocytes. Studies revealed that the SVF serves as a reservoir of heterogenous cell groups like endothelial progenitor cells, preadipocytes, mesenchymal stem cells (MSCs), pericytes, macrophages, T-cells and erythrocytes (Trevor et al., 2020, Bourin et al., 2013, Sarantopoulos et al., 2018) (Fig. 6).
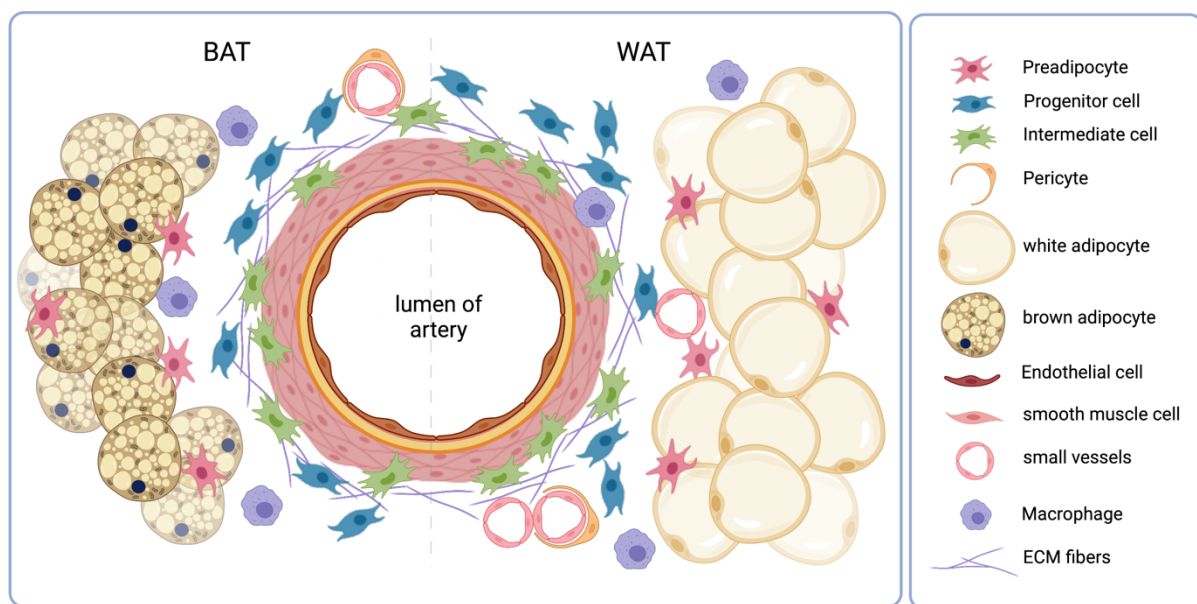
Figure 6: The perivascular niche of adipose tissue
The stromal vascular fraction arranges around the endothelium and comprises of heterogenic cell groups like endothelial progenitor cells, preadipocytes, mesenchymal stem cells (MSCs, like intermediate and progenitor cells), pericytes and macrophages. Every cell type is found in its distinct location until activation. Together, they orchestrate tissue remodeling and homeostasis. BAT: brown adipose tissue; WAT: white adipose tissue (Created with BioRender.com)

1.3.2 SVF, assistance of adipose tissue expansion

The adipose tissue is one of the most plastic organs that constantly remodels to maintain the state of health (Cao, 2007, Cao, 2010). Various stressors can activate

shrinking or tissue expansion. To facilitate adipose tissue adjustment the vascular network is the main component that has to restructure since delivery of nutrition, oxygen, hormones, growth factors, progenitor cells and immune cells are indispensable for tissue repair, growth and expansion (Cao, 2010, Cao, 2007, Folkman, 1995, Lijnen, 2008). Of note, studies have revealed that adipose tissue is already dependent on an established vascular supply during embryogenesis (Crandall et al., 1997, Cao, 2007). However, upon vascularization the interplay of different cell types in the constructive area supports functional tissue growth (Fig. 7).

In obese individuals white adipose tissue experiences hypoxic conditions inducing upregulation of hypoxia-inducible transcription factor 1 (HIF1) and HIF2 which tips angiogenesis by supporting expression of angiogenesis-related factors and downregulation of angiogenic inhibitors (Cao et al., 2001, Hosogai et al., 2007, Trayhurn et al., 2008, de Fraipont et al., 2001). Besides that, obesity represents a state of chronic inflammation that is accompanied with infiltration of inflammatory cells (Cao, 2010). Here, activated macrophages and leukocytes secrete pro-angiogenic factors and cytokines like vascular endothelial growth factor A (VEGFA), tumor necrosis factor (TNF), interleukin-6 (IL-6) and IL-8, too (Cao, 2010, Hotamisligil, 2006, Powell, 2007, Lazar, 2005, Lehrke and Lazar, 2005). Interestingly, adipocytes secrete self-regulating adipokines like leptin, which promotes angiogenesis and inflammation but also adiponectin, which is inhibiting neovascularization (Cao et al., 2001, Cao, 2010, Fantuzzi and Faggioni, 2000, Brakenhielm et al., 2004, Mahadev et al., 2008). These observations indicate a well titrated system of activation *vs* inhibition of angiogenic modulators in the adipose tissue. Moreover, both mature adipocytes and inflammatory cells initiate extracellular matrix (ECM) remodeling by producing metalloproteinases like MMP-2 and MMP-9 that are linked to promote preadipocyte differentiation and micro-vessel maturation since matrix-bound factors can be released (Cao, 2007, Kawaguchi et al., 2002, Bouloumié et al., 2001, Bergers et al., 2000, Christiaens and Lijnen, 2006, Park et al., 2001).

However, adipo-derived stromal cells (ADSCs) represent a stem cell like population within in the SVF which was recognized to significantly contribute to adipose tissue modulation and regenerative processes (Cao, 2010, Meliga et al., 2007, Tang et al., 2008, Gesta et al., 2007, Nakagami et al., 2006). First, secretion of pro-angiogenic molecules and second, the heterogenic cell pool that can differentiate into various cell types like endothelial cell, pericytes and preadipocytes enable efficient tissue

expansion (Grenier et al., 2007, Meliga et al., 2007, Cao, 2010). Taken together, mature adipocytes as well as macrophages regulate angiogenesis and facilitate ECM remodeling. The ADSC compartment on the other hand provides different types of progenitors to populate the obtained space (Fig. 7).

A catabolic stimulus *via* the β3-adrenergic receptor (ADRB3) activation has also been described to initiate adipose tissue remodeling. Here, ADRB3 recruits its downstream target cAMP-dependent protein kinase (PKA) which thereafter induces hormone-sensitive lipase (HSL) and adipose triglyceride lipase (ATGL) to mediate lipolysis (Lee et al., 2012, Lee et al., 2014, Granneman et al., 2005, Lee et al., 2013b). Since ADRB3 stimulates death of vulnerable adipocytes, non-inflammatory macrophages (M2) infiltrate the tissue (Lee et al., 2014, Lee et al., 2013b, Camell et al., 2017, Feingold et al., 1992). Of note, at that state a temporary niche forms: the "crown-like-structure (CLS)" - M2 macrophages clear apoptotic adipocytes and thereby recruit progenitor cells from the ADSC compartment which replenish the space with newly formed brown / beige adipocytes due to catabolic stimuli (Lee et al., 2014, Lee et al., 2013b). In summary, environmental cues regulate tissue remodeling by activating angiogenesis, the immune cell response and recruitment of different progenitor from the ADSC compartment (Fig. 7).
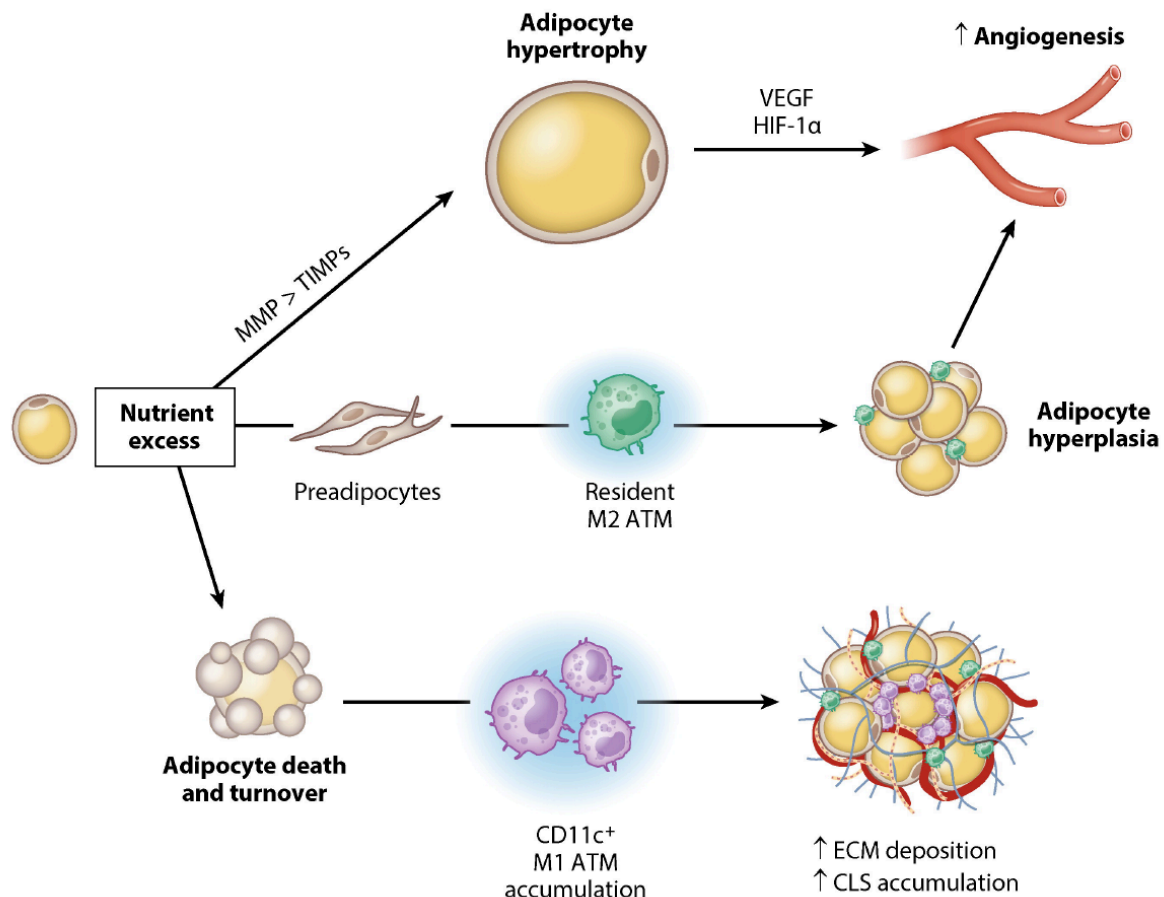
Figure 7: Adipose tissue remodeling
With nutrient excess numerous events are provoked that influence adipose tissue appearance. Titration between adipocyte hypertrophy, hyperplasia and death dictates the energy storage capacity of a fat depot. Both, hypertrophy and hyperplasia are connected to angiogenic cues to support vascular expansion and nutrient availability to adipocytes. Adipocyte death, an indicator of adipose tissue stress, is a consequence of accumulating inflammatory adipose tissue macrophages (ATMs) that form crown-like structures (CLSs). Extracellular matrix (ECM) is reorganized throughout secretion of matrix metalloproteinases (MMP) upon hypertrophy or an inflammatory response. Abbreviations: CD11c+: cluster of differentiation 11c or integrin alpha X; HIF: hypoxia-inducible factor; TIMPs: tissue inhibitors of metalloproteinases; VEGF: vascular endothelial growth factor. (Martinez-Santibanez, 2015)

1.4 The adipogenic progenitor pool

As mentioned before the adipogenic niche serves as a heterogenous progenitor reservoir to enable tissue remodeling. In the last decades intensive work has been performed to disentangle the repertoire of pre-adipogenic progenitors (APs). Fluorescence-activated cell sorting (FACS) strategies were used to separate along different combinations of cell surface markers or reporter mouse lines to specify cell types residing in the SVF. A common observation was that the endothelial and haemopoietic lineage expressing CD31, Ter119 and CD45 (Lin+) do not hold a

significant adipogenic capacity (Rodeheffer et al., 2008, Joe et al., 2009, Sacco et al., 2008, Steinbring et al., 2017, Lee et al., 2012). However, after Lin+ depletion from the SVF cell pool, markers that identify divergent mesenchymal progenitors were used to select for potential adipogenic progenitors.

1.4.1 Established signatures

Studies on subcutaneous white adipose tissue using the Lin- cells and a sequence of mesenchymal progenitor markers: CD29 (β1-integrin), CD34, *stem cell antigen 1* (Sca1) and CD24 confirmed an adipogenic identity upon *in vitro* adipogenic differentiation and transplantation experiments (Rodeheffer et al., 2008, Shackleton et al., 2006, Sidney et al., 2014). The Rossi lab in 2009 identified a similar cell population from Lin- cells expressing: CD34+ and Sca1+ cells in subWAT and vWAT (Joe et al., 2009). Interestingly, cells from white adipose tissue that express CD34, Sca1 and *platelet derived growth factor receptor alpha* (PDGFRα) have been described as a bi-potential progenitor population that forms either a white or brown/beige adipocyte (Joe et al., 2009, Lee et al., 2012, Wankhade and Rane, 2017), highlighting once again the plasticity of the adipogenic niche. Alike, brown adipose tissue was investigated whether brown adipogenic progenitors reside in the SVF too. Work from the Schulz group showed that the Lin- cell fraction expressing Sca1+ and PDGFRα+ hold a brown adipogenic capacity upon *in vitro* adipogenic differentiation (Steinbring et al., 2017). Fascinatingly, flow cytometric screening and cell isolation from the skeletal muscle demonstrated that the Lin-: Sca1+ muscle interstitial cells feature a brown adipogenic potential as well (Schulz et al., 2011). Moreover, single cell RNA sequencing confirmed that Lin-: Sca1+ cells from vWAT are sufficient to study the heterogeneity and adipogenic progenitor landscape in the SVF in the context of obesity (Cho et al., 2019). Altogether, the Lin-: Sca1+ signature seem to be precise enough to measure the full plasticity of the AP pool in adulthood.

However, it is possible to specify the AP signature further by targeting a SVF sub-compartment of interest. This was done in a study that investigated smooth muscle cells of the SVF via CD105+ (endoglin) that validated the adipogenic capacity *in vitro* (Cîmpean et al., 2007, Piao and Tokunaga, 2006, Lv et al., 2012). In a different work an inducible alpha smooth muscle actin (αSMA)-RFP (red fluorescent protein) lineage tracing mouse model was used to study the mural compartment of the vascular niche.

In vivo and *in vitro* experiments proved that the αSMA-lineage+ PPARγ+ cell pool is required for adipose tissue homeostasis (Jiang et al., 2014). In the same study, investigations of the AdipoTrak mouse: a PPARγ^{tTA} ("Doxycycline Off" system) combined with a supplementary reporter system (e.g., *TRE-H2B-GFP; TRE-Cre, R26R^{lacZ}*) highlighted the fact that depletion of the PPARγ+ pool from embryonic stage E0 – E10.5 specifically failed to perform sufficient tissue homeostasis in adulthood. These observations were raising the point that the adipogenic niche is specified before embryonic stage E10.5. Also, depletion of the PPARγ+ pool from E0 – P10 displayed a serious loss of adipose tissue (Jiang et al., 2014, Tang et al., 2008). These data outline that the embryonic signature of pre-adipogenic progenitors deserve higher attention.

As mentioned before, it remains a challenging task to define the pre-adipogenic founder cell signature since their heterogeneity and dynamic distribution creates extra complexity during embryogenesis. Nevertheless, the first thorough embryonic brown adipogenic progenitor signature was defined by a combinatory approach. A study from 2013 introduced the new preadipocyte marker *early B cell factor-2* (Ebf2) which has been confirmed to implement and maintain the brown adipogenic identity pre- and postnatally (Rajakumari et al., 2013). One year later it was stated that the Ebf2+ PDGFRα+ cells hold a much higher adipogenic potential as the Ebf2- group (Wang et al., 2014). With this knowledge, generated transcriptomic data from the E14.5 Ebf2+ PDGFRα+ fraction was correlated with the transcriptomic data of the embryonic E14.5 Myf5 lineage since previous studies of Myf5+ progenitor cells have proven a high level of BAT contribution (Wang et al., 2014, Sanchez-Gurmaches and Guertin, 2014b, Sanchez-Gurmaches and Guertin, 2014a). Genes which were enriched in the Ebf2+ PDGFRα+ and Myf5 lineage+ PDGFRα+ group have been validated as the first brown adipogenic progenitor signature which interestingly did not yield an adipogenic key marker (Wang et al., 2014).

1.5 Programming the adipogenic cell identity

It has been stated that mesenchymal progenitor cells undergo a sequential process to form mature adipocytes. This event is well orchestrated and involves chromatin remodeling, changes in the epigenetic landscape, and finally results in activation of a

transcriptional cascade that defines the adipogenic identity (Jiang et al., 2014, Rauch and Mandrup, 2021, Rosen and MacDougald, 2006, Cristancho and Lazar, 2011).

1.5.1 Mesenchymal cell fate restriction

The determination process in first place implies commitment of a pluripotent stem cell (embryonic stem cell, ESC) to a distinct lineage. Thus, the conversion of mesenchymal stromal cell to a preadipocyte identity (Rosen and MacDougald, 2006).

Interestingly, on a low level, MSCs express various genes from different lineages that suppress each other to maintain the undifferentiated state (Rosen and MacDougald, 2006). At the timepoint of environmental changes, the balance is tipped, and new established conditions enable one lineage to be favored over the others, entering a final cell fate decision process (Rosen and MacDougald, 2006). One of the most prominent examples is the *vice versa* repressive regulation between the adipogenic master regulator PPARγ and osteogenic lineage specifier runt-related transcription factor 2 (RUNX2). Data on RUNX2$^{-/-}$ cells showed an elevated potential to form adipocytes, while PPARγ$^{+/-}$ mice developed increased bone mass (Rosen and MacDougald, 2006, Jeon et al., 2003, Akune et al., 2004). A similar regulatory scenario was described between the myogenic and adipogenic fate. Here, Rho family of small GTPases have been demonstrated to regulate whether RHO-associated kinase (ROCK) translocates into the nucleus and promotes the myogenic cell fate or in case of Rho GTPase inactivation *via* p190B RHO-specific GTPase-activating protein (p190-B RhoGAP) the adipogenic lineage (Cristancho and Lazar, 2011, Rosen and MacDougald, 2006). This has been confirmed on p190-B RhoGAP lacking mice that developed reduced adipose tissue and mouse embryonic fibroblasts (MEFs) with decreased adipogenic competence (Sordella et al., 2003). Moreover, treatment of C2C12 myotubes with insulin growth factor 1 (IGF1)- and ROCK- inhibitor induced lipid accumulation (Bryan et al., 2005, Rosen and MacDougald, 2006, Cristancho and Lazar, 2011). Together, these observations define a sensitive regulatory system which can after disbalance result in a cell lineage commitment.

1.5.2 Chromatin remodeling and enhancer communities

Dynamical changes in the three-dimensional (3D) architecture of chromatin have been associated to be decisive for transcriptional adaption of a cell to environmental changes (Madsen et al., 2020, Rauch and Mandrup, 2021, Inagaki et al., 2016). Therefore, genome organizers like CCCTC binding factors (CTCFs) and cohesion modulate chromatin compartmentation by binding together strands of desoxyribonucleic acid (DNA) which in turn result in chromatin looping and or mounting to structures like the nuclear lamina (Phillips and Corces, 2009, Guelen et al., 2008, Hou et al., 2008). A homodimer of CTCFs has also been described as an inhibitor of transcription since their DNA binding prevents interaction between enhancers and promoters (Yusufzai et al., 2004). As mentioned above a CTCF homodimer defines the boundary of DNA loops which conversely describe a self-interacting genomic unit- also named topologically associated domain (TAD). Within TADs, DNA sequences physically interact with each other more frequently than with sequences outside of a TAD (Pombo and Dillon, 2015). Also, it has been observed that highly interconnected enhancers localize at their boundaries which actively regulate gene expression (Madsen et al., 2020) (Fig. 8).
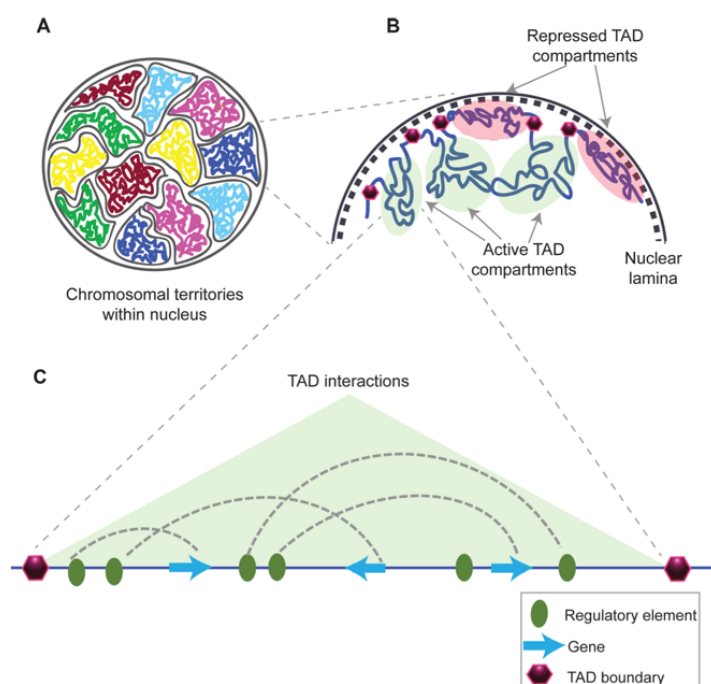
Figure: 8: Structural organization of chromatin. A) Chromosomes are found to occupy specific nuclear spaces, termed chromosomal territories. B) Each chromosome is segmented into topological associated domains (TADs). TADs with repressed transcriptional activity (red) tend to arrange close to the nuclear lamina (dashed line), whereas active TADs (green) tend to localize more in the center of a nucleus. Each TAD is framed by regions with low interaction frequencies "TAD boundaries" (magenta hexagon). C) An active TAD demonstrates several interactions between distal regulatory elements and genes within it. (Matharu and Ahituv, 2015)

Moreover, different enhancer communities have been described to be involved in the 3D chromatin modulation process and cell fate definition. Data from enhancer-capture

Hi-C experiments introduced and characterized firstly "regular enhancer communities" that showed less than eight enhancer-to-enhancer interactions and contained mainly motifs for transcription factors (TFs) that maintain the stem cell state (Madsen et al., 2020). Secondly, "highly interconnected enhancer communities" (HICEs) were identified as organizing structural domains or 3D hubs (regulatory hotspots) that are highly enriched of CTCF motifs (Fig. 9). HICEs demonstrated much higher connectivity between enhancers as well as an enrichment of the total and dynamic enhancer-promoter connections compared to regular enhancer communities (Madsen et al., 2020) (Fig. 9).
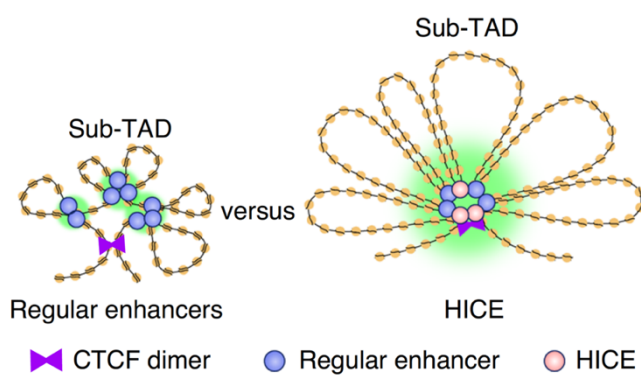
Figure 9: HICEs engage in multiple types of chromatin interactions. Schematic depicting how HICEs, but not regular enhancers, define TAD and sub-TAD boundaries. Regular enhancers rather define smaller sub-TADs with lower numbers of enhancer-enhancer interactions as well es enhancer-promoter connectivity compared to HICEs. Higher connectivity between HICEs and regulator enhancers enable transcriptional control on a higher scale "transcriptional hotspot". (Madsen et al., 2020)

However, super-enhancers (SEs) which have been used to study and analyze master regulators of cell fate and differentiation represent the third party (Hnisz et al., 2013, Whyte et al., 2013). Interestingly, the work from the Mandrup lab revealed that HICEs present distinct differences to SEs. First, HICEs show higher association with differentially expressed genes during differentiation and allow a better assignment of a current cell status. Moreover, HICEs compared to SEs demonstrated to be a more powerful cell fate predictor (Madsen et al., 2020). Altogether, HICEs are functional, preestablished structural domains in the stem cells that can upon differentiation drive possible fates of MSCs (Fig. 10) (Madsen et al., 2020, Rauch and Mandrup, 2021). Thus, PPARγ as an adipogenic master regulator induces changes in the connectivity of functional units like promoter and enhancers that finally directs the adipogenic program (Rauch and Mandrup, 2021, Madsen et al., 2020).
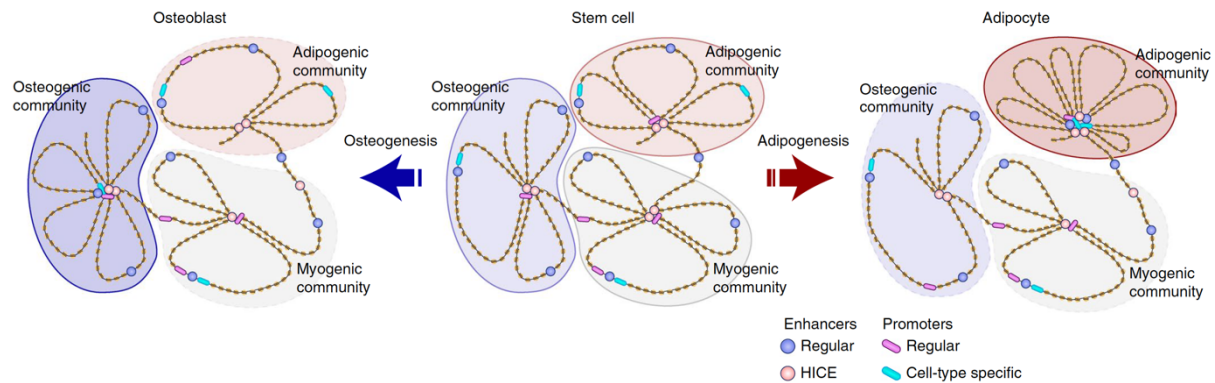
Figure 10: HICE communities define lineage choice. Schematic demonstration how HICE communities conceive lineage choices in human mesenchymal stem cells (hMSCs). In stem cells established HICEs simultaneously modulate gene expression of all lineages to maintain pluripotency. During differentiation to osteoblasts (blue) or adipocytes (red), connectivity within lineage-specific HICE communities is gained, while connectivity decreases in the other lineage-specific HICE communities. (Madsen et al., 2020)

1.5.3 Modulations in the epigenetic landscape control the adipogenic transition

Epigenetics generally describes regulatory modifications that effect gene expression activity which can be mitotically and/or meiotically inherited but do not arise from changes in the DNA sequence (Weinhold, 2006, Dupont et al., 2009). Thus, the modulatory units are histone variants, covalent modifications of DNA bases, and posttranslational modifications of amino acids on the amino-terminal tail of histones (Dupont et al., 2009, Biswas and Rao, 2018). The main epigenetic actors which have been associated with these modifications are firstly, epigenetic writers – a large collection of enzymes proficient of modifying nucleotide base and distinct amino acid residues on histones, secondly, epigenetic erasers - a group of enzymes competent in erasing these modifications, and lastly epigenetic readers - a heterogenous group of proteins that own specialized domains capable of recognizing distinct epigenetic marks in a locus (Biswas and Rao, 2018).

The most investigated epigenetic modifications are methylation and acetylation. Of note, methylation marks were observed on DNA and histone proteins whereas acetylation is exclusively associated with histones. Both modifications have been demonstrated to regulate gene expression pattern in a cell by controlling the state of transcriptional activation or repression (Biswas and Rao, 2018). Thus, epigenomic factors are recognized to play an important role in controlling cell-type-specific gene

expression during cell commitment and differentiation (Reik, 2007, Ong and Corces, 2011, Lee et al., 2019).

For example, the epigenetic landscape of the adipogenic program in embryonic stem (ES) cells has been shown to hold a bivalent signature of active H3K4me3 and repressive H3K27me3 marks. That combination of bivalent histone modifications keeps the adipogenic lineage specific genes like PPARγ and CCAAT enhancer binding protein alpha (CEBPα) in a "poised" state by pausing the RNA polymerase II (Pol II) (Voigt et al., 2012, Bernstein et al., 2006, Chen and Dent, 2014) (Fig. 11, upper right). In contrast, an active chromatin state was observed in ES cells for pluripotent gene loci since acetylation on H3K27 at enhancer regions, H3K4me3 modifications in the promoter and H3K36me3 marks in the gene body represent an active state of transcription (Chen and Dent, 2014, Meissner et al., 2008, Guenther et al., 2007) (Fig. 11, upper left).

However, in preadipocytes pluripotent genes hold repressive H3K9me3 and H3K27me3 modifications at the promoter region and gene body as well as DNA hypermethylation at the promoter summarizing the state of heterochromatin (Meissner et al., 2008, Mikkelsen et al., 2007).

The lineage specific genes of the adipogenic program though demonstrates an active motif of H3K4me1 and H3K27ac marks in the enhancer region. These marks were revealed to be established by epigenomic writers like MLL3/4 and CBP/p300 that got recruited by the pioneer adipogenic TF, CEBPβ (Lee et al., 2013a, Lee et al., 2019). The epigenomic writers in turn recruited the epigenetic reader: bromodomain and extra terminal domain (BET) protein Brd4 to activate enhancers by recruitment of Pol II and co-activators (Lee et al., 2019, Brown et al., 2018). Moreover, the promoter region is labeled with active H3K4me3 marks and the gene body with H3K36me modifications describing transcriptional activity (Mikkelsen et al., 2007).

At the same time genes of other lineages carry repressive marks like H3K27me3 and DNA methylation at their promoter regions (Fig. 11, bottom right), concluding that the epigenetic profile of a cell can describe the actual state of a cell.
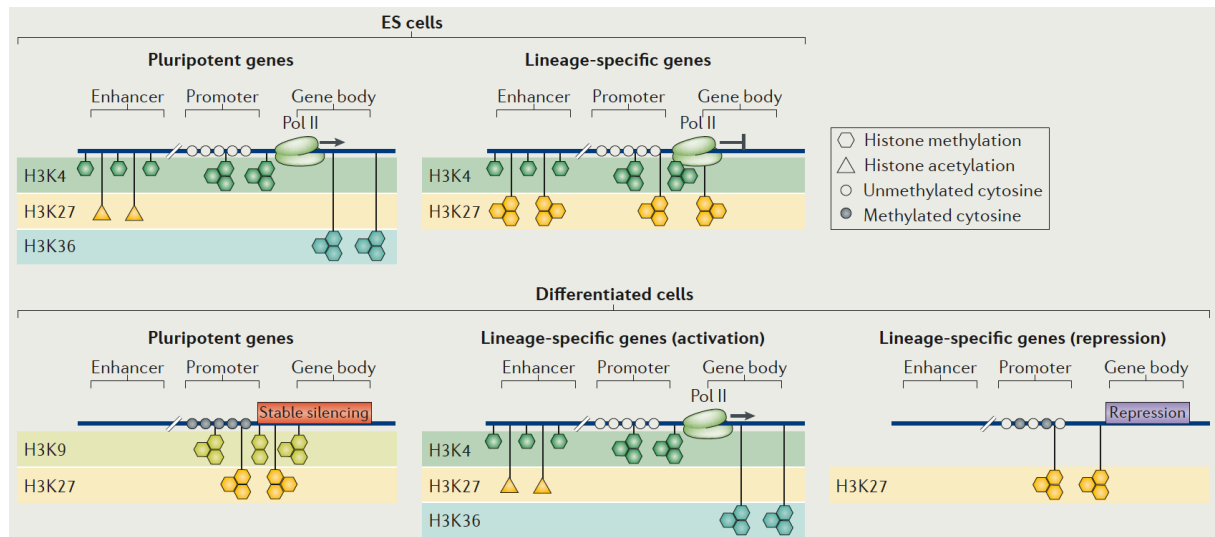
Figure 11: Chromatin modifications describe the actual state of a cell.
The epigenetic signature in embryonic stem (ES) cells show an active chromatin state as H3K4me and H3K27ac mark the enhancer region and H3K4me3 the promoter to maintain the pluripotent state (upper left). Lineage-specific genes instead, hold a bivalent signature such as H3K4me (active) and H3K27me3 (repressive) in the enhancer and promoter region representing a "poised" state of transcription (upper right). In contrast, cells that have differentiated hold repressive marks for genes of other lineages and pluripotent genes comprising of DNA methylation and H3K27me3 in the promoter region (bottom left and right). However, the lineage-specific genes of the differentiated cell demonstrate an activate histone profile: H3K4me and H3K27ac in the enhancer and H3K4me3 in the promoter region (bottom center). (Inagaki et al., 2016)

1.5.4 Key regulators of the early adipogenic transcriptional cascade

To sequentially activate the adipogenic program CCAAT enhancer binding proteins are crucial (Lee and Ge, 2014, Lee et al., 2019, Farmer, 2006, Zuo et al., 2006, Lane et al., 1999, Barak et al., 1999). CEBP proteins belong to the basic leucine zipper family TFs that can form homo- and hetero-dimers to bind to their target sequences to regulate gene transcription (Lee et al., 2019, Landschulz et al., 1989). In the initial phase of adipogenic differentiation, CEBPβ and CEBPδ become immediately activated by either adipogenic chemicals like isobutylmethylxanthine (IBMX) and dexamethasone (DEX) *in vitro* or through other inducive cues (hormones) like insulin *in vivo* (Cao et al., 1991, Lee et al., 2019, Tang et al., 2005) (Fig. 12). The relevance of these TFs has been confirmed by overexpression of CEBPβ alone or together with CEBPδ, which in turn promoted PPARγ expression in a non-adipogenic NIH3T3 cell line (Wu et al., 1995, Wu et al., 1996, Lee and Ge, 2014). Two isoforms of PPARγ exist, PPARγ1 is ubiquitously expressed, whereas PPARγ2 expression is specifically restricted to adipose tissues (Cho et al., 2009). From now onwards, PPARγ2 will be referred to as PPARγ.

However, double knockout of CEBPβ and CEBPδ in mice decreased adipose tissue weight significantly (Tanaka et al., 1997). Also, ChIP-Seq data revealed that CEBPβ functions as a pioneer TF in the initial state of adipogenesis since CEBPβ was observed to bind to adipogenic enhancer regions and thereby enables the recruitment of other pro-adipogenic TFs to form adipogenic enhancers and consequently active expression of late acting TFs such as PPARγ and CEBPα (Siersbæk et al., 2012, Siersbæk et al., 2011).

CEBPα, like PPARγ, is a pro-adipogenic TF, is decisive for adipogenesis since loss of CEBPα in mice leads to lack of white adipose tissue and smaller brown fat depots (Wang et al., 1995). Interestingly, the expression of CEBPα is observed relatively late during adipogenesis as compared to CEBPβ and CEBPδ (Lee and Ge, 2014, Farmer, 2006, Lane et al., 1999) (Fig. 12). Of note, it is stated that the PPARγ2 promoter sequence, contains two CEBP recognition elements which can be recognized by three CEBPs to activate PPARγ2 expression (Zhu et al., 1995). Experiments support that CEBPα binding replaces early CEBPs such as -β and -δ at later stages, which recapitulates their expression patterns (Salma et al., 2006, Clarke et al., 1997) (Fig. 12). Additional data from Chromatin immune precipitation DNA-Sequencing (ChIP-Seq) analyses confirmed that CEBPα, CEBPβ and PPARγ activate PPARγ transcription itself as they bind to enhancer-like regions effecting the PPARγ gene locus in a positive feedback loop driving adipogenesis (Lee et al., 2013a) (Fig. 12).
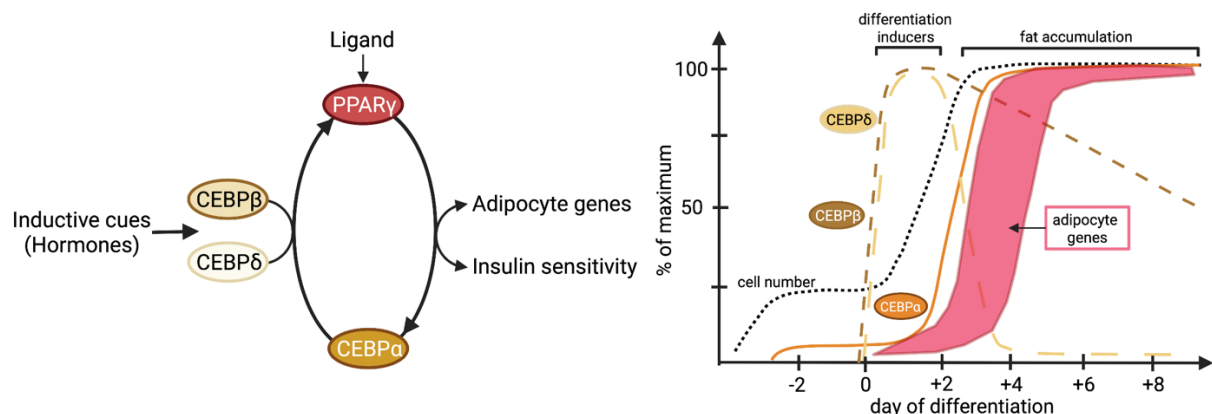
Figure 12: The regulatory cascade controlling adipogenesis.
Adipogenesis is dependent on a sequential activation and interaction of transcription factors, CEBPs and the master regulator PPARγ. CEBPβ and δ peak immediately after adipogenic induction and are crucial to activate PPARγ expression (day 0). Endogenous ligands potentiate the transcriptional activity of PPARγ. Upon ligand activation, PPARγ promotes the expression of CEBPα as well as other adipocyte genes later during adipogenesis (day 2). A positive feedback loop drives CEBPα to maintain the expression of PPARγ. Both, PPARγ and CEBPα promote adipocyte differentiation and insulin sensitivity.(Wu et al., 1999, Lane et al., 1999).

1.6 Modulators of the adipogenic program

1.6.1 Signaling pathways regulate adipogenesis

Several extracellular signaling molecules or hormones were involved in the decision-making process between activation or inhibition of the adipogenic program in mesenchymal progenitor cells (Ghaben and Scherer, 2019).

As already mentioned in the beginning of this study, insulin and insulin growth factor 1 (IGF1) signaling have been confirmed to be highly pro-adipogenic stimulators (Rosen and MacDougald, 2006, Ghaben and Scherer, 2019). Inhibition of single factors of the intracellular signaling cascade including the insulin receptor, insulin receptor substrates (primarily IRS1) its downstream target phosphatidylinositol-3 kinase (PI3K) and finally protein kinase B (AKT-1 or -2) has been demonstrated to block adipogenesis (Blüher et al., 2002, Accili and Taylor, 1991, Tseng et al., 2004, Xu and Liao, 2004) (Fig. 13). Under normal conditions this pathway would activate cyclic AMP (cAMP) response element-binding protein (CREB) as well as regulate mammalian target of rapamycin (mTOR) and the family of forkhead proteins (FOXOs) to drive the adipogenic program in its early stages (Martin et al., 2015, Nakae et al., 2003, Haeusler et al., 2018, Klemm et al., 2001).

Steroid hormones like glucocorticoids (GCs) that signal through glucocorticoid receptors (GCRs) represent another important pro-adipogenic regulator, as dexamethasone (Dex) - a synthetic GR ligand - accelerated adipogenic differentiation *in vitro*. GC expedites adipogenesis by recruiting histone acetyltransferase CBP to activate CEBP-primed enhancers in culture and drives upregulation of several transcription factors, including CEBPs (Lee et al., 2019, Ghaben and Scherer, 2019, Wiper-Bergeron et al., 2007). Furthermore, the glucocorticoid signaling pathway activation sensitizes preadipocytes to insulin signaling which in turn promotes the pro-adipogenic actions of the insulin pathway (Tomlinson et al., 2010, Ghaben and Scherer, 2019) (Fig. 13).

Bone morphogenic proteins (BMPs) belong to the superfamily of transforming growth factor-β (TGFβ) proteins. BMPs are conserved signaling molecules that have been first recognized for their competence to promote cartilage and bone formation (Rosen and MacDougald, 2006). To date it is well described that BMPs are involved in many processes in the entire body (Sieber et al., 2009). The effect of BMPs on mesenchymal

cells have been described to be very heterogeneous depending on the BMP molecule, its concentration, type of precursor cell and presence of other regulators (Rosen and MacDougald, 2006). Activation of the BMP pathway involves BMP molecules binding to the BMP receptors, which induces intracellular phosphorylation and activation of SMAD proteins. Phosphorylated SMADs thereafter translocate to the nucleus and regulate transcription of their target genes (Ghaben and Scherer, 2019, Rosen and MacDougald, 2006) (Fig. 13). It was shown that C3H10T1/2 pluripotent stem cells need BMP signaling to commit to the adipogenic lineage *in vitro* and that SMAD4 can activate PPARγ transcription to enable adipogenesis (Huang et al., 2009, Bowers et al., 2006, Tang et al., 2004). Expectedly, BMP molecules were confirmed to promote either white- or brown adipocyte formation. BMP4 have been recognized to be involved in white adipocyte- and BMP7 in brown adipocyte development (Modica et al., 2016, Tseng et al., 2008).
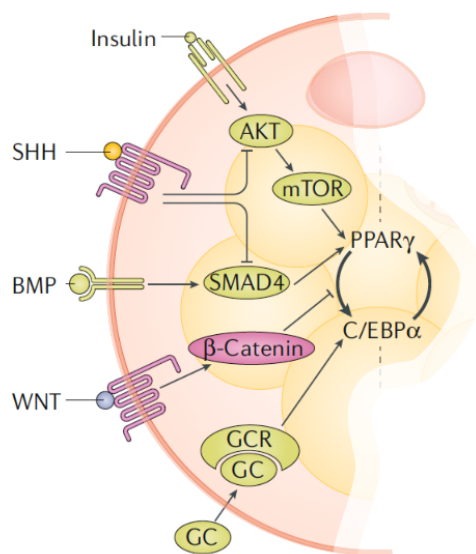
Figure 13: Extracellular regulators of adipogenesis.
Extracellular signaling ligands, including insulin, glucocorticoids (GC) and bone morphogenetic proteins (BMPs), directly activate PPARγ and/or CEBPα to drive preadipocyte differentiation. In contrast, signaling molecules, of the WNT and Hedgehog families (SHH), suppress adipogenesis through direct repression of the PPARγ–CEBPα complex or through intervention of other pro-adipogenic signaling cascades, such as inhibition of insulin and BMP signaling by Hedgehog. GCR: glucocorticoid receptor; mTOR: mammalian target of rapamycin (Ghaben and Scherer, 2019)

WNTs belong to a highly conserved family of paracrine and autocrine molecules which have been demonstrated to be important in the cell fate determination process and development (Ghaben and Scherer, 2019, Rosen and MacDougald, 2006). WNT proteins bind to the frizzled receptors and induce intracellular activation and stabilization of β-catenin that modulates gene expression of its targets (Logan and Nusse, 2004). Apart from their pro-growth roles, Wnt10b, Wnt10a and Wnt6 have been shown to suppress the adipogenic program by inhibition of CEBPα and PPARγ transcription (Ross et al., 2000, Cawthorn et al., 2012) (Fig. 13). At the same time, it has been recognized that WNT treated cells shift towards an osteoblastic identity

(Cawthorn et al., 2012, Cristancho and Lazar, 2011). Moreover, *in vivo* data have revealed that WNT signaling from the vascular endothelium is regulating the adipogenic niche by inhibiting additional adipocyte formation (Rajashekhar et al., 2008). These data emphasize the importance of a negative regulator to control tissue growth.

Hedgehog signaling represents another highly conserved pathway that was recognized as an important regulator in controlling the body patterning during embryogenesis (Ghaben and Scherer, 2019). The Hedgehog family of ligands bind to patched (PTC) receptors to activate downstream signaling by releasing smoothened (SMO) which induces gene expression through members of the GLI family (Hooper and Scott, 2005) (Fig. 13). Sonic hedgehog (SHH) and or activated PTC was demonstrated to reduce the adipogenic potential in rodent fibroblasts due to interference with BMP-2 downstream signaling and alteration of insulin sensitivity (Zehentner et al., 2000, Fontaine et al., 2008). Interestingly, both, WNT and Hedgehog signaling convert adipose precursors into an osteogenic like cell *in vivo* (Suh et al., 2006).

1.7 Aims of the study

Adipose tissue development has been introduced to be a highly complex process in which various lineages together orchestrates tissue organogenesis in a spatial and temporal manner (Sanchez-Gurmaches and Guertin, 2014b, Sanchez-Gurmaches and Guertin, 2014a, Sebo et al., 2018). In the last decades, studies that focused on the description of the initial pre-adipogenic progenitor mainly used lineage tracing strategies to underline the adipogenic competence of target genes at late embryogenesis or in adulthood. However, it still remains an open question when and where the first PPARγ expressing cells appear and whether the newly identified markers overlap with other adipogenic regulators during development. Noteworthy, several pro-white and pro-brown pre-adipogenic markers have been identified but never brought together in one picture to reconstruct postulated developmental strategies to organize adipose tissue development. Thus, initial steps of the adipogenic fate determination in mesenchymal progenitor cells during early embryogenesis remain poorly described.

The overarching question of this thesis therefore is:

May Osr1 represent a key factor characterizing adipogenic progenitor pools and mediating adipogenic cell fate determination in the early embryo?

To achieve this, the early Osr1 expressing cell pool will be challenged in many aspects to decipher the gradual process of adipose tissue formation by approaching the following points:

1. Does the early Osr1 cell pool hold a pre-adipogenic signature? To test that, single cell RNA-Seq data of the E9.5 and E11.5 Osr1+ cell pools will be investigated.

2. Systematic assessment of the adipogenic contribution pattern of the Osr1 lineage. In this case, inducible lineage tracing experiments will be performed during embryogenesis and in adulthood. Moreover, the Osr1-lineage in mature adipose tissue will be challenged by external stressors to prove their adipogenic potential.

3. Is embryonic adipogenesis dependent on Osr1 expressing cells? E14.5 Osr1-knockout embryos will be analyzed and GFP+ cells from E13.5 Osr1^{GCE} embryos will be extracted to assess their adipogenic potential *in vitro*.

4. Is the Osr1 lineage appropriate to capture the event of adipogenic cell fate commitment? To approach this, an *in vivo* expression analysis of multiple pro-adipogenic markers will be performed during early embryogenesis.

5. Mechanistically, how does Osr1 promote the adipogenic fate? Interactive proteomics data in mouse embryonic fibroblasts (MEFs) as well as lineage tracing experiments in Osr1 mutants will provide further details.

In summary, this research will provide new insights into the process of the adipogenic lineage segregation in the embryo. Consequently, the obtained data contribute to develop a detailed understanding in how adipose tissue organogenesis and

homeostasis is established. In the far future this research could serve as new starting point to search for regulatory players that have high potential to modulate adipogenesis.

2 MATERIAL

2.1 Mouse lines

The animal facility of the Max Planck Institute for Molecular Genetics under the supervision of Dr. L. Hartmann maintained the mouse lines used in this study. All mouse lines were maintained on a C57BL/6 background except for the Osr1$^{GCE/+}$ line that was breed on a CD-1 background. The following list introduces the used mouse lines:

Osr1$^{GCE/+}$ reporter line (Mugford et al., 2008). A transgene that expresses the GCE (eGFP-Cre-ERt2) cassette under the control of the Osr1 promoter.

Osr1$^{LacZ/+}$ reporter line (Stumm et al., 2018). A transgene that expresses the β-galactosidase enzyme under the control of the Osr1 promoter.

Osr1$^{fl/+}$ line: This line was generated from the Osr1$^{LacZ/+}$ reporter line introduced in (Stumm et al., 2018). In Stumm et al., the line carried a LacZ-reporter cassette on a multifunctional allele which through mating to the FLP recombinase mouse (Rodríguez et al., 2000) turned into a Osr1 exon 2 floxed mouse.

The Osr1$^{fl/+}$ line is a transgene that carries loxP sequences (fl) flanking the Osr1 exon 2 which by mating to a Cre-recombinase mouse results in excision of exon 2. Moreover, a GFP sequence upon inversion, can be used as a reporter of the Osr1 promoter activation.

Myf5$^{Cre/+}$ line (Tallquist et al., 2000b) provided by Prof. Carmen Birchmeyer, is a transgene that expresses under the control of the Myf5 promoter a Cre-recombinase gene.

Pax7$^{CreERt2/+}$ line (Murphy et al., 2011) is a transgene that expresses a Cre-recombinase gene under the control of the Pax7 promoter. This line was provided by Prof. Gabrielle Kardon and Prof. Tim Schulz

Rosa26$^{mTmG/+}$ line (Muzumdar et al., 2007) was provided by Prof. Andreas Kispert and is a conditional fluorescence reporter mouse, constitutively expressing a conditional td-Tomato transgene (mT). Cre mediated recombination converts the expression from mT to an EGFP (mG).

CAGG$^{CreERt2/+}$ line (Hayashi and McMahon, 2002) is a transgene that expresses a Cre-recombinase gene under the control of the Cagg promoter. This line was provided by Dr. Heiner Schrewe.

In addition to this, different X$^{Cre/+}$;Osr1$^{fl/+}$ mouse lines were generated, breeding the Osr1$^{fl/+}$ mice either to the constitutive Myf5$^{Cre/+}$, the inducible Pax7$^{CreERt2/+}$ or the inducible CAGG$^{CreERt2/+}$ line.

For lineage tracing experiments, different Cre lines such as the Osr1$^{GCE/+}$, the Pax7$^{CreERt2/+}$ and the Myf5$^{Cre/+}$ was breed to the Rosa26$^{mTmG/+}$ animals to generate the X$^{Cre/+}$; Rosa26$^{mTmG/+}$ genotype. For tracing the Osr1-knockout lineage, a modified mouse model was used to overcome that both Osr1 alleles carry a Cre-enzyme. Thus, the Osr1$^{GCE/+}$; Rosa26$^{mTmG/+}$ line was breed to Osr1$^{LacZ/+}$ reporter animals to generate the Osr1$^{GCE/LacZ}$; Rosa26$^{mTmG/+}$ genotype.

To recognize Osr1 expression in lineage tracing experiments, the Osr1$^{LacZ/+}$ reporter line was breed to the X$^{Cre/+}$; Rosa26$^{mTmG/+}$ animals to obtain the X$^{Cre/+}$; Rosa26$^{mTmG/+}$;Osr1$^{LacZ/+}$. Of note, "X" refers to Myf5 and Pax7.

2.2 Cell lines

Table 1: Cell lines

CELL LINE	CELL TYPE	SUPPLIER
Wt1	Brown adipogenic progenitor	Cell bank of Tim Schulz
3T3-L1	White adipogenic progenitor	Cell bank of Petra Knaus
C2C12	Myoblast	Cell bank of Stefan Mundlos

2.3 Instruments

Table 2: Instruments

NAME	TYPE	SUPPLIER
Thermal PCR cycler	ProFlex PCR System	Thermo
Real time PCR cycler	ABI Prism HT 7900	Applied Biosystems
Microwave	DO2329	DOMO
Thermomixer	compact 5350	Eppendorf
Water bath	MD	Julabo
Microscope	IX50	Olympus
Florescence microscope	DMi8	Leica
Confocal laser scanning microscope	SP8	Leica
Confocal laser scanning microscope	LSM 700	ZEISS
FACS	Aria II SORP	BD Pharmingen™
Protein electrophoresis equipment	Mini	Bio-Rad
Protein transfer system	Mini Trans-Blot	Bio-Rad
Power supply	EPS301	Amersham Bioscience
Nandrop	2000	Thermo Scientific
TissueLyser	LT	Qiagen
Cryotome	H560	Microm
Microtome Cool Cut	HM355S	Microm
Embedding station	EC 350-1&2	Microm
Dehydration station	TP 1020	Leica
pH meter	HI2211	HANNA instruments
Automated Cell Counter		Luna™

2.4 Chemicals

If not otherwise specified, chemicals were purchased from Roth, Merck, Roche and Thermo Fisher.

Table 3: Buffers and solutions

BUFFER	FORMULA
Tamoxifen solution	Dissolve 30 mg/ml tamoxifen in 95%Corn Oil / 5% ethanol solution and incubate at 37°C, protect from light
10x PBS	80g NaCl; 2g KCl; 14.4g Na_2PO4; 2.4g KH_2PO4; add 800ml bidest H_20 and set pH to 7.4; Final volume: 1l
PBX	100 ml of 10x PBS solution. 1 ml of TritonX-100. Add bidest to 1l
10x TBS	24g Tris- HCl; 5.6g Tris base; 88g NaCl, dissolved in 900 ml bidest H_20; adjust pH to 7.6; add H_20 to 1l
TBST	Mix 100 ml of 10x TBS solution with 1 ml Tween-20. Add bidest H_20 to 1l.
RIPA buffer	10mM Tris-HCl, pH 7.5; 150mM NaCl; 0.5mM EDTA; 1% Triton-X100; 1% NA-Deoxycholate; 0.1% SDS
Protein lysis buffer	200μl RIPA buffer; 1mg/ml DNase1; 2.5mM $MgCl_2$; 1mM PMSF
10x Transfer buffer	30.2g Tris; 144g Glycine; dissolve in bidest H_20 to 1l
10x Running buffer	30g Tris base; 144g Glycine; 10g SDS; dissolve in bidest H_20 to 1l
1x Transfer buffer	Mix 100 ml of 10x transfer buffer with 200 ml methanol and 700 ml bidest H_20
1x Running buffer	Mix 100ml 10x running buffer with 900 ml bidest H_20
4% Stacking gel (2 gels)	Mix 990μl 30% Acrylamid; 1.89ml 0.5M Tris-HCl pH 6.8; 75μl 10% SDS; 6.03ml bidest H_20; 7.5μl TEMED; 75μl 10% APS (total volume: 15ml)
10% Separation gel (2 gels)	Mix 5ml 30% Acrylamid; 3.75ml 0.5M Tris-HCl pH 8.8; 150μl 10% SDS; 4.5ml bidest H_20; 7.5μl TEMED; 37.5μl 10% APS (total volume: 7.5ml)

6x Protein loading buffer	Mix 3.75 ml 1M Tris pH 6.8; 1.2 g SDS; 6 ml Glycerol; 0.006g bromophenol blue; 0.462g DTT; Total volume: 10 ml
50x TAE buffer	242g Tris; 18.61g EDTA; 57.1g Glacial acetic acid; add bidest water to 1l
6x Orange G DNA loading dye	Mix 2ml of 50x TAE buffer; 0.15 g Orange G, 60 ml Glycerol and add bidest H_2O to 100 ml
Blocking buffer I (Paraffine)	4.11g/l Citric acid, 10.76g/l $Na_2HPO_4 \cdot 2H_2O$, add bidest H_2O to 1l
Blocking buffer II (Paraffine)	242 g/l Tris-Base, 18.6 g/l EDTA pH 9 (with HCl), add bidest H_2O to 1l. Dilute for use 1:50 in H_2O
3% IF blocking solution	Dissolve 3g BSA powder in 100ml 1x PBS
1% IF Staining solution	Dilute 3,33ml blocking solution with 6.66ml 1x PBS
0,3% Sudan black solution	Dissolve 0.3g Sudan black powder in 100ml, 70% ethanol (store stock solution in the dark)
0.5% Oil Red O solution	Dissolve 0.5g ORO powder in 100ml pure isopropanol (store stock solution in the dark)
Rinsing buffer	Mix 2 ml $MgCl_2$ (stock: 1M), 0.2ml NP-40 and 0.1g Na-deoxycholate and add 1xPBS to 1l
β-Galactosidase staining solution	0,01% sodium deoxycholate, 0.02% Nonidet™ P40, 0.4mg/ml $MgCl_2$, 1.7mg/ml $K_3Fe(CN)_6$, 2.1mg/ml $K_4Fe(CN)_6 \cdot 3H_2O$, 1mg/ml X-Gal-substrate
Duolink Buffer A	Dissolve 0.88g NaCl; 0,12g Tris base; 50µl Tween20 in 80ml bidest H_2O; adjust pH to 7.4; add H_2O to 100ml; filter
Duolink Buffer B	Dissolve 0.58g NaCl; 0,424g Tris base; 2.6g Tris-HCL in 50ml bidest H_2O; adjust pH to 7.5; add H_2O to 100ml; filter

2.5 Medium and supplements for cell culture

Table 4: Cell culture products

PRODUCT	SUPPLIER
DPBS	PAN BIOTECH
FBS	PAN BIOTECH
100U Penicillin / 10mg/ml Streptomycin	PAN BIOTECH
Poly-lysine	Millipore / Merck
Trypsin	Gibco
DMEM 4.5g/l glucose	PAN BIOTECH
Insulin	Kindly provided by Prof. T.J. Schulz
Indomethacin	Kindly provided by Prof. T.J. Schulz
Dexamethasone	Kindly provided by Prof. T.J. Schulz
IBMX	Kindly provided by Prof. T.J. Schulz
T3	Kindly provided by Prof. T.J. Schulz
BMP2	Kindly provided by Prof. P. Knaus
BMP7	Kindly provided by Prof. T.J. Schulz
Rosiglitazone	Kindly provided by Prof. T.J. Schulz
SCR	Ambion® , Cat#: AM4635
siOsr1	Ambion® , Cat#: AM16706
Opti-MEM	Gibco™ 31985070
FuGENE HD transfection reagent	Promega E2311
Lipofectamine™ RNAiMAX Transfection Reagent	Thermo Fisher Scientific Cat#: 13778075

Table 5: Cell culture medium

MEDIUM	COMPOSITION
Growth medium	500ml DMEM; 50ml FCS; 5ml 100x Penicillin/Streptomycin
Adipogenic induction medium (50ml)	1ml FCS (2%), 5 µg/ml Insulin, 18 µg/ml Indomethacin, 0.1 µg/ml IBMX, 0.4 µg/ml Dexamethasone, 0.7 µg/ml T3, 1x Penicillin/Streptomycin in DMEM ↑ glucose

Adipogenic maintainment medium (50ml)	1ml FCS (2%), 5µg/ml Insulin, 0.7µg/ml T3, 1x Penicillin/Streptomycin in DMEM ↑ glucose

Table 6: Enzymes

NAME	SUPPLIER
Collagenase A	Roche
Taq-Polymerase	Mundlos lab
Trypsin-EDTA	Gibco
M-MuLV Reverse transcriptase	enzymatics
DNase 1	Quiagen
Duolink® Ligase	Merck
Duolink® Polymerase	

2.6 Plasmid
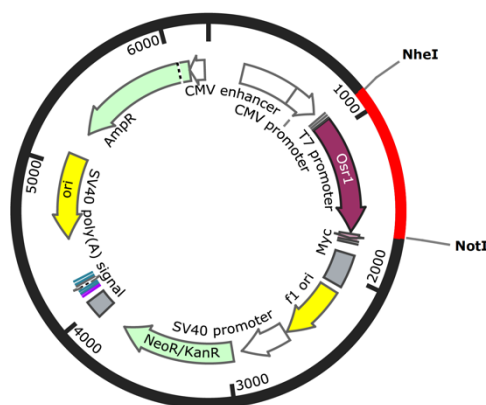
Osr1_c-myc_6xHis_pcDNA3.1_
6259 bp

The Osr1 c-Myc 6xHis pcDNA3.1 plasmid was used to overexpress Osr1 in C2C12 cells. This plasmid was created by David Warschkau whom I supervised in an internship.

Table 7: Reagent Kits

KIT	SUPPLIER
Direct-zol RNA Miniprep	Zymo Research
Biozym Blue S'Green qPCR Kit Separate ROX	Biozym
M-MuLV Reverse transcriptase kit	enzymatics
Duolink® PLA	Merck

2.7 Antibodies

Table 8: Primary antibodies

NAME	HOST	DILUTION	SUPPLIER
PPARγ	Rabbit	1:100	Cell Signaling T.® 81B8
OSR1	Rabbit	1:100	Sigma® life science HPA015525
GFP	Chicken	1:800	Aves labs 1020
FABP4	Rabbit	1:300	Abcam ab66682
phosphoSMAD1/5/8	Rabbit	1:500	Milipore AB3848
PAX7	Guinea pig	1:100	Kindly provided by Prof C. Birchmeier
DLK1	Rabbit	1:500	Santa Cruz sc-25437
Myosin heavy chain	Mouse	1:800	Merck 05-716
EBF2	Sheep	1:20	R&D systems AF7006
EP300	Rabbit	1:250	Novusbio NB100-507
CEBPβ	Rabbit	1:200	Antibodies-online.com ABIN205523
α-TUBULIN	Mouse	1:400	Santa Cruz sc-32293
PECAM-1	Hamster	1:250	DSHB 2H8
αSMA	Rabbit	1:250	Abcam ab5694
FLK1 (KDR)	Rat	1:25	BD Pharmingen™ 550549
MYF5	Rabbit	1:150	Santa Cruz sc-302
KI67	Rabbit	1:1000	Abcam ab833
KI67	Mouse	1:100	BD Pharmingen™ B66
SCA1	Rat	1:50	Abcam ab51317
LAMININ	Rabbit	1:1000	Abcam ab11575
GLP	Mouse	1:200	R&D systems PP-B0422-00
Perilipin A/B	Rabbit	1:300	Sigma P1873-200UL

Table 9: Conjugated antibodies

NAME	CONJUGATE	DILUTION	SUPPLIER
KI67	Alexa Fluor ® 555	1:100	BD Pharmingen™ 558617
CD31	APC	1:33	eBioscience 17-0311-82
CD45	APC	1:33	eBioscience 17-0451-83
SCA1	PE	1:67	BioLegend 108126
Ter119	APC	1:33	eBioscience 17-5921-81
Phalloidin	Texas Red®-X	1:200	Invitrogen™

Table 10: Secondary antibodies

NAME	REACTIVITY	DILUTION	SUPPLIER
Alexa Fluor ® 488, 568, 680	Anti-rabbit		
Alexa Fluor ® 568, 680	Anti-mouse		
Alexa Fluor ® 488	Anti-chicken	1:500	Invitrogen™
Alexa Fluor ® 568, 680	Anti-hamster		
Alexa Fluor ® 568, 680	Anti-guinea pig		
Alexa Fluor ® 568, 680	Anti-rat		
Alexa Fluor ® 568, 680	Anti-sheep		
IgG-HRP	Anti-mouse	1:1000	Kindly provided by Prof. S. Mundlos
IgG-HRP	Anti-rabbit	1:1000	Kindly provided by Prof. S. Mundlos

A negative control for the Co-IP was used: normal mouse IgG diluted 1:400 (Santa Cruz B.: sc-2025) (see: 3.7.4).

2.8 Ladders

Table 11: DNA and protein ladders

LADDER	SUPPLIER
100bp bp DNA ladder	Fermentas
1kb DNA ladder	
Protein Ladder, Page Ruler™ Plus Prestained 10-250kDa	Thermo Scientific™

2.9 Primer

Table 12: Genotyping primer list

PRIMER NAME	PRIMER SEQUENCE (5' → 3')
Reverse Osr1-WT	CTGGCTTAGGGTGAATGACG
Reverse Osr1-KO	GTAGGTCAGGGTGGTCACGA
Forward Osr1-WT/KO	CCCTCTTCCTGTCTTTGCAG
Forward LacZ	CGCTGGATAACGACATTGG
Reverse LacZ	TAGCGGCTGATGTTGAACTG
mTmG-WT-F	CTCTGCTGCCTCCTGGCTTCT
mTmG-WT-R	CGAGGCGGATCACAAGCAATA
mTmG-MUT-R	TCAATGGGCGGGGGTCGTT
Cre-F	GAGTGATGAGGTTCGCAAGA
Cre-R	CTACACCAGAGACGGAAATC
Osr1-spec1-F	GCTTAGAATTCAGGAACTGGG
Osr1-spec1-R	CTG GCA GAG ACA TAC ATG TTG

Table 13: qRT-PCR primer list

PRIMER NAME	PRIMER SEQUENCE (5' → 3')
Ebf2_fw	GCTGCGGGAACCGGAACGAGA
Ebf2_rv	ACACGACCTGGAACCGCCTCA
Dlk1_fw	TGTCAATGGAGTCTGCAAGG
Dlk1_rv	CTTTCCAGAGAACCCAGGTG

Meox1_fw	TGGCCTATGCAGAATCCATTCC
Meox1_rv	TGGATCTGAGCTGCGCATGTG
Pax7_fw	CGATTAGCCGAGTGCTCAGAA
Pax7_rv	CCAGACGGTTCCCTTTGTCG
PPARγ2_fw	GCATGGTGCCTTCGCTGA
PPARγ2_rv	TGGCATCTCTGTGTCAACCATG
Cebpα_fw	CAAGAACAGCAACGAGTACCG
Cebpα_rv	GTCACTGGTCAACTCCAGCAC
Cebpβ_fw	ACGACTTCCTCTCCGACCTCT
Cebpβ_rv	CGAGGCTCACGTAACCGTAGT
Cebpδ_fw	CGACTTCAGCGCCTACATTGA
Cebpδ_rv	CTAGCGACAGACCCCACAC
Myf5_fw	CAGCCCCACCTCCAACTG
Myf5_rv	GGGACCAGACAGGGCTGTTA
Myod1_fw	CGCCACTCCGGGACATAG
Myod1_rv	GAAGTCGTCTGCTGTCTCAAAGG
Mck_fw	GCAAGCACCCCAAGTTTGA
Mck_rv	ACCTGTGCCGCGCTTCT
Gapdh_fw	CTGCACCACCAACTGCTTAG
Gapdh_rv	GGATGCAGGGATGATGTTCT
Adipoq_fw	GGCAGGAAAGGAGAACCTGG
Adipoq_rv	AGCCTTGTCCCTCTTGAAGAG
Osr1_fw	CCTGTATGGTTTCAGCGCTC
Osr1_rv	TGGCTTAGGGTGAATGACGT
Ap2_fw	ATGCCTTTGTGGGAACCTGGA
Ap2_rv	CGCCCAGTTTGAAGGAAATC

2.10 Tools and Software

Table 14: Software

PURPOSE	NAME	SUPPLIER
Microscopy / imaging	ZEN 2010	ZEISS
Microscopy / imaging	LAS-X 3.7.0	Leica
Image processing	Fiji	Wayne Rasband
Image processing	Photoshop 23.0.2	Adobe
Image processing	CorelDRAW X7	Corel Corporation
Documentation and data analysis	Excel, Word, PowerPoint	Microsoft Office
Data analysis	Prism 8.0.2	GraphPad
Data analysis	RStudio V 1.2.1335	RStudio, Inc.
RTqPCR analyses	SDS 2.4	Applied Biosystem
FACS analyzing data	FlowJo	BD Bioscience
Reference management	EndNote X9.3.3	Clarivate Analytics

Table 15: Online Sources and Tools

NAME	URL
String	https://string-db.org
Sivisca	https://shiny.mdc-berlin.de/sivisca/
NCBI: Primer-BLAST	https://www.ncbi.nlm.nih.gov
NCBI: GEO	https://www.ncbi.nlm.nih.gov
CIPR: Cluster Identity Predictor	https://aekiz.shinyapps.io/CIPR/

Table 16: GSE accession numbers for single cell analysis

GSE	GEO TITLE	PUBLICATION
GSE87038	Single-cell RNA-seq analysis unveils a prevalent epithelial/mesenchymal hybrid state during mouse organogenesis	Pijuan-Sala et al., 2019
GSE119945	The dynamic transcriptional landscape of mammalian organogenesis at single cell resolution	Cao et al., 2019
GSE164528	Defining the lineage of thermogenic perivascular adipose tissue	Angueira et al., 2021

3 METHODS

This work is based on the findings generated in my master thesis. Of note, listed methods have been established and explained in my master thesis: "Adipogenic potential of Osr1 expressing progenitor cells", before. For completeness, experiments used in this work again were specified in the following chapter.

3.1 Animal and tissue preparation

3.1.1 Tamoxifen administration for lineage tracing experiments

The lineage tracing approach was performed using the inducible Pax7$^{CreERt2/+}$; Rosa26$^{mTmG/+}$, the Osr1$^{CreERt2/+}$; Rosa26$^{mTmG/+}$ mouse lines as well as the constitutive Myf5$^{Cre/+}$; Rosa26$^{mTmG/+}$. In case of an inducible lineage tracing model, tamoxifen (TAM), an estrogen receptor agonist/antagonist (ERAAs) was administered to enable Cre translocation into the nucleus (Gallo and Kaufman, 1997, Zhong et al., 2015). It was stated that TAM can cause an early embryo abortion (Nakamura et al., 2006, Nguyen et al., 2009). Thus, progesterone (2 mg/40 g bodyweight) was administrated to reduce the negative side effects of TAM.

For prenatal fate mapping experiments, the Cre recombinase was induced with TAM at a desired timepoint. Therefore, as indicated in the table 17, different amounts of tamoxifen were used dependent on the embryonic stage and was injected in the abdominal space (intraperitoneal) of a pregnant mouse. Importantly, at E11.5 the reported side effects of TAM were reduced, and progesterone was expendable.

Table 17: Tamoxifen injection strategies

INJECTION TIMEPOINT	TAM CONC.	PROGESTERONE CONC.	AGE OF INVESTIGATION
E9.5	3mg /40g bw	2mg /40g bw	≥ E18
≥ E11.5	3mg /40g bw	-	≥ E18
E11.5 +E12.5	1.2 mg /40g bw	2mg /40g bw	11 weeks

3.1.2 Preparation of embryonic tissue

Breeding was scheduled to harvest embryos at the preferred stages. Pregnant mice were killed by cervical delocalization and embryos were taken from the uterus. For genotyping, a small biopsy was sampled from the tail. The fixation of E9.5-E11.5 embryos were performed with 4% paraformaldehyde (PFA)/ 1xPBS for 20 to 30 min at 4°C. In contrast, embryos of stage E18.5 were dissected into two pieces between the trunk and the abdominal portion. The fixation with 4% PFA/PBS was carried out overnight (o/n) at 4°C. To remove the PFA properly, three 10 min washing steps with 1xPBS were carried out. Next, sucrose treatments were applied to dehydrate the tissues and to ensure the tissue rigidity. Embryos were treated with 15% sucrose solution o/n at 4°C. On the next day, the 15% sucrose solution was replaced by a 30% sucrose solution. The incubation was performed o/n at 4°C. The prepared samples were transferred in O.C.T. compound, a viscose liquid, that provides a proper matrix for tissue orientation and for cryo-sectioning. The O.C.T. soaked tissues were embedded and orientated in O.C.T. filled chambers. A tank filled with dry ice chilled 100% ethanol was prepared to freeze the tissues. The frozen tissue-blocks were stored at -80°C. For tissue investigations frozen samples were dissected with the cryostat in 10 - 12 µm thin sections.

3.1.3 Tissue preparation of adult mice and paraffine embedding

Adult mice were killed at the age of eight to eleven weeks. Different adipose tissues and organs were collected. Tissues were fixed in 4% formalin 1xPBS solution o/n at room temperature. Three 10 min washing steps with 1xPBS were performed to remove formalin. For paraffin embedding, tissues were dehydrated stepwise. Hence, an increasing ethanol concentration-series (25% for 4 h, 50% for 4 h and 70% o/n) was carried out at 4°C. Afterwards, tissues were transferred into the Dehydration station TP 1020. The machine dehydrated and passaged the tissues from ethanol to the organic 1:1 UltraClear / liquid paraffin mixture. Processed tissues were embedded in liquid paraffin and finally stored at 4°C. For tissue analysis paraffin embedded tissues were dissected with the microtome in 6 µm sections.

3.2 Genotyping

3.2.1 DNA extraction

Sampled biopsies (embryonic tail tissue, adult ear material) were used for DNA extraction. The tissues were prepared on ice and separately loaded with 50 µl QuickExtractTM solution. The incubation was conducted on a thermomixer for 6 min at 65°C. To stop the reaction, enzymes were deactivated by a 2 min heat shock at 98°C. The obtained DNA extracts were ready to use for genotyping.

3.2.2 PCR protocol to identify the Osr1^{GCE} genotypes

The polymerase chain reaction (PCR) depicted in table 18 was performed to identify the possible genotypes. The base pair (bp) length of the amplified PCR-products was quantified through agarose gel electrophorese (WT: 355bp; GCE: 300bp).

Table 18: Osr1 reaction master mix and PCR temperature profile

VOLUME	REAGENT	TEMP.	TIME (min)	CYCLE
15 µl	bidest H$_2$O	95°C	2	
2.5 µl	10x PCR buffer (15mM)	95°C	0.5	
2 µl	dNTP (1.25 mM)	65°C ↓	0.5	10x
1 µl	Reverse Osr1-WT (10 mM)	60°C		(-0.5°C/cycle)
2 µl	Forward Osr1-WT/KO (10 mM)	72°C	0.5	
1 µl	Reverse Osr1-KO (10 mM)	95°C	0.5	
0.5 µl	Taq polymerase 10 U/ µl	60°C	0.5	
1.5 µl	Template	72°C	0.5	25x
25.5 µl	Total	72°C	0.5	
		4°C	∞	

3.2.3 Genotyping protocol to identify the Osr1^LacZ

Table 19 introduces the PCR reaction protocol that identifies the LacZ cassette in the Osr1 locus. The amplified PCR-product was quantified via agarose gel electrophorese (LacZ $\approx$ 600bp).

Table 19: LacZ reaction master mix and PCR temperature profile

VOLUME	REAGENT
19 µl	bidest H_2O
2.5 µl	10x PCR buffer (15mM)
2 µl	dNTP (1.25 mM)
1 µl	Reverse LacZ (10 mM)
1 µl	Forward LacZ (10 mM)
0.5 µl	Taq polymerase 10 U/ µl
1.5 µl	Template
27.5 µl	Total

TEMP.	TIME (min)	CYCLE
95°C	5	
95°C	1	
58°C	1	35x
72°C	1	
72°C	10	
4°C	∞	

3.2.4 Genotyping protocol to identify the ROSA^mTmG

To identify mTmG constructs in the ROSA locus a PCR was performed (Table 20). The amplified PCR-products were quantified through agarose gel electrophorese (WT: 330bp; mTmG: 250bp).

Table 20: mTmG reaction master mix and PCR temperature profile

VOLUME	REAGENT
12 µl	bidest H_2O
2.5 µl	10x PCR buffer (15mM)
2 µl	Mg^{2+} (25 mM)
2 µl	dNTP (1.25 mM)
1 µl	mTmG-WT-F (10 mM)
1 µl	mTmG-WT-R (10 mM)
2 µl	mTmG-MUT-R (10 mM)
0.5 µl	Taq polymerase 10 U/ µl
1.5 µl	Template
24.5 µl	Total

TEMP.	TIME (min)	CYCLE
95°C	5	
95°C	1	
66°C	1	35x
72°C	1	
72°C	7	
4°C	∞	

3.2.5 Genotyping protocol to identify the Cre recombinase

The Cre sequence of the Pax7-CreERt2, the CAGG-CreERt2 as well as the Myf5-Cre line was identified with the general Cre-PCR, introduced in table 21. The amplified PCR-products were quantified through agarose gel electrophorese (Cre: 650bp).

Table 21: Cre reaction master mix and PCR temperature profile

VOLUME	REAGENT
16 µl	bidest H_2O
2.5 µl	10x PCR buffer (15mM)
2 µl	dNTP (1.25 mM)
1 µl	Reverse LacZ (10 mM)
1 µl	Forward LacZ (10 mM)
0.5 µl	Taq polymerase 10 U/ µl
1.5 µl	Template
24.5 µl	Total

TEMP.	TIME (min)	CYCLE
95°C	5	
95°C	0.5	
66°C	0.5	35x
72°C	1	
72°C	10	
4°C	∞	

3.2.6 Genotyping protocol to identify the Osr1[floxed]

Table 22 introduces the PCR reaction protocol that identifies the LacZ cassette in the Osr1 locus. The amplified PCR-product was quantified via agarose gel electrophorese (WT: 356bp; MUT: 295bp).

Table 22: Osr1[floxed] reaction master mix and PCR temperature profile

TEMP.	TIME (min)	CYCLE
95°C	2	
95°C	0.5	
57°C ↓	0.5	10x
52°C		(-0.5°C/cycle)
72°C	0.5	
95°C	0.5	
60°C	0.5	
72°C	0.5	25x
72°C	0.5	
4°C	∞	

VOLUME	REAGENT
17 µl	bidest H_2O
2.5 µl	10x PCR buffer (15mM)
2 µl	dNTP (1.25 mM)
1 µl	Reverse Osr1-WT (10 mM)
1 µl	Reverse Osr1-KO (10 mM)
0.5 µl	Taq polymerase 10 U/ µl
1.5 µl	Template
25.5 µl	Total

3.2.7 Agarose gel electrophoresis

A 1.5% agarose gel was preparade during the PCR reaction. 1.5g agarose powder was dissolved in 100ml 1x TAE buffer in the microwave. Under the hood, EtBr was added in a 1:14000 dilution. After 30min, the gel was ready to use. In the meantime, the PCR products were supplemented each with 4.5 μl 6x DNA loading buffer. Samples and a 100 bp DNA ladder were loaded on the gel. 1 x TAE buffer, was used as a running buffer. The voltmeter was set to 130V and the run was done after 20 min. UV light was used to visualize the PCR products in a gel documentation system.

3.3   Staining procedures

3.3.1 Immunolabeling on paraffine-sections

To achieve paraffin removal and rehydration, slides were treated for 1 h with UltraClear. Afterwards, a treatment with a descending ethanol concentration-series from 100% down to 95%, 70% and 30% was carried out. Finally, slides were washed in bidistilled water (bidest) for 4 min. Next, the tissue sections were exposed for 15 min to a H_2O_2 containing blocking buffer I (table 3). This was done to enable endogenous peroxidases inhibition. Prepared slides were rinsed with bidest to remove H_2O_2. To unmask the antigen epitopes, tissue sections were treated with an antigen retrieval. The treatment was accomplished by using the blocking buffer II (table 3) and a 3-5 min cooking step in the microwave. The sections were shortly rinsed with 1xPBS. Thereafter, prepared sections were treated for 20 min with filtered 0,3% Sudan black solution that was dissolved in 70% ethanol. The dye was applied to reduce the autofluorescence of tissues. Three 10 min washing steps with 1xPBS were required to remove Sudan black particles. Before primary antibodies were applied on the tissue section, a 1 h blocking step with 1% bovine serum albumin (BSA) was conducted to prevent unspecific bindings. The primary antibodies were diluted, as required (table 8) in 1% BSA. The incubation was carried out o/n at 4°C. Three washing steps with 1xPBS (each 10 min) were performed to remove excessive material and eliminate unspecific bindings of antibodies. The secondary antibodies and DAPI (1:1000) were applied on the tissue sections for 1 h at room temperature. The secondary antibodies

were removed with three 10 min washing steps of 1xPBS. Finally, sections were mounted with Fluoromount-G and stored in the dark at 4°C.

3.3.2 Immunolabeling on cryo-sections

Cryo-sections were carefully thawed: 30min room temperature in the unopened box which was followed by 15min incubation on the 37°C heating board. A 10min 1xPBS washing was done to remove the O.C.T. matrix. The following incubation steps were conducted in a humid chamber. 0,4% TritonX-100 solution was applied on the sections for 10 min at room temperature. TritonX-100 is detergent and permeabilizes tissues for better primary antibodies penetration and epitope targeting. The permeabilized tissues were blocked for 1h at room temperature with a 3% blocking solution (table 3), to prevent unspecific bindings. Primary antibodies were diluted in 1% staining buffer (table 8). The sections were treated o/n at 4°C with the primary antibody solution. Three 10 min washing steps were performed with 1xPBX (1xPBS contained 0.1% of TritonX-100) to ensure the complete removal of the excess primary antibodies. Before the secondary antibodies and DAPI were applied, a short rinsing step with 1xPBS was conducted to remove the detergent. The sections were treated with the fluorescent secondary antibodies (1:500) and DAPI (1:1000) for 1 h at room temperature. Three 10 min washing steps with 1xPBX were carried out to remove the excess antibody material. Finally, the sections were mounted with Fluoromount-G and stored in the dark at 4°C.

3.3.3 Oil red O staining

3.3.3.1 On cryo-sections and embryos

O.C.T. was removed from the tissue-sections with 1xPBS as described previously. The Oil Red O (ORO) 0.5% stock solution was prepared with isopropanol in a water bath (table 3). The stock solution was diluted down to 0.3% with bidest water. The staining solution had to rest for 10 min and was filtered afterwards. The prepared slides were rinsed in 60% isopropanol before they were stained for 30 min in the ORO staining solution at room temperature. To remove the excess material, a short rinsing step with 60% isopropanol was processed. If necessary, an immunolabeling was performed

(see: 3.6.2). Finally, the stained tissues were rinsed with 1xPBS and mounted with Fluoromount-G and stored at 4°C.

3.3.3.2 On whole embryos

E18.5 embryos were carefully skinned and fixed for 1h with 4% PFA. The embryos were treated with 0,4% TritonX-100 solution for 15 min. A rinsing step with 60% isopropanol was performed. The ORO staining solution was prepared as described before and added to the skinned and permeabilized embryos for 30min. Excessive staining solution was removed with 60% isopropanol. 60% isopropanol was replaced with fresh one if necessary. Washing was continued until the background staining was removed. Finally, the embryos were washed three times with 1xPBS.

3.3.4 β-Galactosidase color reaction

3.3.4.1 On cryo-sections

The O.C.T. was removed from the cryo-sections with 1xPBS as described above. An additional PBX washing step was performed to permeabilize the tissue sections. The slides were transferred into the staining solution, which contained the artificial substrate (5-bromo- 4-chloro-3-indolyl-β-D-galactopyranoside, X-Gal) of the β-galactosidase. Exposure of X-Gal to β-galactosidase positive tissues initiated the enzymatic color reaction (blue) and enabled identification of reporter expression. The incubation was conducted in the dark at 37°C. The staining process took 3 h to 8 h, depending on the embryonic stage. On the next day, the slides were washed with 1x PBS and mounted with Fluoromount-G and stored in the dark at 4°C.

3.3.4.2 On organs that need paraffine embedding

For β-galactosidase staining on mature adipose tissue, a whole mount staining was conducted. Therefore, freshly dissected tissue was fixed in 4% formalin 1xPBS solution for 1h at 4°C. That was followed by 4x30min washing steps using the rinsing buffer. The buffer contained $MgCl_2$, NP-40 and Na-Deoxycholate (table 3) to further permeabilize the tissue. Upon permeabilization, the tissues were transferred into the X-GAL containing staining solution. The staining was performed overnight at 37°C in

the dark. On the next day, the stained tissues were washed with rinsing buffer and prepared for paraffine embedding (see: 3.1.3).

3.3.5 Eosin staining on paraffine-sections

To do an Eosin staining on paraffin sections, a one-hour incubation with UltraClear to achieve paraffin removal and a treatment with a descending ethanol concentration-series from 100% down to 95%, 70% and 30% was carried out to rehydrate the tissue slides. Afterwards, the slides were washed with bidistillated water for 4 min. In the meantime, 200ml Eosin was activated using 1ml of Glacial acetic acid. The slides were stained for three seconds to 1min. Before the slides were mounted with Entellan, a dehydration process had to follow. An increasing ethanol concentration-series was applied, starting from 70% ethanol (very short incubation), next 95% ethanol (5 min) which was replaced by 100% ethanol (5 min). Finally, the slides were treated with UltraClear for 10min.

3.4 RNA and Protein extraction and assays

3.4.1 RNA extraction with Direct-zol RNA Miniprep (Zymo)

3.4.1.1 Tissue

Adipose tissue samples were dissected from adult mice. The following steps were conducted on ice and with pre-cooled reagents. First, the tissue was lysed using 600 μl TRI Reagent®. A clean grinding ball was added to each tube. The TissueLyser set to 30Hz, was used for tissue homogenization for 3x 1min intervals. The tissue lysate was centrifuged at 20.000xg for 20min at 4°C. The supernatant was transferred to a new tube. An equal volume (600 μl) of ethanol (95-100%) was added to each sample and mixed thoroughly. (Continue as described in: Cells, second paragraph)

3.4.1.2 Cells

Directly in the dish, cells were resuspended in 300 μl TRI Reagent®. An equal volume (300 μl) of ethanol (95-100%) was added to each sample lysed in TRI Reagent® and mix thoroughly.

The following steps were performed at room temperature and centrifugation at 10,000-16,000 x g for 30 seconds, unless specified.

The TRI Reagent® / ethanol mixture was transferred into a Zymo-SpinTM IICR Column which was inserted in a collection tube. A centrifugation step was conducted. The flow-through was discarded and the column was transferred into a new collection tube and discard. 400 μl RNA Wash Buffer was added to the column and another centrifugation step was performed. For DNase I treatment, an RNase-free tube was used, to mix 5 μl DNase I (6 U/μl) with 75 μl DNA Digestion Buffer. The DNase I supplemented buffer was added directly to the column matrix. A 15min incubation step at room temperature was implemented. 400 μl Direct-zolTM RNA PreWash was added to the column and another centrifugation step was conducted. The flow-through was discarded and the treatment was repeated. 700 μl RNA Wash Buffer was added to the column and a 1min centrifugation step was performed to ensure complete removal of the wash buffer. The column was transferred carefully into a RNase-free tube for elution. To elute RNA, 20 μl of DNase/RNase-Free water was added directly to the column matrix and a centrifugation step after a 5min incubation step was implemented. This final step was repeated. The mRNA concentration was measured right after extraction, using the Nanodrop2000. MRNA was stored at -80°C.

3.4.2 Reverse transcription

For one reverse transcription reaction, 1 µg of mRNA was used. For the reaction mix, 1 µg of mRNA was supplemented with 1 µl of Rnasin (40 U/ µl) and RNase free water was added to a volume of 40.5 µl. The components of the master mix for one reaction are listed in the following table 23, as well as the program of the thermal PCR cycler. The total volume (mRNA mix + master mix) for each reaction was 100 µl. Complementary DNA (cDNA) was stored at -20°C.

Table 23: Master mix per reaction

VOLUME	REAGENT
10 µl	10x M-MuLV Buffer
22 µl	$MgCl_2$ (25mM)
20 µl	dNTP (2.5 mM)
5 µl	Random Hexamer (50 µM)
2.5 µl	M-MuLV Reverse Transcriptase (200,000 U/µl)
59.5 µl	Total

TEMP.	TIME (min)
25°C	10
48°C	30
95°C	5
4°C	∞

3.4.3 Quantitative polymerase chain reaction (qPCR)

Biozyme Blue S'-Green-based method was used for real-time qPCR. The cDNA was diluted with Rnase free water 1:10. For a qPCR, 980 µl of the 2x Blue S'-Green mix was combined with 20 µl of the 50 µM ROX additive. 6 µl of blue S'-Green / ROX additive was used per reaction. 4 µl of the 1:10 cDNA was added to the well. Finally, 2 µl of the 2,4 µM primer mixture (14,4 µl of forward and reverse primer stock solution (100 µM) were diluted in 571.2 µl pure water) was added to complete the reaction mix for a 384 well plate. The total qPCR reaction volume was 12 µl. All reactions were performed in triplicates. For negative controls, the cDNA was replaced by 4 µl water for each gene. *Gapdh* was used as a housekeeping gene to target genes relative expression and enabled normalization. A 7900 HT Fast Real-Time PCR Cycler was used to run the qPCR reaction. Raw data extraction and plate analysis was done in the SDS 2.4 data analysis system. Extracted data were further analyzed and visualized in Excel.

3.4.4 Co-immunoprecipitation

Whole WT embryos from stage E11.5 and E13.5 were dissected. The following steps were conducted on ice and with pre-cooled reagents. First, the tissue was lysed using 600 to 1000 µl proteinase inhibitor supplemented lysis buffer. A clean grinding ball was added to each tube. The TissueLyser set to 30Hz, was used for tissue homogenization for 3x 1min intervals. The tissue lysate was centrifuged at 20.000xg for 20min at 4°C. Only the supernatant was transferred to a new tube. The NanoDrop was used to estimate the protein concentration. 120 µg of the protein extract was used as input and thus mixed with an equivalent volume of 2x sample buffer. The input was denatured on a thermomixer at 400rpm for 5min at 98°C. The input was stored for a western blot analysis at -20°C.

In the meantime, a defined volume of agarose G beads were equilibrated by a single washing step with 1 ml proteinase inhibitor supplemented RIPA buffer. A centrifugation step at 3000 rpm at 4°C was conducted and the supernatant was discarded. RIPA buffer was used to set the beads back to the original volume.

In this case, 60 µl of the G bead solution was added to 490 µl embryonic protein extract to perform a pre-clearing on a rotating device for 1h at 4°C. After a centrifugation step at 3000 rpm at 4°C, the supernatant was transferred to a new tube. 300 µl of the pre-cleared protein extract was used per Co-IP reaction. The primary antibody GLP was diluted 1:1000 in 300 µl protein extract. As a negative control, an anti-mouse IGg antibody was used 1:200 in a separate reaction. The primary antibodies in the protein extract were incubating on a rotating device over night at 4°C. On the next day, 35 µl of the agarose G beads were added to each Co-IP reaction. The beads were mixing with the antibody-protein extract on a shaking device for 2h at 4°C. A centrifugation step at 3000 rpm at 4°C was implemented to discard the supernatant. The beads were washed 3x with 1xPBS carefully. PBS was removed after another centrifugation step at 3000 rpm at 4°C. Finally, the agarose G beads were resuspended in 30 µl 2x sample buffer. The denaturation was done on a thermomixer at 98°C for 10min. A short centrifugation step was performed to separate the supernatant from the beads. The Co-PIs were further investigated in a western blot assay (see SDS-Page).

3.4.5 SDS-PAGE

Sodium dodecyl sulfate-polyacrylamide gel electrophoresis (SDS-PAGE) was used to separate proteins through a gel matrix. According to their size, proteins will migrate with different pace, meaning that smaller proteins for example, migrate faster (Laemmli, 1970). A 10% polyacrylamide gel was prepared to separate GLP (~130kDA) from OSR1 (~35kDa). The stacking gel was prepared with 4% polyacrylamide (formulation, see materials). First the separation gel was prepared and covered with 100% ethanol to prevent contact with oxygen. After 45 min, ethanol was removed carefully. Second, the stacking gel was poured on top, and a comb was inserted to allow the acrylamide to polymerize.

Gels were placed into a gel chamber and covered with 1x running buffer. Samples were loaded in the center of the gel flanked by a lane of protein ladder. As long as the samples were migrating in the stacking gel, the voltage was set to 80V (~30min) and was increased to 120V (~1h) for the separation gel.

3.4.6 Western blot

After protein separation, a western blot was performed. For this purpose, a transfer buffer (table 3) was prepared during the SDS-PAGE run and stored at -20°C, until needed. In this study, only the wet transfer was conducted. The SDS-PAGE was stopped as the blue dye and the protein ladder reached the bottom of the gel. Next, the stacking gel was discarded, whereas the remaining separation gel was measured in size to cut the PVDF (polyvinylidene fluoride) membrane based on that. Pure methanol was used to activate the PVDF membrane for 30 sec. Right after, the membrane was transferred to 1x transfer buffer to equilibrate. All components of the transfer sandwich were soaked in chilled transfer buffer before use. Transfer sandwich assembly: sponge, three layers of Whatman paper, gel, PVDF membrane, three layers of Whatman paper, and another sponge. Air bubbles between the different layers were removed by rolling a falcon over it. The transfer sandwich was placed in the transfer chamber, the gel near to the cathode. Before additional transfer buffer was added, freezer packs were arranged around the transfer sandwich to ensure cooling. Moreover, the transfer chamber was put on ice, to prevent that the heat production affects the transfer. A 1.5h transfer at 100V was implemented. Directly after the

transfer, the PVDF membrane was stained with ponceau for 10min to validate efficient protein transfer. PBST was used to remove the red dye from the membrane. 5 % milk powder in TBST was prepared to block the membrane for 1h on a shaking device at room temperature. In the meantime, the primary antibody solutions were mixed, using 5 % milk/TBST with either OSR1 1:100 or GLP 1:2000. The membrane was cut in two, to stain one half with GLP and the other with OSR1. Incubation was done shaking at 4°C overnight. Excessive primary antibodies were removed with 3x 10min TBST washing steps. The secondary antibodies (anti-rabbit and anti-mouse) were diluted 1:1000 in TBST. The membranes were stained with the secondary antibody mixtures for 1h at room temperature. Again, excessive antibodies were removed with 3x 10min TBST washing steps. An ECL solution was prepared just before result documentation. The membranes were incubating with the ECL solution for 1min at room temperature. The excessive ECL solution was removed before the membrane was imaged with the western blot gel document system.

3.5 Fluorescence-activated Cell Sorting

3.5.1 Embryo and organ preparations for FACS analysis

Embryos of the Osr1^{GCE} reporter line as well as the adipose tissue from Osr1$^{GCE/+}$; Rosa26$^{mTmG/+}$ lineage tracing experiments were collected as explained in point 3.1.2. To specifically investigate the Osr1 expressing cells as well as the Osr1 lineage FACS sorting was performed.

3.5.2 FACS sorting to perform a single cell mRNA-Seq

For the single cell mRNA-Seq, GFP+ cells from E9.5 and E11.5 embryos of the Osr1$^{GCE/+}$ line were isolated. Single embryos were dissociated in 2ml tubes, containing 400 μl GM and 3 μl of Col A (100 μg/μl). Embryos were minced and placed in a 37°C pre-warmed thermomixer. For E9.5 embryos, the incubation was timed to 5min and for E11.5, to 10-15min. The cell suspension was pipetted carefully up and down. The cells were centrifuged at 300xg for 5min. The supernatant was discarded, and the cell pellet was washed with 1x PBS. After another centrifugation step, 1xPBS was replaced by the FACS sorting medium, containing 1% FCS, 2mM EDTA mixed in 1xPBS (filtered).

Before FACS, the cell suspensions were strained, using a 40 μm mesh to enable cell separation. The isolation of GFP+ cells was done by C. Bräuning in the FACS core facility of the MDC in the Berlin Institute for Medical System Biology (BIMSB, team leader: Dr. T. Conrad) as described in (Vallecillo-Garcia et al., 2017). GFP+ isolated cells were prepared for ICell8 sequencing as described in https://www.takarabio.com by C. Bräuning. The initial steps of the single cell mRNA-Seq analysis was performed by Dr. C. Fischer, a group member of Dr. T. Conrad's Single Cell Technologies Unit.

3.5.3 FACS sorting to obtain GFP+ embryonic progenitor cells

Osr1$^{GCE/GCE}$ and Osr1$^{GCE/+}$ embryos of stage E11.5, E12.5 and E13.5 were dissected. For FACS, distinct parts of the embryonic body were used. The torso without limbs, head and tail was isolated from E11.5 and E12.5. In contrast, the upper torso of an E13.5 embryo was of interest. Each torso was transferred to a single 2ml tube, containing 800 μl GM and 8 μl of Col A (100 μg/μl). The tissue was minced and digested in a 37°C water bath. The incubation was stopped as soon as tissue lumps disintegrated into a single cell suspension (E11.5: 12 min; E12.5: 18min and E13.5: 23 min). Cells were washed and resuspended in FACS sorting medium as described before. FACS sorting was performed in the FACS core facility of the MPI of Molecular Genetics lead by Dr. C. Giesecke-Thiel as described in (Vallecillo-Garcia et al., 2017). Sorted cells were collected in GM. Isolated cells were used for qPCR analysis (see: 3.4.3), in a PLA assay (see: 3.6) and cell culture assay to obtain the adipogenic potential of E13.5 GFP+ cells (see: 3.8.4).

3.5.4 FACS analysis of the Osr1 lineage in the SVF

The E11.5 + E12.5 Osr1 lineage was traced using the Osr1$^{GCE/+}$; Rosa26$^{mTmG/+}$ mouse model. Adipose tissues were dissected from 11 weeks old animals. A piece of each adipose tissue was placed in a 2ml tube, containing 1 ml GM and 10 μl of Col A (100 μg/μl). The samples were incubating for 30min at 37°C on a thermomixer in the dark. The reaction was stopped as described above. The adipocyte layer was aspirated. The cells were resuspended in 1xPBS on ice. To identify mesenchymal progenitors from the SVF, an antibody staining was performed. To remove the hematopoietic cells from the suspension, antibodies identifying Ter119/CD31/CD45 were used. Sca1 was

added to mark cells that function as progenitors of the adipogenic niche. The FACS experiment was done with Dr. P. Vallecillo-Garcia in the FACS core facility of the MPI of Molecular Genetics lead by Dr. C. Giesecke-Thiel.

3.6 Duolink® Proximity ligation assay

To validate protein-protein interactions a proximity ligation assay (PLA) was conducted. OSR1 in combination with GLP, EP300 and CEBPβ was tested. This was conducted either on FACS sorted Osr1-GFP+ cells of embryonic stage E11.5 and E13.5 or on undifferentiated 3T3-L1 cells.

3T3-L1 cells were plated on coverslips and cultured for 2 days until they reached 40% of confluency. Or 20.000 freshly FACS sorted Osr1-GFP+ cells were plated on coverslips for 1h at 4°C. Both were fixed for 10 min with 4% PFA/PBS solution and directly washed twice with 1xPBS. The coverslips were permeabilized with a 0.4% TritonX/PBS solution for 10 min. Per coverslip, 40 μl Duolink® blocking solution was added. The incubation time in a heated humidity chamber was 1h at 37°C. The primary antibodies were diluted in the Duolink® antibody diluent. Then, the Duolink® blocking solution was replaced by 40 μl primary antibody-Duolink® antibody diluent. The primary antibody mix was incubating in the humidity chamber over night at 4°C. On the next day, the Duolink® PLA probes PLUS and MINUS were diluted 1:5 in 40 μl Duolink® antibody diluent. The primary antibody-Duolink® antibody diluent solution was removed from the coverslips and washed 2x 5 min with wash buffer A (table 3). The PLA probe solution was added to the coverslips and was incubating in a humidity chamber for 1h at 37°C. To do the ligation, a 5x Duolink® ligation buffer was diluted 1:5 in pure water. Before ligation, the coverslips were washed 2x 5 min with wash buffer A. Then, just before adding the diluted ligation solution to the coverslips, the ligase enzyme was diluted 1:40 in 40 μl 1x Duolink® ligation buffer. The incubation was conducted in a humidity chamber for 30 min at 37°C. In the meantime, the 5x Duolink® amplification buffer was diluted 1:5 in pure water. This solution is light sensitive and had to be kept in the dark. Upon Duolink® ligase reaction, the coverslips were washed 2x 5 min with wash buffer A. Just before the washing steps finished, the polymerase enzyme was diluted 1:80 in 40 μl Duolink® amplification reaction buffer. The amplification was again done in a humidity chamber for 100 min at 37°C. Finally, the coverslips were washed 2x 10 min with 1x wash buffer B (table 3) that was mixed prior with DAPI (1:1000). The

last washing step was done with 0.01x wash buffer B for 1min. The coverslips were mounted with Fluorumount-G.

3.7 Osr1 BIO-ID

The Osr1 BIO-ID was performed in collaboration. The lab of Prof. M. Koch (Dr. T. Imhof) together with the CECAD / CMMC Proteomics Facility (Dr. Jan-Wilm Lackmann) of the University of Colone performed on SV40 immortalized mouse embryonic fibroblasts (MEFs) an Osr1 protein-protein interaction assay. Therefore, the DNA sequence of TurboID His tag was fused to the C-terminus of murine Osr1 (NP_035989, aa: 1-266) and cloned into sleeping beauty transposon vectors. A control plasmid was generated by cloning of TurboID His tag into sleeping beauty vectors. MEFs were stably transfected with FuGENE HD transfection reagent (#E2311, Promega, Mannheim, Germany). The protein expression was then induced with 1 µg/ml doxycycline (#D9891, Sigma-Aldrich, St. Louis, MO, USA) for 24 h. Next, the medium was replaced by 50 µM biotin containing DMEM and the cells were incubated for 1 h. After two washing steps with 1xPBS, cell pellets were lysed with 50 mM Tris, pH 7.4, 500 mM NaCl, 0.4 % SDS, 1 mM dithiothreitol, and 1x cOmplete protease inhibitor (#11697498001, Roche, Basel, Switzerland). Triton X-100 was added to the cell lysate to a final concentration of 2 %. Next, the samples were liquefied by sonication, diluted with an equal volume 50 mM Tris (pH 7.4) 500 mM buffer, and cleaned by centrifugation at full speed. The supernatant was then collected and purified with MagStrep type 3 XT magnetic beads (#2-4090-002, IBA Lifesciences, Göttingen, Germany), washed 2x with lysis buffer, 2x 50 mM Tris, 1 M NaCl, pH 8 buffer, 2x 50 mM Tris, pH 8 and eluted with 8 M Urea 50 mM NaOH. The elution was then neutralized by 50 mM HCl and 50 mM triethylammoniumbicarbonate buffer (#T7408, Merck KGaA, Darmstadt) were added. The samples were then incubated with DTT (5 mM) (#43819, Merck KGaA, Darmstadt) for 60 min followed by 2-chloroacetamide (40 mM) (#22790, Merck KGaA, Darmstadt) for 30 min in the dark at room temperature for reduction and alkylation of disulfide bonds. Next, the samples were digested by lysyl endopeptidase (#V1671, Promega, Walldorf) for 4h. The sample urea concentration was then reduced to 2M urea by adding triethylammoniumbicarbonate buffer and trypsin (#V5280, Promega, Walldorf) digestion was performed overnight. Finally, the digestion was stopped by 1% formic acid and peptides were purified with SDB-RP

METHODS

stage tips as previously described (Nat Protoc doi: 10.1038/nprot.2007.261.). Samples were analyzed using a Q Exactive Plus Orbitrap (#IQLAAEGAAPFALGMBDK, Thermo Fisher Scientific, Waltham, MA, USA) mass spectrometer coupled to an EASY nLC LC (#LC140, Thermo Fisher Scientific, Waltham, MA, USA). The mass spectrometric raw data were processed with Maxquant (version 1.5.3.8) with default settings.

3.7.1 Mass spectrometer set up

All samples were analyzed by the Proteomics Facility at CECAD on a Q Exactive Plus Orbitrap mass spectrometer that was coupled to an EASY nLC (both Thermo Scientific). Peptides were loaded with solvent A (0.1% formic acid in water) onto an in-house packed analytical column (50 cm — 75 μm I.D., filled with 2.7 μm Poroshell EC120 C18, Agilent). Peptides were chromatographically separated at a constant flow rate of 250 nL/min using the following gradient: 3-5% solvent B (0.1% formic acid in 80 % acetonitrile) within 1.0 min, 5-30% solvent B within 40.0 min, 30-50% solvent B within 8.0 min, 50-95% solvent B within 1.0 min, followed by washing and column equilibration. The mass spectrometer was operated in data-dependent acquisition mode. The MS1 survey scan was acquired from 300-1750 m/z at a resolution of 70,000. The top 10 most abundant peptides were isolated within a 1.8 Th window and subjected to HCD fragmentation at a normalized collision energy of 27%. The AGC target was set to 5e5 charges, allowing a maximum injection time of 110 ms. Product ions were detected in the Orbitrap at a resolution of 35,000. Precursors were dynamically excluded for 10.0 s.

3.7.2 Raw data processing

All mass spectrometric raw data were processed with Maxquant (version 1.5.3.8) using default parameters. Briefly, MS2 spectra were searched against the canonical murine Uniprot FASTA (UP000000589, downloaded at: 26.08.2020) database, including a list of common contaminants. False discovery rates on protein and PSM level were estimated by the target-decoy approach to 1% (Protein FDR) and 1% (PSM FDR) respectively. The minimal peptide length was set to 7 amino acids and carbamidomethylation at cysteine residues was considered as a fixed modification. Oxidation (M) and Acetyl (Protein N-term) were included as variable modifications. The

match-between runs option was enabled. LFQ quantification was enabled using default settings.

3.8 In vitro approach

3.8.1 BMP treatment

This experiment was conducted in a 12 well plate. 35.000 WT1 cells / well were seeded in GM. On the next morning, a cell confluence of 55% was reached. The cells were starved for three hours. Right after, the cells were treated with BMP supplemented GM or pure GM, as depicted in table 24.

Table 24: BMP treatment scheme

BMP	CONC.	RNA ISOLATION after
BMP2	2.5 nM	24h, 48h
BMP2	5 nM	24h, 48h
BMP7	3.3 nM	3h, 24h, 48h, 72h
BMP7	8 nM	3h, 24h, 48h, 72h
Negative Ctrl	0	0h, 3h, 24h, 48h, 72h

RNA was isolated to measure Osr1 expression levels *via* qPCR.

3.8.2 Osr1 knockdown in Wt1 cells

This assay was conducted in 24 well plates. A reverse transfecting siRNA assay using Lipofectamine™ RNAIMAX reagents was performed. For one well, add 9 pmol siOsr1 (or SCR) mixed with 100 μl Opti-MEM® and 1 μl Lipofectamine™ RNAIMAX to an empty well (table 4). The plate was moved thoroughly to enable mixing. The reagents were incubating for 20 min. 500 μl GM containing 18000 cells were added to the mixture (cell confluence should reach 30%-50% in the next 24h). The transfection-cell solution was mixed by rocking the plate back and forth (Pin liu, 2017 from Thermo fisher scientific). On the next day, the transfection was stopped by replacing the medium with 8 nM BMP7 supplemented GM. The cells were cultured for three consecutive days under the same conditions. MRNA was sampled from one day, two and three days

after transfection to test the knockdown efficiency. After three days of BMP7 treatment, an adipogenic differentiation was conducted. For two days, cells were treated with an adipogenic induction medium (table 5). The medium was replaced by an adipogenic maintenance medium, which was changed every second day. After four days maintenance medium, mRNA samples were collected for qPCR and additionally, cells were fixed to perform an ORO staining (see: 3.8.5).

3.8.3 Osr1 overexpression in C2C12 myoblasts

This assay was conducted in 12 well plates. 60.000 cells / well were plated on coverslips with GM. On the next day, C2C12 cells were transfected with Osr1-Myc plasmid (or GFP plasmid) using the FuGENE reagent. A 3:1 ratio was chosen, meaning 98 μl Opti-MEM$^\circledR$ was mixed with 2 μg plasmid. Upon vortexing, 6 μl of FuGENE was added. The master mix was incubating for 5-10 min.

Each well was already prepared with only 500 μl GM to which 75 μl transfection mixture was added. After six hours, the medium was replayed by pure GM. In the afternoon of the following day, adipogenesis was induced by using the adipogenic induction medium supplemented with 1 μM rosiglitazone (ROSI). The induction medium was removed after 2 days and replaced by adipogenic maintenance medium supplemented with 1 μM ROSI. The differentiation was stopped three days later. Coverslips were fixed with 4% PFA for 10min and stained with PLIN and MYHC (see: 3.8.5). Of note, mRNA was collected 24h after transfection to measure Osr1 expression.

3.8.4 Adipogenic differentiation assay on E13.5 GFP+ cells

Collected GFP+ cells from FACS were centrifuged at 300xg for 5 min. The supernatant was replaced by normal GM. 80.000 cells / well were plated in a 24 well-plate. Afterwards, the cells were kept in the incubator at 37°C overnight in GM. On the next day, the cells were confluent enough to start the adipogenic differentiation.

The components of the adipogenic induction medium were 5 µg/µl insulin, 1 µM dexamethasone, 0.5 µM 3-isobutyl-1-methylxanthine (IBMX), 1 nM 3,3′,5-triiodo-Lthyronine (T3) and indomethacin. After the two days treatment with induction medium, the medium was replaced by adipogenic maintenance medium that was composed of

insulin (c = 5 µg/µl) and T3 (c = 1 nM). After seven days of adipogenic differentiation, cells were fixed and stained as described in point 3.8.5.

3.8.5 Oil red O and immunolabeling in vitro

For ORO and immunolabeling, cells were plated in wells equipped with coverslips. After an adipogenic differentiation, coverslips were fixed with 4% PFA for 20 min at room temperature to perform an ORO staining. The PFA was directly replaced by the ORO staining solution, which was prepared like explained previously (see: 3.6.3). The incubation was carried out for 1 h at room temperature in the dark. 60% isopropanol was used to wash off excessive staining solutions. Another three 10 min washing steps were conducted with bidest H_2O to remove precipitated dye. The cell culture plates were air-dried and stored at room temperature. If necessary, ORO-stained cells were further analyzed for adipogenic markers by performing an immunolabeling.

For this purpose, coverslips were removed carefully from the cell culture plate and washed shortly with 1xPBS. The cells were permeabilized with 0,4% TritonX-100 solution for 10 min at room temperature. The prepared coverslips were blocked with 3% BSA/PBS to avoid unspecific bindings of primary antibodies. The blocking step was performed for 1 h at room temperature. The followed staining procedure was carried out like described in point 3.3.2.

4 RESULTS

Extensive work has been done on the identification of early BAT-progenitors in late embryogenesis and adult mice. Since development is a complex procedure and heterogenic cell types come in action – the process itself is not yet fully understood. This research applies latest techniques combined with traditional approaches to shed light on the very early steps of brown adipose tissue progenitor specification in the Osr1-lineage.

4.1 ICell8 single cell RNA Seq data of the E11.5 Osr1+ cell pool provides novel details of a pre-adipogenic-progenitor source

A study in 2017 introduced Osr1 as a marker of embryonic fibro-adipogenic progenitors and provided first evidence of the adipogenic capacity in the *Osr1* lineage (Vallecillo-Garcia et al., 2017). Genetic lineage tracing captured adipogenic potential of Osr1 cells at the stage of E11.5. To identify the Osr1 adipogenic progenitor cell pool at E11.5 whole Osr1$^{GCE/+}$ embryos were used to sort out Osr1-green fluorescent (GFP) cells to perform an ICell8 single-cell RNA-seq experiment.

4.1.1 Computational evaluation of Osr1-cluster identities through integration of a reference dataset

The E11.5 *Osr1+* single-cell transcriptome dataset was mapped to a reference study of a whole E11.5 embryo (Cao et al., 2019) to ensure quality and to verify overlap of the isolated *Osr1+* cell pool with the endogenous *Osr1* expressing cells of the reference dataset (Fig. 14A-B).
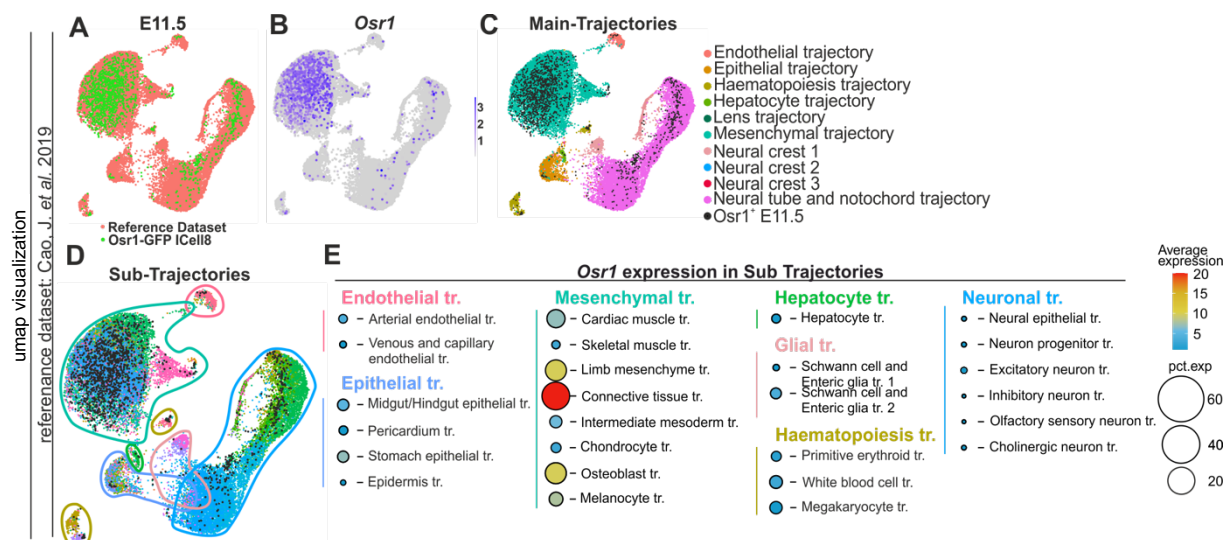
Figure 14: Representative mapping of the *Osr1*⁺-E11.5 scRNAseq dataset to an equivalent reference

A) displays the E11.5 *Osr1*+ single-cell dataset in green, mapped to the reference dataset of a whole E11.5 embryo in coral (Cao et al., 2019). B) represents the actual *Osr1* expression in the reference data. The Main-Trajectories of the Cao et al. dataset is visualized in C). The reference data defined Sub-Trajectories, which are depicted in D). The color-coded outlines in D) represent the Main-Trajectories in C). The color-code of the depicted cells refers to the Sub-Trajectories (see appendix). Both C) and D) show the Osr1-dataset in black. The expression profile of *Osr1* in the Cao et al. 2019 data is listed in E).

The Osr1 cells cluster within the reference dataset and strongly overlap with the cells from Cao et al. where active expression of *Osr1* can be detected (Fig. 14A-B), supporting successful purification of the complete Osr1+ cell pool at E11.5. The color-coded main-trajectories of the reference-object hold first insights of possible identities within the extracted Osr1+ cell pool. Clearly, Osr1 cells (depicted in black) are most abundant in the mesenchymal trajectory (Fig. 14C). Investigations of the Sub-Trajectories allow further specifications regarding the isolated cell types of the E11.5 *Osr1* dataset. The reference object displays highest *Osr1* expression levels and cell abundance inside the mesenchymal trajectory -specifically in the connective tissue compartment (Fig. 14D-E). In conclusion, the main cell type in the isolated *Osr1*+-dataset has mesenchymal identity.

4.1.2 Identification and annotation of 11 UMAP clusters

The first impressions of the proposed cell identities using the Cao et al. dataset provided an ideal basis to address the final cell annotation.

Figure 14A presents a UMAP plot which divides the Osr1 cell pool in 11 clusters. Three main cluster build the center of the UMAP: cl0, cl1 and cl2. Furthermore, a density plot

demonstrates that the core clusters hold the highest cell density (Fig. 14B). The scaled level of density highlights explicitly cl0 as the most abundant cell type – closely followed by cl2 and cl1. The core clusters are surrounded by nine smaller clusters. It is important to note that the nine peripheral cluster consist of very low cell numbers (Fig. 15B). Moreover, the signature genes of the peripheral clusters show a clear expression profile, which enabled direct cell type annotation (Fig. 15D). To determine the overall level of differentiation a pseudotime analysis was performed which identified cl1 as the most developed cluster (Fig. 15B).
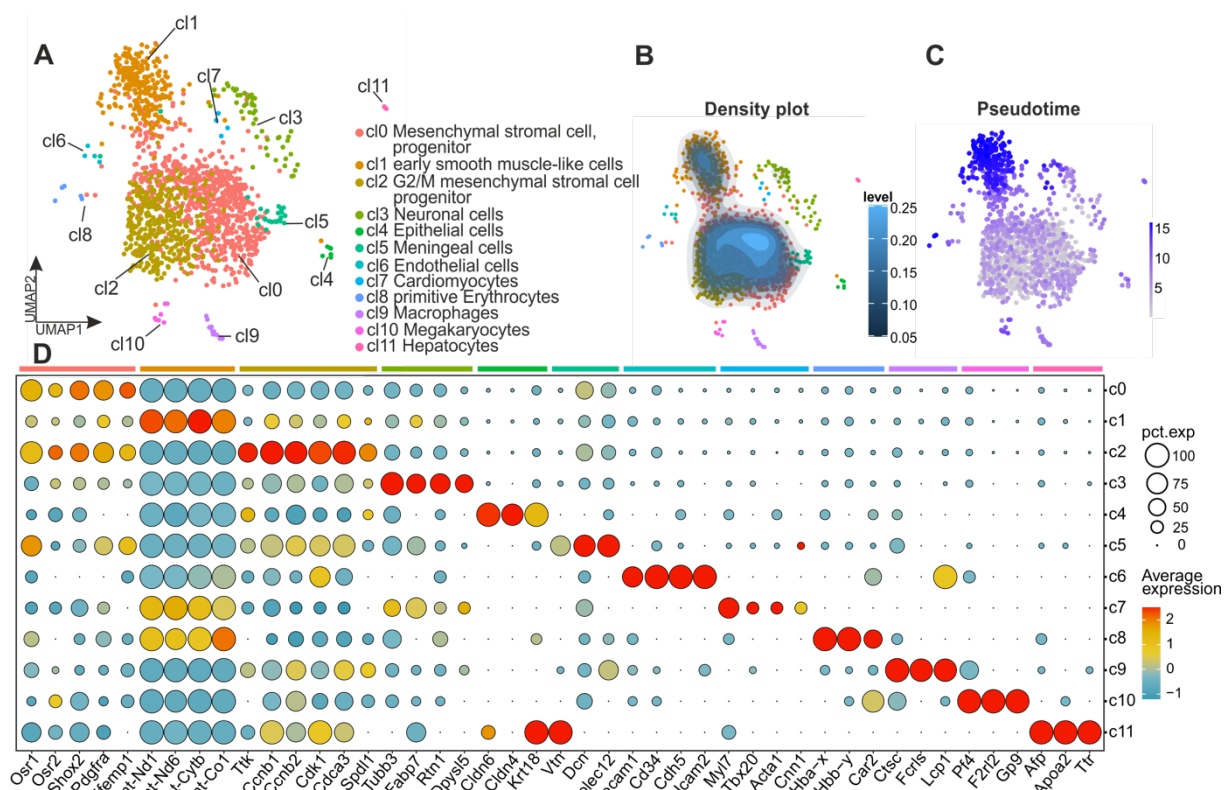
Figure 15: 11 cluster define the Osr1 cell pool at E11.5
The UMAP visualization of the 11 Osr1 clusters is displayed in A), highlighting that there are only three major cell types that define the Osr1 single cell RNA-object. The density plot in B) reveals that cl0 has highest number of cells followed by cluster cl2 and cl1. C) demonstrates the pseudotime, which ranks cl1 as the most developed cell type. Signature genes are used to define cluster identities in D). The signature genes in D) show that cl0 and cl2 are very similar, cl2 is characterized by expression of cell cycle genes too.

Looking at the signature genes of the main clusters, it is obvious that cluster cl0 and cl2 show a very similar expression profile. Both are high in genes which are widely expressed in the embryonic body. Especially strong *Osr1* expression (Fig. 15D) marks cell types with fibroblastic identity. Apart from that, *Osr2* and *Pdgfrα* show a similar expression profile as *Osr1*, which postulates a mesenchymal stromal cell identity for cl2 and cl0 (Fig. 15D) (Farahani and Xaymardan, 2015, Stricker et al., 2012). The

significant difference between cl0 and cl2 is that genes which define the G2/M phase of the cell cycle e.g., *Ccnb1* and *Cdk1* are enriched in cl2. Cl1 on the other hand, does not show any of these markers, it is rather very high in mitochondrial genes that are well known to identify tissue with myogenic potential: like heart and skeletal- or smooth muscle cells (Fig. 15D and 16) (Gabella, 1989, Kuznetsov et al., 2009, Wang et al., 2020, Thul PJ, 2017). Supportingly, cl7 shows expression of *Acta1* and *Myl7* and identifies a mature cardiomyocyte cell type which is also rich in mt-genes (Fig. 15D). To further validate the predicted cluster identities, a gene ontology (GO) analysis was performed by using the top 50 marker genes (Fig. 16).

Descartes Cell Types and Tissue 2021 E11cl0

	p-value
Stromal cells in Thymus	$2,93*10^{-8}$
Stromal cells in Muscle	$1,23*10^{-7}$
Stromal cells in Kidney	$1,84*10^{-7}$
Vascular endothelial cells in Cerebrum	$6,98*10^{-7}$
Mesothelial cells in Spleen	$1,18*10^{-6}$
Stromal cells in Adrenal	$1,60*10^{-6}$
Stromal cells in Eye	$3,89*10^{-6}$
Stromal cells in Stomach	$7,92*10^{-6}$
Stromal cells in Heart	$8,33*10^{-5}$
Mesothelial cells in Liver	$1,97*10^{-3}$

Descartes Cell Types and Tissue 2021 E11cl2

	p-value
Erythroblasts in Stomach	$2,98*10^{-3}$
Stromal cells in Stomach	$7,22*10^{-3}$
Stromal cells in Thymus	$3,34*10^{-2}$
IGFB1 DKK1+ cells in Placenta	$3,79*10^{-2}$
Retinal progenitors and Muller glia in Eye	$4,65*10^{-2}$
Stromal cells in Adrenal	$5,10*10^{-2}$
Stromal cells in Liver	$5,48*10^{-2}$
Stromal cells in Kidney	$6,54*10^{-2}$
Stromal cells in Heart	$8,17*10^{-2}$
Stromal cells in Intestine	$9,31*10^{-2}$

Descartes Cell Types and Tissue 2021 E11cl1

	p-value
Smooth muscle cells in Muscle	$5,07*10^{-3}$
SLC4A4 PEX5L+ cells in Cerebellum	$1,18*10^{-2}$
Thymic epithelial cells in Thymus	$1,80*10^{-2}$
EnS neurons in Intestine	$1,05*10^{-1}$
Inhibitory interneurons in Cerebellum	$1,09*10^{-1}$
Stromal cells in Splenn	$1,43*10^{-1}$
Mesangial cells in Kidney	$1,84*10^{-1}$
Smooth muscle cells in Placenta	$2,07*10^{-1}$
Stromal cells in Muscle	$2,61*10^{-1}$
Chromaffin cells in Adrenal	$3,09*10^{-1}$

Figure 16: Gene ontology analysis of the main clusters cl0, cl1 and cl2
The online tool "Enrichr" https://maayanlab.cloud/Enrichr/ prognosed based on the respective top 50 cluster signature genes possible identities. The used reference database is "Descartes Cell Types and Tissue 2021". The length of the bars as well as the red color-code represents the level of significance. The green frames highlight the most common cell type for the respective clusters, depicting that cl0 and cl2 on the left show stromal cell type characteristics, whereas cl1 on the right, presents myogenic identity.

Enrichr is a powerful online tool to define cell types with a representative signature list (Chen et al., 2013, Kuleshov et al., 2016, Xie et al., 2021). The readout for cl0 and cl2 exhibits stromal cell identity from any possible tissue. That goes together with the previously proposed cluster status: "mesenchymal stromal cell, progenitor". Furthermore, cl1 is assigned to a smooth - / skeletal muscle identity which supports once again the potential "early smooth muscle like cell" character (Fig. 15A and 16).

Considering the obtained cluster definitions and the *Osr1* expression pattern at E11.5 a map was developed- visualizing possible cluster to tissue assignment (Fig. 17B-C).

Osr1 expression in for e.g limb mesenchyme, the branchial arches, the stomach, the pharynx, the esophagus, lung tissue (Fig. 17C) and a cell collective lining the abdominal wall (Fig. 17B) are regions that overlapped with tissues considered to represent stromal cell identity and thus could indicate cl0 and cl2. Noteworthy, immunolabeling reveals OSR1^{+} expression in specific parts of the dermomyotomal derivate intermingling with the PAX7 cell pool (Fig. 17B-C).

Smooth muscle like cells of cl1 are found around the main vasculature – the dorsal aorta and outflow tract of the heart. The *Osr1*^{+} neuronal cluster 3 demonstrates *tubulin, beta 3 class III* (*Tubb3*) expression and explicitly marks cells of the dorsal root ganglion and the ventral horns of the spinal cord, where motor neurons reside (Kinameri et al., 2008) (Fig. 17A and 17C). Expression of tight-junction proteins claudin-5 and 6 (*Cldn5*, *Cldn6*) define epithelial cells (Sugimoto et al., 2013, Zhang et al., 2018). Here, *Osr1* expressing cells residing in the inner epithelial cell layer of the stomach and the diaphragm could represent cl4. Finally, the meningeal cluster 5 is forming a multi layered cell group, that surrounds the central nerve system along the cranial to caudal axis (Fig. 17B-C).

In summary, Osr1 is widely expressed but also defines specific areas providing different sources to the developing embryo. However, the main interest of this study is to investigate the *Osr1+* pool for an adipogenic progenitor identity.
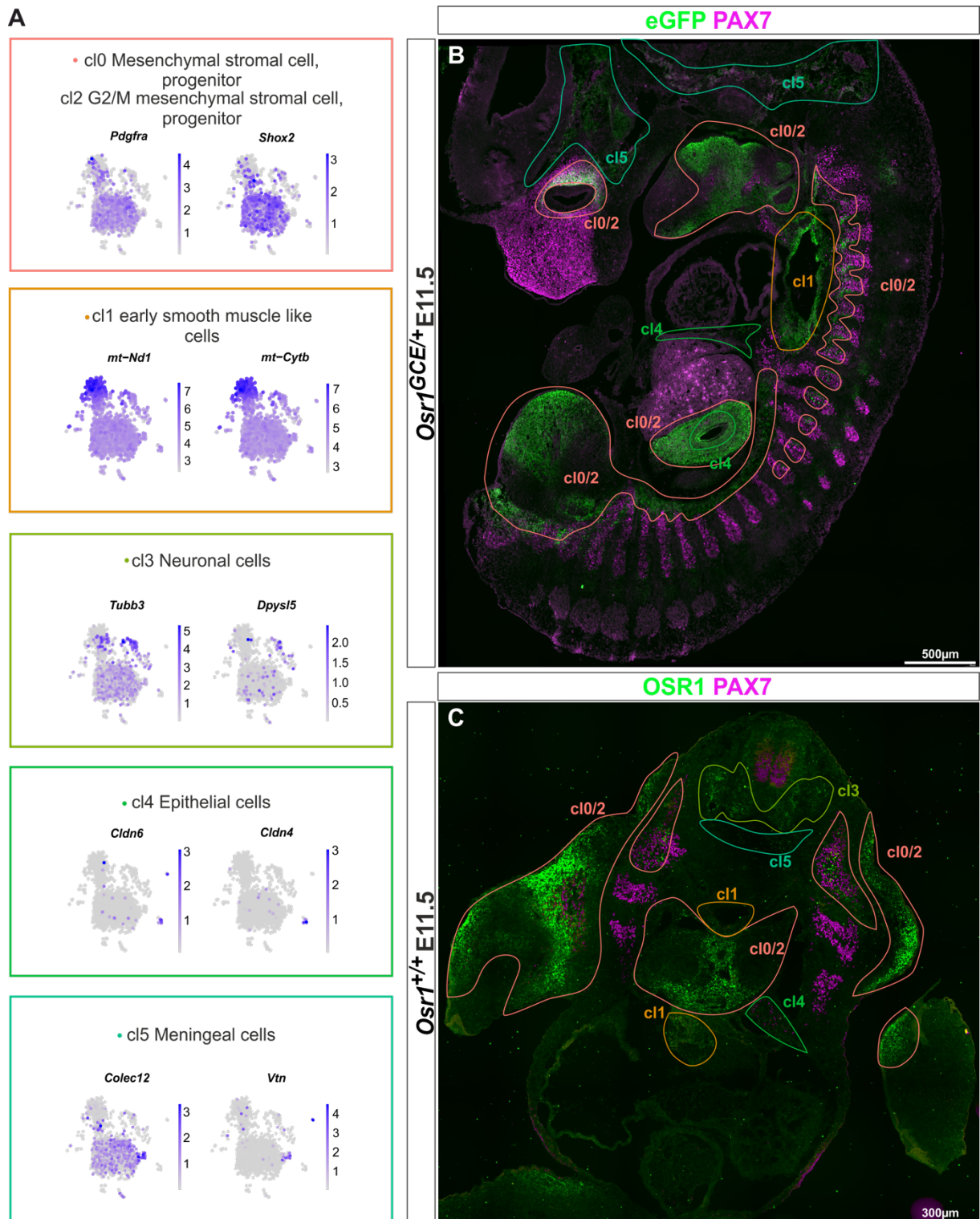
Figure 17: Merging clusters with the OSR1 expression map of an E11.5 embryo
A) depicts UMAP-feature plots, highlighting expression of cell type defining signature genes. As genes listed in A) are found in specific regions of an embryo, it can be assumed that OSR1 is colocalizing. B) and C) displays the expression pattern of OSR1 in green at embryonic stage E11.5. B) illustrates a longitudinal – and C) a cross section with a co-staining of PAX7 in magenta to discriminate OSR1+ locations. Regions of OSR1 expression were assigned to their most likely cluster identity.

4.1.3 Cluster 0 holds a pre-adipogenic identity

To unmask the adipogenic potential of the Osr1 dataset a computational strategy was chosen.

The earliest brown adipogenic precursor signature in development has been described in the Seale lab (Wang et al., 2014). They investigated freshly sorted *Ebf2+Pdgfra+* cells and *Pdgfra+* cells of the Myf5 lineage at the stage of E14.5. After revealing brown adipogenic potential of those cells, an Ebf2 pre-brown adipogenic gene signature (Ebf2 pre-BAT) of the most strongly enriched genes was defined. This Ebf2 pre-BAT signature was mapped on the Osr1 dataset and a signature enrichment in cl0 was observed (Fig. 18A). This finding indicates that the mesenchymal stromal cluster 0 could hold an adipogenic potential. For further validation a recent single cell RNA sequencing (scRNA-Seq) dataset derived from perivascular adipose tissue of P3 thoracic aorta was used. Importantly, this scRNA-Seq dataset provides information about different types of fibroblasts that serve as a source of adipose tissue remodeling (Angueira et al., 2021) (Fig. 18B). Interestingly, they identified three different fibroblast populations that reside in discrete anatomical compartments within the developing perivascular adipose tissue (PVAT) niche of the thoracic aorta. "Intermediate" fibroblasts express *Clec11a*, *Bace, Cd124* and are intimately associated with smooth muscle cells. Those showed enriched hedgehog signaling and did not reveal an adipogenic potential *in vitro*. In contrast, the identified *Ly6a* expressing "Progenitor" pool that resides in the adventitial cell region as well as the *Pparγ* and *Pdgfra* expressing "Preadipocytes" that locate at the periphery of adipose tissue lobes were highly adipogenic (Fig. 18B)(Angueira et al., 2021). However, signatures from the main Osr1 clusters (cl0, cl1 and cl2) were used to correlate with the identities of the P3 thoracic aorta object in figure 18B, confirming that cl0 has highest potential of pre-adipogenic identity (Fig. 18C). The dot plot shows that cl0 has the best overlap with the signatures of "Intermediate cells", "Progenitor cells" and "Preadipocytes". The cl1-signature on the other hand, is rich in cell types which hold smooth muscle characteristics like "SMC-a/b/c". Cl2 does not correspond very well with the object since cell cycle genes peak in cl2. Figure 18D displays the quality of the match between the Osr1-signatures and the PVAT-object, recapitulating the information of the dot plot in figure 18C. Finally, the same approach was used in opposite direction to test the PVAT-fibroblast identities on the main body of the Osr1 dataset (Fig. 18E). In summary,

it can be stated that cluster 0 holds the highest potential to provide a source of adipogenic progenitors to the developing embryo.
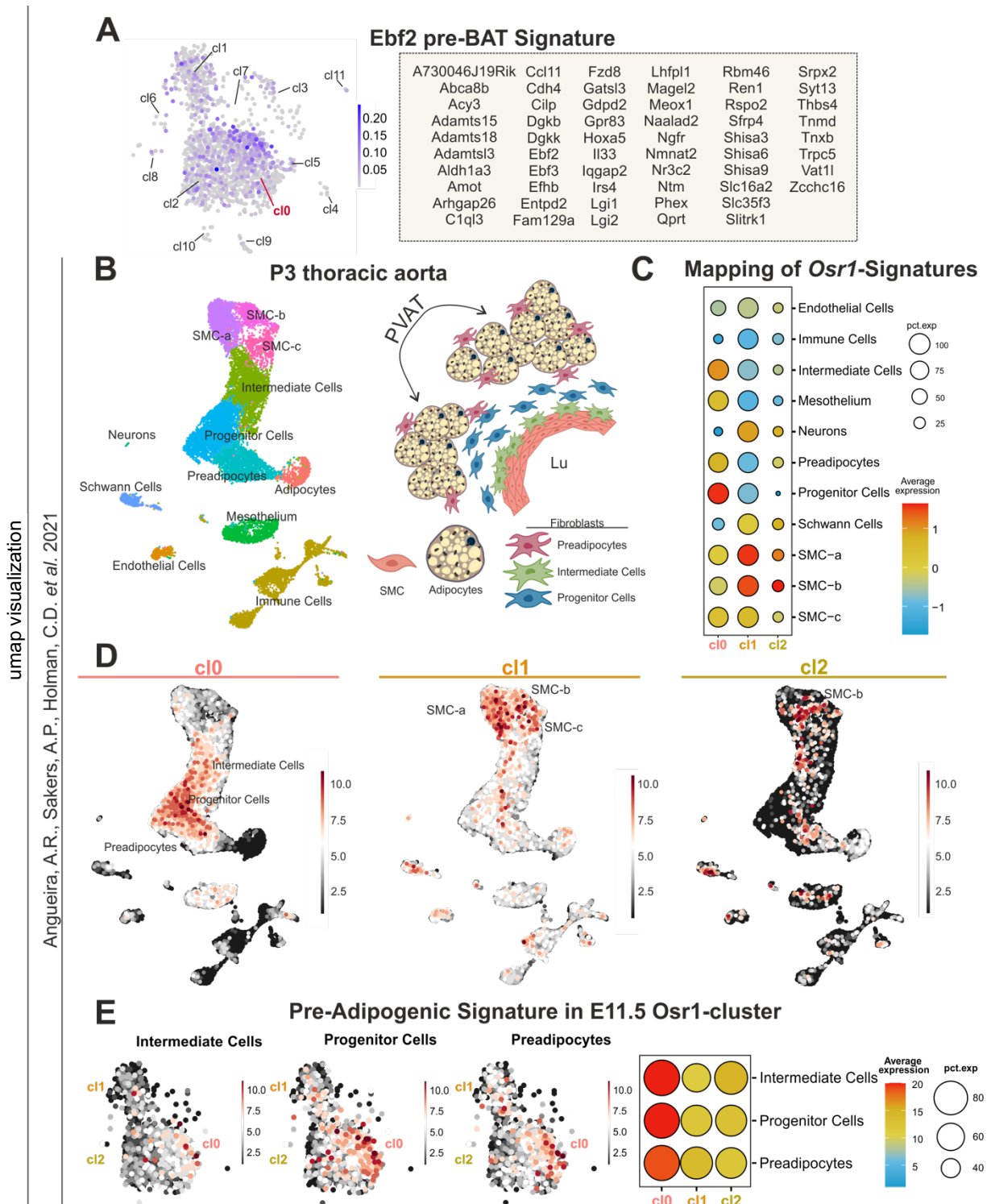
Figure 18: Identification of a pre-adipogenic signature in the Osr1+ scRNA-Seq dataset
A) shows a feature plot of the Osr1-object which highlights the overlap with the Ebf2 pre-BAT signature. An overview of a scRNA-Seq project on P3 thoracic aorta is displayed in B). The signature expression level of cl0, cl1 and cl2 from the Osr1-dataset is correlated with the P3 thoracic aorta project and represented in a dot plot in C). D) recapitulates the dot plot in C), highlighting the best fit of the three main Osr1 identities. In E) the signatures of most interesting cell types from P3 thoracic aorta-object were used to find the best match with the Osr1-main body.

4.1.4 Osr1+ cells colocalize with pre-adipogenic markers in distinct regions of an E11.5 embryo

Many studies have been focusing on the detection of new key markers that pinpoint the ultimate adipogenic progenitor pool during embryogenesis but have not been able to capture them *in vivo* as early as stage E11.5.

The E11.5 Osr1-scRNA-Seq dataset holds first evidence that a subpopulation of cl0 carries a pre-adipogenic identity. Combining published information of well-defined pre-adipogenic markers and the *Osr1* expression profile enabled one of the first visualizations of an initial pre-adipogenic cell pool. Since an Ebf2 pre-BAT signature has been used, it is pivotal to prove co-expression (Fig. 19). Immunolabeling (IF) for EBF2 and OSR1 on longitudinal Osr1$^{GCE/+}$ sections display co-expression in distinct regions. Section 1 displays a very lateral plane of the embryo which shows the OSR1 staining in green - marking the midline of the body. Although EBF2 seem to be expressed widely and especially in the periphery of the OSR1 labeled area -they do co-express in the very center of the embryo (Fig. 19.1A). A more medial plane of the embryo is shown in figure 19.2. Here, it becomes clear that co-labeling of both markers is detected in the surrounding tissue of the aorta or outflow tract of the heart (Fig. 19.2A). Further monitoring carried out that a small subset of cells in the dermomyotomal derivate (dmd) co-express OSR1 and EBF2 too (Fig. 19.2B). The scheme in figure 19B represents the expression pattern of the stained candidates. In summary, the analysis of IF supports that OSR1 and EBF2 co-express indeed in regions close to the heart and in the dermomyotomal derivates (dmd).
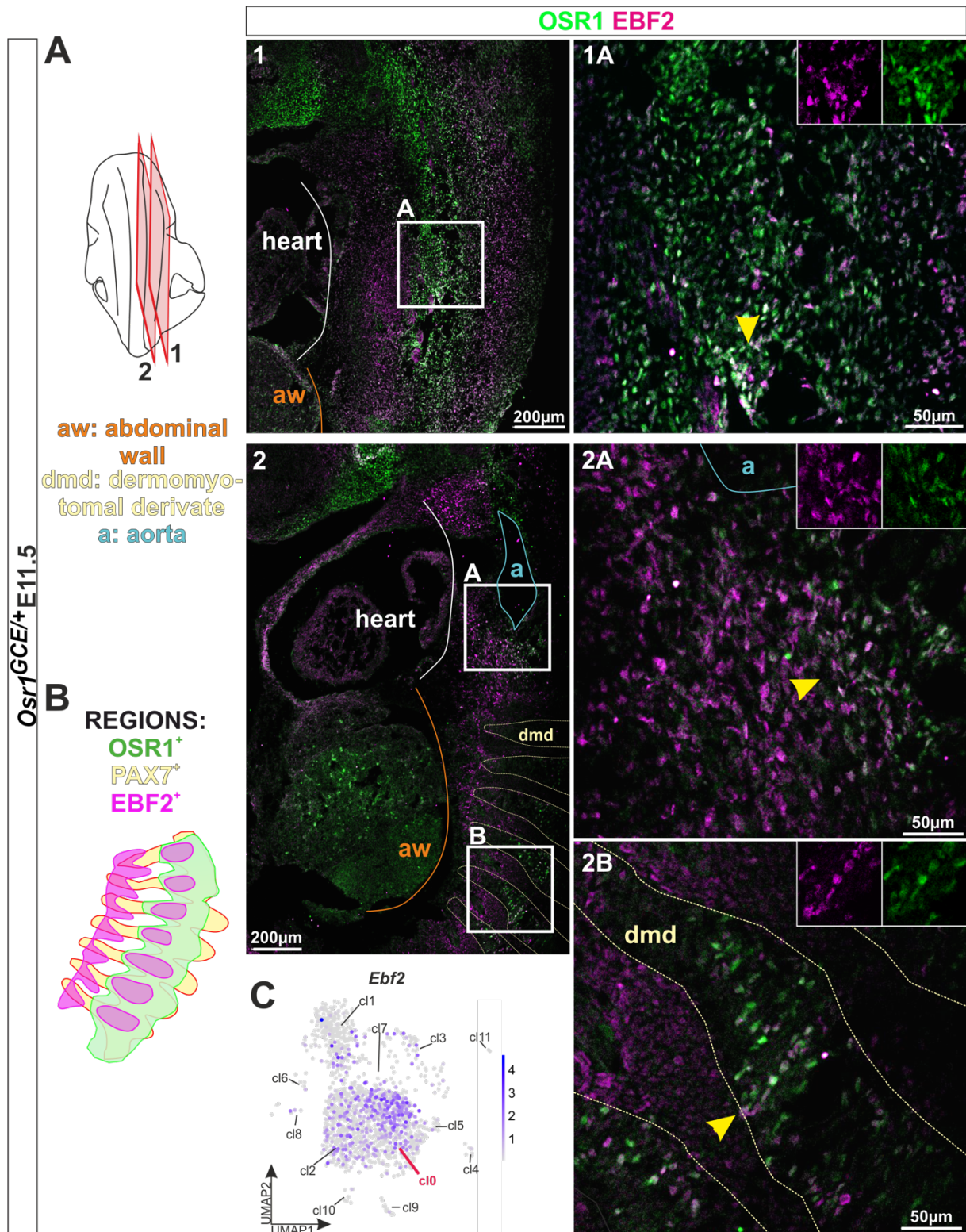
Figure 19: The pre-BAT marker *Ebf2* colocalizes with *Osr1* expressing cells
A) displays longitudinal sections of an E11.5 Osr1^GCE/+ embryo. An immunofluorescent staining for OSR1 in green and EBF2 in magenta was conducted. Section 1 represents a more lateral region than section 2. Yellow arrow heads in the closeups 1A, 2A and 2B point at the magnified inserts proving co-expression in the Osr1+ midline of 1A, in proximity to the aorta next to the heart (2A) and within the dmd region (2B). The schemata in B) illustrates a map of PAX7, OSR1 and EBF2 expression pattern at E11.5. A UMAP feature plot of the Osr1-dataset for *Ebf2* expression is shown in C).

Further validation was needed to prove the identified location of the early pre-adipogenic cell pool. Another well-known marker for pre-adipogenic progenitors in the embryo is Dlk1- also known as Pref1 (Hudak et al., 2014, Nueda et al., 2007). Investigations of the same regions has been done to test whether Dlk1+ cells gather in the same region as Ebf2+ cells (Fig. 20A). The magnified regions in figure 20.1A-1D and 20.2A-2D presents the expression pattern of DLK1, which is quite similar to the EBF2 expression, depicted in figure 19. The most interesting differences are depicted in figure 20.2A-2D: here, DLK1+ cells cluster in proximity to the abdominal wall which express OSR1-GFP too. In contrast, DLK1+ was not observed in the PAX7+ dmd as EBF2 showed. These findings indicate that there are two different anatomical locations that hold adipogenic progenitors: first the dmd and second the space around the abdominal wall (Fig. 19.2B and 20A.2). However, *Dlk1* is highly enriched similar to *Ebf2* in cl0 of the Osr1-object (Fig. 19C, 20C).
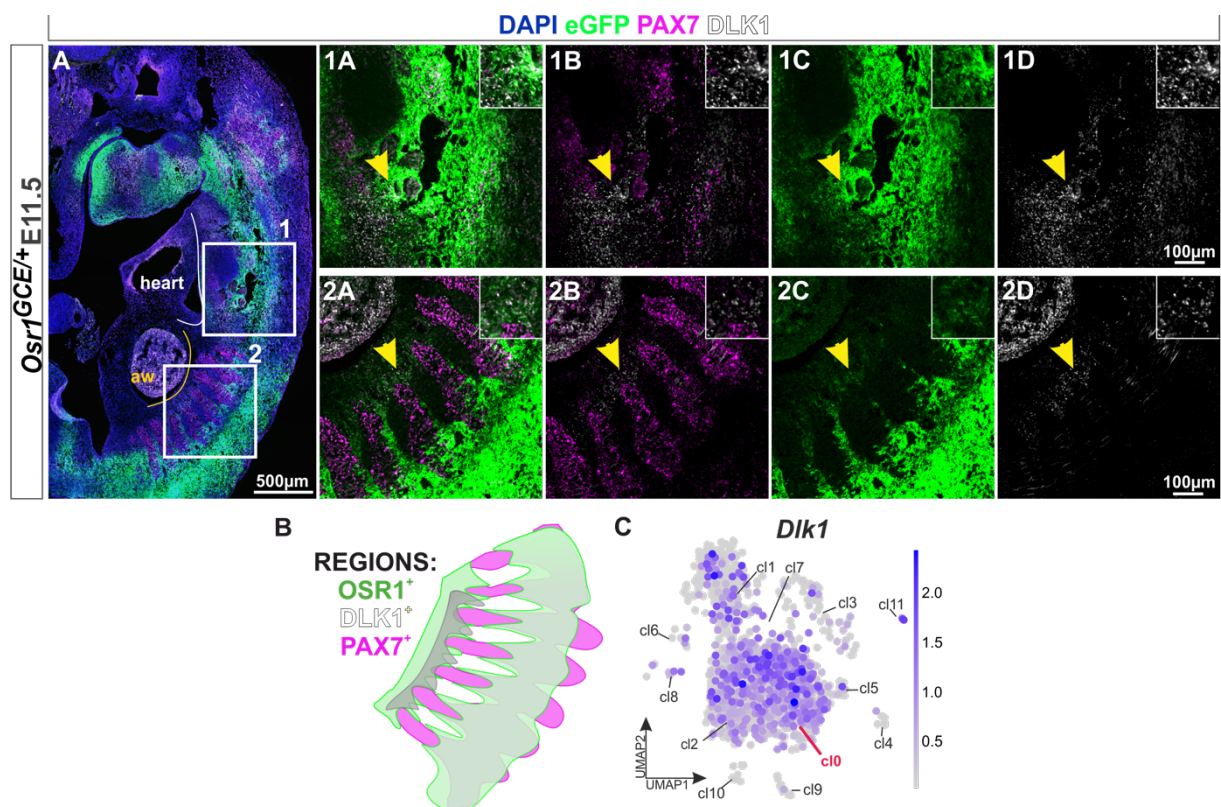
Figure 20: *Dlk1* and *Osr1* co-express in proximity of the heart and along the abdomen
An immunostaining for GFP in green (OSR1), DLK1 in white and PAX7 in magenta is shown on an Osr1[GCE/+] embryo. The overview-section in A) presents the areas of interest. In both regions 1 and 2 co-expression of DLK1 and OSR1 was detected. Yellow arrowheads in 1A-D and 2A-D point to double positive cells that are magnified once again and highlighted in respective inserts. B) presents a schematic summary of the investigated expression patterns of OSR1, PAX7 and DLK1. The *Osr1* single cell dataset in C) displays high expression of *Dlk*1 in cl0.

4.1.4.1 Osr1+ cells at E11.5 mark a small subpopulation of the dermomyotomal derivate

Since PAX7+ cells were identified as a source of brown adipogenic progenitors (Lepper and Fan, 2010) the overlap and co-expression pattern of PAX7 and Osr1 was studied. The PAX7+ cells define the dmd region that expands along the dorsal to ventral axis. Strikingly, OSR1-GFP staining is observed in a subset of PAX7+ cells which locate in the midline of the PAX7 dmd stream (Fig. 212A-C). To date, it has nerve shown that a small pool of OSR1+ PAX7+ cells exist. Most likely the subpopulation of OSR1+PAX7+ cells could represent the same cell pool identified in figure 19.2B co-expressing EBF2.
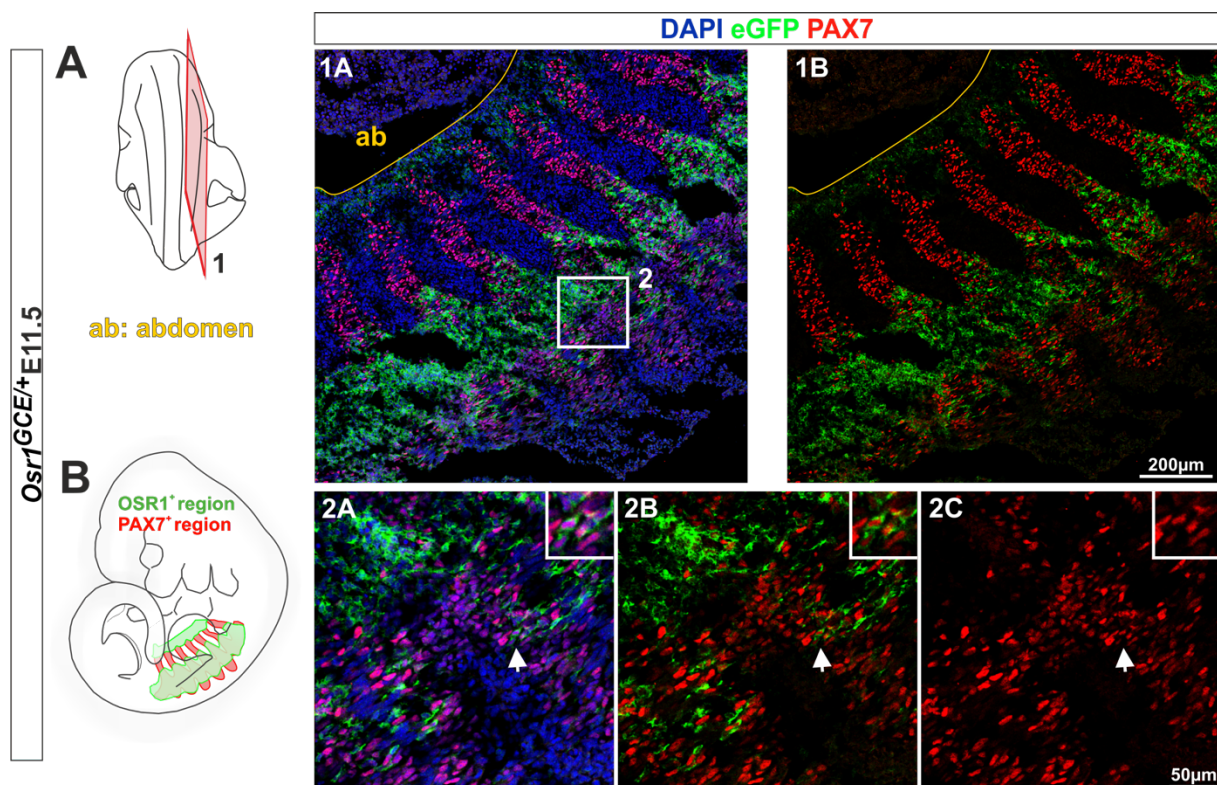
Figure 21: OSR1+ cells in the dermomyotomal derivate
A) a co-staining of GFP in green (OSR1) and PAX7 in red was performed on longitudinal sections of an E11.5 Osr1$^{GCE/+}$ embryo. The overview images 1A-B demonstrate distinct expression patterns of both proteins. OSR1-GFP labels the midline along the cranial to caudal axis and PAX7 marks the dermomyotomal derivate which propagates from the ventral to dorsal part of the embryonic body. The indicated area 2 magnifies the overlapping space of PAX7 and OSR1. The white arrows specify cells that express both markers. The schematic overview of the PAX7- and OSR1- expression pattern is depicted in B).

Another observation was that the tips of the dermomyotomal derivates end in a pool of OSR1-GFP+ cells that do not show co-expression with PAX7, which indicate that the OSR1-GFP+ cell pool near the peritoneum has different capacities than those cells

that co-express PAX7. To test whether the two OSR1 marked compartments hold different pre-adipogenic potentials, a staining for PPARγ was conducted.

Finally, the expression profile of the key marker of adipogenesis PPARγ was investigated (Rosen et al., 2002). So far, the very early pattering of PPARγ during embryogenesis has only been shown a few times as whole mounts using a GFP-Reporter of the AdipoTrak mouse model (Jiang et al., 2014). Unfortunately, the published data do not provide many details. Here, figure 22 presents the distribution profile of PPARγ cells on a new level at E11.5.
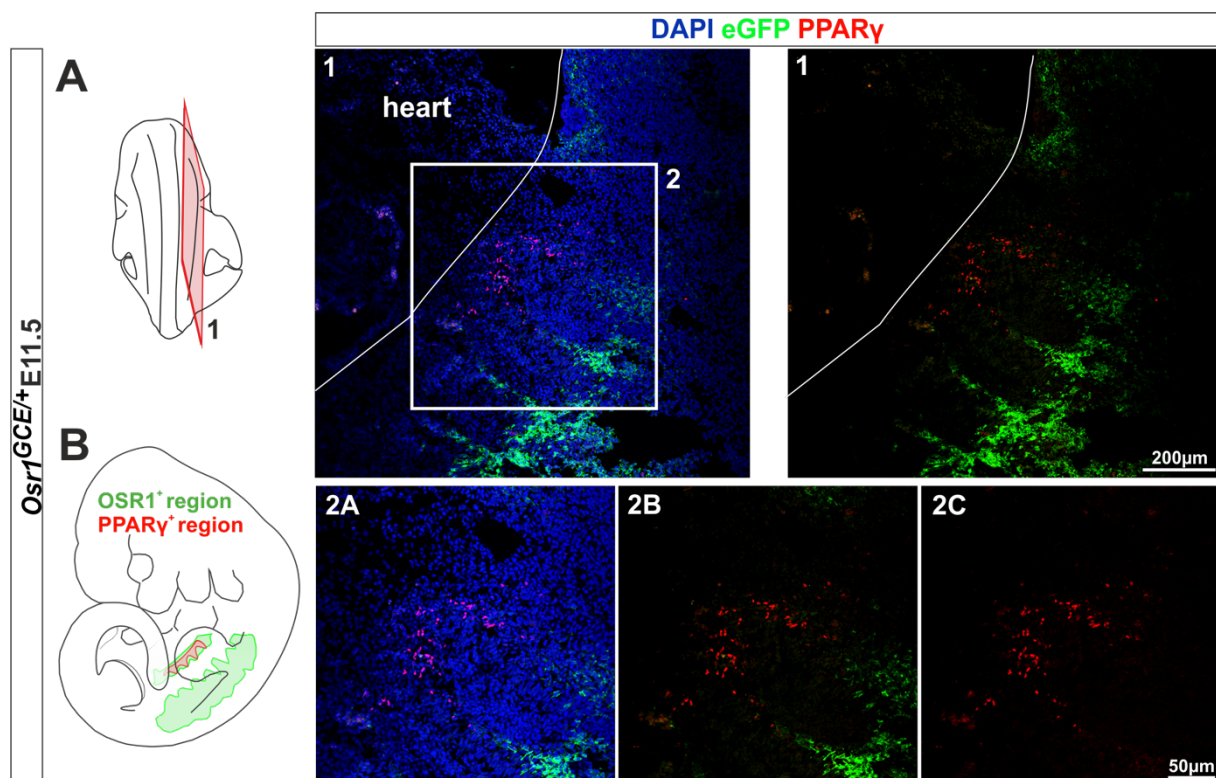
Figure 22: First observed PPARγ+ cells cluster near the embryonic heart
A co-immunostaining on E11.5 Osr1[GCE/+] longitudinal sections in A) demonstrates the first detectable PPARγ+ (red) cell pool near the heart. The Osr1-GFP is labeled in green and recapitulates the same patterning that is found in the area where PAX7^{+} cells would be expected. B) simplifies the distribution map of OSR1-GFP and PPARγ.

The images in figure 22A demonstrate that the PPARγ cells cluster near the heart, close to the ventral tips of the dmd. OSR1 in green, labels the midline of the dmd compartment in the embryo that most likely overlaps with the PAX7+ cells, as observed in figure 21.

To fully understand the distribution profile and overlap of PPARγ, PAX7 and OSR1 regions cross section were studied. Figure 23 clearly demonstrates that PAX7+ and OSR1+ cells at E11.5 merge in two region of the dermomyotome (Fig. 23.1 and 23.2).
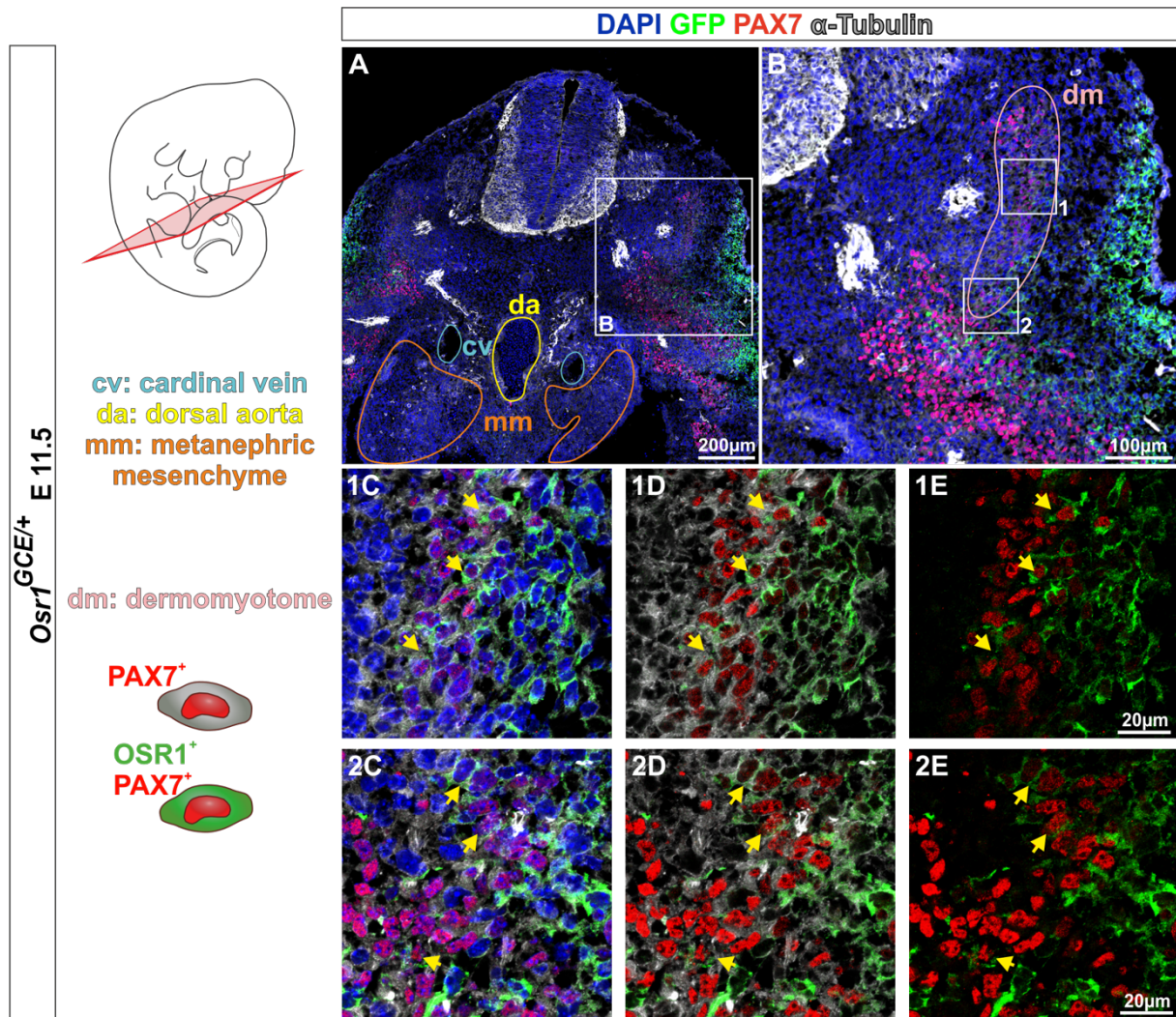
Figure 23: PAX7+ and OSR1+ cells merge only in distinct zones of the dermomyotome
Cross sections of an E11.5 Osr1$^{GCE/+}$ embryo highlight PAX7 in red, OSR1-GFP in green and α-TUBULIN in grey. A) and B) provide an overview of the expression pattern of PAX7 and OSR1. B) specifies two regions (1-2) of the dermomyotome where both markers colocalize. The yellow arrows mark co-expression in the central part (1C-1E) and in the hypaxial (2C-2E) dermomyotome.

A graphical scheme in figure 24A simplifies the OSR1 expression pattern within the dermomyotome summarizing that OSR1 was detected only in the central part and ventral tip. The UMAP-feature blot of the Osr1-scRNA-Seq in figure 24B validated that a few cells express *Pax7* in cl0 and cl2 which goes in line with the fact that cl0 harbors pre-adipogenic progenitors.
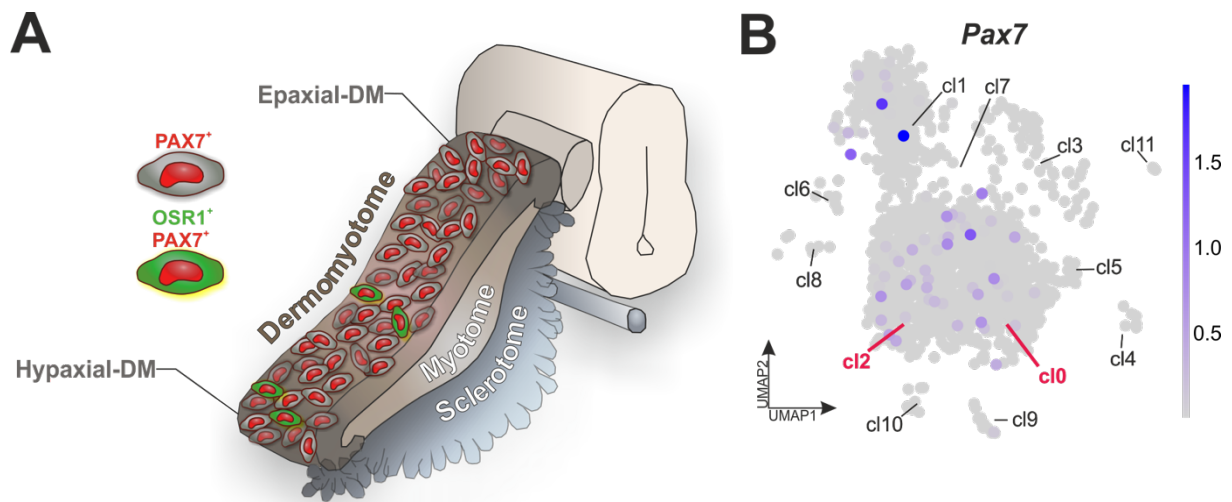
Figure 24: Schematic representation – distribution of OSR1+ cells in the dermomyotome
The graphic in A) demonstrates the somites which divides into the sclerotome, myotome and dermomyotome. The latter is rich in *Pax7* positive cells. Only a few cells of the dermomyotome-exclusively those in the central and the hypaxial lip show *Osr1* expression. A UMAP-feature plot of *Pax7* in B) demonstrates that there are once again very few Osr1 cells that are *Pax7* positive but manly cluster in cl0 and cl2.

Cross sections of an embryo at stage E11.5 gave a more detailed picture of how the organization of OSR1, PPARγ and PAX7 looks like. Figure 25.1A-1C and 25.2A-2C clearly show several PPARγ+ OSR1+ cells that arrange themselves along the abdominal wall. PAX7+ cells on the other hand, do not combine with the PPARγ+ population, concluding that they represent two distinct populations with different characteristics: adipogenic *vs*. myogenic. OSR1 instead is detected in both the myogenic and adipogenic cell population. That implicates that OSR1 might has different functions – for example: PAX7+ cells are more prone to become myogenic, but a myogenic contribution has never been reported of the E11.5 Osr1-lineage (Vallecillo-Garcia et al., 2017). Here, one could assume that Osr1 reprograms the PAX7 cell to become a pre-adipogenic progenitor. *Osr1* expression in the PPARγ+ cell instead, might rather support the pre-adipogenic state to allow further proliferation, migration and a gradual specification process throughout development.
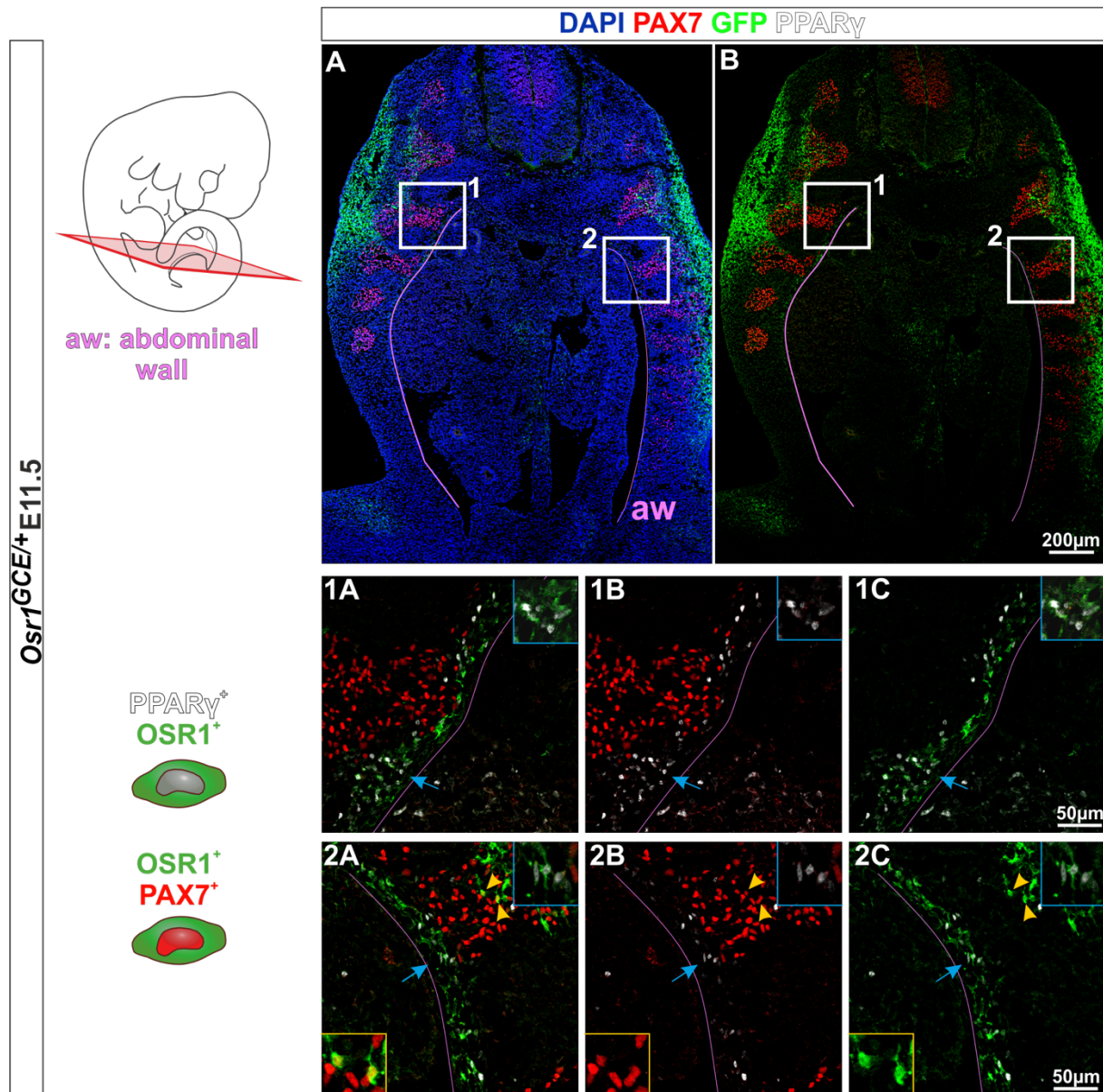
Figure 25: OSR1 positive PPARγ cells reside along the abdominal wall
A cross section from an E11.5 Osr1[GCE/+] embryo displays a staining for PAX7 (red); OSR1-GFP (green) and PPARγ (white). A) and B) give an overview of the expression patterns and tissue context. The two highlighted areas (1A-1C and 2A-C) convey the distribution of all three markers at the same time. Blue arrows point at OSR1+ PPARγ+ positive cells detected along the abdominal wall. The colocalization of PAX7 and OSR1 is marked with yellow arrowheads. Interestingly, the distance between the OSR1+PAX7+ cells and the OSR1+PPARγ+ cell pool appears to be small. Co-stainings of PAX7 and PPARγ were not observed.

In summary, a computational approach highlighted cl0 with mesenchymal stromal cell identity as the candidate that holds highest pre-adipogenic potential of the Osr1-single cell-object. The application of traditional methods enabled the visualization of well-known pre-adipogenic markers like EBF2, DLK1, PAX7 and PPARγ in E11.5 OSR1 expressing cells. Once again, all investigated markers are clearly enriched in cl0.

The graphical overview in figure 26 demonstrates that OSR1 and PPARγ co-express in the ventral part of the embryo. Figure 20 shows that DLK1+ cells reside in the same

region – specifying the early pre-adipogenic cell pool. Furthermore, the co-expression of PAX7 and OSR1 is observed in the midline of the dmd region (Fig. 21; 23 and 26). EBF2 and OSR1 also display colocalization in the same region and might label a common myogenic-to-adipogenic progenitor.
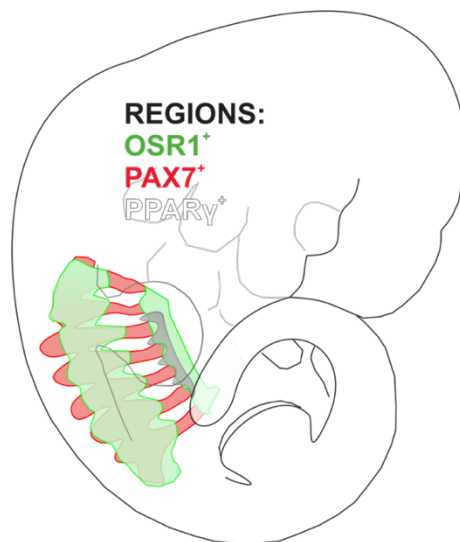
Figure 26: Graphical summary of the OSR1, PAX7 and PPARγ expression analysis
The lateral view on an E11.5 embryo shows the expression map of PAX7 in red that is recapitulating the dermomyotomal derivate. The OSR1 expression profile is depicted in green and overlaps with the center of the PAX7+ region where the forelimb buds. Apart from that, the PAX7 extensions culminate ventrally in the OSR1+ region along the peritoneum which overlap with the initial PPARγ population (grey).

According to these findings it can be concluded that a Osr1 marks pre-adipogenic progenitor cells in the lateral region along the dorsal to ventral axis.

A further question to be addressed is to elucidate what might drive the adipogenic fate commitment during embryogenesis?

4.1.5 Active BMP signaling is observed in Osr1+ cells around the vasculature in the area of early brown adipose tissue

It has been described that BMPs are required to develop brown adipose tissue through embryogenesis. Especially studies on BMP7 provided evidence that BMP signaling is involved in the fate determination process between the myogenic and adipogenic identity (Tseng et al., 2008, Schulz et al., 2011, Schulz et al., 2013). Thus, investigations of active BMP signaling *via* the pSMAD1/5/8 mark was performed to detect its localization in the early BAT anlagen of embryonic stage E12.5 and E13.5 (Fig. 27). Widespread pSMAD1/5/8 signal-positive cells were found in the neural system and in the early muscle masses where co-expression with PAX7 and MyHC can be seen (Fig. 27.1D; 27.3D). Importantly, in the early developing BAT anlage, sparse pSMAD1/5/8 labeled cells were observed arranged around the vasculature

(Fig. 27.1C, 2C, 3C, 4C). That finding is interesting since it is reported that the vasculature is a known source of BMPs and thus possibly act as signaling centers in the BAT anlage (Saito and Takahashi, 2015, Katagiri and Watabe, 2016).
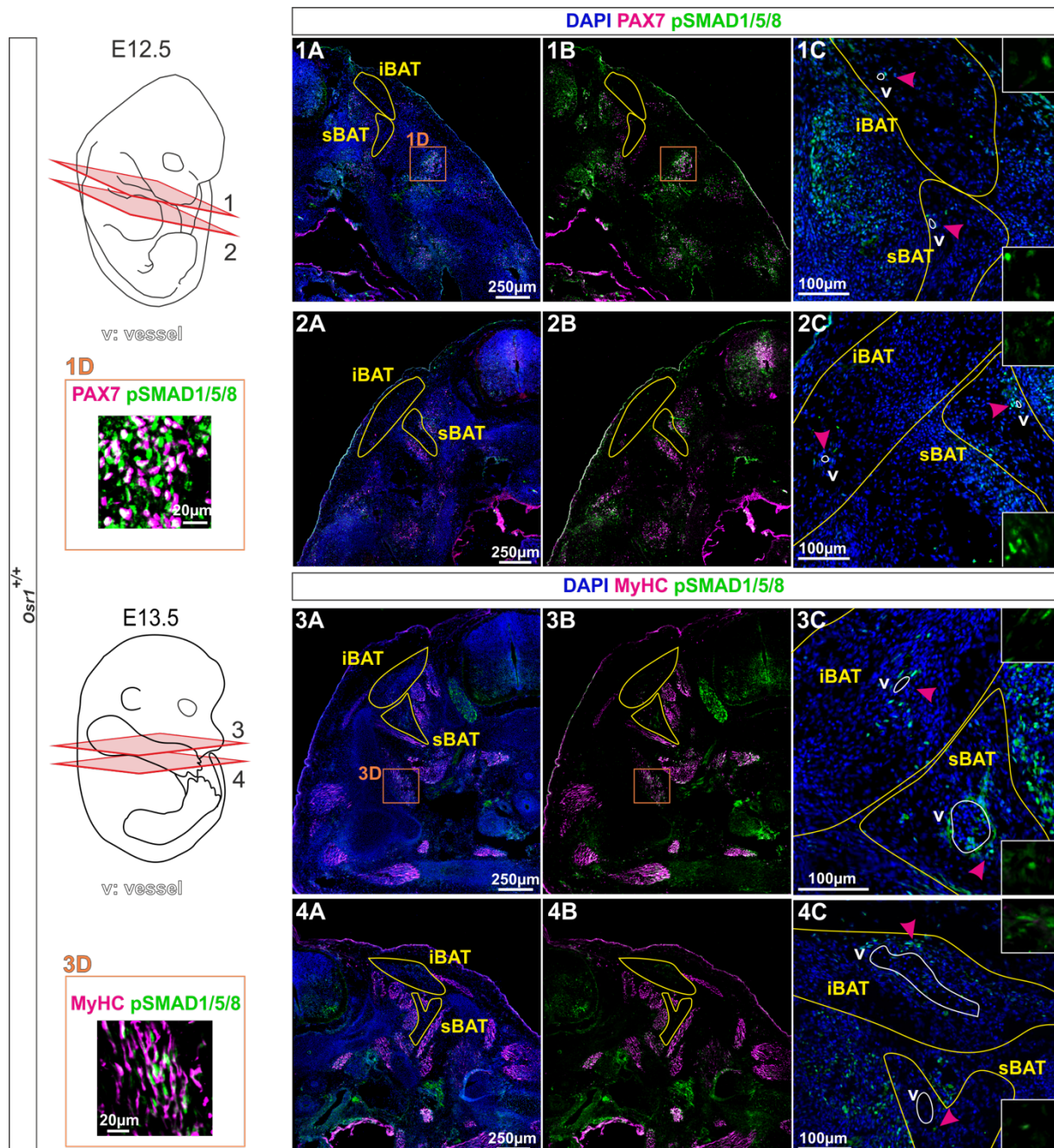
Figure 27: pSMAD1/5/8+ cells localize around the early BAT vasculature
1A-2C) shows IF stainings for PAX7 in magenta and pSMAD1/5/8 in green on two different sections of an embryo at E12.5. 1A-1B) and 2A-2B) provide an overview of the anatomical location of the early BAT anlage. 3A-4C) displays IFs from MyHC in magenta and pSMAD1/5/8 in green on two different sections of an embryo at E13.5. The overview images in 3A-3B) and 4A-4B) allocate tissue context. 1C, 2C, 3C and 4C present closeups from the iBAT and sBAT. Violet arrowheads point at vessels that show a pSMAD1/5/8+ signal in proximity. 1D and 3D demonstrate that pSMAD1/5/8 is enriched in myogenic cells as co-localization with Pax7 and MyHC expression was found (orange square). iBAT: interscapular brown adipose tissue; sBAT: subscapular brown adipose tissue

This study has already proved that Osr1+ cells label a PPARγ+ pre-adipogenic progenitor pool at E11.5 but is not yet clarified how the Osr1 expression is controlled to drive adipose tissue development?

4.1.5.1 BMP molecules modulate *Osr1* expression

The previous observations raise the question, whether Osr1+ is regulated through bone morphogenic protein (BMP) signaling to mediate BAT development? To test that, a brown pre-adipogenic cell line "Wt1" was used to investigate the expression levels of *Osr1* after BMP treatment (Tseng et al., 2005, Tseng et al., 2004). Different BMP molecules were tested to identify whether Osr1 specifically responds to one or rather follows a general expression pattern upon BMP stimuli. First BMP2 was used, which is known to signal through receptor BMPR-IA and BMPR-IB to promote bone formation (ten Dijke et al., 1994, Miyazono et al., 2010, Lin et al., 2019). Figure 28 presents that *Osr1* expression has almost doubled after 24h treatment with 5nM BMP2 and reaches even higher levels after 48h compared to its respective controls. Apart from that, a lower concentration of BMP2 could not significantly recapitulate the effect due to high inter-experimental variability.
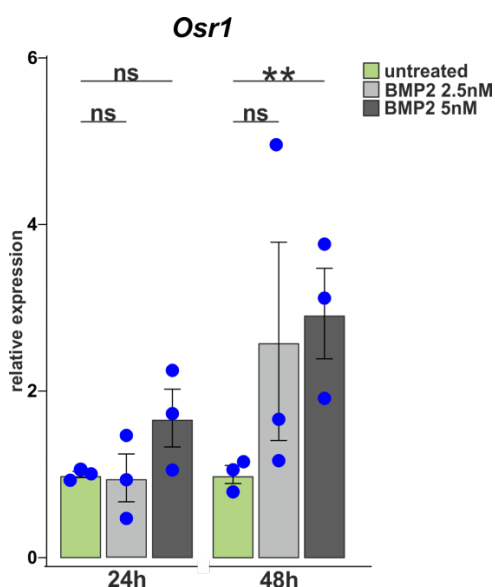
Figure 28: BMP2 titration modulates *Osr1* expression *Osr1* expression levels were measured *via* RT-qPCR on undifferentiated Wt1 cells. Cells were starved for 3hs and cultured with BMP2 2,5nM (light grey) or 5nM (dark grey) for 24hs and 48hs. The control group (green) was starved but not treated with BMP. Relative expression of *Osr1* is slightly upregulated after 24hs and significantly upregulated after 48hs upon a 5nM BMP2 treatment. The lower BMP2 concentration showed no statistically significant *Osr1* upregulation. Data are presented as mean ± SEM (n = 3); statistical analysis was done using two-tailed Student's t tests: * $p<0.05$, ** $p<0.001$.

Interestingly, the experiments with BMP7 showed something different (Fig. 29). A 1,5nM BMP7 treatment demonstrated a significant enrichment of *Osr1* transcripts after the first 3h only (Fig. 29A). However, using 8nM BMP7 instead of 1,5nM demonstrated the opposite results. The expression level of *Osr1* was notably higher after 48h and 72h compared to 3h and 24h (Fig. 29B). In summary, it can be seen that BMPs regulate

Osr1 expression to a certain extent. This suggests that dependent on the BMP type and its local concentration, the expression of *Osr1* can be titrated.
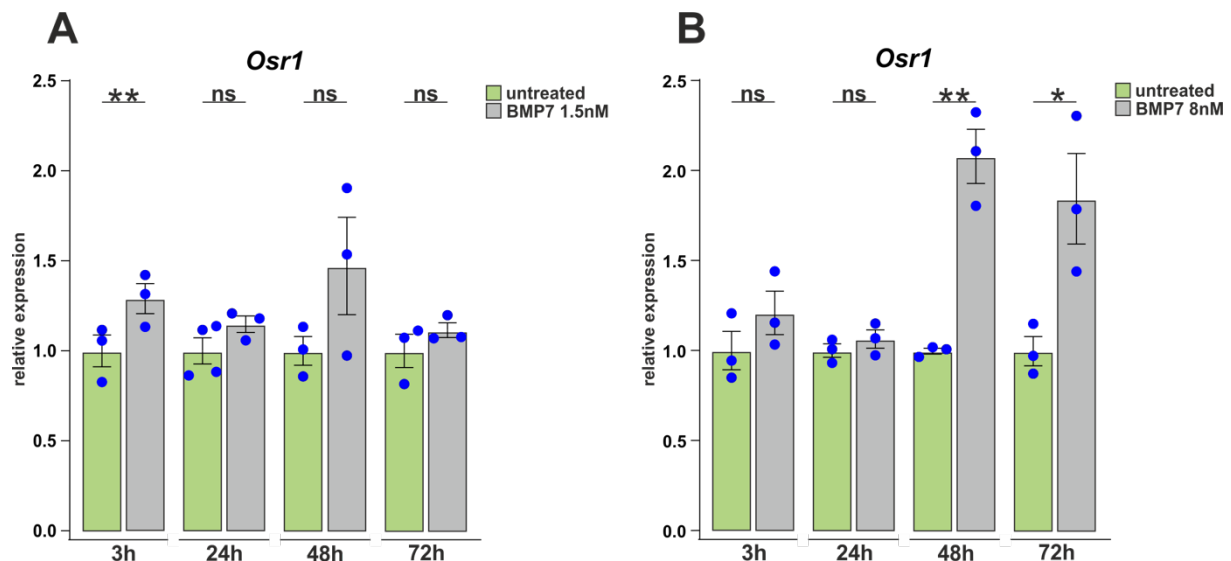
Figure 29: Different BMP7 concentrations affect the time-course of *Osr1* expression
Osr1 expression levels were measured *via* RT-qPCR on undifferentiated Wt1 cells. Cells were starved for 3h and cultured with BMP7 (light grey) for 3hs, 24hs, 48hs and 72hs. The control group (green) was starved but not treated with BMP. A) Relative expression of *Osr1* is significantly upregulated after 3hs of BMP7 1.5nM treatment compared to its respective controls. The following timepoints do not demonstrate notable changes. B) 8nM of BMP7 present a different time course of *Osr1* expression. With higher BMP7 concentration significantly higher *Osr1* levels were recognized at 48hs and 72hs. Data are presented as mean ± SEM (n = 3); statistical analysis was done using two-tailed Student's t tests: * $p<0.05$, **$p<0.001$.

Next it remained to be clarified whether BMP-downstream targets are detected in the Osr1-scRNA-dataset. Figure 30 visualizes the UMAP-feature-plots for *Id1*, *Id2* and *Id3* which clearly demonstrate active BMP signaling in the Osr1+ cell pool of stage E11.5.
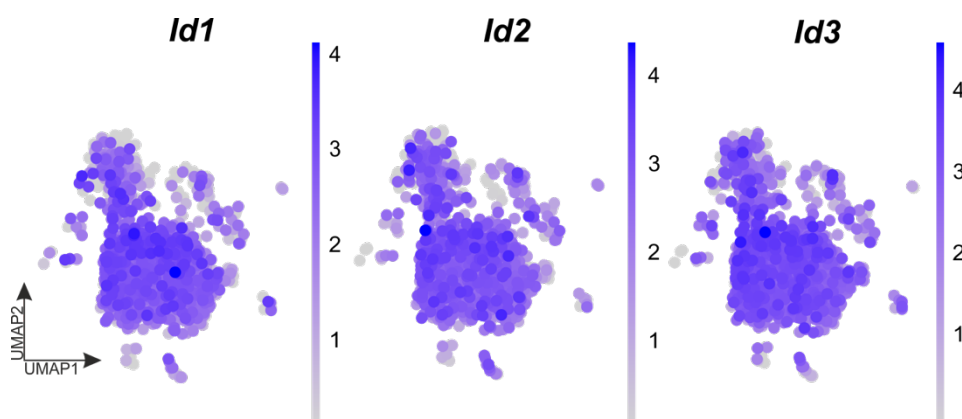
Figure 30: Osr1+ cells at E11.5 are high in expression of BMP downstream targets
Here, three different downstream targets of BMPs - *Id1*, *Id2* and *Id3* - are tested for their expression levels in the Osr1-scRNA-object. The feature-plots highlight that the Ids are well expressed in the entire dataset. Demonstrating that the Osr1+ cells respond to BMP molecules.

The only missing information here is the distribution profile of pSMAD1/5/8 labeled cells at stage E11.5. This is required to understand if the Osr1+ pre-adipogenic progenitor cell pool colocalizes with the BMP activated once. To approach that immunofluorescent stainings for OSR1, myogenic markers and pSMAD1/5/8 were performed on cross sections (Fig. 31, 32). Since both pSMAD1/5/8 and Osr1 antibodies were produced in the same host a co-immunostaining was not possible. However, pSMAD1/5/8 expressing cells were manly observed around the dorsal aorta. Only here, a spatial overlap of OSR1 and pSMAD1/5/8 was detected (Fig. 31.1A-4B; Fig. 32.3A-3B). In dmd regions, pSMAD1/5/8 signals were exclusively detected in the early myotubes, but not in Osr1+ cells (Fig. 32.1A-2C).
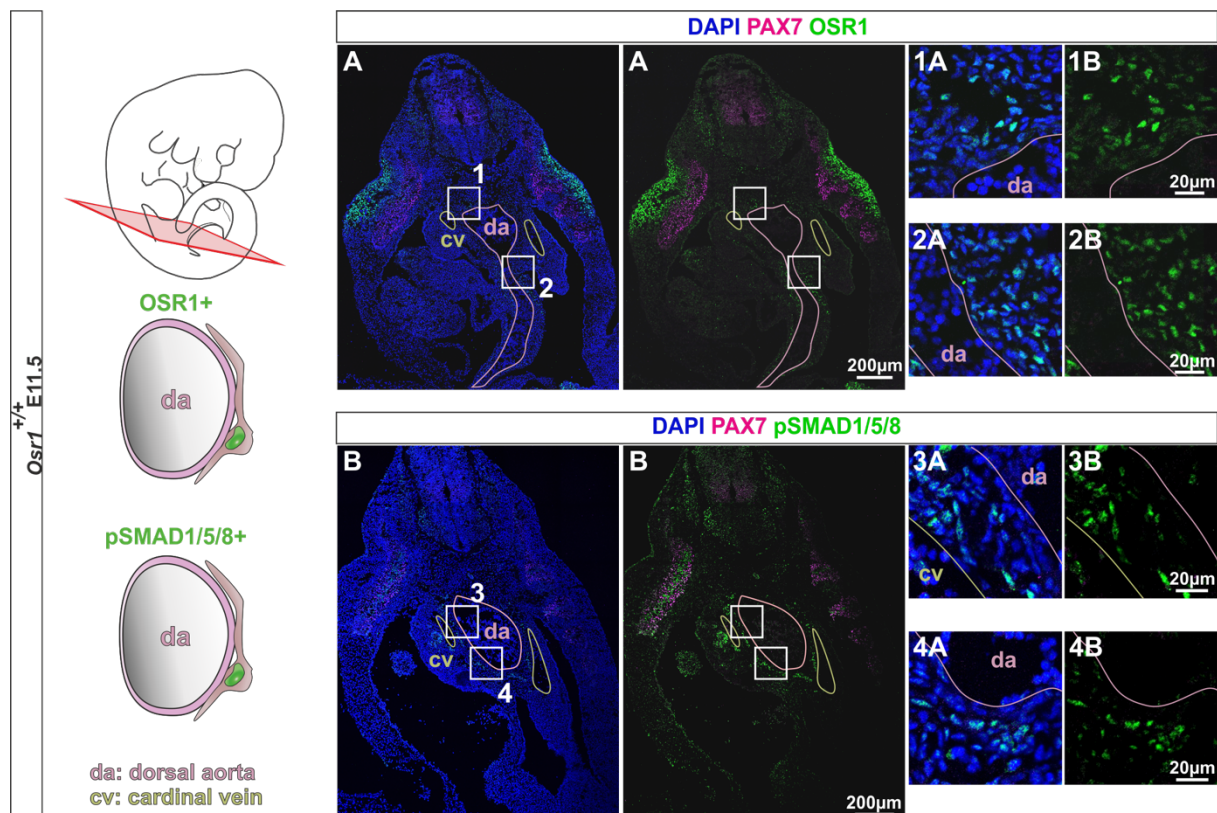
Figure 31: OSR1+ and pSMAD1/5/8+ cells reside along the dorsal aorta at E11.5
Immunostainings for PAX7 (magenta) and OSR1 (green) are displayed in A.1A-2B. A) represents an overview image with the dorsal aorta in its center. Indicated regions in A.1 and A.2 are magnified on the right side. The closeups capture that OSR1+ cells arrange along the dorsal aorta (1A-1B). B) shows an IF for pSMAD1/5/8 (green) and PAX7 (magenta) on a similar section to A. Indicated regions in B.1 and B.2 are magnified on the right side. The closeups in 3A-4B) almost recapitulat the expression pattern of OSR1 in the dorsal aorta compartment. Considering the distribution pattern from OSR1 and pSMAD1/5/8, it is very likely that both markers merge in the dorsal aorta region. da: dorsal aorta; cv: cardinal vein
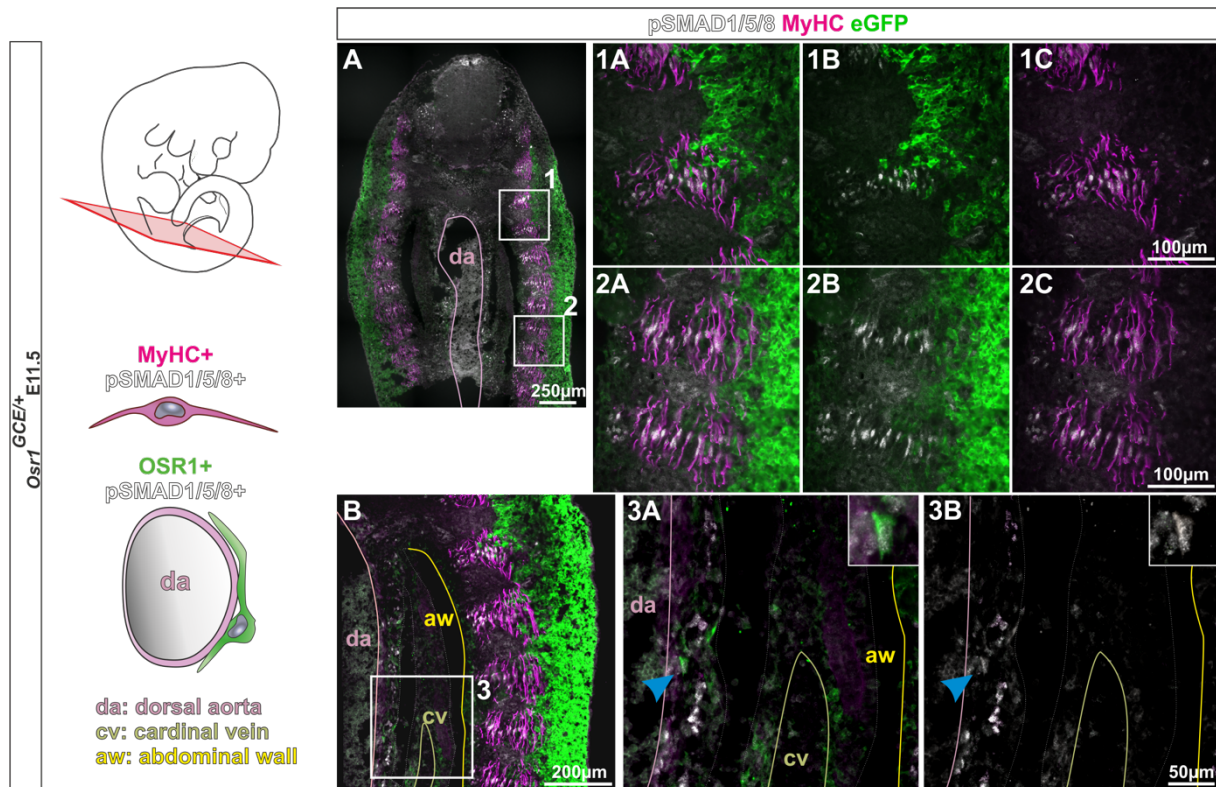
Figure 32: At E11.5 the dorsal aorta compartment holds BMP activated OSR1+ cells
The IF for pSMAD1/5/8 (white), MyHC (magenta), OSR1-GFP (green) was performed on E11.5 Osr1$^{GCE/+}$ embryos. In A) an overview image shows the distribution pattern of all markers. The indicated regions A.1) and A.2) are magnified in 1A-2C. The closeups display that most of the pSMAD1/5/8 labled cells are detected in the MyHC positive myotubes. No colocalization of GFP and pSMAD1/5/8 was obsereved in the dmd region. B) represents the dorsal aorta compartment. The magnified region 3A-3B) demonstrate that both - GFP and pSMAD1/5/8 – are recognized in the the same cell (blue arrowhead).

4.1.6 BMP signaling is not involved in the process of very early pre-adipogenic progenitor specification

Finally, a PPARγ staining was performed to test whether early PPARγ+ cells show BMP/pSMAD1/5/8 signaling. Cross sections were investigated where PAX7+ cells almost touch the abdominal wall, where (as shown above) the first PPARγ+ cells arise (Fig. 33A). The staining for pSMAD1/5/8 in figure 33.1A-1C labeled cells that intermingle with the PAX7+ cells. In this region just very few OSR1+ cells show pSMAD1/5/8 expression. The same was observed for the PAX7+ population. In figure 33.2A-2C, PPARγ+ cells were detected more closely to the peritoneum instead of mixing with the PAX7 cell pool. Co-expression of PPARγ and pSMAD1/5/8 was not detectable. However, OSR1 could be observed colocalizing with all three markers.
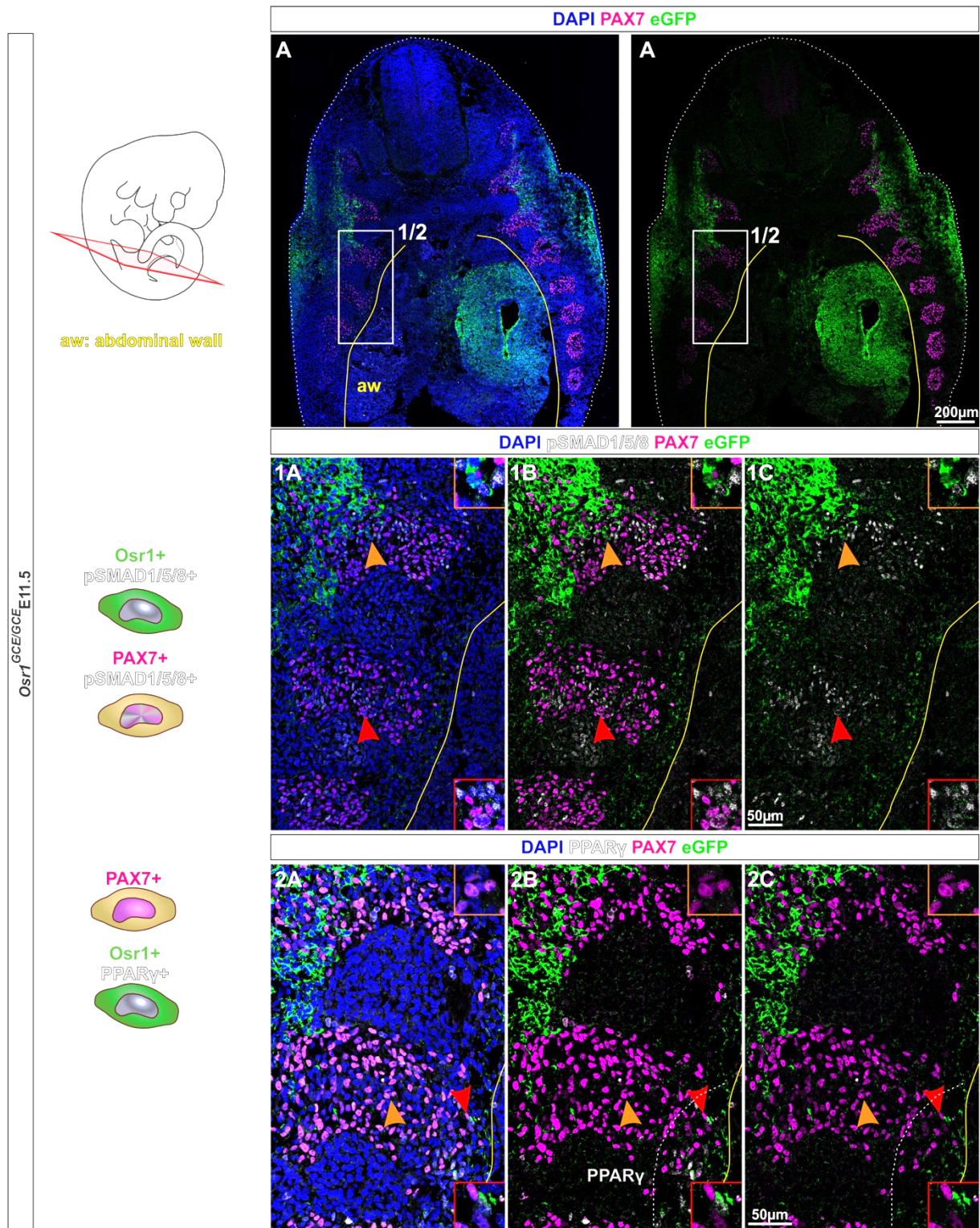
Figure 33: The PPARγ labeled cells are pSMAD1/5/8 negative at E11.5
A) presents an overview of an IF staining for PAX7 (magenta), OSR1-GFP (green) on E11.5 Osr1$^{GCE/+}$ embryos. The specified area A1/2) was investigated on adjacent sections more closely for pSMAD1/5/8 (white) expression pattern 1A-1C. The red arrowhead points at cells that show co-expression for PAX7 and pSMAD1/5/8. A orange arrowhead highlights cells that express pSMAD1/5/8 and GFP. The same investigations have been performed with a PPARγ (white) co-immunolableing (2A-2C). PPARγ was not detected in the center of the PAX7+ cell pool (orange arrowhead), which was the opposite for pSMAD1/5/8. However, GFP expression was observed in the PPARγ+ cells close to the abdominal wall (red arrowhead). PPARγ+ cells reside in the indicated region (white dashed line). No pSMAD1/5/8+ cells were observed in this region (1A-C).

The expression profile of pSMAD1/5/8, OSR1, PAX7 and PPARγ is simplified in the graphical summary in figure 34, focusing once again on the lateral view of an E11.5 embryo. The graphic highlights that pSMAD1/5/8 mixes with dermomyotomal derivate but is not recognized in the same region with PPARγ. Within the dmd, active BMP/pSMAD1/5/8 signaling was detected predominantly in nascent myotubes.
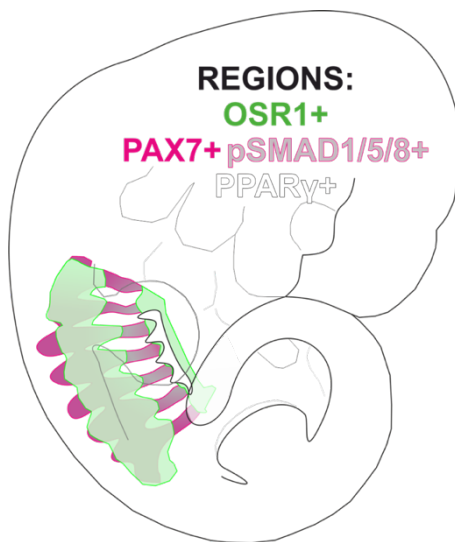
Figure 34: Graphical summary: BMP activated cells map with the myogenic but not adipogenic cell pool
A lateral view of an E11.5 embryo map displays the expression profile of PAX7, pSMAD1/5/8, OSR1 and PPARγ. The graphic summarizes that BMP activated cells mix with PAX7 cells but mostly express MyHC (not shown here). PPARγ only overlaps with the OSR1+ region but not with the PAX7-pSMAD1/5/8 zone. Thus, the OSR1-PPARγ cell pool is clearly separated from the myogenic party.

It can be concluded that BMP signaling in the Osr1+ cell pool of E11.5 occurs but it is not clear that BMP signaling is involved in the very first steps of adipogenic fate commitment.

4.2 The Osr1 lineage is a source of individual adipogenic progenitor populations of the developing adipose tissue

4.2.1 Inducible genetic lineage tracing of the E11.5 Osr1+ population confirms adipogenic contribution

The Osr1 single cell RNA-Seq dataset from E11.5 embryos gave evidence that cells of mesenchymal stromal cell identity (cl0) harbor pre-adipogenic progenitor potential. Furthermore, immunolabeling *in vivo* proved that E11.5 OSR1+ cells express pre-adipogenic progenitor markers like PAX7, EBF2, DLK1 and PPARγ. These findings indicate that the Osr1 cell pool at E11.5 may contribute to adipose tissue development. To test this, an inducible Cre-loxP based lineage tracing approach was chosen using

the Osr1$^{CreERt2/+}$;ROSA$^{mTmG/+}$ mouse model. Cre recombinase expression is controlled by the Osr1 promoter. At a desired timepoint, Cre translocation into the nucleus was induced by tamoxifen administration. The Cre enzyme recognizes loxP sites in the ROSA locus which flank the membrane Tomato (mT) gene and a transcriptional stop signal. After recombination, the mT sequence as well as the stop signal is removed which results in membrane GFP (mGFP) transcription in *Osr1+* cells and its descendants exclusively.

The Osr1 progeny that have been labelled by a TAM pulse at E11.5, were traced until stage E18.5 to investigate the adipose tissue, which is anatomically apparent at this stage (Fig. 35). The chased Osr1 descendants are, as mentioned above, marked by recombination-mediated expression of mGFP. FABP4 was used to label and identify mature adipocytes. Figure 35 introduces that the E11.5 Osr1-lineage contributes to cBAT, sBAT and latBAT (upper panel) and to axiWAT, subWAT (lower-panel). The only exception is the interscapular brown adipose tissue (iBAT) (lower panel), which displays very few mGFP cells. This suggests that the iBAT recruits a different source than the Osr1+ progenitors.

Figure 35: E9.5 and E11.5 Osr1 progeny contribute to adipose tissue (next page)
Inducible lineage tracing experiments starting from E9.5 or E11.5 till E18.5 were conducted on the Osr1$^{CreERt2/+}$;ROSA$^{mTmG/+}$ mouse model. FABP4, depicted in red, is expressed in the central nerve system and in mature adipocytes. The Osr1 lineage is labeled with mGFP. A and E) show cross sections to provide an overview of adipose tissue patterning at E18.5 at different rostro-caudal levels of the fetus. A whole-mount Oil Red O (ORO) staining is displayed on skinned E18.5 embryos to highlight the organization of different subcutaneous white adipose tissues; brown adipose tissues are not visible, as they are covered by WAT (B, C and D). The dashed line in B, C and D refers to the section planes in A) and E). mGFP+ FABP4+ adipocytes were detected in all fat depots for the E9.5 and E11.5 Osr1 lineages. The only exception with very few mGFP+ cells is presented in interscapular brown adipose tissue (iBAT). cBAT: cervical Brown adipose tissue; sBAT: subscapular brown adipose tissue; latBAT: lateral brown adipose tissue; iBAT: interscapular brown adipose tissue; axiWAT: axillary white adipose tissue; subWAT: subcutaneous white adipose tissue.
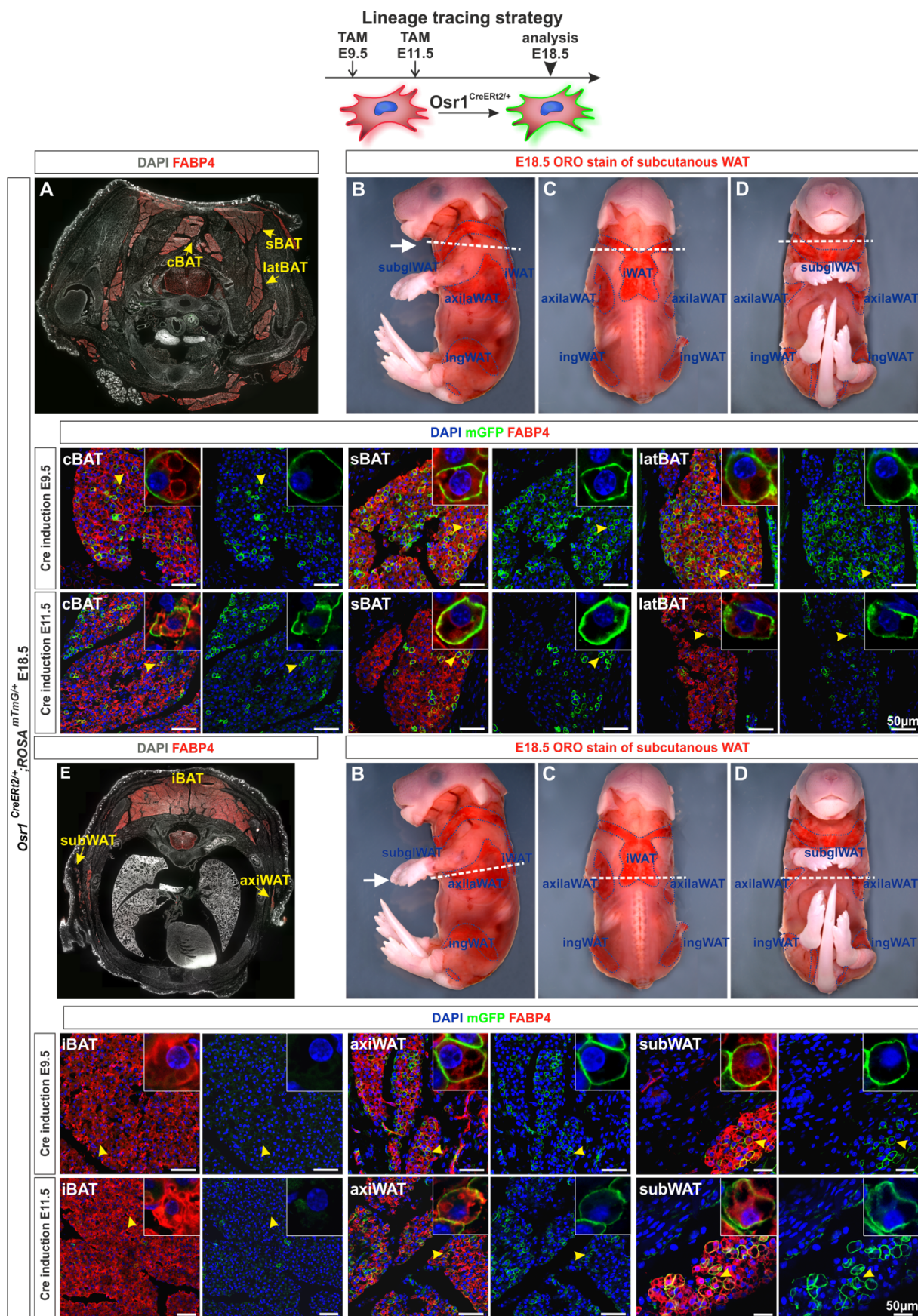
4.2.2 Adipogenic potential in the Osr1+ lineage is captured earlier than E11.5

Osr1 is expressed in mesenchymal cells before E11.5. To assess, if even earlier Osr1+ cells show adipogenic potential, Cre-recombinase was activated at stage E9.5. The analysis was done again at stage E18.5 using the same markers and comparable sections as described above. Figure 35 demonstrates that, indeed, E9.5 Osr1 progeny contributes to mGFP+ FABP4+ adipocytes of the same depots (cBAT, sBAT, latBAT, axiWAT and subWAT) as the E11.5 Osr1-lineage. Once again, the E9.5 Osr1 lineage does not provide adipocytes to the iBAT. The mGFP+FABP4+ cells of the E11.5 and E9.5 Osr1 lineage were quantified in three well-defined brown fat depots: the cervical brown adipose tissue (cBAT), interscapular brown adipose tissue (iBAT) and subscapular adipose tissue (sBAT). As expected already from the IFs the iBAT showed very low contribution from the Osr1 lineage. The percentages of adipogenic contribution from E9.5 and E11.5 are completely comparable between each other: around 25% in the sBAT and approximately 15% in the cBAT (Fig. 36).

Here, the question arises whether the Osr1 lineage would provide up to 100% contribution to brown fat- except the iBAT- in a constitutive lineage tracing model? Unfortunately, there was no constitutive Osr1-Cre mouse line available.
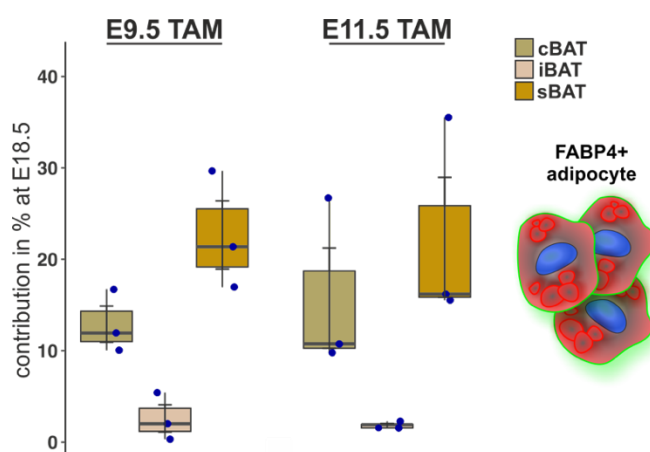
Figure 36: Quantification of the Osr1 lineage to adipose tissue contribution
The quantification was done on the E9.5 and E11.5 Osr1 lineage. Three well definable brown adipose depots: cBAT, iBAT and sBAT were investigated. Obviously, both lineages follow a similar trend and show a comparable adipogenic contribution pattern. The highest contribution was observed for the sBAT ($\approx$ 25%). The smallest contribution was measured in the iBAT ($\approx$ 2%). The cBAT instead shows roundabout 15% of adipogenic contribution. Data are presented as mean ± SEM (n = 3). cBAT: cervical brown adipose tissue; iBAT: interscapular brown adipose tissue; sBAT: subscapular brown adipose tissue

Lastly, an even earlier Cre induction timepoint was used to identify the initial pre-adipogenic source of the Osr1 pool. Thus, tamoxifen was administered at stage E7.5. The adipose tissue was investigated using an immunolabeling strategy for PPARγ and CD31 (also known as PECAM1) at stage E18.5 (Fig. 37). Interestingly, the immuno-stainings for mGFP in figure 37 disclosed that the Osr1 progeny from E7.5 contribute mainly to interstitial cells or CD31+ cells of the brown- and subcutaneous adipose tissue. These data suggest that the E7.5 Osr1 pool is not as adipogenic as opposed to the lineage from E9.5 or E11.5.
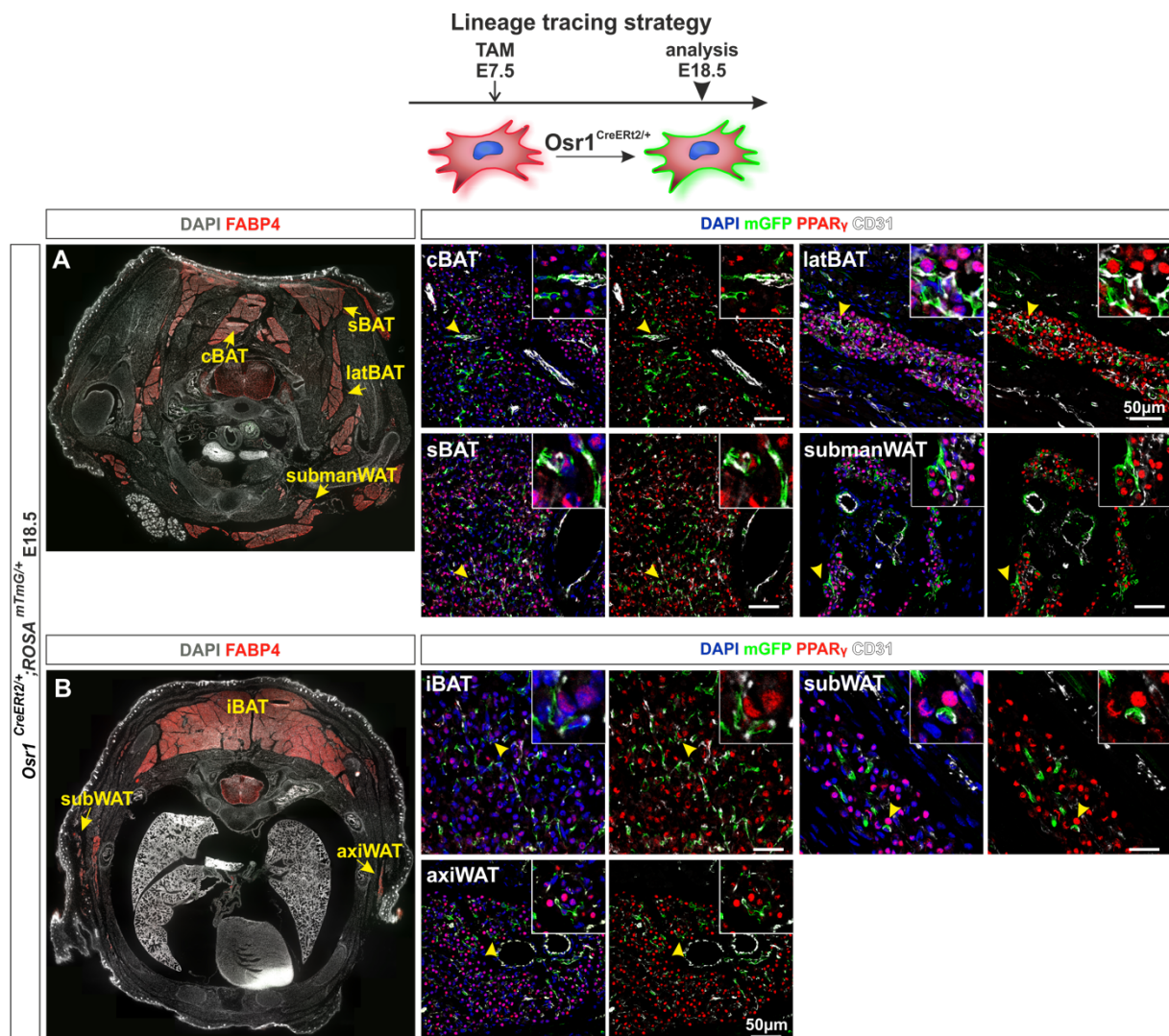
Figure 37: E7.5 Osr1 progeny contribute to endothelial and interstitial cells of adipose tissue Inducible lineage tracing experiments starting from E7.5 till E18.5 were implemented on the Osr1^CreERt2/+; ROSA^mTmG/+ mouse model. PPARγ, depicted in red, marks the nucleus of adipogenic cells. The Osr1 lineage is labeled with mGFP. A and B) show cross sections to provide an overview of adipose tissue patterning at E18.5. mGFP+ PPARγ+ cells are rare in sBAT, latBAT, submanWAT, iBAT and axiWAT but mGFP+ CD31+ cells instead, were found more often cBAT, sBAT, latBAT, submanWAT and iBAT.

Since the distribution pattern of the E7.5 Osr1 descendants is highly different to E9.5 or E11.5 a more detailed contribution profile was generated (Fig. 38).

For direct comparison, E9.5 and E7.5 lineage tracing tissue sections were immunolabeled for mGFP to visualize the Osr1 progeny, PLIN to label mature adipocytes and MyHC to show the muscle patterning. Figure 38 confirms that the E9.5 Osr1 lineage gave rise to adipose tissue (F1-2, I1-2), and muscle interstitial cells as expected (F1-2, G1-2, I1-2, J1-2). Surprisingly, the E9.5 Osr1 lineage in addition contributed to skeletal muscle of forelimbs (G1-2, J1-2), the pectoral muscle (I1-2) as well as the panniculus carnosus muscle (F1-2). This was never observed when tracing the Osr1 lineage at E11.5 or later (this study, Vallecillo 2017, Master thesis Verena). No recognizable contribution was seen to bone marrow (H1-2). The contribution pattern of the E7.5 Osr1 lineage on the other hand displayed that almost all tissue types: endothelium (A1-2), bone marrow (C1-2), myotubes (A1-2, B1-2, D1-2) as well as muscle interstitial cells (A1-2, B1-2, D1-2, E1-2) hold mGFP cells. Notably, the global amount of mGFP+ cells per tissue appears lower compared to the E9.5-lineage. In conclusion at E7.5 the Osr1 pool represents a more undefined multipotent progenitor cell type, which is able to convert into a wide range of cell types like muscle, connective tissue, adipose tissue, bone marrow and endothelial cells throughout development.

The lineage tracing experiments confirmed that the Osr1 cell pool at E9.5 and E11.5 hold an adipogenic potential. This raises the question, whether the adipogenic Osr1+ cells at E9.5 and E11.5 represent an overlapping pool, or distinct lineages. To further investigate the cell identities of the E9.5 Osr1 pool, a single cell RNA-Seq was performed, which was compared to and integrated into the E11.5 Osr1 dataset.
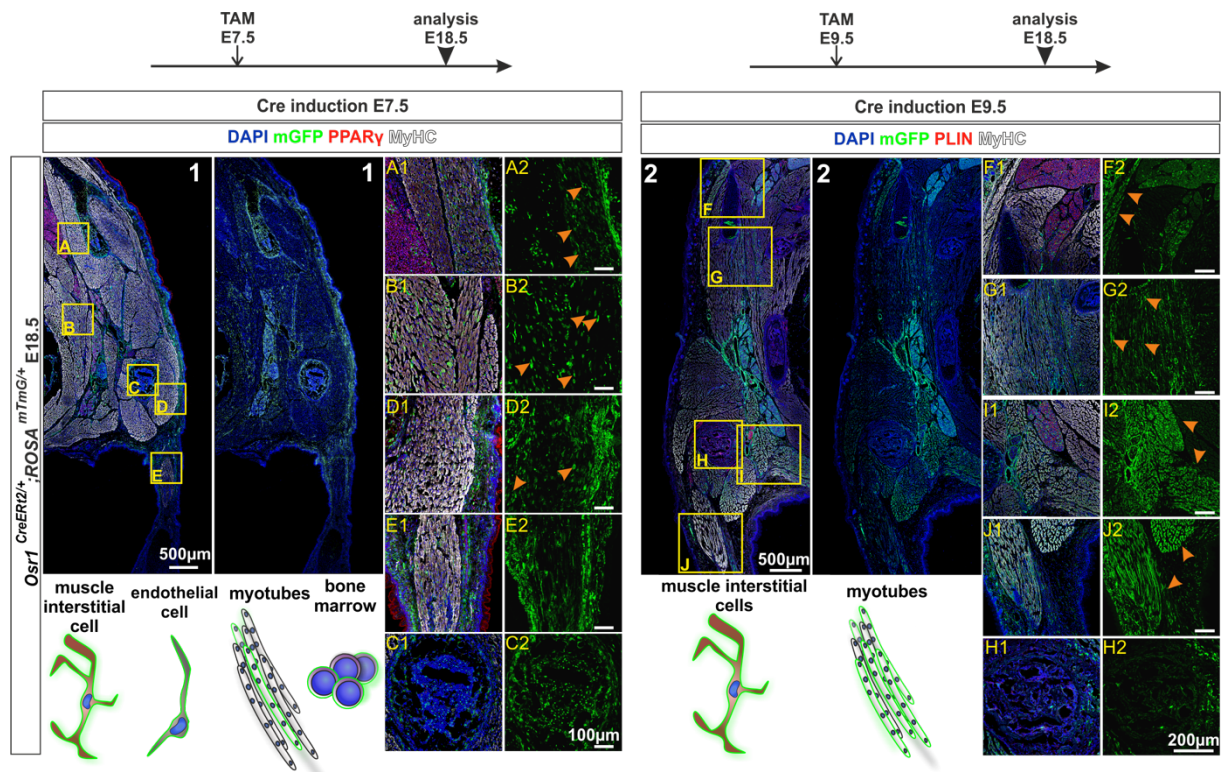
Figure 38: The E7.5 Osr1 lineage has various differentiation potentials
Inducible lineage tracing experiments starting from E7.5 or E9.5 till E18.5 were performed on the Osr1[CreERt2/+]; ROSA[mTmG/+] mouse model. Immunolabeling for myogenic tissue (MyHC in white), adipogenic (PLIN in red) and the Osr1 lineage (mGFP in green) was conducted to compare and assess the differentiation potentials of both lineages. 1 and 2) show cross sections to provide an overview of the investigated regions. Myogenic tissue contribution is indicted with orange arrowheads. At Cre induction timepoint E9.5, MyHC+mGFP+ are observed in the following regions: 2F, G, I, J. The E7.5 Osr1 lineage shows myogenic contribution too (1A, B, D), but not to the same extent as the E9.5-lineage. Furthermore, at Cre induction timepoint E7.5 the mGFP cells locate in the bone marrow (1J) which was not observed for the E9.5-lineage (2H). The adipose tissue (1A and 2F) confirmed that the E7.5 lineage provides endothelial and interstitial cells, but not mature adipocytes. In general, the mGFP pattern from 1A-E confirms that the Osr1 cell pool of E7.5 has various differentiation potential.

4.3 ICell8 RNA-Seq dataset of E9.5 Osr1+ cells present distinct differences to the embryonic stage E11.5

A general investigation of the E9.5 Osr1 scRNA-seq dataset was done as described for the E11.5 Osr1-object in the beginning. To do so the dataset from E9.5 was mapped to the reference project from Cao et al.. Here, the reference specimen was subsetted before to cells of an E9.5 embryo (Fig. 39).
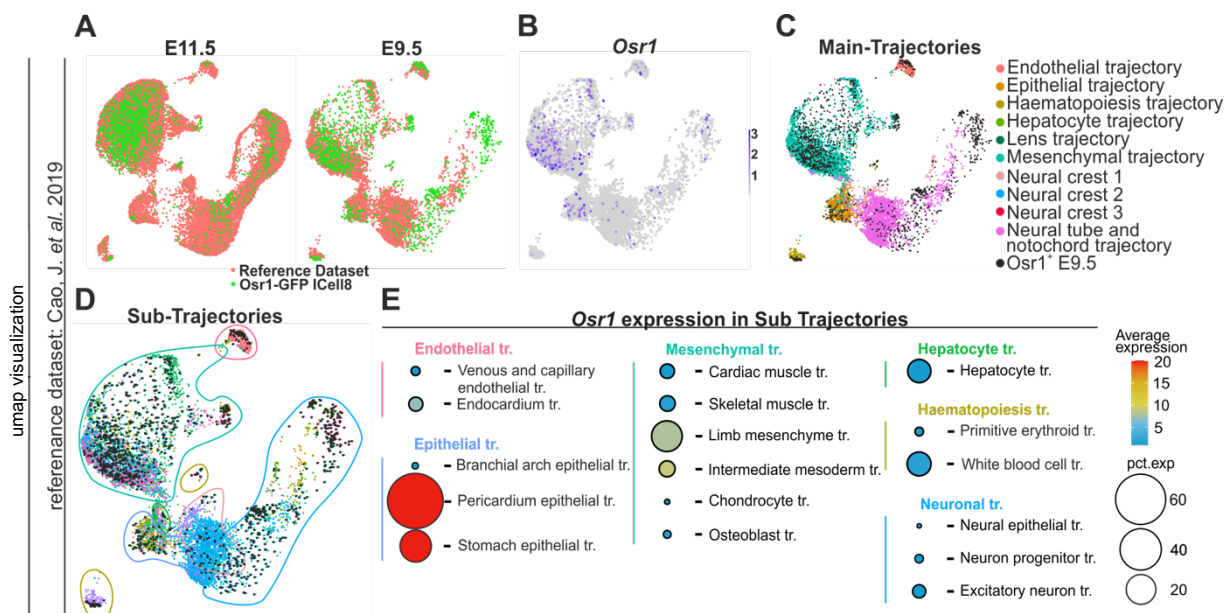
Figure 39: Representative mapping of the *Osr1*+-E9.5 scRNAseq dataset to an equivalent reference

A) displays the distribution pattern of the *Osr1*+ E11.5 and E9.5 single-cell dataset (in green) mapped to its respective reference object of an E11.5 embryo and E9.5 embryo (in coral) for direct correlation (Cao et al., 2019). Comparing the two stages with each another it becomes obvious that the Osr1 pool at E9.5 is distributed more evenly in the reference object. B) shows the actual *Osr1* expression in the reference dataset that recapitulates the pattern of the E9.5 Osr1-dataset. The Main-Trajectories from the Cao et al. file are visualized in C). The reference data defined Sub-Trajectories, which are depicted in D). The color-coded outlines in D) represent the Main-Trajectories in C). The color-code of the depicted cells refers to the Sub-Trajectories (see appendix). Both C) and D) display the Osr1 E9.5 dataset in black. The cell types that have enriched the most in the Osr1+ object are from endothelial-, cardiomyocyte-, epithelial- and the haematopoiesis trajectory. The expression profile of *Osr1* in the E9.5 Cao et al. 2019 data is listed in E).

The dataset comparison of E11.5 (E11.5 data from Fig. 14A) and E9.5 showed that the Osr1 cells from E9.5 are more evenly distributed among the reference object (Fig. 39A), suggesting that the cell pool is much more diverse. Furthermore, the profile of the Osr1-sc-dataset was correlated with the distribution pattern of the Osr1 expressing cells of the E9.5 reference object (Fig. 39A and B). The provided Main-trajectories in figure 39C introduced that the E9.5 Osr1 cell pool has higher content of endothelial-, epithelial-, haemopoietic cells and cardiomyocytes. Analyzing the Osr1 expression level of the reference Sub-trajectories in figure 39E indicated that the Osr1-sc-dataset hold epithelial cells from the pericardium and stomach, limb mesenchymal cells, cells of the intermediate mesoderm, endothelial cells as well as very few cells from muscle trajectories. All together the E9.5 dataset shows much higher variability than the E11.5 object.

4.3.1 Computational correlation and ID prediction of the Osr1 scRNA-dataset through a reference single-cell-map of gastrulation and early organogenesis

Next, the whole Osr1-dataset was aligned to a single cell object of mouse gastrulation and early organogenesis (Pijuan-Sala et al., 2019) to evaluate where and when the Osr1 cells emerge in the time context of development (Fig. 40).
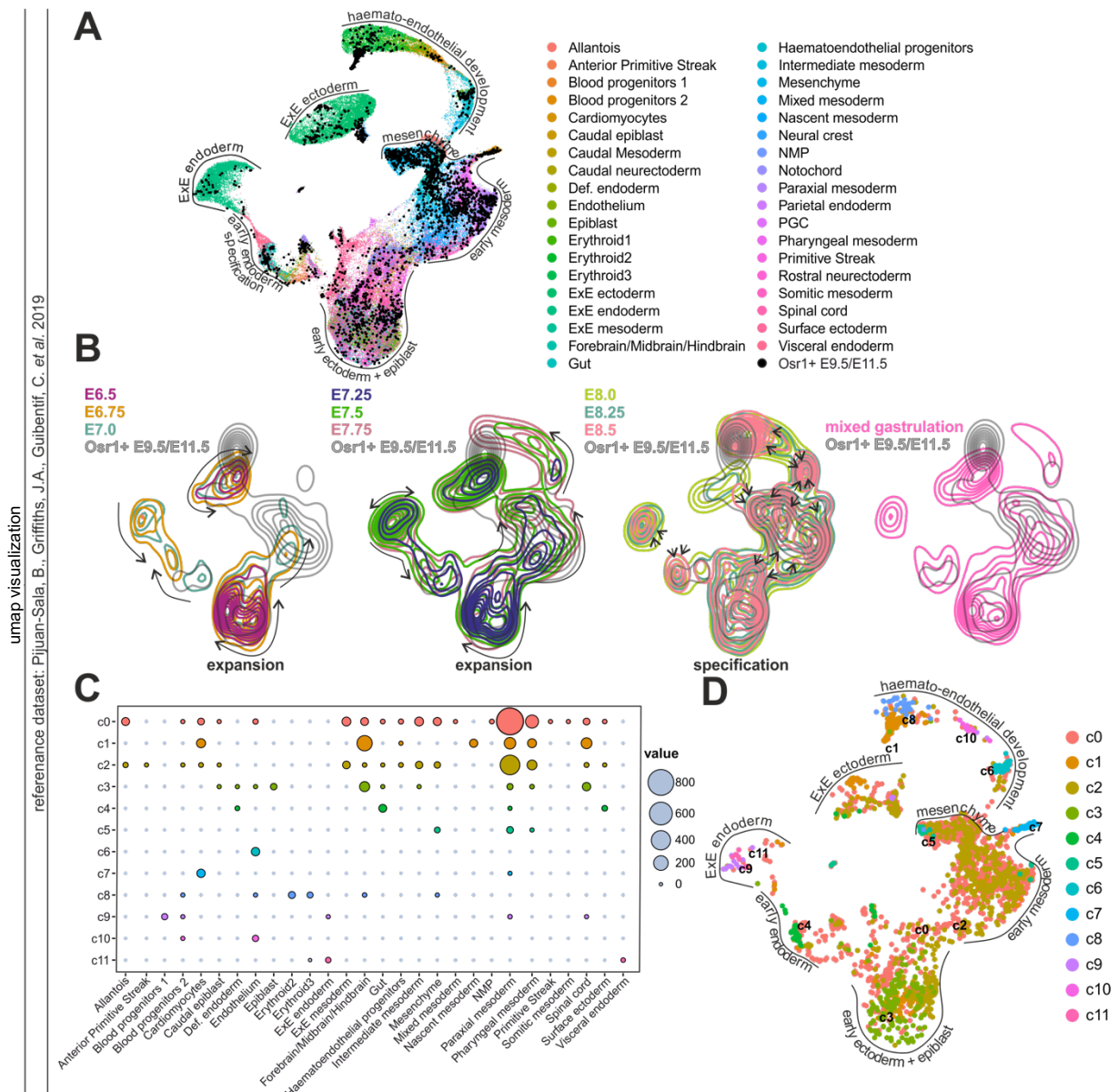
Figure 40: Integration of the Osr1-object into a mouse gastrulation and early organogenesis dataset
A) displays the reference dataset from (Pijuan-Sala et al., 2019) with a color-coded list of sub-trajectories on the right. The main-trajectories are directly assigned to the UMAP plot. The reference dataset comprises the embryonic stages from E6.5-E8.5. B) presents small groups of overlayed cell density landscapes of indicated embryonic stages. Each color represents a different stage. The Osr1-dataset is plotted in grey that showed first similarities with the dataset of stage E8.5 (in salmon). The table in C), in the color-code of the Osr1 sc-dataset highlights that especially signatures of mesodermal identity match with the Osr1-specimen. The UMAP-plot in D) prognosticates where the clusters of the Osr1-dataset arrange.

The whole object from Pijuan-Sala et al. is depicted in figure 40A. The project summarizes the early embryonic stages from E6.5 to E8.5. Figure 40A provides a colorcoded list of sub-trajectories which can be recognized in the UMAP-object in their respective main trajectories of early development. Within the Pijuan-Sala dataset, cells from the Osr1-specimen (depicted in black) specifically align with the main trajectoies of early mesoderm, mesenchyme, early endoderm and heamato-endothelial develoment. These observations go in line with the proposed identities of the Cao et al. reference dataset of stage E9.5 and E11.5.

Furthermore, the cell density landscape of all available embryonic stages of the Pijuan-Sala-specimen were plotted and aligned in groups to trace the developmental time course (Fig. 40B). The Pijuan-Sala dataset starts of with stage E6.5 that manly consists of two islands: the epiblast and extra embryonic ectoderm. These two founder populations progressively expand until stage E7.75. The final stages (E8.0, E8.25 E8.5), on the other hand, appear to evolve backwards, which can be explained by specification processes – cell commitment. Thus, new smaller centers appear in the cell density landscape. However, as expected, the Osr1 object from E9.5 and E11.5 cells do not overlap much with the objects of the stages: E6.5, E6.75 and E7.0, indicating that Osr1 cells represent a more advanced mesodermal population than the naïve mesoderm. The same was observed for the datasets of E7.25, E7.5 and E7.75, although the landscapes seem to match each other better compared to the earlier stages. Focusing on the last stages E8.0, E8.25 and E8.5, the Osr1-profile can be almost recapitulated from the E8.5-dataset. There are only a few cells that do not cluster within the Pijuan-Sala dataset, that probably can be explained by developmental progression. Notably, the contours of the E8.5 dataset demonstrate more cell-density-centers within single trajectories whether the Osr1 density landscape shows only one per main trajectory (Fig. 40B). This finding suggests that the Osr1-object consists of a more general cell type of each main trajectory, which again is observed in figure 40B, demonstrating that the main Osr1 clusters: cl0, cl1 and cl2 distribute within the mesenchyme, early mesoderm and early ectoderm /epiblast trajectories of the Pijuan-Sala UMAP plot. Only the small peripheral clusters of the Osr1-object (Fig. 15A and 41A) take specific positions (Fig. 40D).

Additionally, the Pijuan-Sala-object was used to predict cluster identities of the Osr1-dataset from a developmental point of view (Fig. 40C). The findings demonstrate that the main cluster cl0, cl1 and cl2 are high in mesodermal identity. It should be noted

that cl1 seems to carry a higher myogenic identity than the others. Unclear is the predicted neurogenic potential for cl1. This could be an artifact from the computational analysis since a comparision from early embryonic stages with later stages is not always conclusive. Altogether, the correlation of both datasets showed that the Osr1-object holds a rather general progenitor identity of different tissues as indicated among the density plots in figure 40B and the UMAP plot in figure 40D.
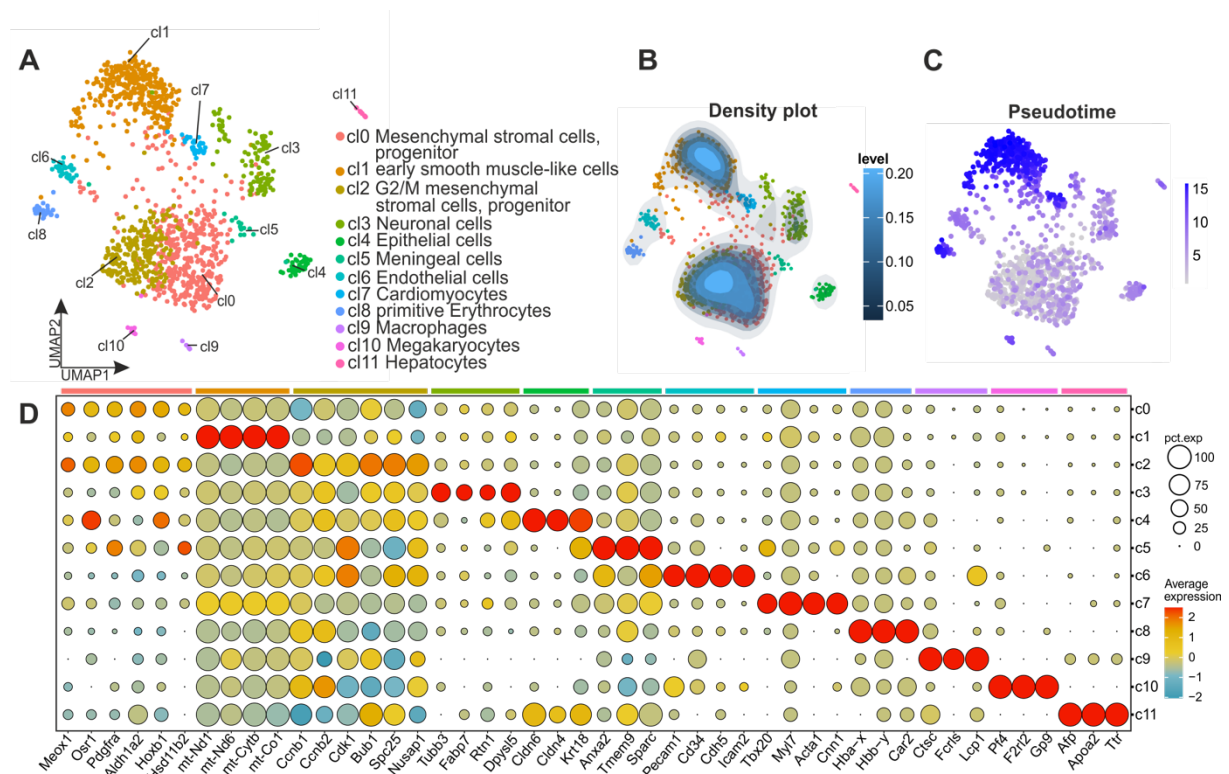
Figure 41: Integration of the E9.5-Osr1-dataset into the E11.5-object
The UMAP visualization of the E9.5 Osr1 clusters is displayed in A). Obviously, the small satellite clusters grew in cell numbers. That is also demonstrated in the density plot in B). The new centers are again cl0, cl2 and cl1. C) presents the pseudotime, which ranks cl1, cl7 and cl8 as the most developed cell types. The cluster signature genes are listed in D). The signature genes recapitulate to a greater extent the E11.5 dataset.

Reference datasets from Pijuan-Sala et al. and Cao et al. were applied to facilitate cell type predictions of the entire Osr1 single cell dataset. Next, the Osr1-E9.5 sc-dataset was further specified after integration into the Osr1-E11.5 UMAP visualization pattern (Fig. 41), meaning that the distribution of E9.5 cells as well as their gene signatures pattern based on the E11.5 Osr1-dataset. Thus, the global structure of the UMAP remained unchanged (Fig. 41A). The density plot, on the other hand, revealed that more cells localize in the satellite clusters compared to the Osr1-E11.5 dataset. Furthermore, cell density differences have been recognized within the main clusters: It seems like that the cl1 and cl2 embodies more cells than detected in the E11.5

specimen (Fig. 41B; Fig. 15B). The pseudotime analysis presents that cl1, cl7 and cl8 have a higher grade in differentiation than the other clusters (Fig. 41C). That is consistent with the pseudotime of stage E11.5. The signature genes of the clusters are listed in figure 41D. Cl0 and cl2 again show a very similar expression profile with one exception that cl2 is highly enriched of G2/M genes. Furthermore, the signature genes like: *Aldh1a2, Pdgfra, Meox1* and *Hoxb1* are broadly expressed in mesenchyme along the cranial to caudal axis at stage E9.5 (Mic et al., 2004, Kirilenko et al., 2011, Niederreither et al., 2003, Qian et al., 2017). Notably, since *Osr1* expression is not present in the head at this stage, the focus for further investigations was laid on the main body of the E9.5 embryo (Wang et al., 2005). Cl1 shows the same signature as described before in the E11.5 Osr1-dataset. Both record expression of myogenic genes, which were also detected in the cardiomyogenic cl7. One of the main differences between the E9.5- and E11.5- objects is that the small peripheral clusters consist of a significant higher number of cells. Thus, E9.5 shows a higher variability in cell types: especially (cl4) epithelial-, (cl6) endothelia-, (cl7) cardiomyocyte as well as cells of the haemato-endothelial trajectory (cl8, cl9, cl10). This was already proposed from the E9.5 Cao et al. reference object in figure 39.

4.3.2 Osr1 expressing cells pattern around the central body axis of an E9.5 embryo

Next, immunostainings were performed to validate the sc-dataset of E9.5 Osr1+ cells. Figure 42 presents a sequence of cross sections throughout a whole E9.5 embryo. OSR1 in green was used together with PAX7 in red to mark the early dermomyotome and PECAM1 in white, to identify the endothelial cells. Obviously, OSR1 was mainly detected in the central-axis or midline of the embryo (Fig. 42A-F). Regions with OSR1 staining are found in the pharynx and in the heart (A), the trachea and lung buds (B), the intermediate mesoderm, urogenital ridge, gut (C, D) and finally the dorsal aorta compartment (E). The detected OSR1 expression pattern is summarized in the scheme of figure 42F. Obviously, there are clear differences in the OSR1+ cell distribution between E9.5 and E11.5.
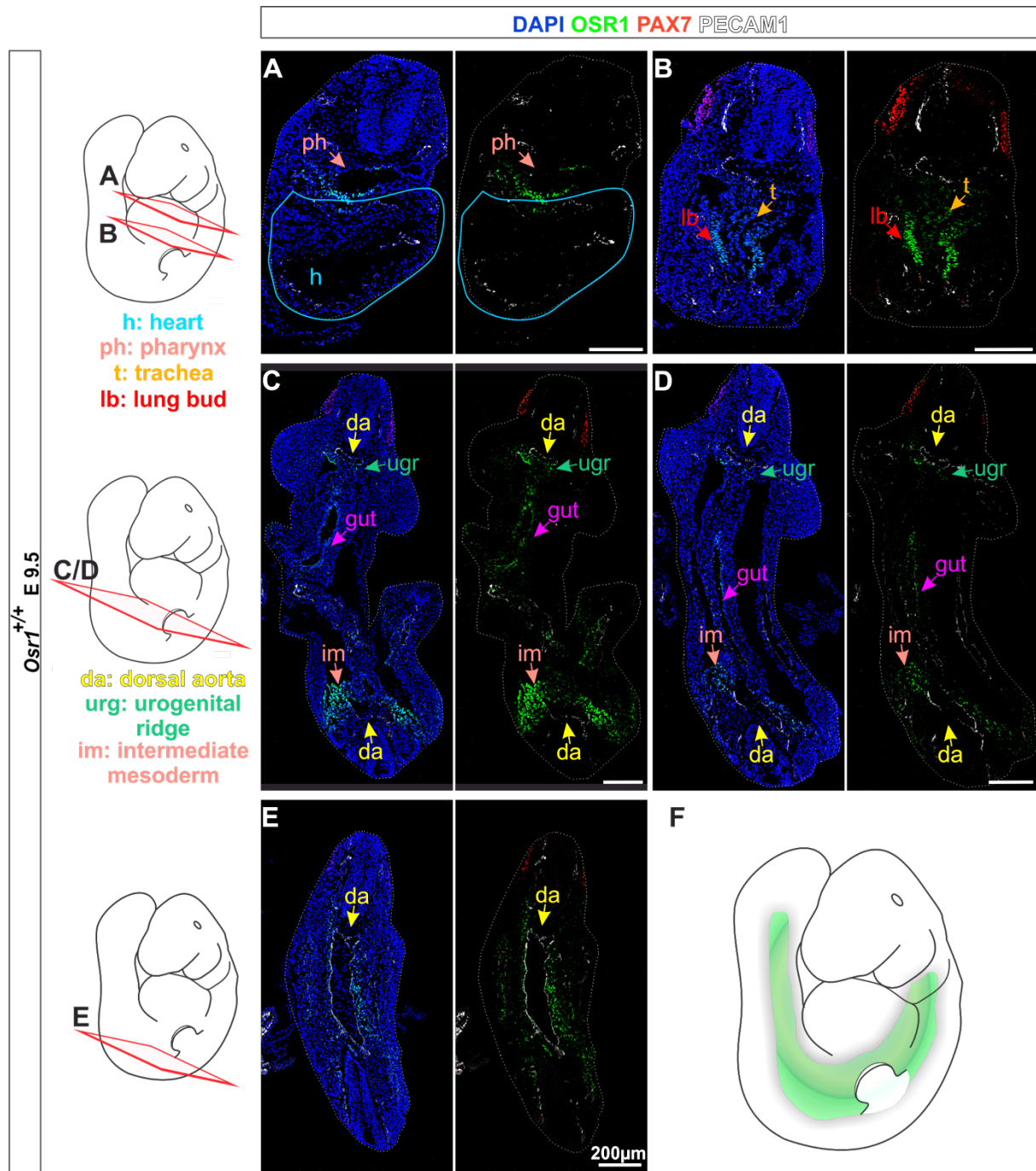
Figure 42: The distribution pattern of OSR1 at stage E9.5

A-E) displays immunostainings on indicated cross sections for OSR1 in green, PAX7 in red and PECAM1 in white. A and B) revealed that Osr1 is expressed in the pharynx, the outflow tract of the heart and the primitive structures of trachea and lung buds. In the more caudal part of the embryo OSR1 is observed in the gut-epithelium, urogenital ridge, the intermediate mesoderm and the dorsal aorta compartment (C-E). In none of the section was OSR1 and PAX7 co-expression recognized. F) summarizes the more centralized OSR1 expression pattern in a graphical schema. h: heart; ph: pharynx; t: trachea; lb: lung bud; da: dorsal aorta; urg: urogenital ridge; im: intermediate mesoderm

Most importantly, there is no evidence that the OSR1+ cell pool colocalizes with the PAX7+ cells (Fig. 42B-E and 43.1/2/4). This was further investigated in figure 43 on comparable sections to figure 42B and E, which demonstrates magnifications of the early dermomyotome. In none of the cases co-expression of PAX7 and OSR1 was observed.
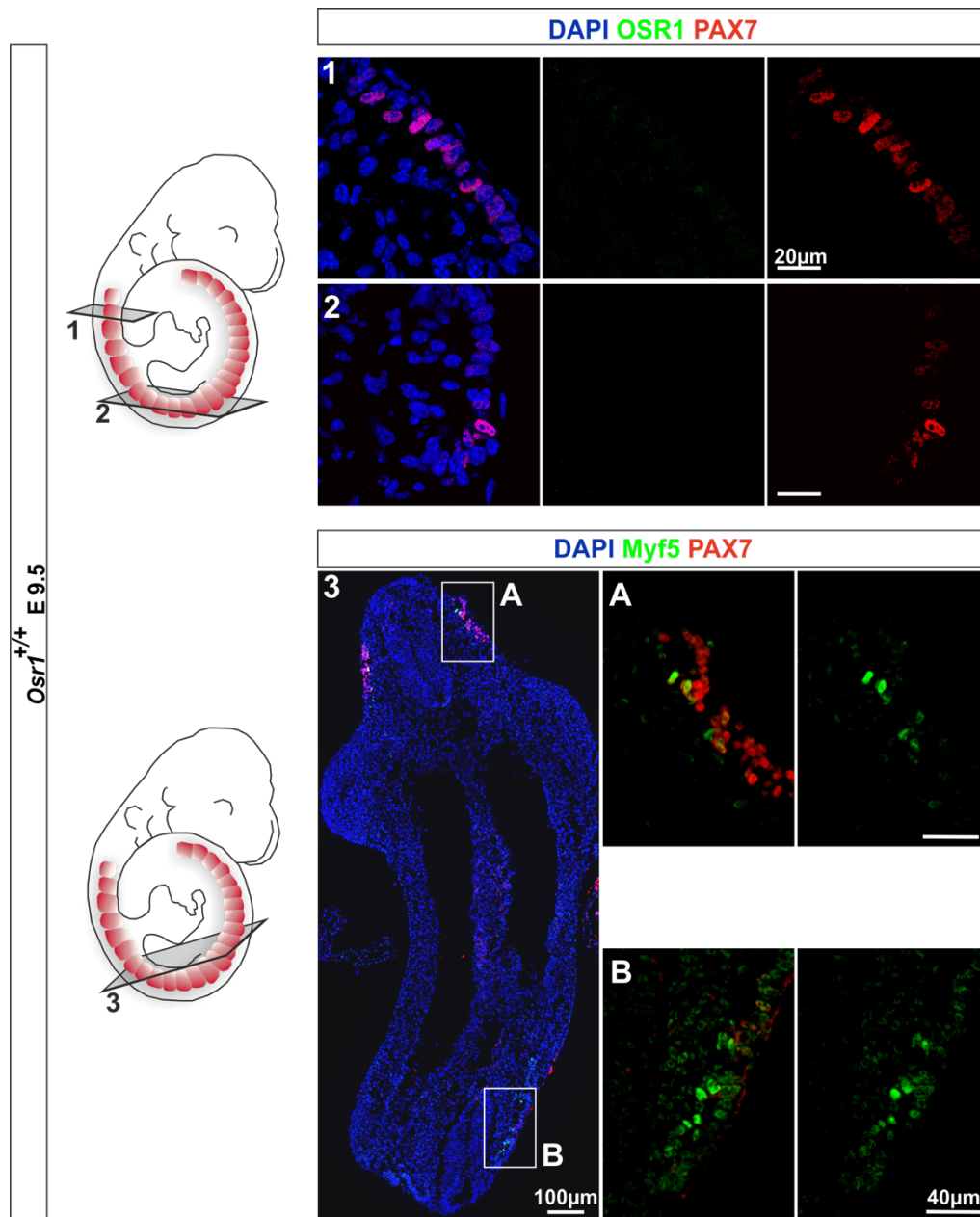
Figure 43: OSR1 is not expressed in the somites of stage E9.5
Respective sections from figure 42 were further analyzed in area 1) and 2) whether OSR1 (green) and the myogenic marker PAX7 (red) colocalize. Both indicated regions are negative for OSR1. Section 3) reveals that MYF5 (green) - another early myogenic marker - is only expressed in a subset of the PAX7+ (red) cells, concluding that OSR1 and MYF5 clearly not overlap.

4.3.3 At E9.5 the myogenic lineage is separate from the Osr1+ cell pool

On the one hand, BAT progenitors arise from the myogenic lineage; on the other hand, the Osr1 lineage tracing experiments demonstrated that the E9.5 Osr1 cell pool holds a myogenic potential (Fig. 38.2). Immunolabeling suggested no overlap of Osr1 expression with early myogenic markers at E9.5, however, to confirm that Osr1 is not expressed at this stage in cells of the myogenic lineage or their progeny, the Myf5 lineage was examined via genetic lineage tracing. Here, the constitutive Myf5$^{Cre/+}$; ROSA26$^{mTmG/+}$ mouse was used to capture the myogenic lineage; Myf5 was shown to label approx. 95% of the myogenic lineage (Gensch et al., 2008, Picard and Marcelle, 2013) and practically 100% of subscapular BAT progenitors (Sanchez-Gurmaches and Guertin, 2014b). In addition, this line was crossed to an allele that carried a LacZ reporter in the Osr1 locus (Osr1$^{LacZ/+}$). Thus, in the combination line (Myf5$^{Cre/+}$; ROSA26$^{mTmG/+}$;Osr1$^{LacZ/+}$), mGFP labeled cells derive from the Myf5-lineage and the β-Galactosidase activity (X-Gal- staining) identifies Osr1 expression.

The investigations of the Myf5$^{Cre/+}$; ROSA26$^{mTmG/+}$; Osr1$^{LacZ/+}$ E9.5 embryo revealed that throughout the entire embryo mGFP+ Myf5-progeny was negative for β-Galactosidase activity (grey) (Fig. 44). That leads to the conclusion that figure 44 provides further proofs that the early myogenic lineage and the Osr1-β-Galactosidase cells intermingled with Myf5-derived cells expression pattern but do not colocalize. Consequently, there must be an independent source of skeletal muscle progenitors apart from the somites.

These findings change the focus of attention. What could be the source of embryonic brown adipose tissue and skeletal muscle apart from the somites? It could be a cell type which is most likely not available in the E11.5 Osr1-sc-dataset since the myogenic potential was not observed later than E9.5. To tackle these questions a direct comparison between the clusters of the E9.5- and E11.5- dataset was performed.
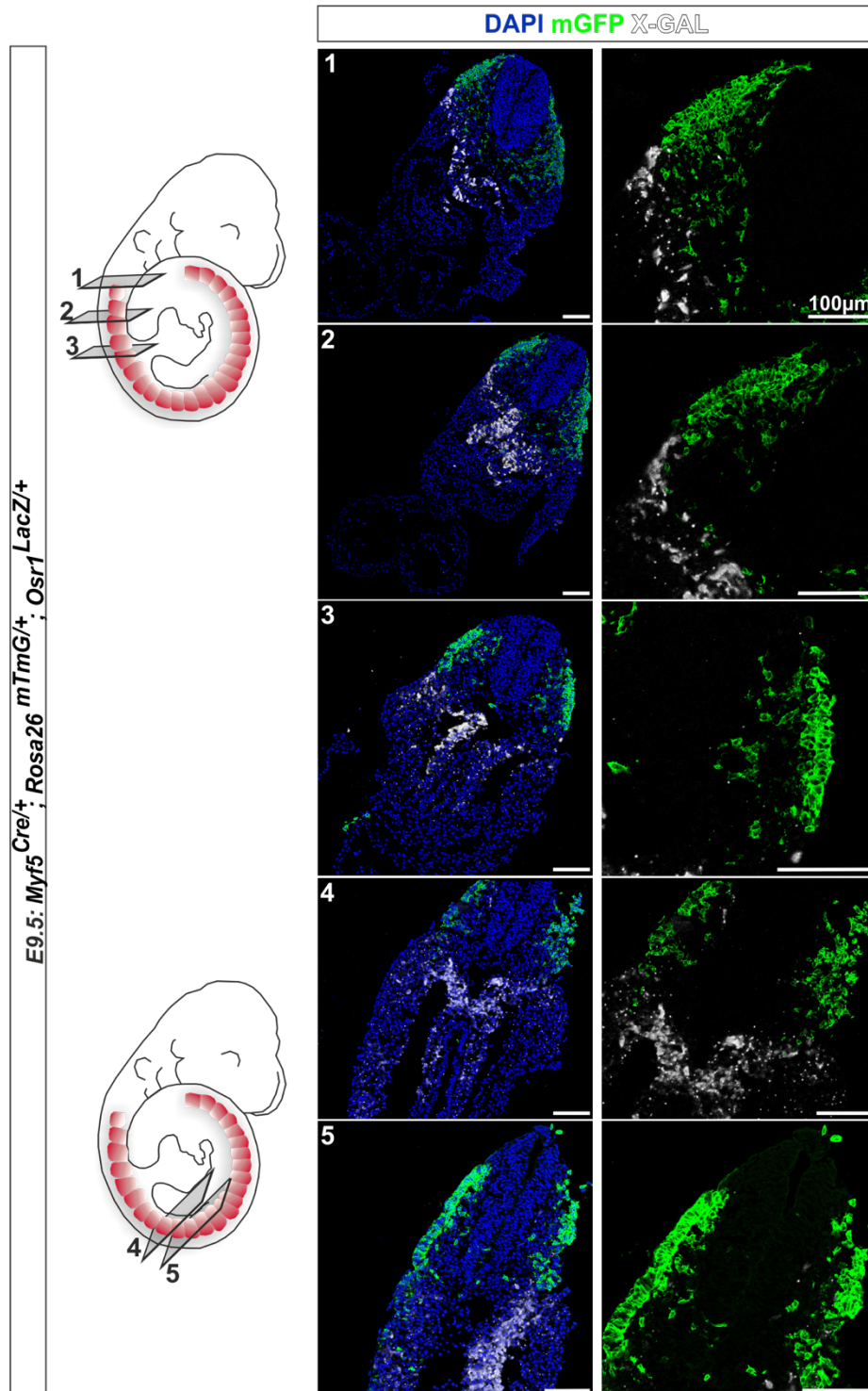
Figure 44: Osr1 is not expressed in the early Myf5 lineage
A constitutive Myf5-Cre was used to trace the entire Myf5 cell population. The Myf5$^{Cre/+}$;ROSA26$^{mTmG/+}$ mouse model that also carries a LacZ cassette in the Osr1 locus to allow Osr1 detection *via* a β-Galactosidase activity staining (X-GAL). Immunolabeling for the Myf5 progeny (mGFP) and a X-GAL staining for Osr1 was performed on consecutive cross section (1-5) of an E9.5 embryo. In none of the investigated areas did the Myf5 lineage overlap with the Osr1 expression, indicating that indeed Osr1 expression is separated from the myogenic progenitor pool.

4.3.4 At E9.5, Osr1 labels a cell population in the dorsal aorta compartment

The observation that Osr1 cells are found in the aorta-gonadal-mesonephros (AGM) region, raised interest, since this region was characterized harboring potent cells like mesoangioblasts. Mesoangioblasts were described to specifically arise from the dorsal aorta, hold an early endothelial signature and which among development, can give rise to different mesodermal tissues such as skeletal muscle, bone and adipocytes (Minasi et al., 2002, Cossu and Bianco, 2003). Thus, the most interesting candidates in the single cell RNA dataset are smooth muscle like cells of cl1 as well as cl6, representing endothelial characteristics. Cl6 has not received much of attention at E11.5 since it harbors only very few cells.

It has been demonstrated that especially the dorsal aorta at E9.5 or the aorta-gonadal-mesonephros (AGM) region of an E10.5 embryo provides a multipotent, self-renewing cell "the mesoangioblast" that can differentiate into most mesodermal tissues (Minasi et al., 2002, Esner et al., 2006). To assess whether the Osr1 cell pool of stage E9.5 holds mesoangioblast identity, additional immunostainings were essential. First, it was addressed whether OSR1+PECAM1+ cells cluster along the dorsal aorta. Figure 45 displays some cells along the dorsa aorta that co-express OSR1 and PECAM1. The amount of detected PECAM1 positive cells nicely represents the cluster size. *Pecam1* expression is exclusively detected in cluster 6 (Fig. 45.3).
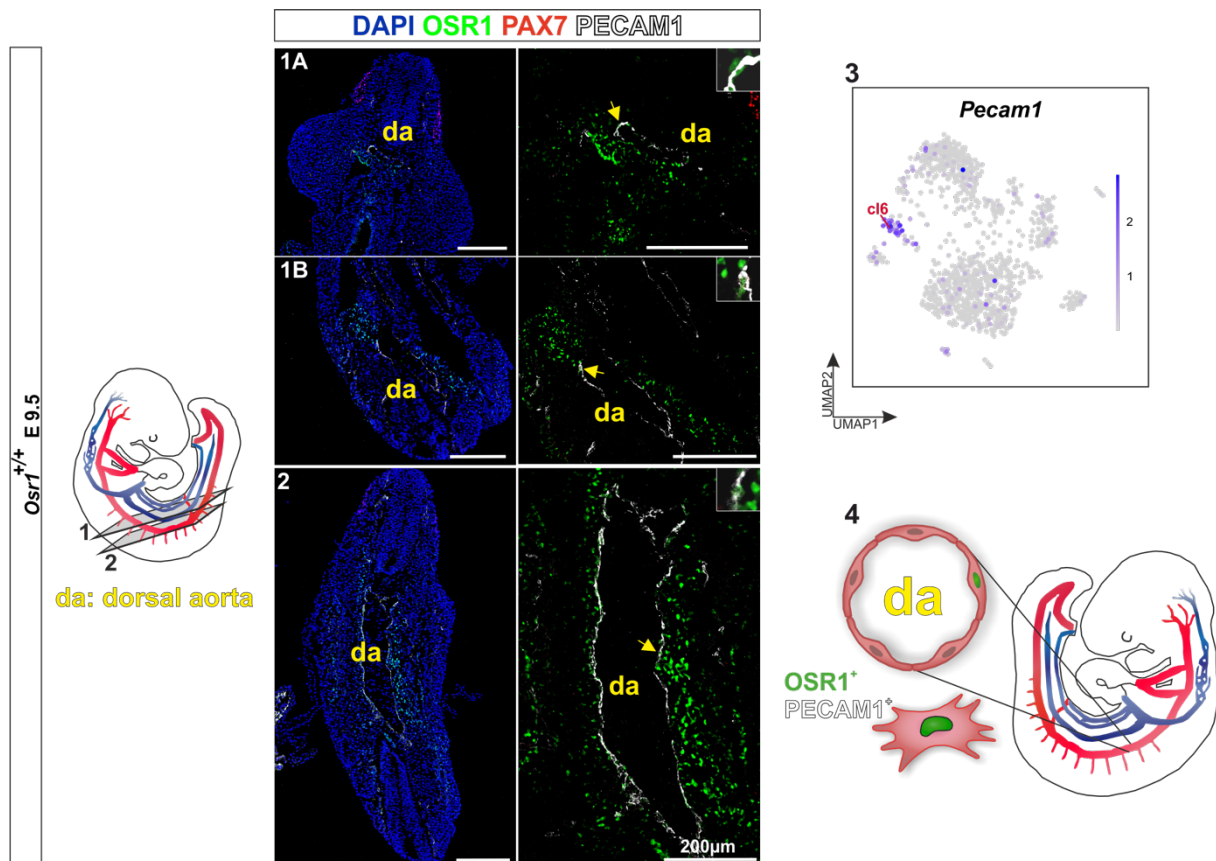
Figure 45: Osr1+ cells reside in the dorsal aorta at E9.5
Cross sections 1 and 2) were studied more closely to confirm that Osr1+ localize in endothelial layer of the dorsal aorta. Immunolabeling for PECAM1 was used to mark the endothelium. All investigated regions of the dorsal aorta hold a few numbers of OSR1+ (green) cells. Yellow arrows indicate some of them. The E9.5 Osr1-object was tested for *Pecam1* expression levels in 3). A relative smaller cluster (cl6: endothelium) was exclusively enriched for *Pecam1* which perfectly reflects the findings on tissue sections.

Since the mesoangioblast signature is defined by a collection of genes like vascular endothelial growth factor receptor 2 (KDR) (also known as FLK1) and CD34 (Cossu and Bianco, 2003). Additional co-expression experiments were conducted on tissue sections to confirm mesoangioblast identity (Fig. 46). Interestingly, the immunolabeling in figure 46A resolves that KDR (in red) is detected in the entire vasculature, like PECAM1 (in white). Consequently, the whole OSR1+ PECAM1+ cell pool expresses KDR+. This is consistent with the UMAP-feature plots of the Osr1 E9.5 object. Furthermore, *Cd34* seems to cluster on a high extent with *Kdr* (Fig. 46B). The only detectable difference between *Pecam1* and *Kdr* or *Cd34* is that also cl1 (early smooth muscle-like cells) includes cells with endothelial identity, which is characteristic of mesoangioblast (Cossu and Bianco, 2003).
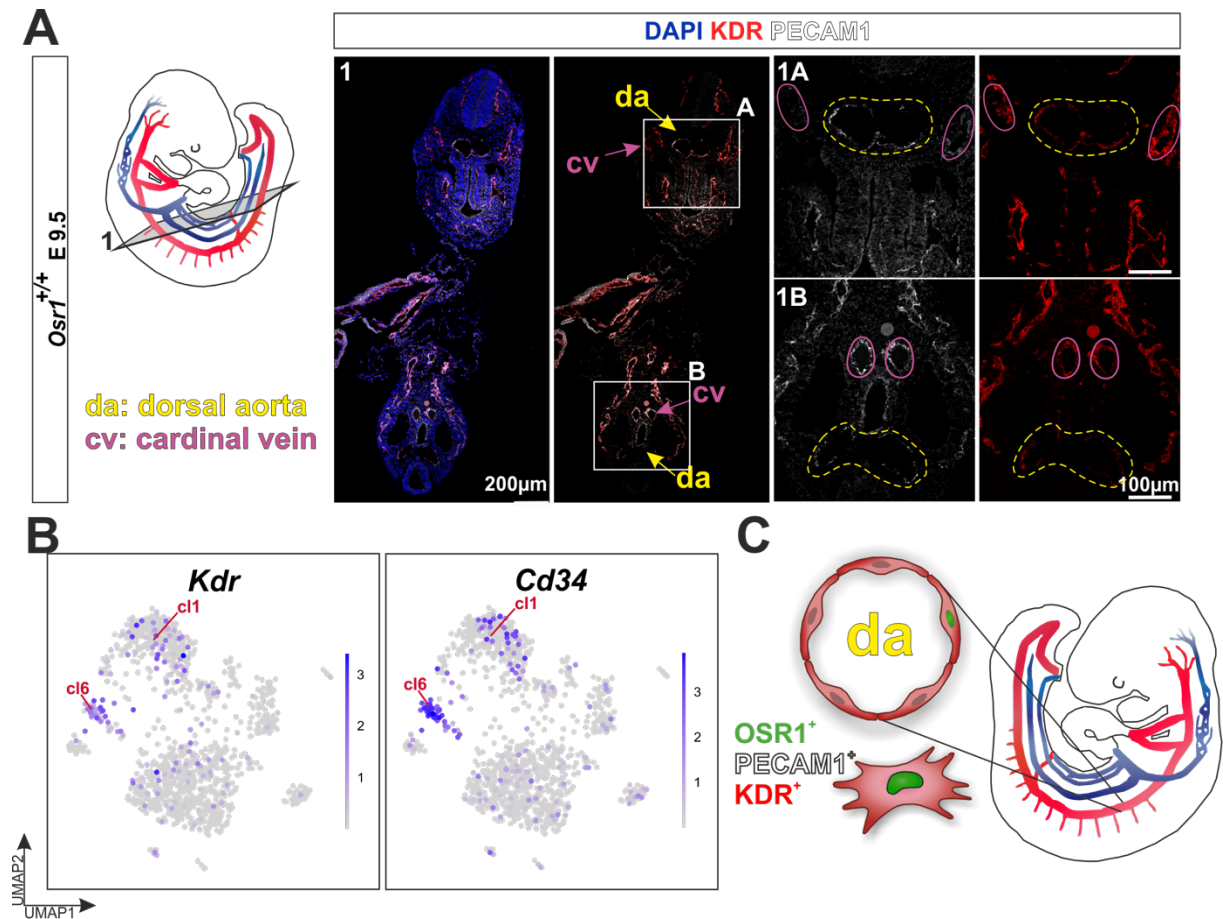
Figure 46: At E9.5 cl6 and cl1 holds mesoangioblast identity
Cross sections of an embryo at E9.5 were immunolabeled for PECAM1 (white) and KDR (red) to detect potential mesoangioblasts. Interestingly, the entire endothelium at E9.5 expresses KDR A). Consequently, the OSR1+ PECAM1+ cell pool expresses KDR+. The E9.5 Osr1-object demonstrates in B) that *Kdr* is mainly enriched in the endothelium but seem to be available in the smooth muscle like cell cluster too. The same expression pattern was observed for *Cd34* – another marker for mesoangioblast identity. C) summarizes that the OSR1+ cells of the dorsal aorta hold mesoangioblast identity.

These findings propose that cl1 and cl6 could be a potential source for skeletal muscle and most likely brown adipose tissue. Therefore, the E9.5 and E11.5 Osr1-object were tested for *Ebf2* expression to assess a pre-adipogenic signature in Osr1 cells at this stage (Fig. 47).

The UMAP-feature-plots in figure 47 show clearly that *Ebf2*+ cells cluster mainly in cl0 at stage E11.5. However, at E9.5 *Ebf2* expression is lower and seem to be randomly distributed, indicating that they might not mark pre-adipogenic progenitors at this point. The same result is visualized in the *Ebf2* dot-plot. Thus, it is not reasonable to use the Ebf2 based pre-BAT signature to identify pre-adipogenic progenitors on the E9.5 Osr1-sc-dataset.
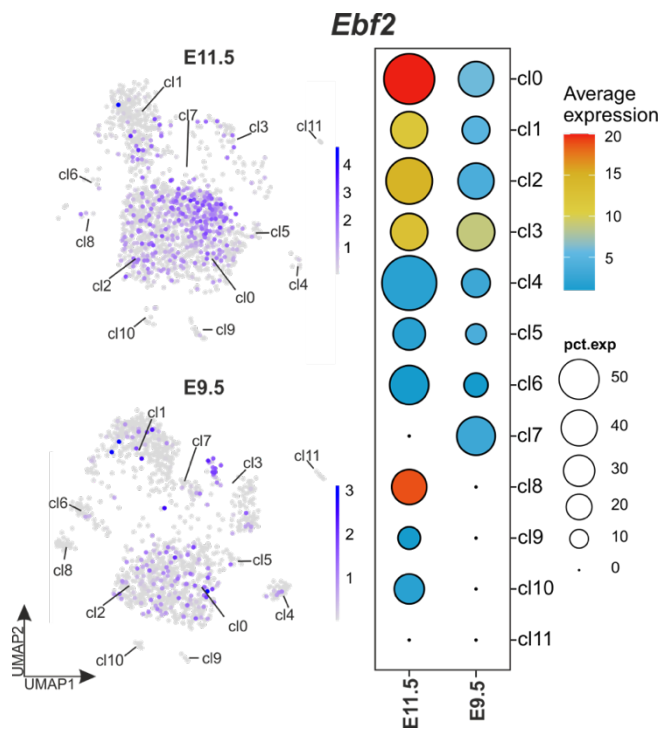
Figure 47: *Ebf2* expression is diminished at E9.5
E11.5 and E9.5 UMAP-feature plots for *Ebf2* are displayed for direct comparison. Obviously, E9.5 demonstrates a smaller number of *Ebf2*+ cells that also follow a random distribution pattern. The dot-plot visualizes and ranks the *Ebf2* expression level among the 11 clusters of both stages. Once more, cl0 of stage E11.5 contains the highest level of *Ebf2*. Notably, the *Ebf2* expression level at E9.5 is comparatively low to stage E11.5.

Nevertheless, the three core clusters of the E9.5 Osr1-object were investigated for adiopgenic potential by using the Angueira-object. Figure 48A displays the project "P3 thoracic aorta"- overview. First, the signatures of the three main E9.5 clusters were used and mapped to the P3 thoracic aorta dataset. Figure 48B demonstrates that cl0 is slightly enriched for the progenitor as well as for the preadipocyte identity. However, recapitulating the signature match from the E11.5-cl0 to the Angueira-object (Fig.18) presented a much better overlap to the fibroblast signatures as shown in figure 48B at E9.5. Cl2 instead, did not significantly change in identity between the E11.5 and E9.5 datasets, not matching the P3 thoracic aorta dataset properly (Fig.18, 48B). Most interesting is that cl1 is highly detectable in the smooth muscle but more importantly in the preadipocyte cluster. This finding could indicate that cl1 represents a more potent progenitor, expressing sigantures of various cell populations as indicated in figure 48B. Second, *vice versa* testing showed that the signatures from the Angueira-object do not match as good as on the E11.5 object depicted in figure 18E. Only cl1 from the E9.5-specimen recapitulates the three fibroblast-signatures to a low extent (Fig. 48C), which is in line with figure 48B. This is an intersting finding since cl1 cells are defined as a smooth muscle-like cell with expression of endothelial progenitor markers: *Kdr* and *Cd34*.
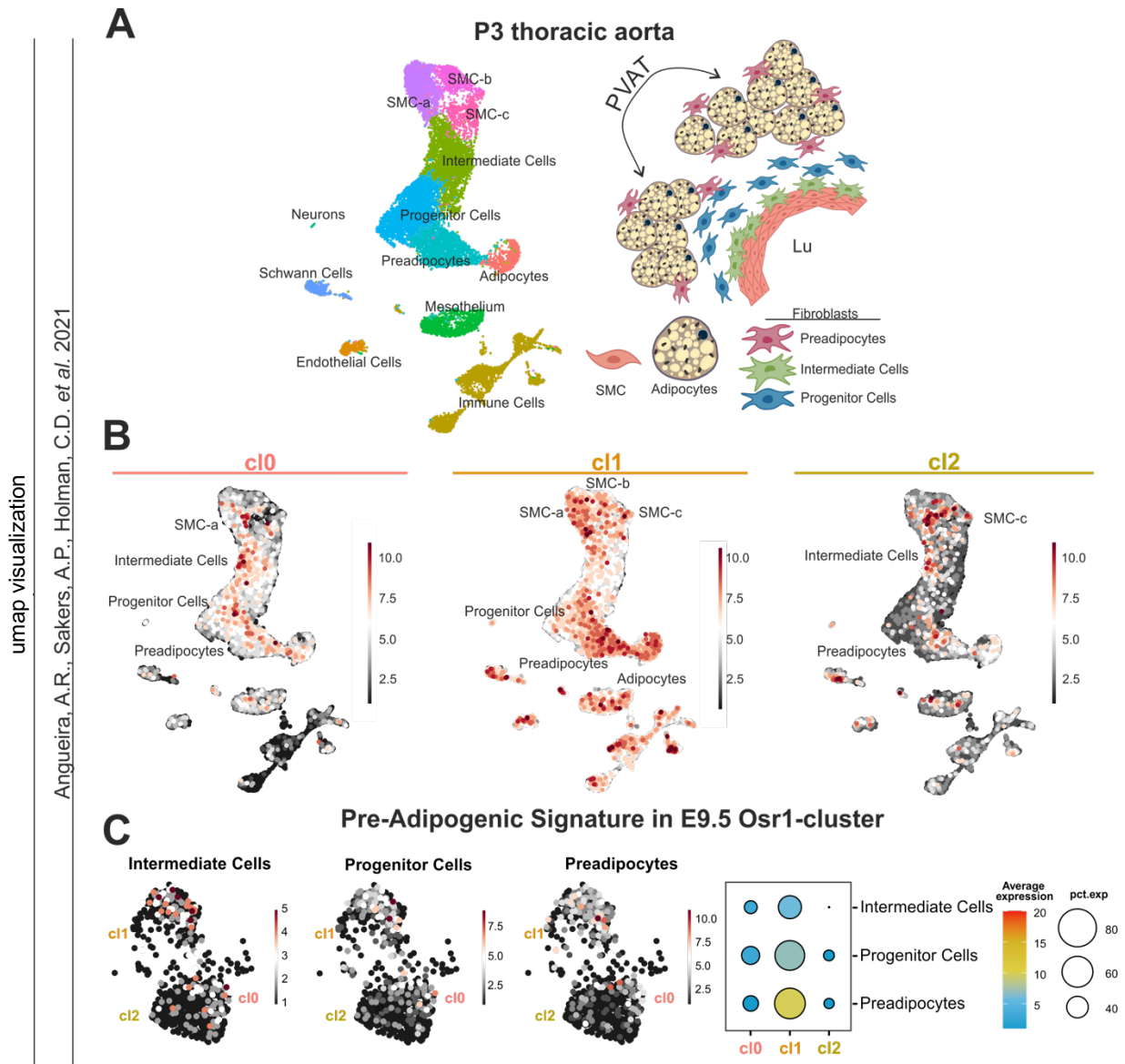
Figure 48: Cl1 could serve as an alternative source for pre-adipogenic progenitors at E9.5
A) shows an overview of the Angueira-object from the P3 thoracic aorta. B) demonstrates the match of the main E9.5 Osr1 cluster signatures to the P3 thoracic aorta object, showing that cl1 clearly recapitulates the reference dataset the best. C) presents the fibroblast signatures from P3 thoracic aorta-dataset in the Osr1-main clusters (cl0, cl1 and cl2). Interestingly, the Intermediate cells-, the Progenitor cells- and the Preadipocyte signature was mainly detected in cl1. The dot-plot recapitulates what is visualized in the Osr1-UMAP-plots. Exclusively cl1 seem to carry pre-adipogenic identity.

4.3.5 The endothelial cluster 6 provides a progenitor pool "the Mesoangioblast" with adipogenic capacity at E9.5

Taken together, these data imply that cl0 and cl2 do not serve as pre-adipogenic progenitor sources as it was observed for E11.5. After all, the smooth muscle- (cl1) and endothelial-cells (cl6) could define a potential root of pre-adipogenic progenitors at E9.5. To test that, considerable signatures for the discussed pre-adipogenic progenitor origins were used on the E9.5 Osr1-object. Figure 49 summarizes how low

the Ebf2 pre-BAT is reflected in the E9.5 dataset. Obviously, the signature is not well represented in the dataset as the scale bare discloses very low expression levels and a diffuse distribution pattern of positive cells. Otherwise, signatures describing the "Mesoangioblast" and "Mesoangioblast- Pericyte" identity (Cossu and Bianco, 2003) seem to specifically match cl6 and to a lesser extent cl1 (Fig. 49B). For direct comparison a dot-plot in figure 49C demonstrates that the Ebf2 pre-BAT signature only matches in the E11.5 cl0 very well. The mesoangioblast identity instead, was exclusively observed at stage E9.5.
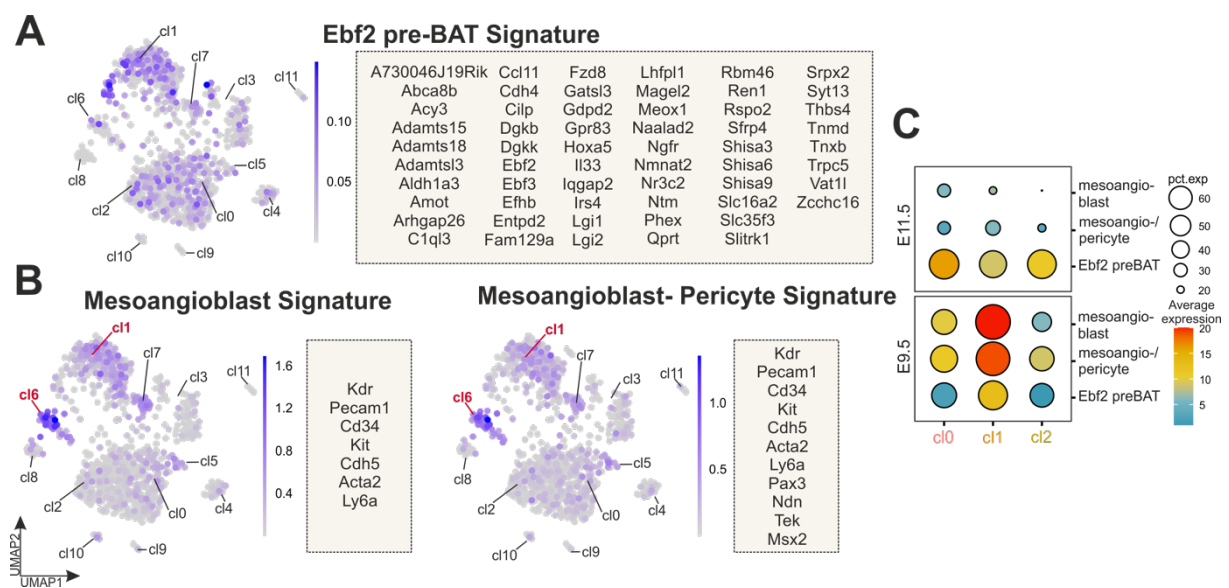
Figure 49: The Mesoangioblast signature is recognized exclusively at E9.5
In A) the Ebf2 pre-BAT signature was tested on the E9.5 Osr1-dataset. The scale bar indicates that the Ebf2 pre-BAT signature is expressed only on a very low level and distributes randomly. The signatures in B) introduce the mesoangioblast identities. Both are well enriched in the endothelium (cl6) and slightly in the smooth muscle like cl1. C) demonstrates that the mesoangioblast signatures are not detected in the E11.5 dataset compared to E9.5. However, the Ebf2 pre-BAT signature seem to be high in the E11.5-object. Only cl1 of the E9.5-specimen implies Ebf2 pre-BAT identity.

These data indicate that stage E9.5 provides an independent source of pre-adipogenic progenitors to the E11.5 Osr1+ cells. To further investigate the idea of an Osr1+ meso-angioblast cell pool at the E9.5, pulse lineage tracing experiments were performed.

4.3.6 Pulse lineage tracing experiments indicate that E9.5 Osr1 progeny provide an independent source from E11.5 to the developing BAT

If Osr1+ cells in the AGM region represent a mesangioblast population, these cells are supposed to migrate to other anatomical locations during the following days of

development. To detect the Osr1+ mesoangioblast cells short pulse lineage tracing experiments using the Osr1$^{CreERt2/+}$; ROSA$^{mTmG/+}$ mouse model were performed. First, the E9.5 Osr1+ cells were chased till stage E10.5 and second, until stage E11.5. Figure 50 displays images of the dorsal aorta in the forelimb and hindlimb region. In both conditions a few mGFP+ cells were discovered to be aligned with the dorsal aorta. Importantly, images of the forelimb region depict that the E9.5 Osr1 progeny resides mainly in organs (Fig. 50.1A, 2, 4) as expected and observed from the OSR1 expression analysis on E9.5 tissue sections (Fig. 42). Furthermore, small vessels in the periphery of the dorsal aorta seem to have proximate mGFP+ cells too (Fig. 50 white arrowheads). Tracing the E10.5 Osr1 population instead, demonstrates lesser density of mGFP cells in the dorsal aorta compartment compared to the E9.5 progeny (Fig. 50.5).
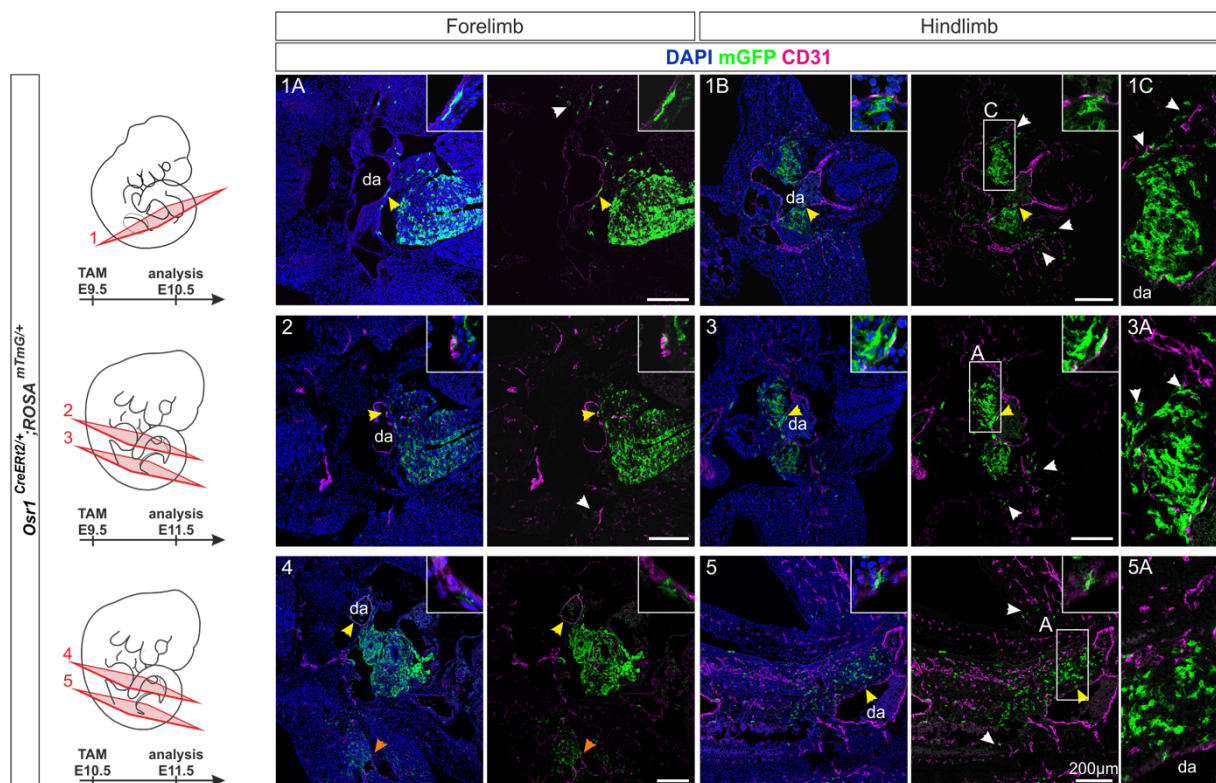
Figure 50: E9.5 Osr1 descendants localize in proximity to the dorsal aorta
The Osr1$^{CreERt2/+}$; ROSA$^{mTmG/+}$ mouse model was used to do pulse lineage tracing experiments. Immunostainings for mGFP (green) to identify the Osr1 descendants and CD31 (magenta) to label the endothelium were conducted in the forelimb and hindlimb region. Yellow arrows indicate mGFP+ cells that are aligned and / or incorporated into the CD31+ endothelium of the dorsal aorta. Section 1A and 1B) represents the lineage from E9.5 to E10.5. Showing that a very few numbers of mGFP arrange closely around the dorsal aorta. The same mGFP distribution pattern was observed for the E9.5 lineage at stage E11.5 in section 2 and 3. White arrowheads mark mGFP+ cells that reside next to smaller vessels in the periphery of the dorsal aorta. The lineage from E10.5 is depicted on sections 4 and 5) of an E11.5 embryo. Here, mGFP+ cells in general seem to be further away from the dorsal aorta and emerge around the forelimb vasculature (orange arrow). da: dorsal aorta

These findings propose that indeed a small population of Osr1+ cells at stage E9.5 arise from the dorsal aorta. In summary the immunostainings could describe the following conceivable scenario: At E9.5 a small subset of OSR1+ PECAM1+ reside in the dorsal aorta. One day later the Osr1+ endothelial population declines and only Osr1 descendants aligned to the dorsal aorta remain. Supportingly, the endothelial cluster 6 at E9.5 holds a significant number of cells but at E11.5, cl6 is strongly decimated (Fig. 15A and 41A). Notably, small mGFP+ colonies of the E10.5 Osr1 lineage were detected close to vessels of peripheral tissues (Fig. 50 orange arrowheads). This can be explained by the gradual process of Osr1+ cells leaving the vasculature and adapting to their surrounding tissue environment (Fig. 51).

E9.5 Osr1+ lineage cells

early muscle mass

pre-adipogenic progenitor

muscle connective tissue
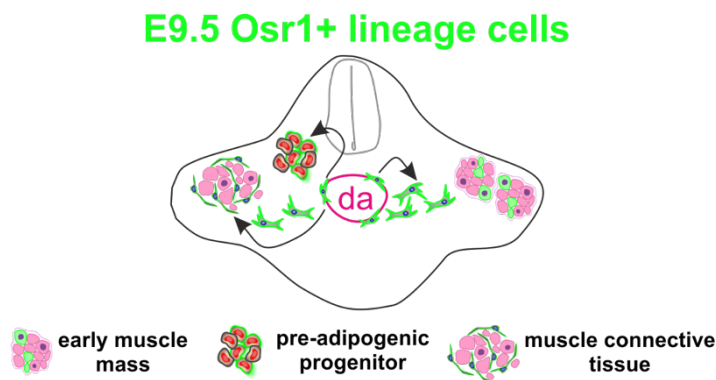
Figure 51: Graphical summary: A subset of the E9.5 Osr1 lineage arises from the dorsal aorta
Gradually, mGFP of the E9.5 Osr1 lineage detach from the dorsal aorta and get recruited from the neighboring tissue which in turn influences the final fate of the Osr1 progeny. da: dorsal aorta

4.3.6.1 The E9.5 Osr1 progeny commit to embryonic BAT at a later stage than the E11.5 lineage

Since pulse lineage tracing experiments uncovered a potential Osr1+ mesoangioblast population, the distribution pattern of the E9.5- and E11.5-progeny needs to be traced longer and investigated more closely. To address that, the Osr1 lineages from E9.5 or from E11.5 were followed to E12.5 (Fig. 52). As expected from the expression data for E9.5 (Fig. 42) or E11.5 (Fig. 17), strong mGFP labeling can be seen in the trachea, esophagus and some parts of the heart. This most likely reflects cells that have been labeled on site and have not changed their position in the tissue. Intriguingly, in peripheral regions, considerably more mGFP+ cells can be traced from E11.5 compared to E9.5, including the proximal limb mesenchyme nearby the vasculature (Fig. 52). This could simply reflect the fact that at E11.5 there are more cells expressing Osr1 and thus amenable to recombination. However, there are two striking differences. Tracing E9.5 cells, already at E12.5, mGFP+ myofibers can be observed in proximal limb muscle (Fig. 52.1C), which is not observed for the E11.5 progeny. This agrees with the lineage tracing data presented in figure 38. And, most importantly, the E9.5 Osr1 lineage was not detected in the area of developing brown adipose tissue yet (Fig. 52.1A), while the E11.5 lineage already shows ample presence in this region. It is important to mention that the cells in the BAT anlagen do not express PPARγ yet. Mainly the E11.5 progeny represents different types of stromal cells in the whole embryo like muscle connective tissue depicted in figure 52.2C and cells in the area of early brown adipose tissue shown in figure 52.2A. However, the broad mGFP distribution pattern of the E11.5 lineage is clearly not myogenic (Fig. 52.2C). Summarizing that, both lineages expand differently and carry distinct capacities, indicating once more that the Osr1+ cells from E9.5 provide an independent progenitor pool to the brown adipose tissue and skeletal muscle.
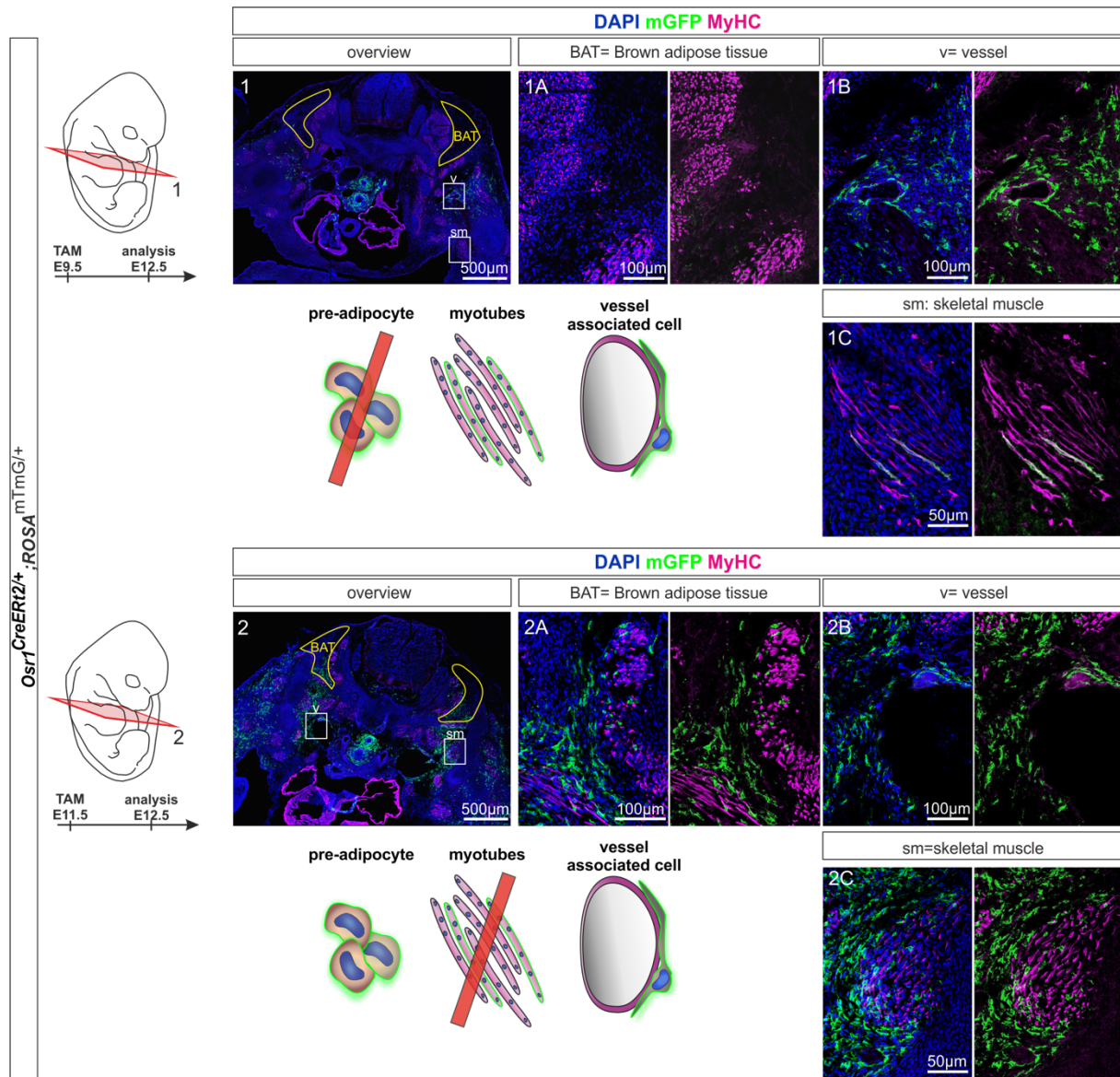
Figure 52: The Osr1 lineages hold distinct differences
The Osr1$^{CreERt2/+}$; ROSA$^{mTmG/+}$ mouse model was used to trace the E9.5- and E11.5- lineage till E12.5. Immunostainings for mGFP (green)- to identify the Osr1 progeny and MyHC (magenta)- to label the myogenic tissue were implemented on comparable cross sections. Section 1 and 2 represent an overview of the investigated regions. The yellow framed area specifies the region of the early BAT anlagen and the white indicated locations show either the vasculature (v) or skeletal muscle (sm). Interestingly, the mGFP+ cells of the E11.5 lineage are high in number and seem to be evenly distributed. The immunostainings confirm that mGFP+ of the E11.5 lineage resides in the area of BAT anlagen (2A) and muscle connected tissue (2A, 2C). Furthermore, 2B) shows that the E11.5 lineage patterns around the cardinal vein. 1A) The E9.5 lineage instead, was not detected in the early BAT anlagen but showed contribution to MyHC+ myotubes (1C). 1B) displays that the E9.5 Osr1 progeny arranged around the limb vasculature and its surrounding tissue.

Finally, the Osr1+ lineages from E9.5 and E11.5 were further investigated to detect first adipogenic contribution. At E14.5 the initial brown adipose tissue anlagen has formed and can be studied for co-expression of PPARγ+ and mGFP+ (Fig. 53). Immunostainings confirm that the E11.5 Osr1 progeny shows a much higher number of mGFP+ PPARγ+ cells compared to the lineage of E9.5. Most probably the

adipogenic contribution of the E9.5 lineage expands later in embryogenesis to reach almost the same level as the E11.5 lineage at embryonic stage E18.5 (Fig. 36).
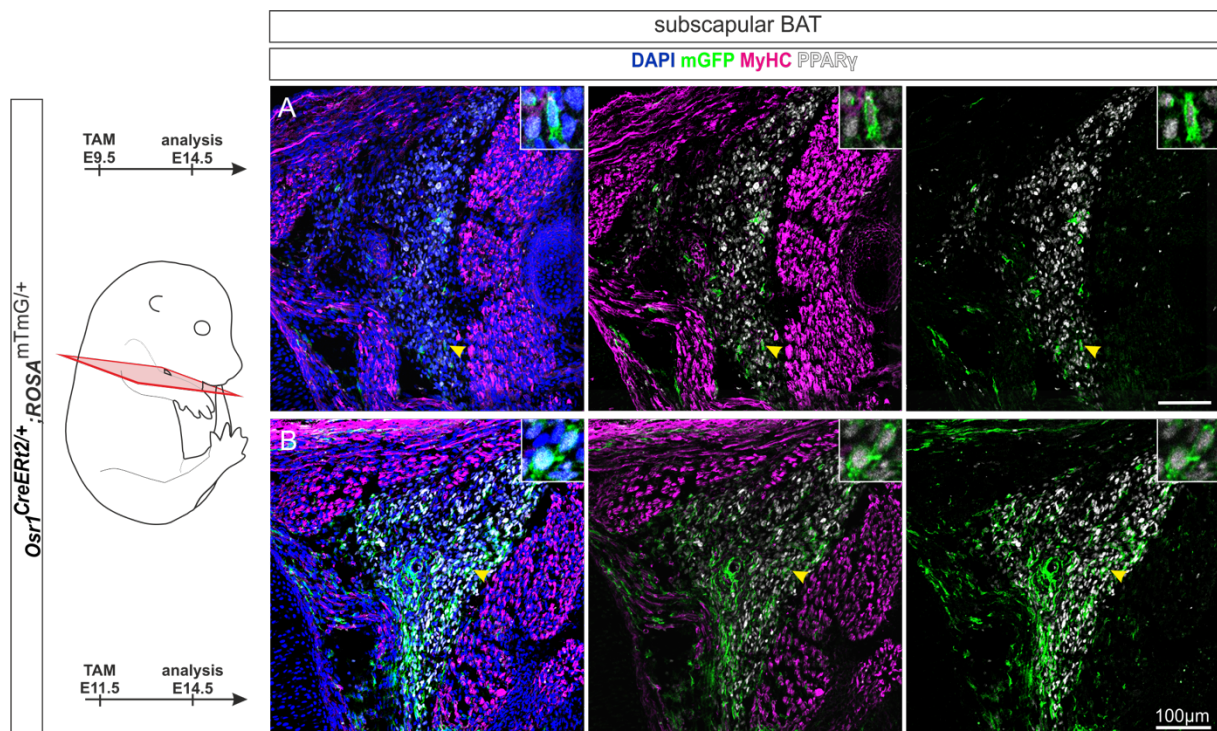
Figure 36: E9.5 Osr1 progeny have lower adipogenic contribution at E14.5 than the E11.5 Osr1 lineage
The Osr1$^{CreERt2/+}$; ROSA$^{mTmG/+}$ mouse model was used to trace the E9.5- and E11.5- lineage till E14.5. Immunostainings for mGFP (green)- to identify the Osr1 progeny, MyHC (magenta)- to label the myogenic tissue and PPARγ (white) to define pre-adipogenic progenitors were performed on comparable cross sections of the subscapular brown adipose tissue. The Osr1 lineage from E9.5 in A) shows less mGFP+ in the PPARγ+ area than the E11.5 Osr1-lineage in B). The yellow arrowhead points at representative PPARγ+ mGFP+ cells which are magnified in the inlays.

4.4 Defining a Osr1+ trajectory tree of the main disparities of the scRNA data

The aim of this study is to shed light on the initial steps of adipose tissue development. To tackle the question which cell types are involved in early adipogenic development the Osr1-sc-object was adjusted. Clusters with neuronal-, hematopoietic- and hepatocyte identity were removed from the Osr1-sc-dataset (Fig. 54A).
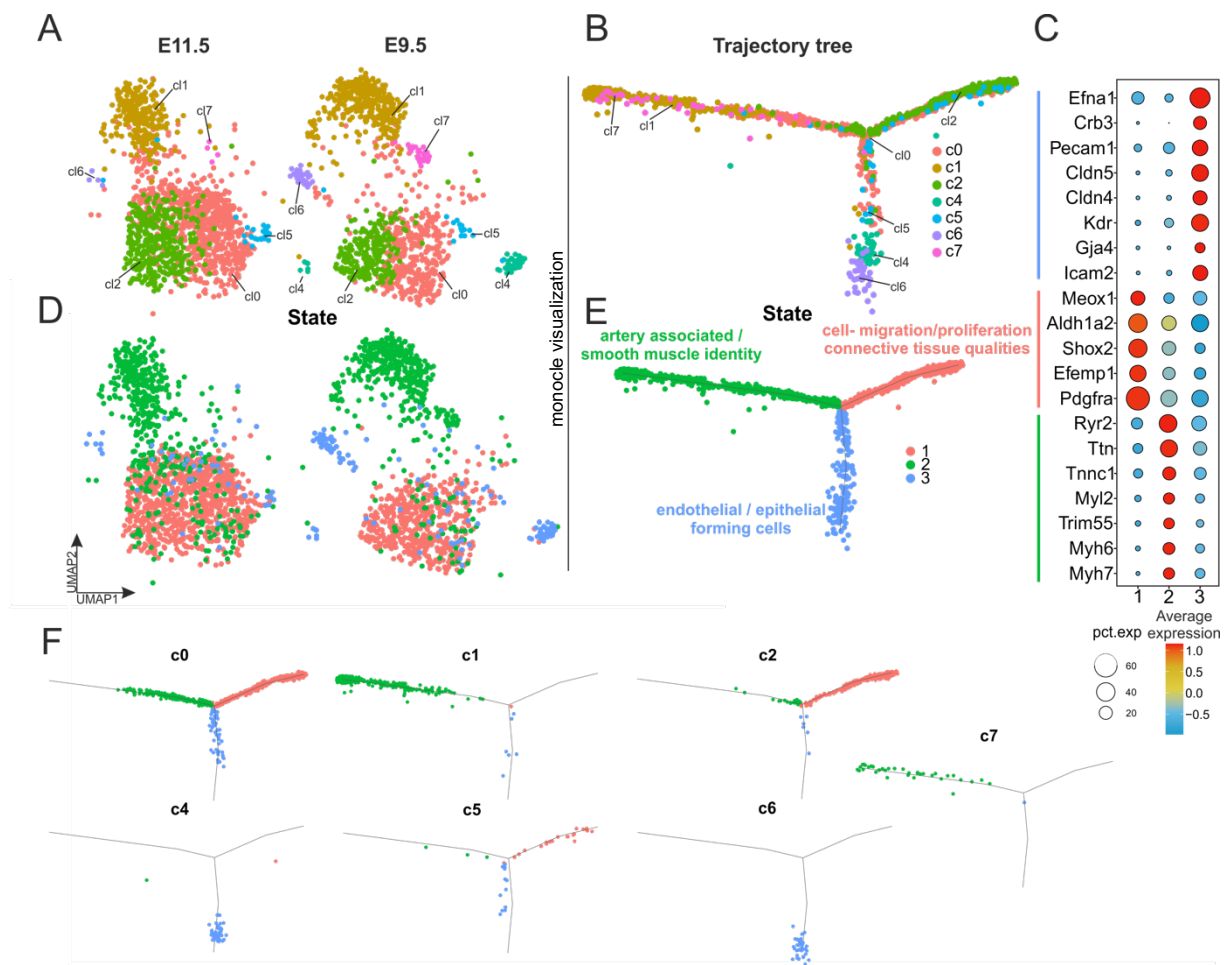
Figure 54: The Osr1-dataset holds three distinctive states
A) represents the adapted UMAP plots of stage E9.5 and E11.5. A computed trajectory tree rearranged all clusters in consideration of their properties in B). C) highlights the signatures of the three possible states. The UMAP plots in D) visualize how the three states arrange along the Osr1-datasets. E) shows that the trajectory tree defines three distinct states which hold different cell type characteristics. Finally, F) highlights where the individual cluster organize themselves and that one cluster can hold more than one state.

The remaining clusters: cl0, cl1, cl2, cl4, cl5, cl6 and cl7 were challenged to arrange into three different states regarding their properties to build a trajectory tree using the monocle tool (Fig. 54B, C, E). Obviously, the three separated arms represent three different states (Fig. 54C). The state 1 signature indicates expression of *Pdgfrα* and *Shox2,* which are associated with connective tissue qualities. In contrast, state 2 is represented through myogenic markers like *Ttn* and *Myh7*. In state 3 the signature genes as *Cldn5*, *Kdr* and *Pecam1* hold epithelial and endothelial features. Figure 54D demonstrates how the three defined states arrange in the UMAP plot compared to the trajectory tree in figure 54B. Interestingly, the states do not necessarily recapitulate the cluster structures (Fig. 54F). Cluster 0 builds the center of the trajectory plot and seems to hold all three states. The smooth muscle like cluster 1 and the cardiomyocytes cl7 represent state 2 only. The proliferative stromal cells of cluster 2 group in state 1

together with a subset of cluster 0. The meningeal cluster 5 is assigned to state1 and 3 since it forms cell sheets and holds mesenchymal characteristics.

This new format simplifies the Osr1-object and combines properties with depiction. Thus, it was necessary to test within the new Osr1-format for the embryonic pre-adipogenic progenitor signatures (Fig. 55). The Ebf2 pre-BAT signature as expected assigns clearly to state 1 of the E11.5 Osr1-dataset. However, the Ebf2 signature was not well represented in the E9.5 cell pool (note the different scale bars in Fig. 55A, top row). That can be explained by the fact that Ebf2 is not detectable in an E9.5 embryo. Instead, both mesoangioblast signatures match perfectly to state 3 and to a much lesser extent to state 2 of the E9.5-specimen (Fig. 55A). In conclusion, at E11.5 the Osr1+ population supplies a fibroblast-like progenitor cell to the developing brown adipose tissue (Fig. 55B).

In summary, the E9.5 Osr1 pool mobilizes an endothelial / smooth muscle arising cell to contribute to the growing skeletal muscle and brown adipose tissue (Fig. 55C).
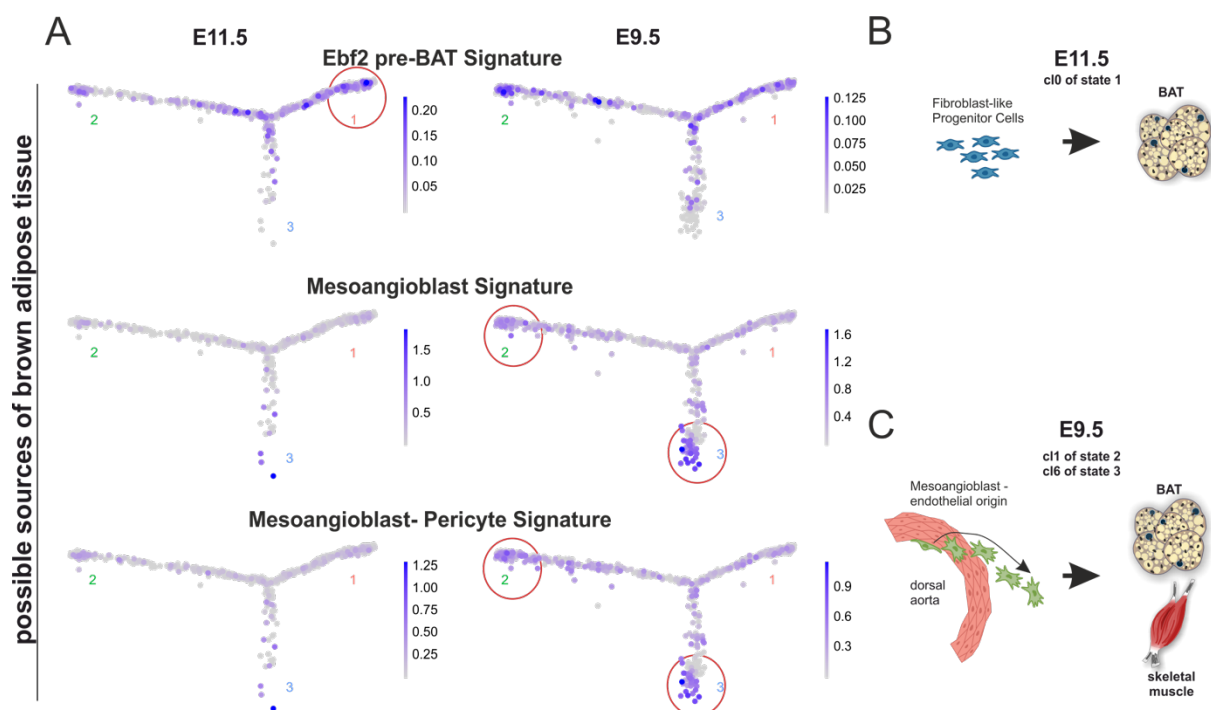
Figure 55: The Osr1+ cell pool changes dynamically and so the source of pre-adipogenic progenitors too
A) the trajectory plots from E9.5 and E11.5 project the three signatures: The Ebf2 pre-BAT signature is specifically enriched in state 1 at E11.5 which is not well represented at E9.5. The opposite was observed for the Mesoangioblast and Mesoangioblast-Pericyte signatures. Those are exclusively recognized at stage E9.5 within state 3 and to a lesser extent in state 2. B) illustrates that at E11.5 most likely a fibroblast-like progenitor cell type serves as a BAT source. C) visualizes that a Mesoangioblast cell with endothelial origin supplies a progenitor pool for skeletal muscle and brown adipose tissue (BAT).

So far, the subject of this work was focused on the identification of pre-adipogenic progenitors in the Osr1-cell pool. Nevertheless, it is still an open issue whether the Osr1 lineage is essential to form adipose tissue. To approach that the adipose tissue of Osr1 knockout embryos was investigated.

4.5 Osr1 mutants show strongly impaired adipogenesis

4.5.1 Embryos that lack Osr1 form smaller fat depots

The $Osr1^{GCE/+}$ mouse line was used to generate Osr1 knockout embryos ($Osr1^{GCE/GCE}$). Embryos that lack Osr1 are lethal at embryonic stage E15.5. Thus, the last possible stage to study the adipose tissue pattern was E14.5. Figure 56A introduces the arrangement of the early adipose depots at E14.5. PPARγ+ cells were counted to assess the size of each depot in $Osr1^{GCE/+}$ and $Osr1^{GCE/GCE}$ embryos. Strikingly, every depot showed reduced numbers of PPARγ+ cells in the $Osr1^{GCE/GCE}$ embryos (Fig. 56B). However, the iBAT and the ingWAT were not as affected as the other fat depots. Supportingly, the observations regarding the iBAT go in line with the lineage tracing data from E9.5 and E11.5 to E18.5 (Fig. 35 lower panel) which confirmed very low contribution to the iBAT.
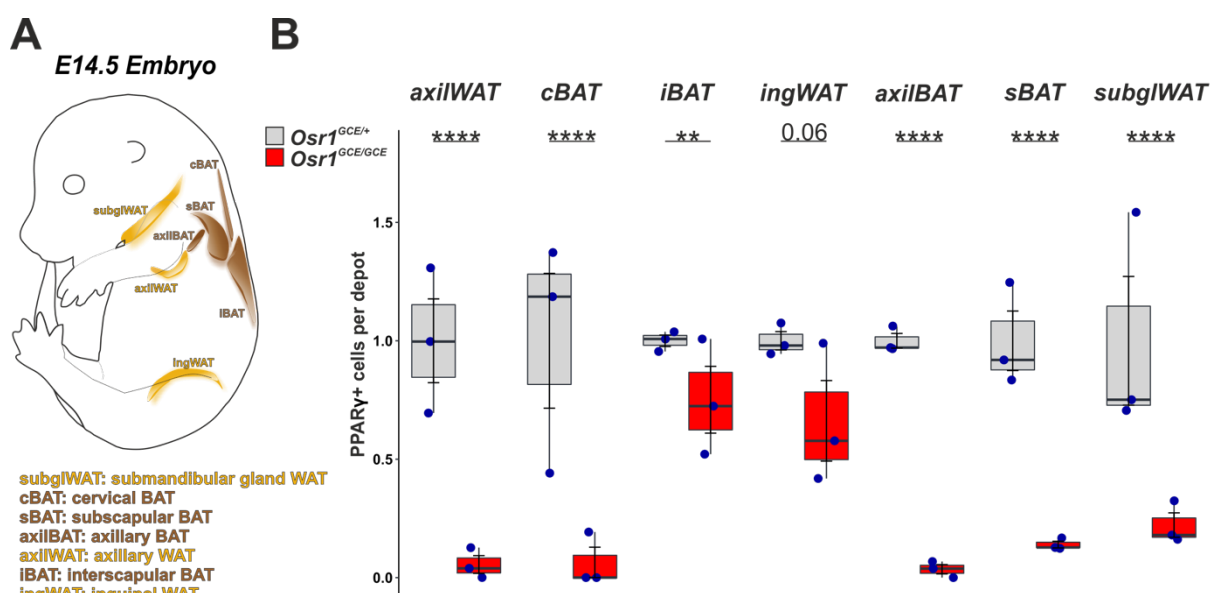
Figure 56: Adipose tissue is remarkably reduced in Osr1 KO embryos
A) shows a schematic representation of the adipose tissue depots of an E14.5 embryo. The box plot in B) illustrates that seven distinct adipose tissues have reduced numbers of PPARγ+ cells per depots in $Osr1^{GCE/GCE}$ (red) compared to the $Osr1^{GCE/+}$ (grey). Data are presented as mean ± SEM (n = 3); statistical analysis was done using two-tailed Student's t tests: * p<0.05, **p<0.001, ***p<0.0001, ****p<0.00001.

4.5.1.1 Osr1 is expressed in distinct locations of the developing adipose tissue

Figure 57 demonstrates the adipogenic phenotype of the brown adipose depots on immunostainings in the Osr1 knockout at E14.5. As already stated above, the $Osr1^{GCE/GCE}$ embryos show decreased numbers PPARγ+ cells in each depot. Another interesting observation is that Osr1-GFP+ cells are detected around the vasculature (Fig. 57A) and in the outer - not center zones of every brown fat depot (Fig. 57A, C, E, G). These observations indicate that the OSR1+ PPARγ+ might be responsible to keep them in a pre-adipogenic and proliferative state to facilitate further depot expansion, whereas OSR1 negative PPARγ positive cells in the center of each depot undergo complete differentiation.
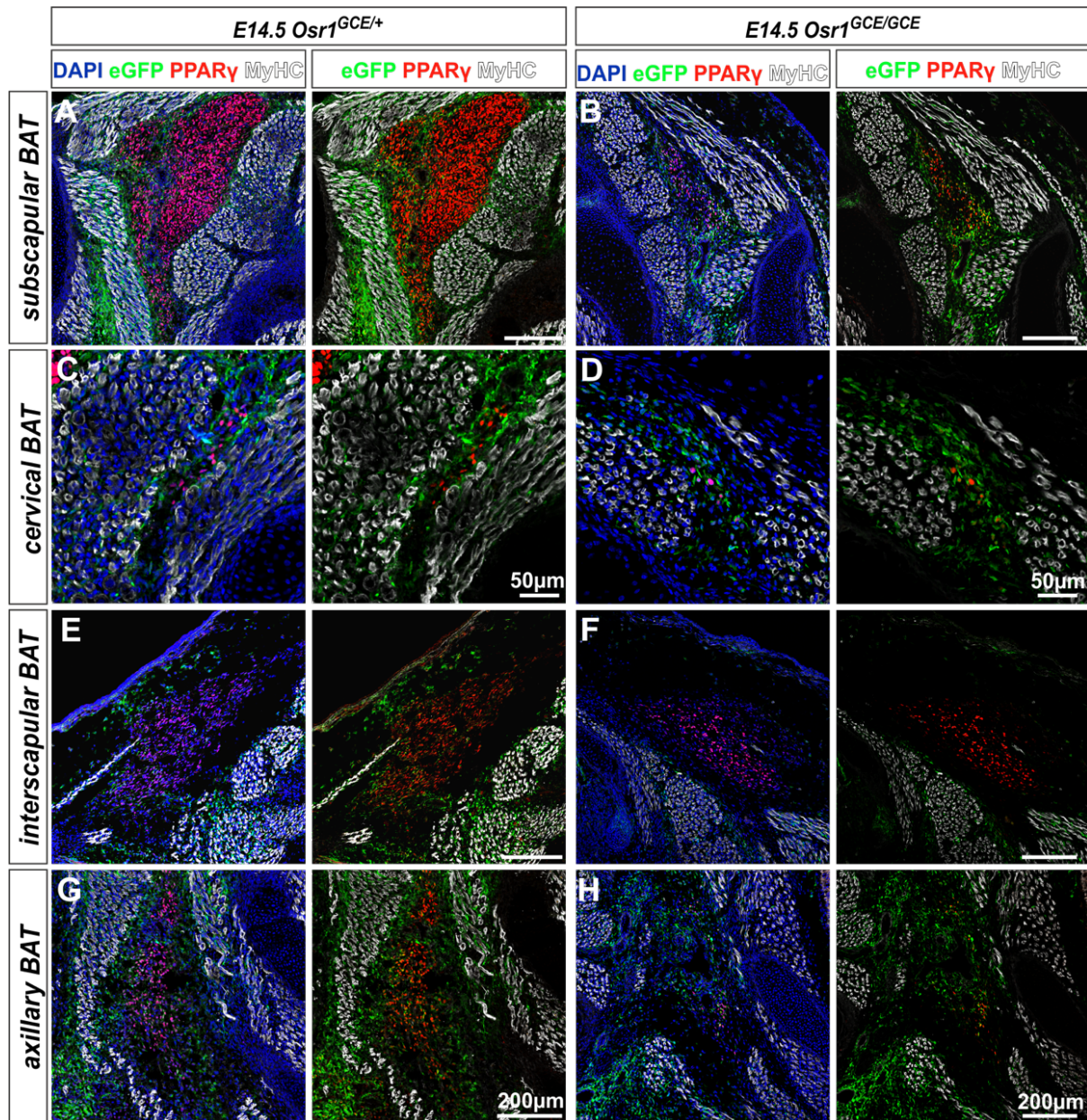
Figure 57: The Osr1 mutant has smaller brown adipose tissues
The left side of the panel exhibits immunostainings from an *Osr1^GCE/+* embryo and the right from an *Osr1^GCE/GCE* embryo at E14.5. The cross sections were labeled for PPARγ+ (red) to visualize the adipogenic cells, MyHC (white) to stain the myogenic tissue and eGFP+ (green) to detect the cells which should actively express OSR1. Each fat depot displays an overlap of GFP+ and PPARγ+ cells in the outer part and/or around the vasculature of the depot- except in image F. Every fat depot of the *Osr1^GCE/GCE* embryo demonstrates a lower number of PPARγ+ cells. BAT: brown adipose tissue

4.5.2 PPARγ+ cells in the Osr1-mutant show a defect in proliferation

To estimate whether Osr1 is indeed affecting the proliferation of PPARγ+ cells, co-immunostainings for PPARγ and the proliferation marker Ki-67 (Ki67) was performed. The KI67+ PPARγ+ cells were counted and normalized to the total number of PPARγ+ cells. Figure 58 summarizes that the number of KI67+ PPARγ+ is diminished in each fat depot of the Osr1 knockout. Notably, fat depots in the *Osr1*^{GCE/GCE} embryo which have significantly reduced PPARγ+ cells also proliferate less (Fig. 58B). These results suggest that Osr1 is involved in the stabilization of the proliferative state.
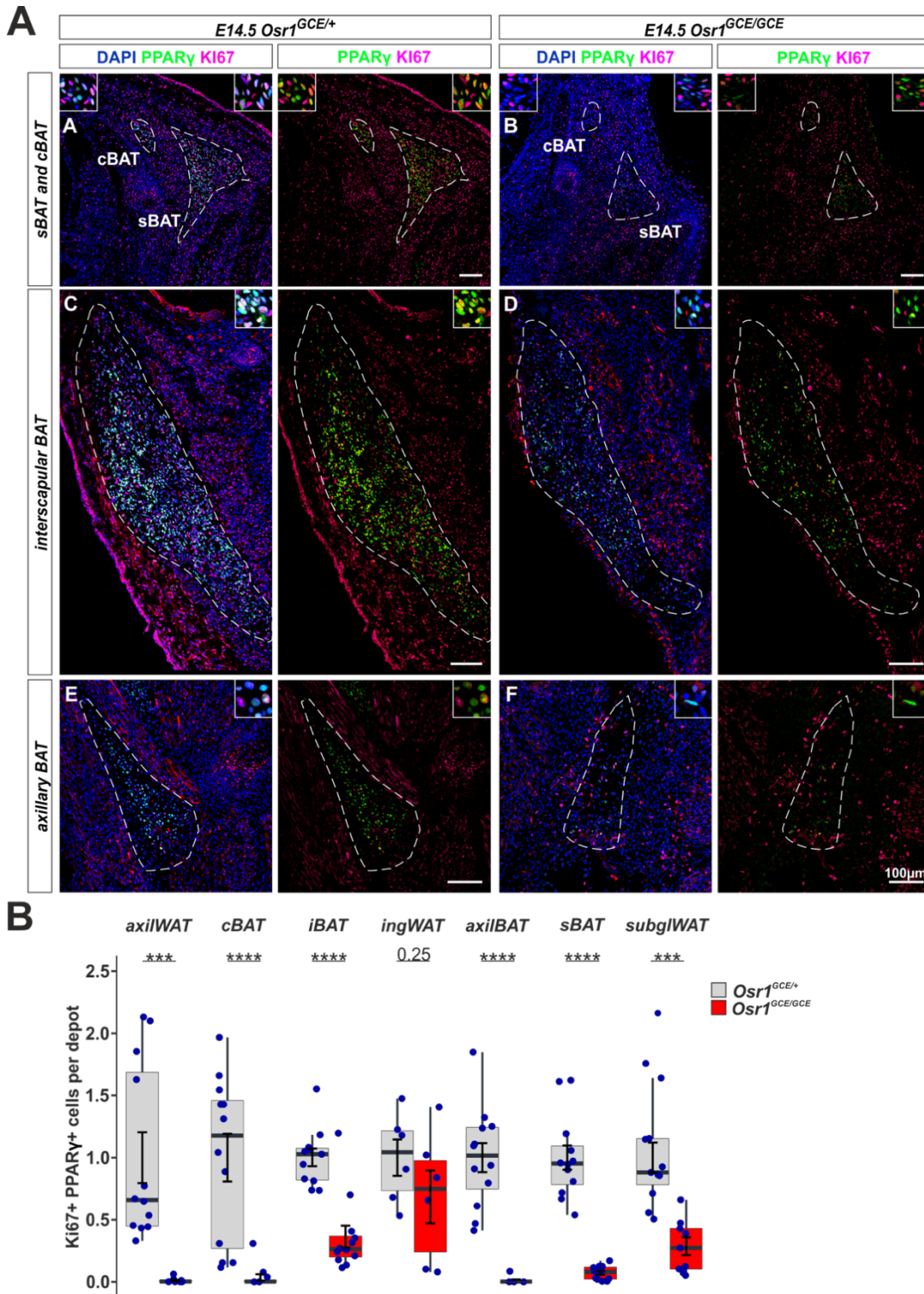
Figure 58: PPARγ+ cells of the Osr1 mutant proliferate less
A) The left side of the panel exhibits immunostainings from a *Osr1*$^{GCE/+}$ embryo and the right from a *Osr1*$^{GCE/GCE}$ at E14.5. The cross sections were labeled for PPARγ+ (green) to visualize the adipogenic cells and KI67+ (magenta) to stain the proliferative cells. The investigated areas are highlighted by a dashed line. The inlays represent co-staining of PPARγ+ and KI67+. The stained sections were quantified for PPARγ+ KI67+ cells relative to the total PPARγ+ population / depot in B). Six fat depots demonstrate a significant reduction of the PPARγ+ KI67+ cell pool in the *Osr1*$^{GCE/GCE}$ (red) embryo compared to the *Osr1*$^{GCE/+}$ (grey) embryo. The inguinal white adipose tissue (ingWAT) instead, displays a mild reduction only. Data are presented as counts/section ± SEM (n = 3); statistical analysis was done using two-tailed Student's t tests: * p<0.05, **p<0.001, ***p<0.0001, ****p<0.00001.

4.5.3 The adipogenic phenotype manifests around stage E12.5 – E13.5

The new arising question is when the adipogenic phenotype would be detectable in the Osr1 knockout? To get first insight, *Osr1$^{GCE/+}$* and *Osr1$^{GCE/GCE}$* embryos of stage E11.5, E12.5 and E13.5 were dissected and FACS sorted for GFP expression (Fig. 59A-B). Immunolabeling introduced the fact that GFP+ pre-adipogenic progenitors reside in specific compartments of the embryonic body. Thus, only those regions were used in the FACS experiment to enrich for pre-adipogenic cells. Known early pre-adipogenic genes were tested in a RT-qPCR analysis to detect the gradual formation of the adipogenic phenotype. Figure 59C displays the expression levels of the adipogenic genes across the three embryonic stages. Obviously, the generated results seem to be not as clear as desired which is because GFP+ cells represent a rather heterogenic cell mix containing only a few pre-adipogenic cells. Nevertheless, the GFP+ from the Osr1-KO at E12.5 (depicted in red) seem to be reduced in *Cebpα, Cebpβ, Cebpδ* and *Dlk1.* Although, a reduction of *Pparγ* is observed first at stage E13.5. *Ebf2*, the marker for brown pre-adipocytes seem to stay unaffected in the Osr1-knockout. These data indicate that the adipogenic phenotype develops between E12.5 and E13.5. However, it is to consider that the isolated GFP+ cells are heterogeneous and not a pure pre-adipogenic population.
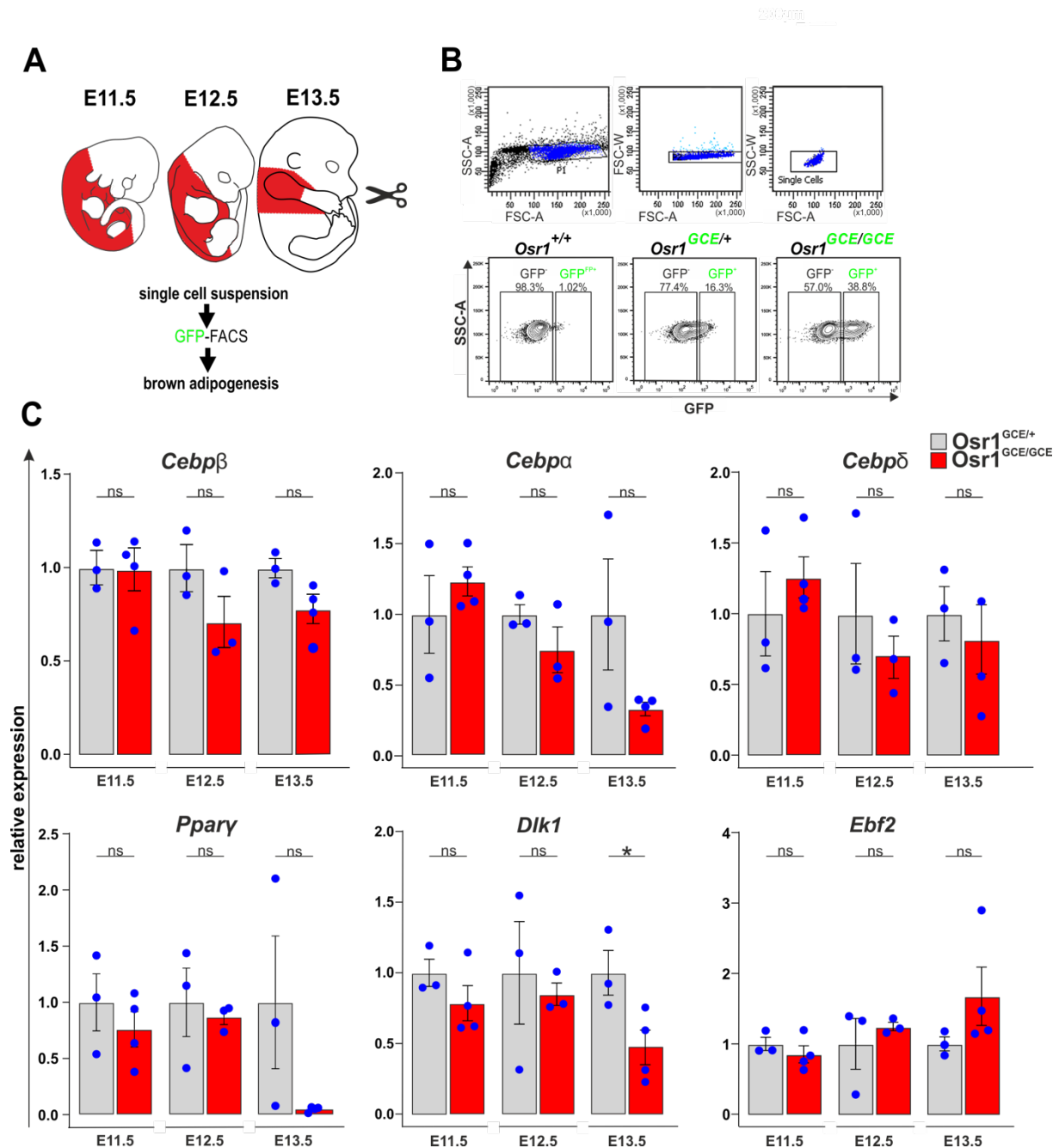
Figure 59: The adipogenic phenotype manifests between E12.5 to E13.5
A) displays the dissected regions (red) of $Osr1^{GCE/+}$ and $Osr1^{GCE/GCE}$ embryos of indicated stages to isolate GFP+ cells *via* FACS. The GFP FACS sorting procedure is illustrated in B). The expression level of pre-adipogenic marker genes was measured in GFP+ cells *via* RT-qPCR and compared between $Osr1^{GCE/GCE}$ (red) and $Osr1^{GCE/+}$ (grey) in C). Gradually, between E12.5 and E13.5 the differences in the pre-adipogenic marker expression levels become more significant among the two groups. Data are presented as mean ± SEM (n = 3 or 4); statistical analysis was done using two-tailed Student's t tests: * $p<0.05$.

4.5.4 Osr1-knockout cells lose their adipogenic potential

Since the RT-qPCR data confirmed that the adipogenic phenotype manifests around stage E12.5 – E13.5. GFP cells from $Osr1^{GCE/+}$ and $Osr1^{GCE/GCE}$ were tested *in vitro* whether they hold or show an altered adipogenic potential. First, the expression pattern

of PPARγ+ and GFP+ in the *Osr1*^GCE/+ embryo at E13.5 was studied (Fig. 60A), highlighting that every detectable fat depot contains a PPARγ+ GFP+ cell pool. Second, GFP+ cells from both genotypes were isolated again from the upper torso and plated with growth medium. Adipogenesis was induced directly on the next day.
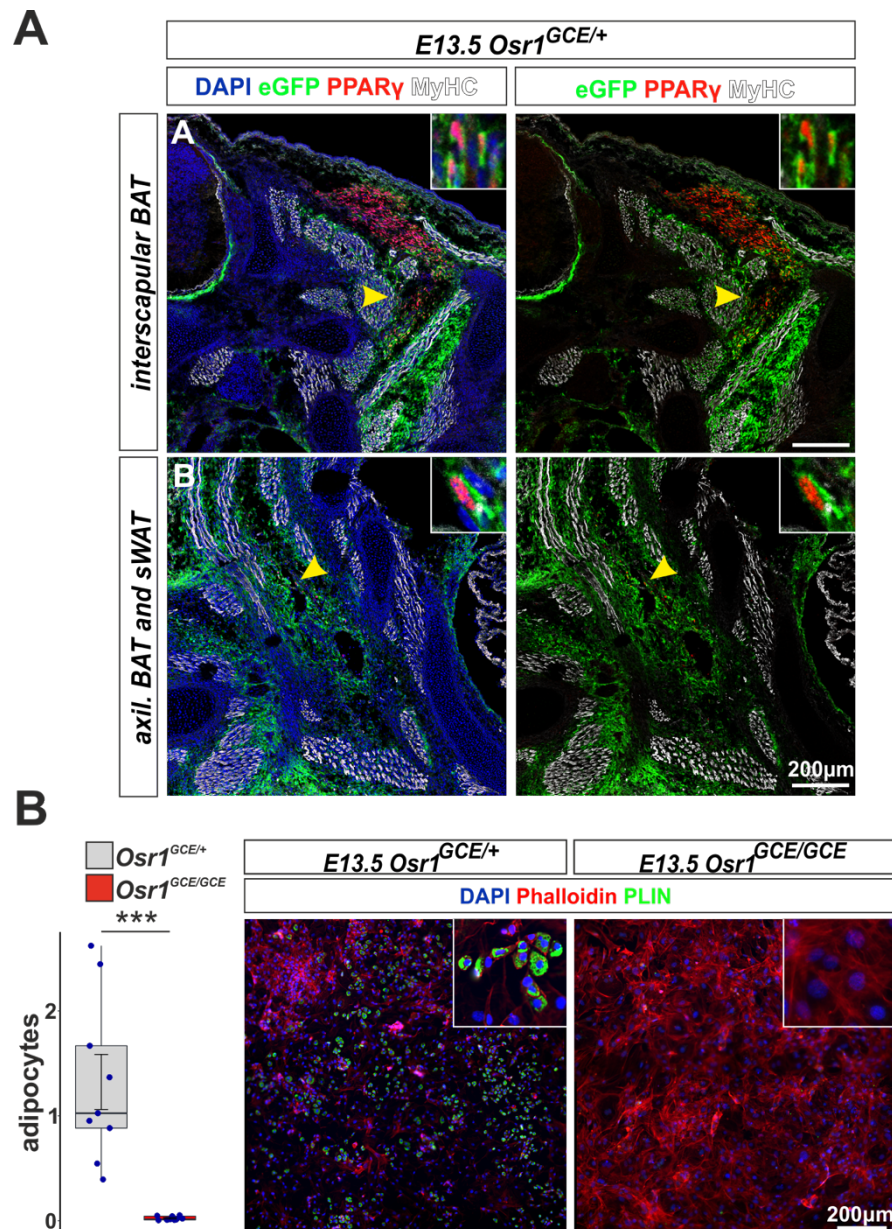
Figure 60: Osr1-knockout cells have reduced adipogenic capacity
Immunostainings on cross sections of an *Osr1*^GCE/+ embryo at stage E13.5 is shown A). PPARγ+ (red) was used to identify the adipogenic progenitors, GFP+ (green) to label the Osr1+ cells and MyHC (white) to stain the myogenic tissue. Two regions are highlighted: (A) the interscapular BAT, (B) axillary BAT and subcutaneous WAT. In both cases co-expression of PPARγ and OSR1-GFP was observed. The magnified area is signified with yellow arrowheads. B) displays the adipogenic capacity of GFP+ isolated cells from E13.5 *Osr1*^GCE/GCE (red) and *Osr1*^GCE/+ (grey) after an *in vitro* adipogenic differentiation assay. Adipocytes were identified with PLIN (green) and the cytoskeleton with Phalloidin (red). PLIN+ cells per total cell numbers were quantified and plotted. The GFP+ cells from the *Osr1*^GCE/GCE (red) embryo have remarkably low adipogenic potential compared to the *Osr1*^GCE/+ (grey) control. Data are presented as mean ± SEM (n = 3); statistical analysis was done using two-tailed Student's t tests: *p<0.05, **p<0.001, ***p<0.0001.

Figure 60B confirmed that the Osr1 knockout cells have remarkably low adipogenic capacity. Only the heterozygous Osr1 cells formed mature adipocytes. Taken together, these data demonstrated that Osr1+ cells show an adipogenic potential, whereas cells that lack Osr1 reveal a diminished adipogenic capacity.

To reproduce these findings in a different experimental design, a brown pre-adipogenic cell line (Wt1) was used. Interestingly, Wt1 cells endogenously express Osr1 (Fig. 61A). Here, a BMP7 stimulus (for 72hs) was used to prime brown adipogenesis. Also, BMP7 was recognized to increase *Osr1* expression after 48hs (Fig. 29). To mimic an Osr1 knockout model siOsr1 was supplemented. Figure 61A displays that *Osr1* knockdown efficacy was not that strong. Only ~50% of the *Osr1* transcripts were successfully removed. Nevertheless, after mature adipocytes appeared, it was tested whether the siOsr1 treated samples had reduced expression levels of mature adipocyte marker genes. Indeed, *AdipoQ*, *Ap2* and *Pparγ* appeared slightly reduced (Fig. 61B). The same was observed for the quantifications of Oil red O stained lipid droplets (Fig. 61C). However, all quantifications were not statistically significant. Very likely, this mild effect can be explained through a low efficient Osr1 knockdown; mind that *in vivo* loss of one Osr1 allele does not produce any obvious phenotype.

The overall essence is that Osr1 is crucial to facilitate adipose tissue development. Firstly, measurements for proliferation demonstrated a reduced rate of proliferative PPARγ+ cells. Secondly, the Osr1-knockout cells at E13.5 diminished their adipogenic potential *in vitro* remarkably. Finally, the $Osr1^{GCE/GCE}$ embryo at E14.5 revealed much smaller fat depots compared to the $Osr1^{GCE/+}$ embryo.

The pending question is: Which lineage misses the *Osr1* expression and thereby fails to commit to the adipogenic fate? Since it has been described that the myogenic pool is a source of brown adipose tissue, it is important to investigate the interaction of Osr1 and the myogenic lineage more thoroughly.
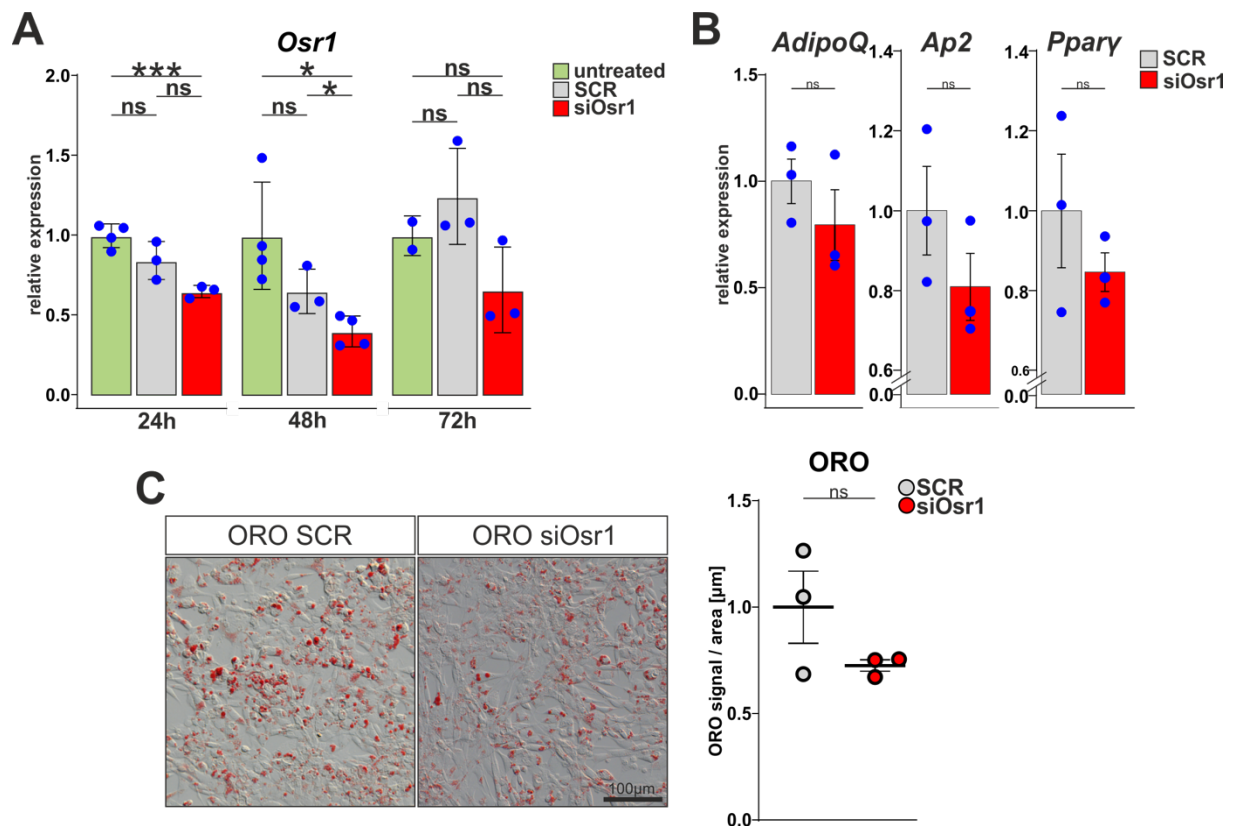
Figure 61: Reduced levels of Osr1 attenuate the adipogenic capacity in Wt1 cells
A) displays RT-qPCR data of *Osr1* expression levels in untreated (green), SCR (grey) and siOsr1 (red) Wt1 cells after 24hs, 48hs and 72hs of the actual Osr1 knockdown. In the meantime, Wt1 cells were stimulated with BMP7 (8nM) to prime brown adipogenic differentiation. Obviously, the Osr1 knockdown reached a maximum of ~50% only. B) The efficacy of adipogenic differentiation was measured between SCR (grey) and siOsr1 (red) treated Wt1 cells *via* RT-qPCR. Genes that represent mature adipocytes were tested: *AdipoQ, Ap2, Pparγ.* A mild reduction of each was detected. The lipid droplet contend was assayed with an Oil red O stain in C). The amount of red stained lipid droplets seems to be slightly reduced in the siOsr1 (red) group compared to SCR (grey) control. Data are presented as mean ± SEM (n = 3 or 4); statistical analysis was done using two-tailed Student's t tests: * p<0.05, **p<0.001, ***p<0.0001.

4.6 Osr1 expression is needed in the myogenic lineage to initiate the adipogenic identity

4.6.1 Osr1 expression is found in the Pax7 lineage at E11.5

The Lepper and Fan paper from 2010 gave the first hint to study the Pax7 lineage together with the actual Osr1 expression pattern to elucidate their relation (Lepper and Fan, 2010) as Osr1 and Pax7 show co-expression at E11.5 (Fig. 21 and 23). Since E11.5 displayed the first PPARγ+ cells, further investigations will be performed on the same or subsequent stages. An inducible lineage tracing model was used: PAX7[CreERt2/+];ROSA26[mTmG/+] to determine the Pax7 lineage. Osr1 was detected *via* the

LacZ reporter cassette in the Osr1-locus. Figure 62 demonstrates that the E9.5 Pax7 lineage patterns at E11.5 in the neural tube and from the very dorsal part of the embryo towards the thoracic cavity and peritoneum, following the maturation process of the dermomyotome and migration of myogenic progenitors. As expected from the previous data, X-GAL+, which represent the Osr1+ cells, colocalize with PAX7+ cells in the dermomyotome derivate at E11.5 (Fig. 23, Fig. 62). This confirmation led to further investigation on the correlation between the Pax7 lineage and the Osr1 distribution profile. Also, it was tested to what extent the Pax7 lineage contributes to brown adipose tissue anlagen. To do so, the E9.5 Pax7 lineage was investigated at stage E12.5, where the niche of the BAT-anlagen was developed.
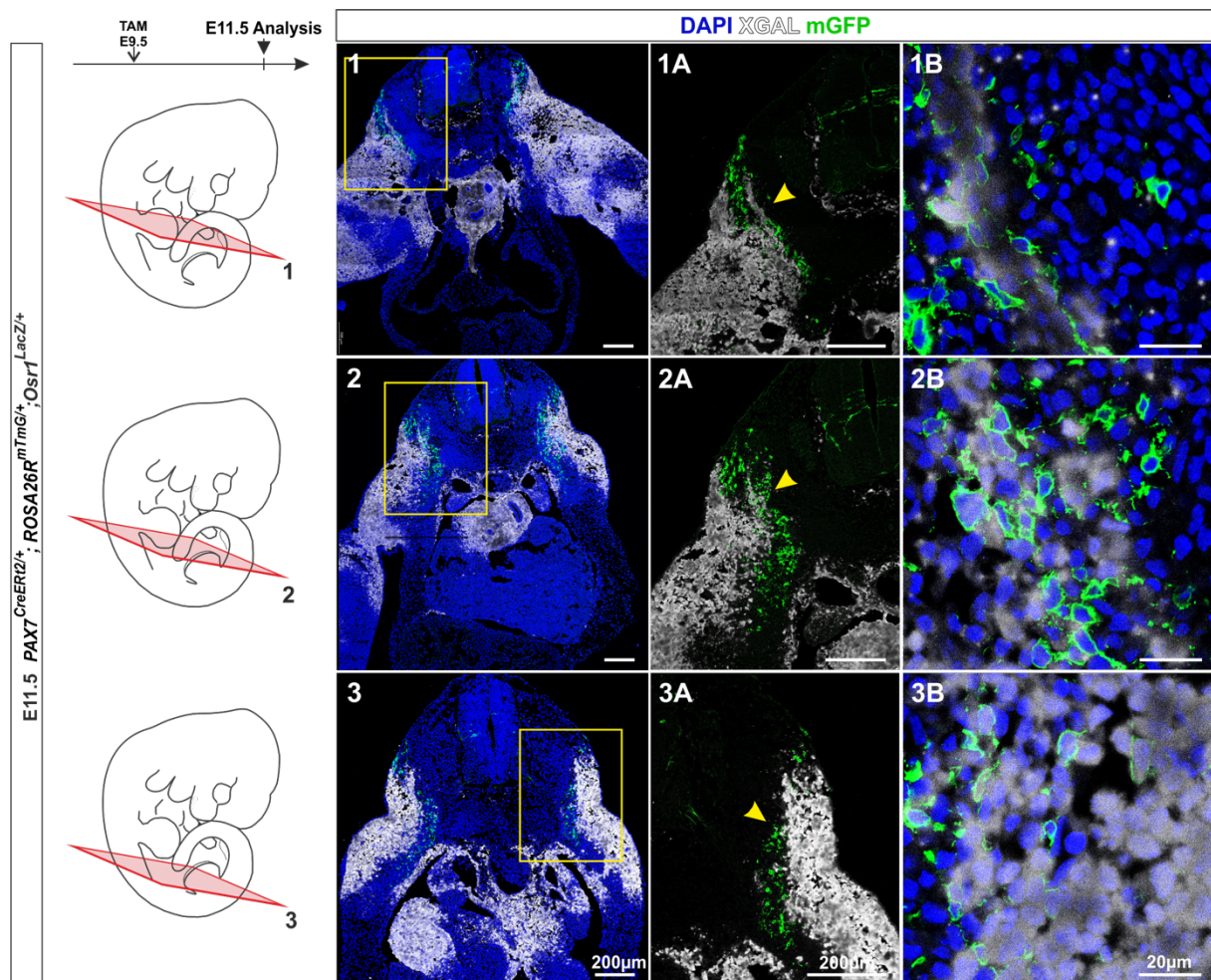
Figure 62: The E9.5 Pax7 lineage co-expresses Osr1 in the dermomyotome derivate at stage E11.5

An X-GAL and immunostaining on cross sections of a PAX7$^{CreERt2/+}$;ROSA26$^{mTmG/+}$;Osr1$^{LacZ/+}$ embryo at stage E11.5 is shown. X-GAL (white) was used to identify the Osr1 expressing cells and mGFP (green) to label the E9.5 Pax7 lineage. Three different regions are depicted: 1), 2) and 3) in which the X-GAL+ cells merge the mGFP+ cell pool exclusively in the dermomyotomal derivate (yellow boxes). The area where Osr1+ cells map with the Pax7 lineage are specified with yellow arrowheads and magnified in 1B, 2B and 3B.

4.6.2 The E9.5 Pax7 lineage reveals low BAT contribution

Figure 63.1 demonstrates that the Pax7-lineage from E9.5 resides in the anatomical region of early BAT at E12.5. Interestingly, the Pax7 progeny in the BAT-anlagen show β-galactosidase activity suggesting that both Osr1 expression and the Pax7 lineage provide a founder pool of pre-adipogenic progenitors. However, Pax7 descendants from E9.5 were also found scattered nearby the abdominal wall, where the initial PPARγ+ cell pool was observed (Fig. 63.2-3). At E12.5, PPARγ+ cells were discovered in the same location as in stage E11.5 intermingling with PAX7+ cells (Fig. 63.2-3). Here, the E9.5 Pax7 progeny was not detected in PPARγ+ cells, instead it was found to label Pax7+ cells in the area close to the abdominal wall defining migrating myoblasts. These findings indicate that at E12.5 the pro-adipogenic Pax7 lineage resides already in the early BAT anlagen to develop brown adipose tissue as depicted in figure 63.1. The work of Lepper et al. stated that the E9.5 as well as the E10.5 Pax7 lineage confirms brown adipogenic contribution only (Lepper and Fan, 2010). This again supports the observation that the pro-adipogenic Pax7 lineage is not found around the abdominal but rather in the early BAT anlagen. To validate the brown adipogenic potential of the E9.5 Pax7 lineage, the adipose tissue was investigated at stage E13.5 (Fig. 63.4). Immunolabeling for PPARγ and mGFP confirmed that the E9.5 Pax7 descendants show a mild contribution to the PPARγ+ pool in the area of the subscapular brown adipose tissue (sBAT). In summary, these data hint that the Osr1+ cells of the Pax7 lineage in early embryogenesis could affect brown fat development.
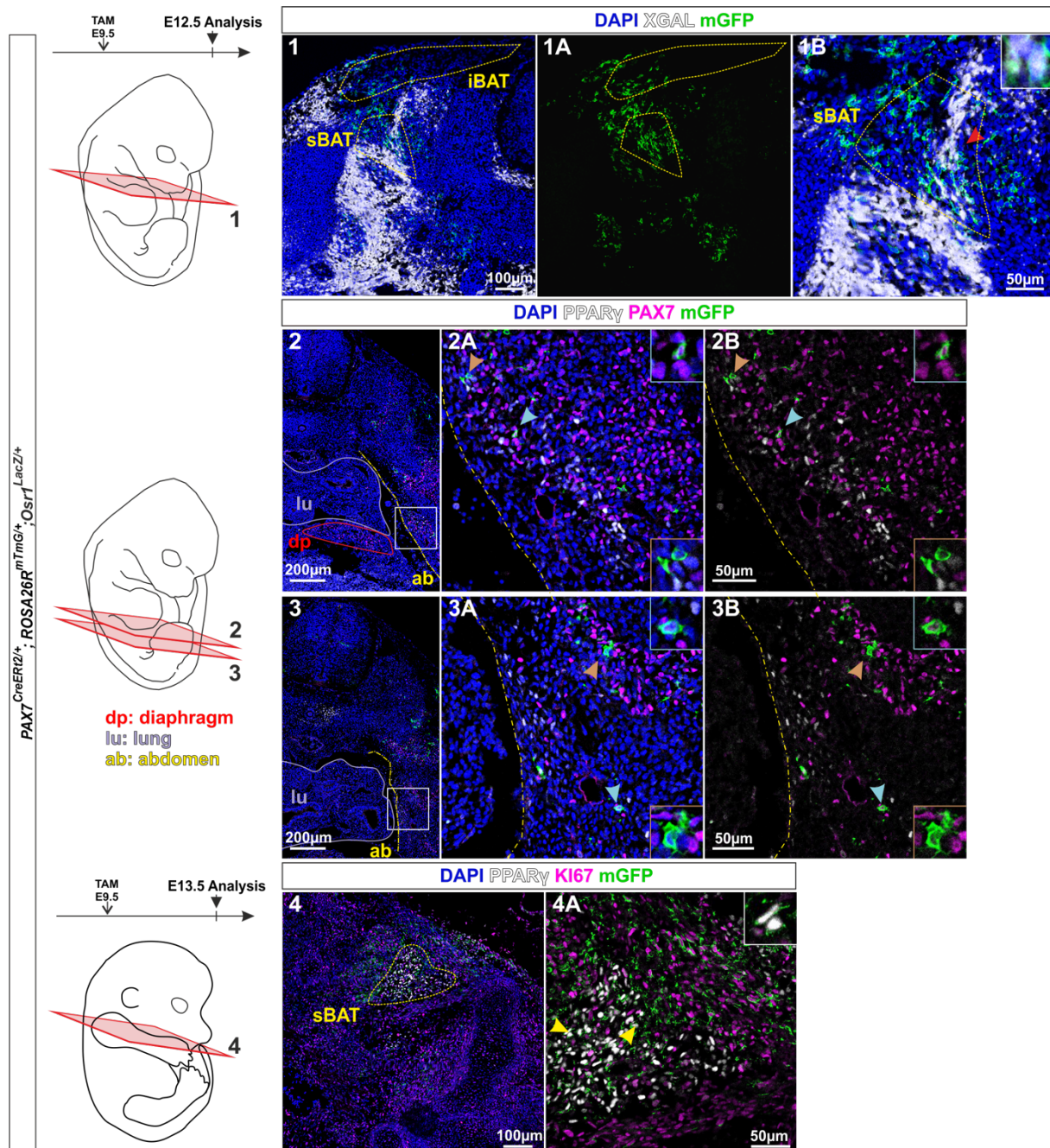
Figure 63: Little number of the E9.5 Pax7 descendants contribute to the early BAT
An X-GAL and immunostaining on cross sections of a PAX7$^{CreERt2/+}$;ROSA26$^{mTmG/+}$;Osr1$^{LacZ/+}$ embryo at stage E12.5 (1-3) and E13.5 (4) is shown. 1) X-GAL (white) was stained to identify the Osr1 expressing cells and mGFP (green) to label the E9.5 Pax7 lineage. The Pax7 lineage locates in the anatomical region of the BAT-anlagen that is indicated with yellow dashed lines. 1B) The red arrowhead confirms the overlap of the Pax7 lineage with Osr1 expressing cells. Of note, the LacZ staining quenches the signal quality of the mGFP. Embryo sections in 2 and 3) focus on the region where PPARγ+ cell cluster. Immunolabeling for PPARγ (white), PAX7 (magenta) and mGFP (green) demonstrates that the Pax7 lineage expresses still PAX7 (light-blue arrowheads) but is negative for PPARγ (orange arrowheads). 4) presents that immunostainings for PPARγ (white), KI67 (magenta) and mGFP+ reveal that a small subset of the E9.5 Pax7 lineage contributes to PPARγ+ cells of the sBAT (yellow arrowhead). dp: diaphragm; lu: lung; ab: abdomen; sBAT: subscapular BAT; iBAT: interscapular BAT

4.6.2.1 The inducible mouse system PAX7^{CreERt2/+};OSR1^{fl/fl} does not show an adipogenic phenotype

For further understand whether the correlation of the Pax7 lineage and Osr1+ expression modulates or primes the pre-adipogenic progenitors, Osr1 was removed from the Pax7 lineage at distinct timepoints (Fig. 64). For this purpose the PAX7^{CreERt2/+};OSR1^{fl/+} mouse was utilized as the control group and the PAX7^{CreERt2/+};OSR1^{fl/fl} mouse as the Osr1 knockout model. In order to ensure targeting of the pre-adipogenic progenitor pool, tamoxifen was administered twice: on E10.5 and on E11.5, when the initial PPARγ cells arise. Only those cells which express Pax7 at stage E10.5 and E11.5 will be recombined and experience the loss of Osr1 but will be able to express GFP instead, under control of the Osr1 promoter. Hence, GFP expression indicates recombined cells that should express Osr1. This genetic modification is stable and will be inherited to their daughter cells. After Cre induction the embryos were analyzed at stage E14.5. Figure 64A displays that the GFP cells (active Osr1-promoter after a recombination event) localize mainly in the area of the sBAT. Of note, only a small subset of GFP+ cells express also PPARγ. The quantification in figure 64B summarizes that the amount of PPARγ+ cells in the sBAT is unaffected.

This finding can be explained by three scenarios: First, Osr1 is not required in the Pax7 lineage to affect the priming process of brown-pre-adipogenic progenitors (Fig. 64). Second, Pax7-CreERt2 is an ineffective recombiner, or the Pax7 lineage targets only a minority of the pool. This is difficulted to discriminate, because all the previous data are generated with the same mouse model.

Figure 64: The Osr1 deficient Pax7 lineage resides in the sBAT exclusively
The control embryo PAX7[CreERt2/+];OSR1^{fl/+} (A1) and the mutant PAX7[CreERt2/+];OSR1^{fl/fl} (A2) embryo were investigated at E14.5. The event of recombination was initiated at E10.5 and E11.5 which is depicted in B). Immunolabeling for PPARγ+ (magenta) was conducted to visualize the fat depots and MyHC (white) to show the myogenic tissue. GFP (green) demonstrates the recombined Pax7 lineage with an activated Osr1 promotor. Noteworthy, only a few GFP+ cells co-express PPARγ+ (light-blue arrowhead). However, they reside in the sBAT depot exclusively. C) demonstrates that the loss of Osr1 expression in the E10.5 and E11.5 Pax7 lineage does not affect the total number of PPARγ+ in the sBAT. Data are presented as mean ± SEM (n = 3); statistical analysis was done using two-tailed Student's t tests: * $p<0.05$.

4.6.3 The Myf5 lineage merges with the actual Osr1 expression pattern in the BAT-anlagen at E12.5

A constitutive myogenic Cre mouse model was used to measure the effect of the Osr1 expression in the myogenic lineage once again. To do so the MYF5[Cre/+];ROSA26[mTmG/+] mouse model was investigated to figure out to what degree the constitutive Myf5 lineage labels the BAT-anlagen (Fig. 65). The embryos were analyzed first at stage E12.5. The Myf5 progeny occupied the complete shoulder gridle compartment, including the highlighted BAT-analgen (Fig. 65.1-2). Interestingly, X-GAL stainings confirm Osr1 expression specifically in the anatomical niche of the BAT-anlagen, matching the Myf5 lineage and concluding that the constitutive Cre model is more suitable to the main concern.
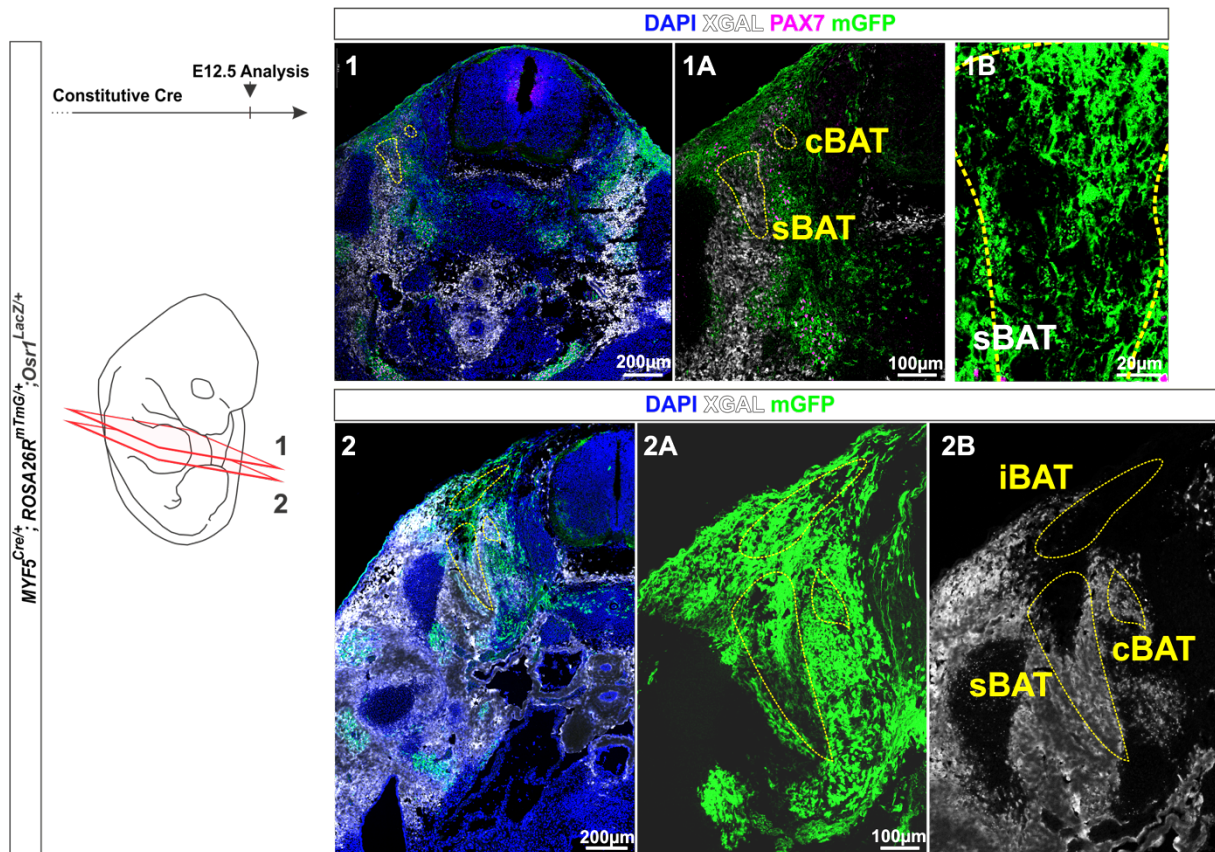
Figure 65: The Myf5 lineage occupies the shoulder gridle compartment at E12.5
An X-GAL and immunostaining on cross sections of a MYF5$^{Cre/+}$;ROSA26$^{mTmG/+}$;Osr1$^{LacZ/+}$ embryo at stage E12.5 is shown in 1 and 2). Two different regions of the forming BAT-anlagen are depicted. X-GAL (white) was used to identify the Osr1 expressing cells and mGFP (green) to label the Myf5 lineage. The mGFP+ cells cover the complete shoulder gridle and reaches out till thoracic cavity. Of note, the LacZ staining quenches the signal quality of the mGFP. Yellow dashed lines indicate the BAT-anlagen which are entirely mGFP+. Interestingly, 2B verifies that the Myf5 lineage and the Osr1+ cell pool merges in the region of sBAT and cBAT. sBAT: subscapular BAT; cBAT: cervical BAT; iBAT: interscapular BAT.

4.6.4 Osr1 deficiency in the Myf5 lineage displays an Osr1 knockout fat phenotype

We then investigated the brown adipose tissue phenotypes in the MYF5$^{Cre/+}$;Osr1$^{fl/+}$ and MYF5$^{Cre/+}$;Osr1$^{fl/fl}$ embryos at stage E14.5 (Fig. 66). Remarkably, we observed that the GFP+ cells, which recapitulate the recombined cells, occupy exactly the space of the cervical (cBAT), subscapular BAT (sBAT) and almost excludes the interscapular BAT (iBAT), confirming again the neglectable contribution of Osr1-expressing cells to this depot. Notably, the GFP distribution pattern correlates with reduction of PPARγ+ cells per fat depot (Fig. 66C), indicating that Osr1 expression in the Myf5 lineage is obligatory to form distinct BAT depots. Also, the MYF5$^{Cre/+}$;Osr1$^{fl/fl}$ BAT phenotype is

very similar to the one observed in the Osr1$^{GCE/GCE}$ embryo (Fig. 57). The sBAT and cBAT showed a strong reduction of PPARγ+ cells, whereas the iBAT was just slightly affected.
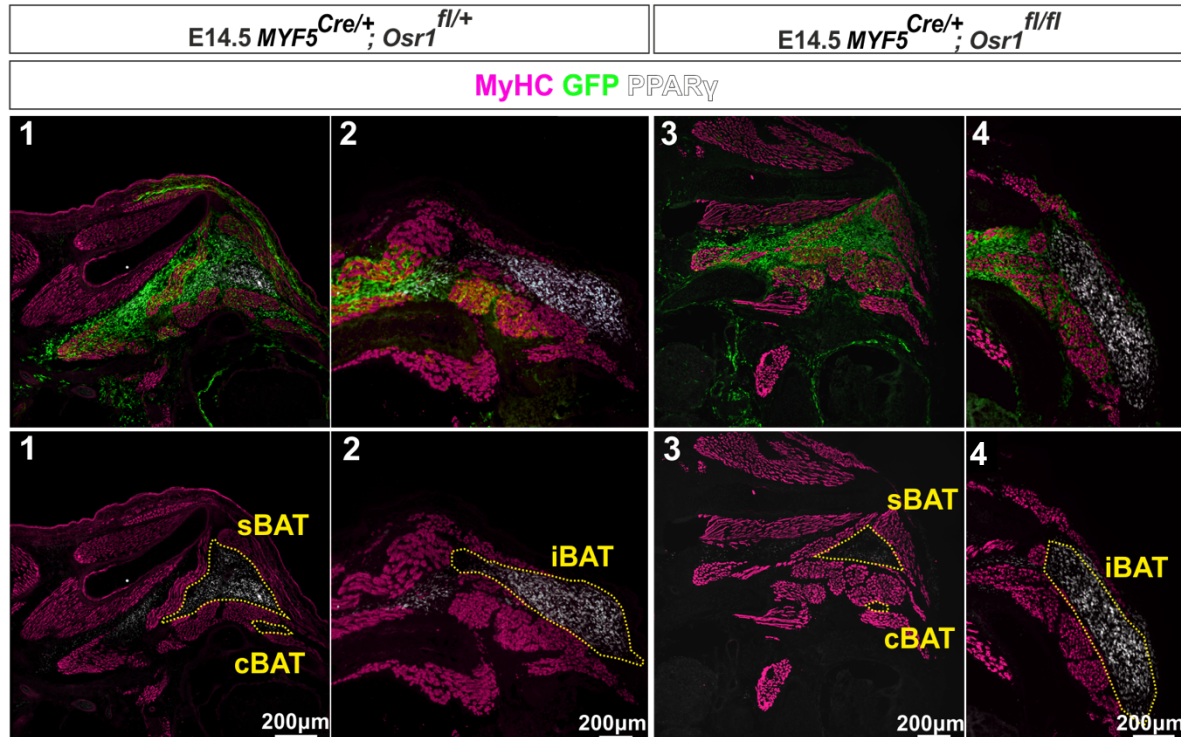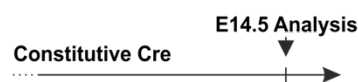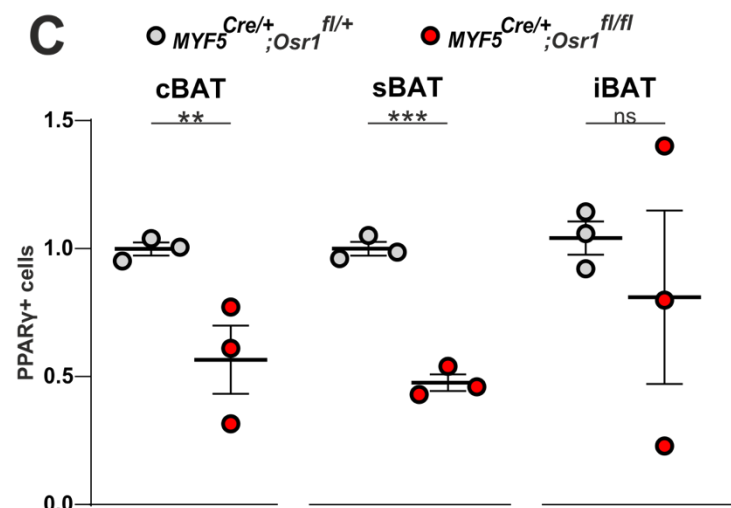
Figure 66: The MYF5$^{Cre/+}$;Osr1$^{fl/fl}$ embryo mirrors the Osr1$^{GCE/GCE}$ BAT-phenotype
The control embryo MYF5$^{Cre/+}$;OSR1$^{fl/+}$ (A-B) and the mutant MYF5$^{Cre/+}$;OSR1$^{fl/fl}$ (C-D) embryo were investigated at E14.5. B) recapitulates the timeline of the experiment. Immunolabeling for PPARγ (white) was conducted to visualize the fat depots and MyHC (magenta) to show the myogenic tissue. GFP (green) demonstrates the recombined Myf5 lineage with an activated Osr1 promotor. The yellow dashed lines define the areas of the different fat depots in A). GFP+ cells pattern in the subscapular space and occupy the sBAT and cBAT (1/3). However, they do not cluster in the iBAT region (2/4). C) demonstrates that the number of PPARγ+ cells per depot is significantly down in the sBAT and cBAT of the MYF5$^{Cre/+}$;OSR1$^{fl/fl}$ (red) embryo compared to the MYF5$^{Cre/+}$;OSR1$^{fl/+}$(grey) embryo. Data are presented as mean of analyzed fat depots ± SEM (n = 3); statistical analysis was done using two-tailed Student's t tests: * p<0.05, **p<0.001, ***p<0.0001, ****p<0.00001.

Finally, the MYF5$^{Cre/+}$;Osr1$^{fl/+}$ and MYF5$^{Cre/+}$;Osr1$^{fl/fl}$ was investigated at a later stage to understand whether the detected BAT phenotype is stable or transient. Figure 67 demonstrates that MYF5$^{Cre/+}$;Osr1$^{fl/fl}$ embryos at stage E16.5 certify that the BAT phenotype is persistent and not transient. Interestingly, immunolabeled GFP cells (i.e. recombined Osr1-expressing cells) cluster around the BAT vasculature and the outer part of each BAT-depot-segment. These compartments have been mainly associated with the stromal vascular fraction which holds the adipogenic progenitors (Brown and Katz, 2019). Also, a DLK1 immunostaining validated that pre-adipogenic progenitors reside in the peripheral parts of the fat depot, similar to the GFP cells (Fig. 67.1C and 2C). These results suggest that the Myf5 lineage may need Osr1 expression to prime the adipogenic progenitors in their niche in order to facilitate adipose tissue growth and preservation. To further support this hypothesis, the MYF5$^{Cre/+}$;Osr1$^{fl/+}$ and MYF5$^{Cre/+}$;Osr1$^{fl/fl}$ was analyzed during adulthood (Fig. 67B). As expected from the previous data, the adipose tissue phenotype is stable. A significant fat depot reduction was observed for cBAT, sBAT and the perirenal white adipose tissue (perireWAT), which only develops after birth. These observations go in line with published data which highlight that the Myf5 lineage is exactly required to develop the three affected depots (Sanchez-Gurmaches and Guertin, 2014a, Sanchez-Gurmaches and Guertin, 2014b). Altogether, the new data demonstrate that the Osr1 lineage influences the adipogenic commitment process in the early Myf5 lineage since a loss of Osr1 results in significantly smaller fat depots.

However, the observations depicted in figure 67 introduce that Osr1 seem to be important in adipose tissue development also postnatally and could therefore also play a role in adult adipose tissue. To investigate that, the Osr1 lineage of E11.5 was analyzed in adulthood.
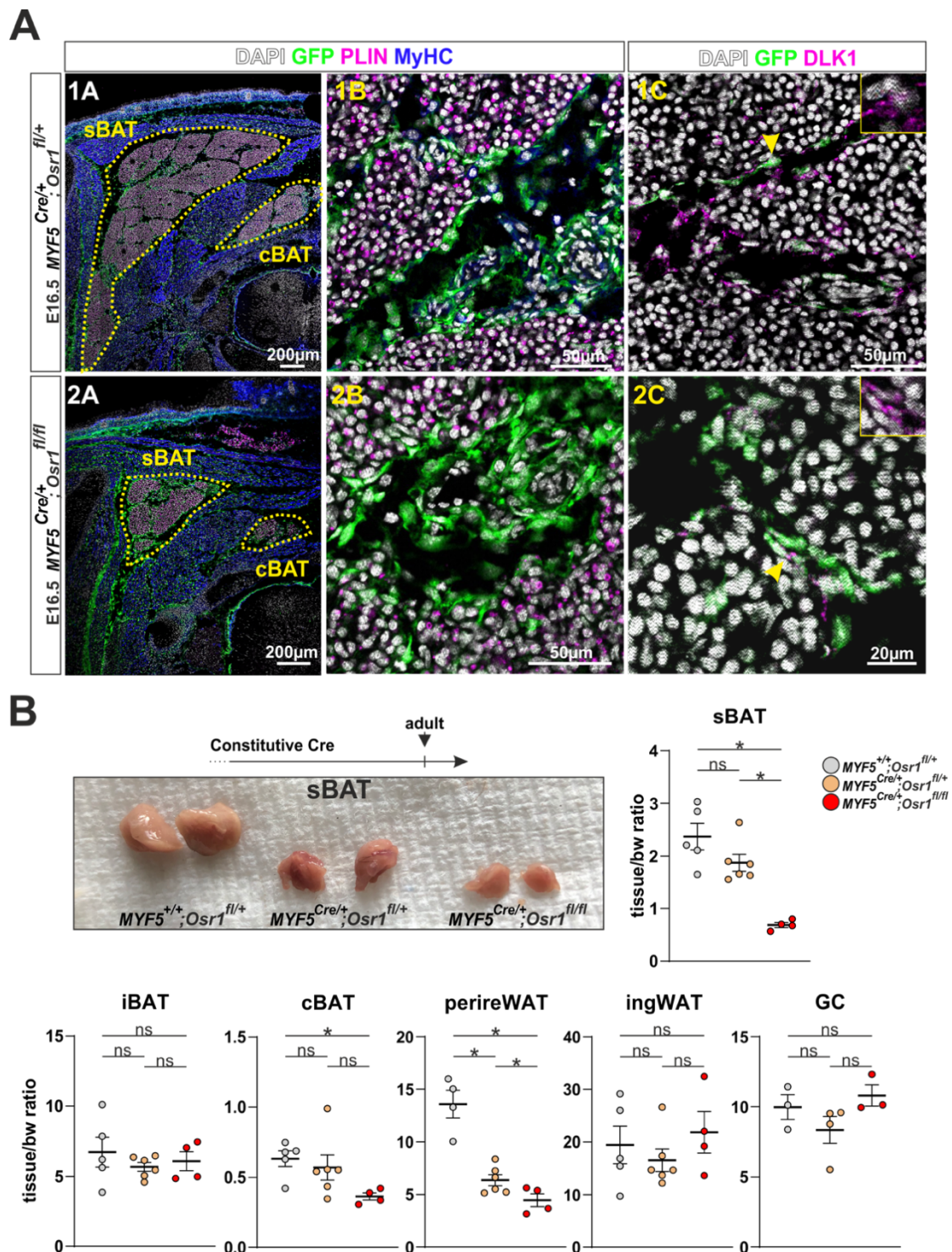
Figure 67: The Osr1 deficient Myf5 lineage displays a persistent fat phenotype
A) The control embryo MYF5$^{Cre/+}$;OSR1$^{fl/+}$ (1A-1C) and the mutant MYF5$^{Cre/+}$;OSR1$^{fl/fl}$ (2A-2C) embryo were investigated at E16.5. Immunolabeling for PLIN (magenta) was conducted to visualize the fat depots and MyHC (blue) to show the myogenic tissue. GFP (green) demonstrates the recombined Myf5 lineage with an activated Osr1 promotor. The yellow dashed lines define the areas of the different fat depots. Obviously, the area of the sBAT and cBAT in (2A) is smaller than in (1A). Furthermore, GFP+ cells pattern in the outer layer of each BAT segment and around the BAT vasculature. The yellow arrowhead in 1C and 2C indicates that GFP+ cells co-express DLK1+. B) depicts the isolated sBAT of adult mice from MYF5$^{+/+}$;OSR1$^{fl/+}$ (grey), MYF5$^{Cre/+}$;OSR1$^{fl/+}$ (beige) and MYF5$^{Cre/+}$;OSR1$^{fl/fl}$ (red). Furthermore, the tissue/bodyweight ratio of indicated adipose tissues and the gastrocnemius (GC) was calculated for the three cohorts. Data are presented as mean ± SEM (n = 3-6); statistical analysis was done using two-tailed Student's t tests: * p<0.05.

4.7 Osr1 is involved in stress response of mature adipose depots

4.7.1 The E11.5 and E12.5 Osr1 lineage contributes to the niche and to mature adipocytes in adult mice

New insights from the investigation of the MYF5$^{Cre/+}$;Osr1$^{fl/+}$ mouse model indicated that Osr1 primes an adipogenic progenitor pool in the myogenic lineage during embryogenesis, may be needed at a later timepoint to promote tissue growth and possibly also adult tissue homeostasis (Fig. 67A). A lineage tracing experiment using the Osr1$^{CreERt2/+}$;ROSA$^{mTmG/+}$ mouse model could shed some light on this thread. Single time point tamoxifen injection proved inefficient for tracing Osr1-descencants postnatally. Thus, for sufficient tracing efficacy, two tamoxifen injection time points E11.5 and E12.5 were chosen. The Osr1 lineage in white and brown adipose tissue was investigated at the age of 11 weeks (Fig. 68). Looking at the results of the sBAT, cBAT and iBAT in figure 68A, it becomes clear that the contribution pattern of the Osr1 lineage did not change. The highest contribution to mature adipocytes was observed in the sBAT (Fig. 55.1) and the lowest in the iBAT. The cBAT ranked in between as expected from prenatal lineage tracing. Furthermore, the thoracic aorta BAT was added to this study that depicts a moderate contribution from the early Osr1-lineage too. The ingWAT recorded almost as many mGFP+ adipocytes as the sBAT. However, the epidydimal WAT, which appears gradually during postnatal life, exhibited as expected a very low contribution from the Osr1 lineage. Remarkably, we observed that in each analyzed adipose tissues the E11.5 and E12.5 Osr1 progeny reside in the αSMA compartments. That once again supports the idea that the early Osr1 lineage provides a pre-adipogenic progenitor pool to a mature fat depot.

A
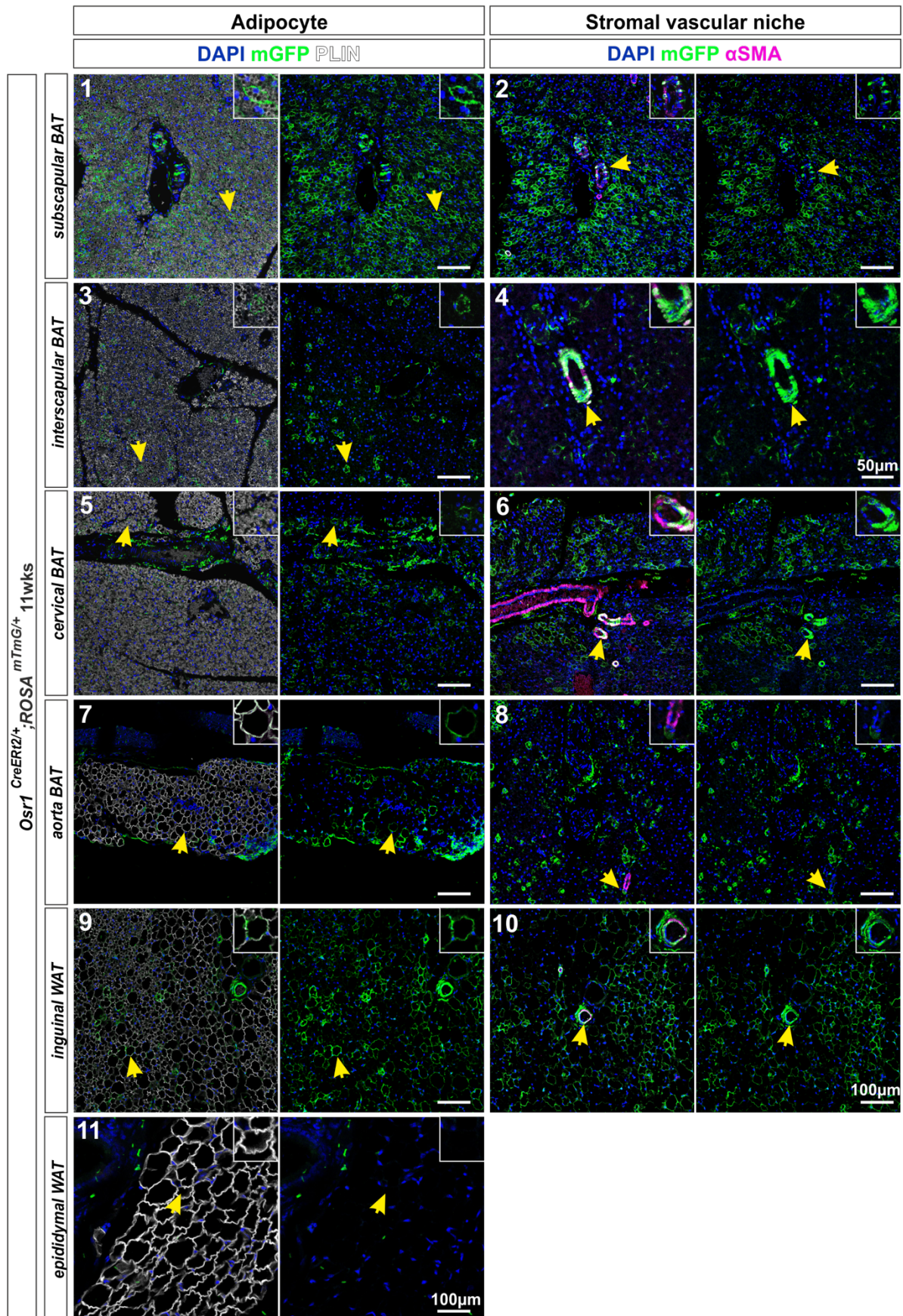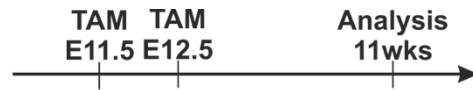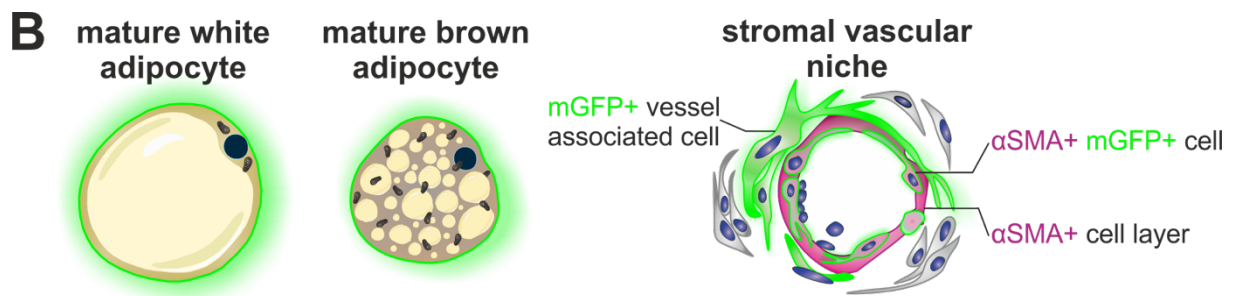
Figure 68: The embryonic Osr1 lineage complements the stromal vascular niche and provides adipocytes to the forming depot
A) displays data from inducible lineage tracing experiments starting from E11.5 and E12.5 till 11 weeks of age on the Osr1$^{CreERt2/+}$; ROSA$^{mTmG/+}$ mice. Immunostainings for PLIN (white), identifies mature adipocytes, αSMA (magenta) detects the smooth muscle layer of the vasculature and mGFP (green) labels the Osr1 lineage. Yellow arrows indicate mGFP labeled adipocytes (left column) and αSMA+ cells (right column) in A). B) summarizes that the Osr1 lineage gave rise to white as well as brown adipocytes. Additionally, mGFP+ cells were also found associated to the vasculature and integrated in the αSMA+ compartment.

To experimentally validate the contribution of embryonically primed Osr1 cells to the stromal vascular fraction (SVF) a FACS analysis was performed (Fig. 69). The total fat depot was dissociated and separated from mature adipocytes. Afterwards the remaining cells were stained for lineage (Lin) markers CD45/TER-119/CD31 to clearance the haemopoietic cells and the endothelium from the stromal fraction. Figure 56b confirmed that the mGFP+ are not detectable in the negative control: Osr1$^{+/+}$;ROSA$^{mTmG/+}$. However, the mGFP+ cells within the Lin- resided exclusively in the SCA1+ cell population, which has been assigned to represent the general progenitor pool (Cho et al., 2019, Joe et al., 2009, Angueira et al., 2021). This observation is repeated in the other adipose tissue samples, indicating that the Osr1 progeny from E11.5 and E12.5 specifically provide progeniture cells to the SVF of mature adipose tissue. Once again, the recognized portion of SCA1+mGFP+ in the BAT-SVF was the highest in the sBAT and lowest in the iBAT. Interestingly, the detected Sca1+mGFP+ cell pool was even bigger in the inguinalWAT depot (~50%). In contrasts, the mesentericWAT revealed a very small Sca1+mGFP+ population, which was expected since the mesentericWAT is formed during postnatal life.
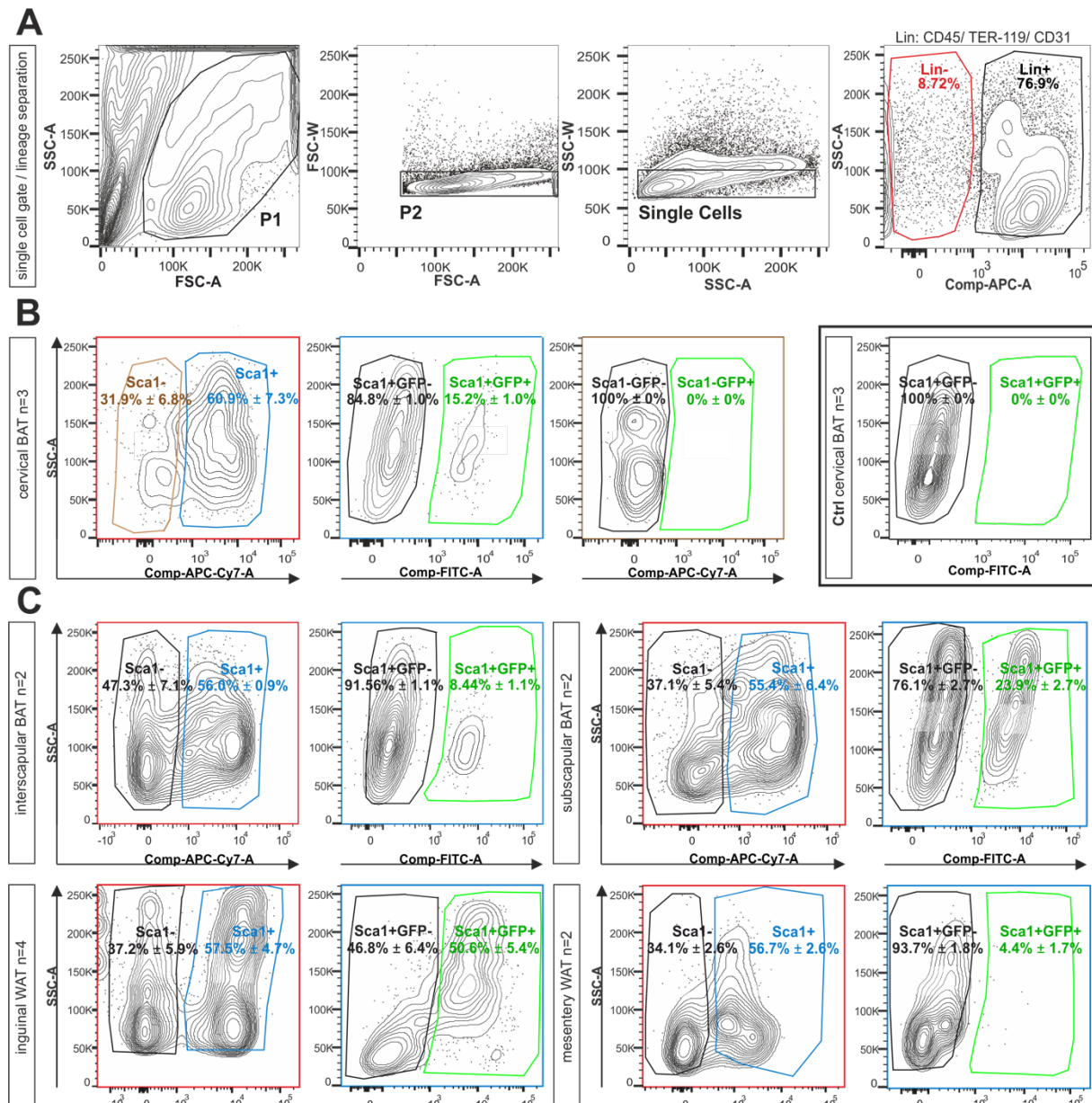
Figure 69: FACS data support that the E11.5 and E12.5 Osr1 progeny merge with the Sca1+ cell pool in the stromal vascular niche

FACS data from inducible lineage tracing experiments starting from E11.5 and E12.5 till 11 weeks on the Osr1$^{CreERt2/+}$; ROSA$^{mTmG/+}$ mice are depicted. A) shows the gating procedure to identify the single cell pool and the separation of Lineage+ (LIN): CD45/TER-119/CD31 cells from the Lin-population. B) presents scatter pots from the cervical BAT indicating that ~60% of the Sca1+ cell pool holds ~8% of Sca1+mGFP+. Of note, the Sca1- population is negative for the Osr1-lineage. Also, the control Osr1$^{+/+}$;ROSA$^{mTmG/+}$ mouse (Ctrl) confirmed that the Comp-FITC-A signal was not detectable. C) displays a collection of the approximate proportion of Sca1+mGFP+ in white and brown adipose tissues. Data are presented as mean ± SEM (n = 2-4).

In summary, the generated results from FACS and immunostainings confirm that indeed the E11.5 and E12.5 Osr1 lineage expresses SCA1+ and αSMA+ in the stromal vascular compartment of adipose tissue (Fig. 69A and 70B). Thus, it appears that the Osr1 lineage has an even greater relevance in the process of organogenesis and tissue homeostasis during embryonic fat depot specification than expected.
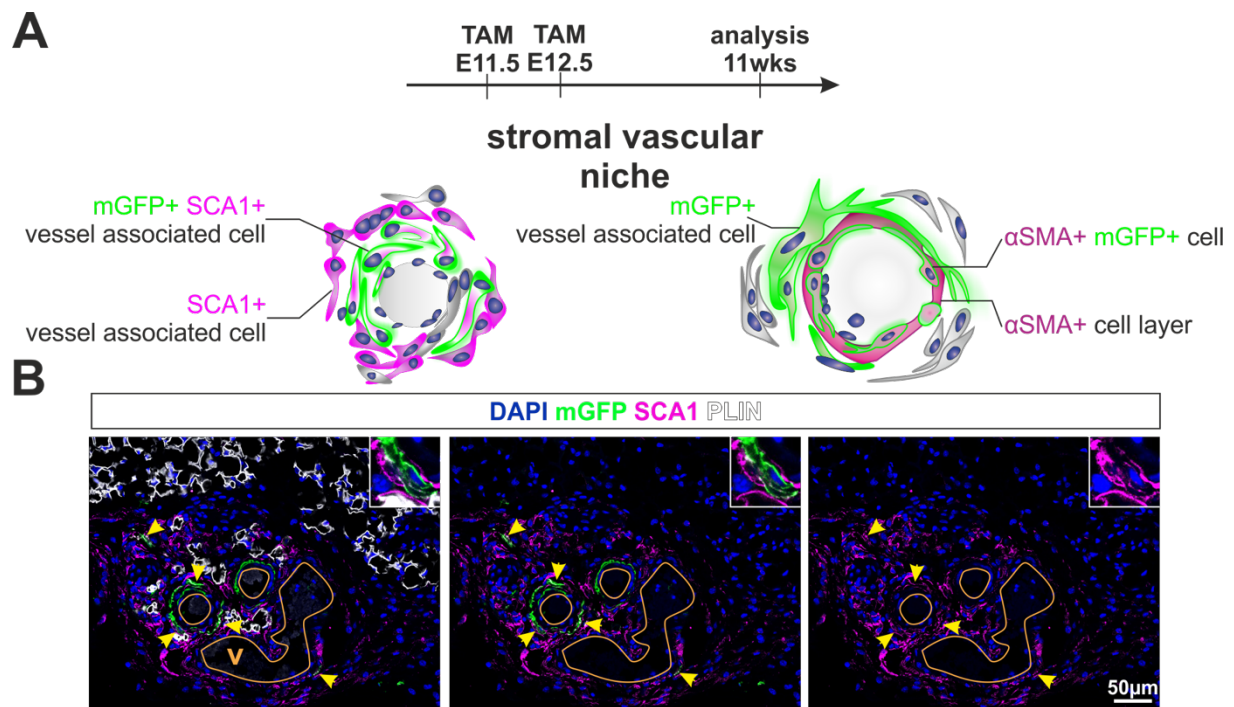
Figure 70: The embryonic Osr1 lineage resides in the stromal vascular nice
A) summarizes that the E11.5 and E12.5 Osr1 lineage primes cells which express SCA1+ or αSMA+ and reside in the vasculature compartment of mature adipose tissue. Immunolabeling in B) show PLIN in white, SCA1 in magenta and mGFP in green. Yellow arrowheads indicate that mGFP+ cells co-express SCA1+ and cluster around the vasculature.

Considering the latest findings, it was an urgent issue to find out whether Osr1 is detectable and if so -what characteristics define the Osr1+ cell pool in mature adipose tissue?

4.7.2 Osr1 marks cells in the stromal vascular fraction

To get a first impression of how the Osr1+ cells pattern in the adipose tissue an Osr1-LacZ reporter mouse (Osr1$^{LacZ/+}$) was used. A whole mount X-GAL staining on interscapular BAT and inguinal WAT (Fig. 71A) suggests that the Osr1+ population resides along the vascular network. Magnifications of both fat depots confirmed that the X-GAL+ cells cluster exclusively around the vasculature. Furthermore, since mature adipocytes did not show β-Galactosidase activity it can be concluded that Osr1 expression seem to be silent. Interestingly, the Osr1+ cells in the thoracic aorta BAT gave a very strong signal in its smooth muscle compartment. These observations were correlated with a reference single cell dataset of the P3 and adult thoracic aorta from Angueira et al. (Fig. 71B) to develop a better understanding of the Osr1+ cell pool in mature adipose tissue.
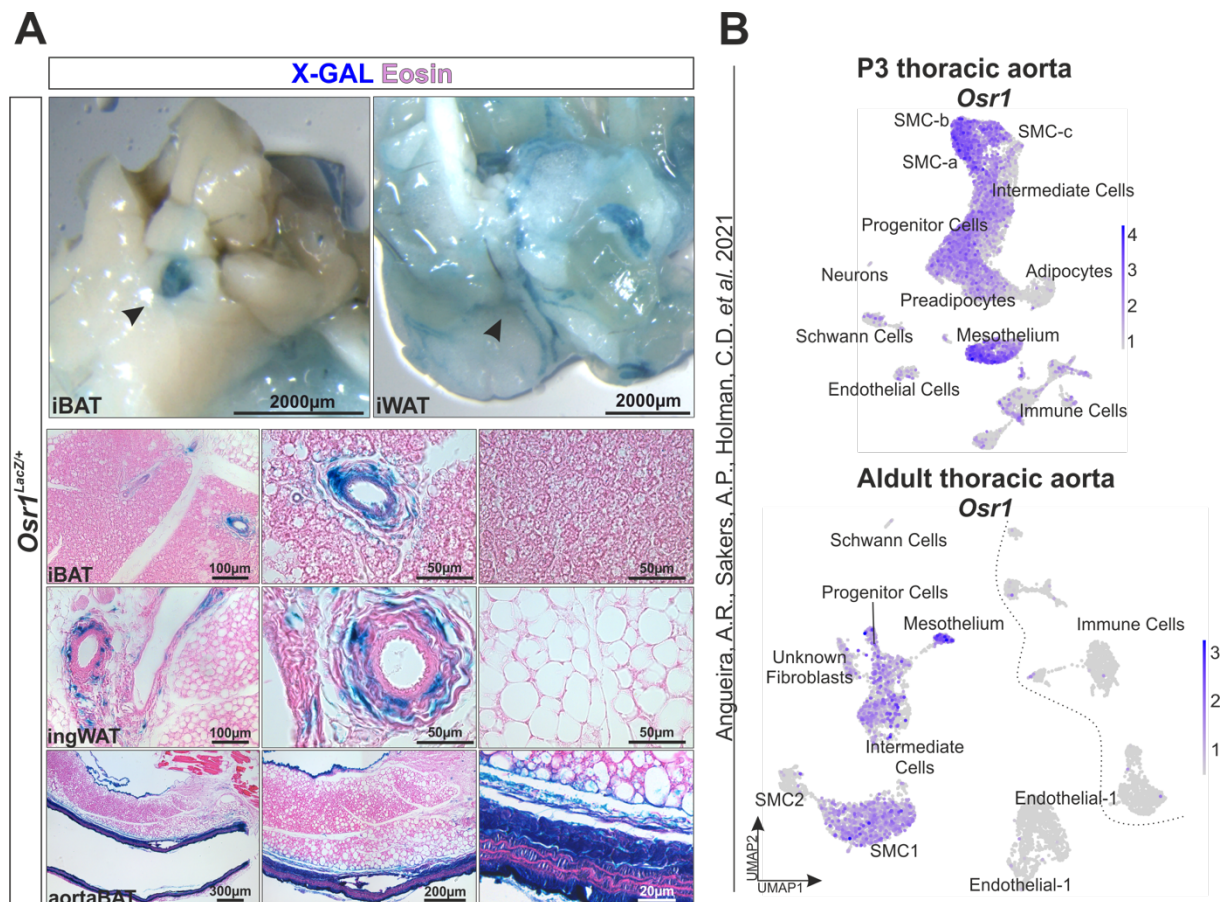
Figure 71: Osr1+ cells clusters within the stromal vascular fraction
A) depicts X-GAL stained wholemount tissue from iBAT and ingWAT of the adult Osr1[LacZ/+]. The black arrowhead points at the X-GAL-stained vascular network. Eosin-stained tissue sections from iBAT, ingWAT and aortaBAT reveal that X-GAL+ cells cluster around the vasculature and does not label mature adipocytes. In the aortaBAT a strong X-GAL signal is observed in the smooth muscle compartment of the thoracic aorta. B) demonstrates *Osr1* expression in the Angueira et. al thoracic aorta dataset.

First, at P3 and in the adult thoracic BAT single cell-dataset, *Osr1* is expressed in the smooth muscle section (Fig. 71 aortaBAT). Second, in the mesothelium and finally in the fibroblast cell types like intermediate cells, progenitors and preadipocytes (Fig. 71 iBAT and ingWAT). In summary, the *Osr1* expression pattern in the reference-datasets is represented in the X-GAL stainings in figure 71A. The single cell dataset provided further evidence about the identity of the Osr1+ cells along the vascular network.

4.7.3 Different types of stress regulate Osr1 expression

4.7.3.1 High fat diet reduces Osr1 expression

Since the Angueira et al. dataset indicated that the Osr1+ cell pool has progenitor and preadipocyte identity, an experimental setup was designed to mobilize the Osr1+ cells. First, for one day mice were fed with high fat diet. Adipose tissue was collected right after and a RT-qPCR was performed to assess the *Osr1* expression levels. Interstingly, the *Osr1* expression in the high fat diet cohort reached only ~50% of the control cohort (Fig. 72), indicating that either the cells just stopped expressing *Osr1* or became activated to undergo adipogenic differentiation. The latter seems to be plausible because mature adipocytes do not express Osr1.
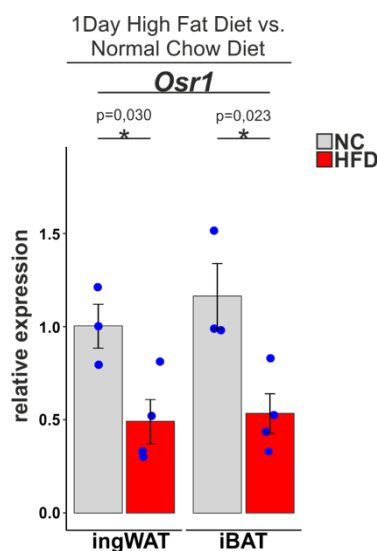
Figure 72: Diet induced stress reduces Osr1+ expression
IngWAT and iBAT was sampled from animals that were fed normal chow diet (grey) or high fat diet (red) for one day. *Osr1* expression was measured *via* RT-qPCR. Data are presented as mean ± SEM (n = 3 or 4); statistical analysis was done using two-tailed Student's t tests: * p<0.05.

To test whether the Osr1+ pool also shows response to temperature induced stress like cold exposure to activate adipose tissue browning, adult Osr1[LacZ/+] mice were kept at 4°C for two days. Right after the adipose tissue was investigated for X-GAL+ cells. Figure 73A demonstrates tissue sections from cold treated and untreated iBAT and ingWAT. The control cohort demonstrated once again that the X-Gal+ cells reside in the vascular compartment. However, animals which experienced cold exposure seem to have a reduced number of Osr1+ cells in the iBAT. In contrast, the ingWAT displayed that X-Gal+ cells seem to leave the vascular niche to migrate into the surrounding tissue. Since there were too few X-GAL+ cells in the iBAT the quantification of how many X-GAL cells reside in their vascular compartment and of how much the Osr1+ cells spread was only assessed within the ingWAT (Fig. 73B). The number of X-GAL+

cells/vessel did not alter in the ingWAT but indeed the X-GAL+ cells seem to be further away from its nearest vessel than detected in the control group. These data suggest, that the Osr1+ cells do not proliferate right after stress induction but migrate into the periphery to overcome the stress by maybe forming adipocytes.
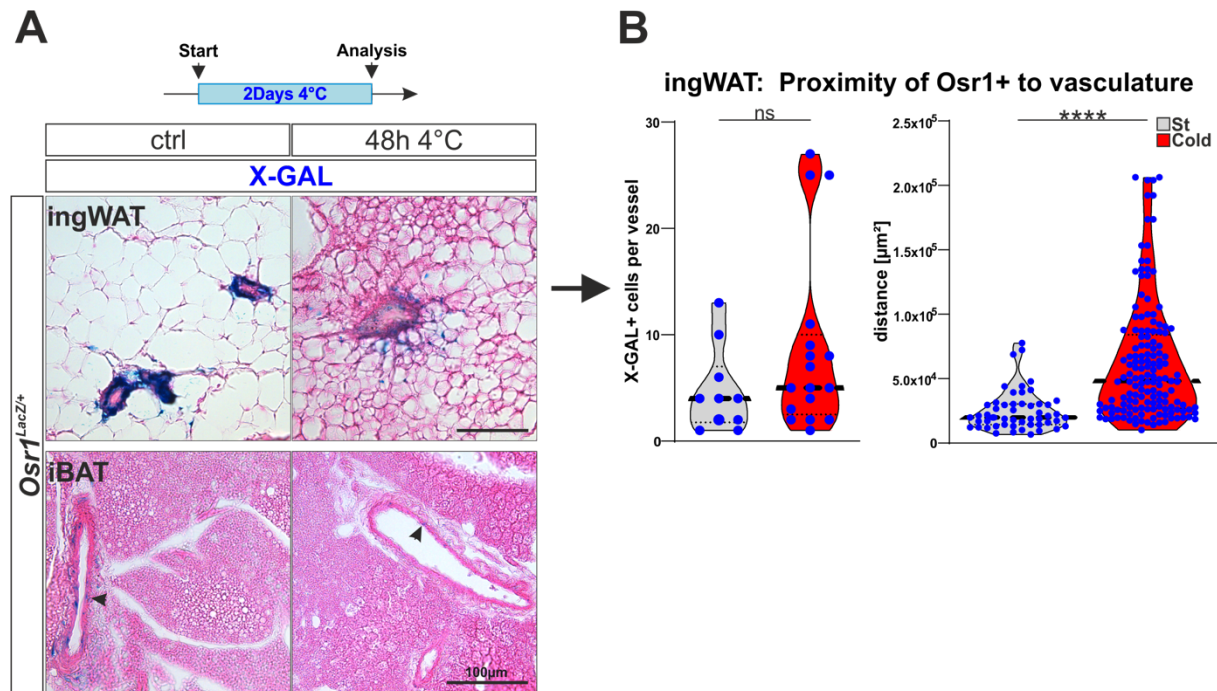
Figure 73: Osr1+ cells diminish or migrate out of their niche after cold induction
A) ingWAT and iBAT of Osr1$^{LacZ/+}$ animals were investigated after 48h of cold exposure or normal animal keeping conditions. Eosin-stained tissue sections show X-GAL signals around the vasculature. In the iBAT it became less after cold exposure and for the ingWAT the X-GAL+ cells cluster further away from the vasculature. B) depicts first that the amount of X-GAL+ cells per vessel does not significantly alter between standard (grey) and cold (red) and second that X-GAL+ cells sit further away from their nearest vessel after cold exposure in the ingWAT. Data are presented as counts per vessel ± SEM (n = 3); statistical analysis was done using two-tailed Student's t tests: * p<0.05, **p<0.001, ***p<0.0001, ****p<0.00001.

4.7.3.2 Osr1 lineage tracing studies during cold exposure recruit adipocytes from Osr1+ preAPC pool

To assess the adipogenic potential of the Osr1+ cell pool during cold exposure lineage tracing experiments were performed. The Osr1$^{CreERt2/+}$; ROSA$^{mTmG/+}$mouse model was used to trace the Osr1 progeny in mature adipose tissue. Tamoxifen was administered seven and six days before the cold exposure treatment. Two injections were chosen to facilitate a complete labeling of the Osr1+ cell pool. After one week the animals were kept at 4°C for two consecutive days. During that phase tamoxifen was injected once more to detect whether the Osr1 cell pool is replenished in the stromal vascular compartment.

Figure 74: After stress induction: Osr1+ cells multiply, migrate and form adipocytes
A) illustrates the experimental timeline of the conducted lineage tracing experiment using the Osr1$^{CreERt2/+}$; ROSA$^{mTmG/+}$ mouse model. The adipose tissue was sampled and immunostained for mGFP+ (green) to visualize the Osr1 progeny and PLIN (magenta) to identify mature adipocytes. A representative image of the iBAT is depicted in B). C) demonstrates that generally the amount of GFP pixel in the area of the SVF is higher, B) the amount of mGFP+ cells in the interstitial space grew and E) the number of mGFP+ adipocytes increased in those samples which experienced cold exposure (red) instead of a constant temperature (grey). Data are presented as counts per area ± SEM (n = 3); statistical analysis was done using two-tailed Student's t tests: * p<0.05, **p<0.001.

The adipose tissue was investigated four days after cold exposure (Fig. 74A). Immunostainings for mGFP and PLIN enabled the identification of mature mGFP+ adipocytes. Furthermore, due to the anatomical location, mGFP+ cells were assigned either to the vascular compartment or defined as an interstitial cell that was surrounded by adipocytes (Fig. 74B).

In general, it was observed that there were more mGFP+ cells in the vascular compartment after cold exposure. Although, this finding seems to be fat depot dependent. The increase of mGFP+ cells was not significant in the iBAT and ingWAT but showed a similar trend. Remarkably, the Osr1 progeny was rather detected outside the vascular niche in-between the adipocytes after cold exposure. The fact that there were more mGFP+ interstitial cells after cold exposure indicated that the Osr1 descendants gradually migrated into the adipose tissue. Also, after cold exposure the number of mGFP+ adipocytes increased per area. These data confirm once again the adipogenic potential of the Osr1-lineage especially in context of stress response (Fig. 74C).

Considering the latest results, it seems like that the Osr1+ cell pool was activated in response to outer stress signals like high fat diet and cold exposure. This on the other hand suggests that the deletion of the Osr1 expression will have a substantial effect on the adipose tissue homeostasis.

4.7.4 Conditional Osr1-knockout animals gain adipose tissue upon tamoxifen injection

In our lab the conditional Osr1-knockout mouse CAGG$^{CreERt2/+}$;Osr1$^{fl/fl.}$ is commonly used for several projects to study different tissues in the absence of Osr1. Here, Osr1 will be excised in cells that express CAGG and have experienced tamoxifen. A study about Osr1 in a muscle injury context used the conditional Osr1-knockout mouse to enlighten the impact of Osr1 on the regeneration process. Thus, adipose tissue was collected from tamoxifen injected animals to measure the effect of Osr1 in tissue homeostasis. In this study the injury as well as the tamoxifen/oil injection, served as an external stress signal. The adipose tissue was investigated whether the loss of Osr1 affects the depot / bodyweight ratio. In the first trail tamoxifen was injected one day before, at the day of muscle injury and the three following days (Fig. 75B). The iBAT and the ingWAT was investigated at 3dpi (three days post injury). Figure 75A depicts

immunostainings for GFP that represents recombined cells with an active Osr1 promotor and SCA1+ to label the progenitors of the stromal vascular niche in the adipose tissue. GFP+SCA1+ cells were observed arranged around the vasculature in both tissues. That finding confirmed that Osr1 is supposed to be expressed after muscle injury in the stromal vascular compartment. To understand whether the Osr1 expression in the SVF is crucial to organize adipose tissue homeostasis the depot / bodyweight ratio was measured at 5dpi (Fig. 75C). Interestingly, it seemed like that the adipose tissue increased in weight after injury. Consequently, the lack of Osr1 promotes adipogenesis. Importantly, tamoxifen was injected with sunflower oil five times before the tissue examination, which should be recognized as a trigger for adipogenesis as well.
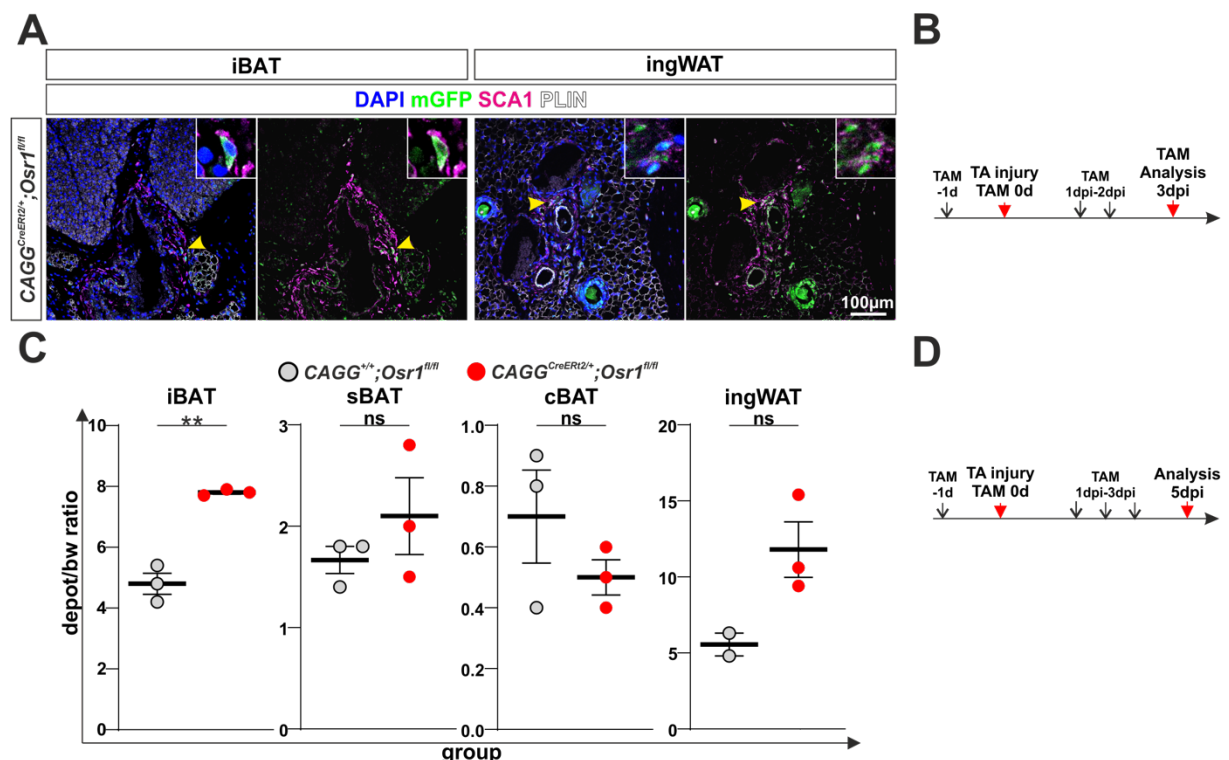
Figure 75: Osr1 deficient adipose tissue increased in weight
A) immunolabeling for GFP (green) - to visualize recombined cells that have an activated Osr1 promotor, SCA1 (magenta) – to identify the progenitor pool and PLIN (white) -to label adipocytes was performed on the iBAT and ingWAT of an adult CAGG$^{CreERt2/+}$;Osr1$^{fl/fl}$ mouse at 3dpi. Yellow arrowheads indicate GFP+SCA1+ cells reside in the stromal vascular compartment. B) depicts the experimental time axis for the images in A). The fat depot per bodyweight ratio was calculated on adipose tissue at 5dpi. The dot-plots indicate that the adipose tissue rather gained than lost weight. D) clarifies the procedure of the experiment in C). Data are presented as measuring points ± SEM (n = 2 or 3); statistical analysis was done using two-tailed Student's t tests: * p<0.05, **p<0.001.

Collectively, each experimental readout assigned Osr1 as an essential factor in the context of embryonic adipose tissue organogenesis and in tissue homeostasis during postnatal life. However, it is not clear yet what mechanism puts Osr1 in that position.

4.8 Protein-protein interaction analysis of Osr1 highlights an epigenetic mechanism in targeting key regulators of the adipogenic program

4.8.1 Osr1 knockout cells hold myogenic identity

4.8.1.1 The Osr1-deficient lineage tracing data prove contribution to myogenic tissue

To understand the mechanism of Osr1 it was required to study the Osr1-lineage in the absence of Osr1. This is feasible by using the Osr1$^{CreERt2/LacZ}$;ROSA$^{mTmG/+}$ mouse model. To not face a CreERt2 dosage problem in the full Osr1 knockout a LacZ cassette was inserted instead of a second CreERt2. Here, the E11.5 lineage was traced till stage E14.5. Strikingly, mGFP+ cells of the E11.5 Osr1-knockout-lineage were detected in MyHC+ myotubes of the subscapular compartment (Fig. 76A). The myogenic contribution was quantified and could reach more than 20%. However, the myogenic potential was not observed in the control embryos: Osr1$^{CreERt2/+}$;ROSA$^{mTmG/+}$. Since the myogenic contribution was assigned to the anatomical region were the sBAT and cBAT develop, it seems to be possible that Osr1 is involved in the fate determination process. To further investigate that, it was tested whether Osr1 can revert the myogenic identity of C2C12 myoblasts to an adipogenic cell.
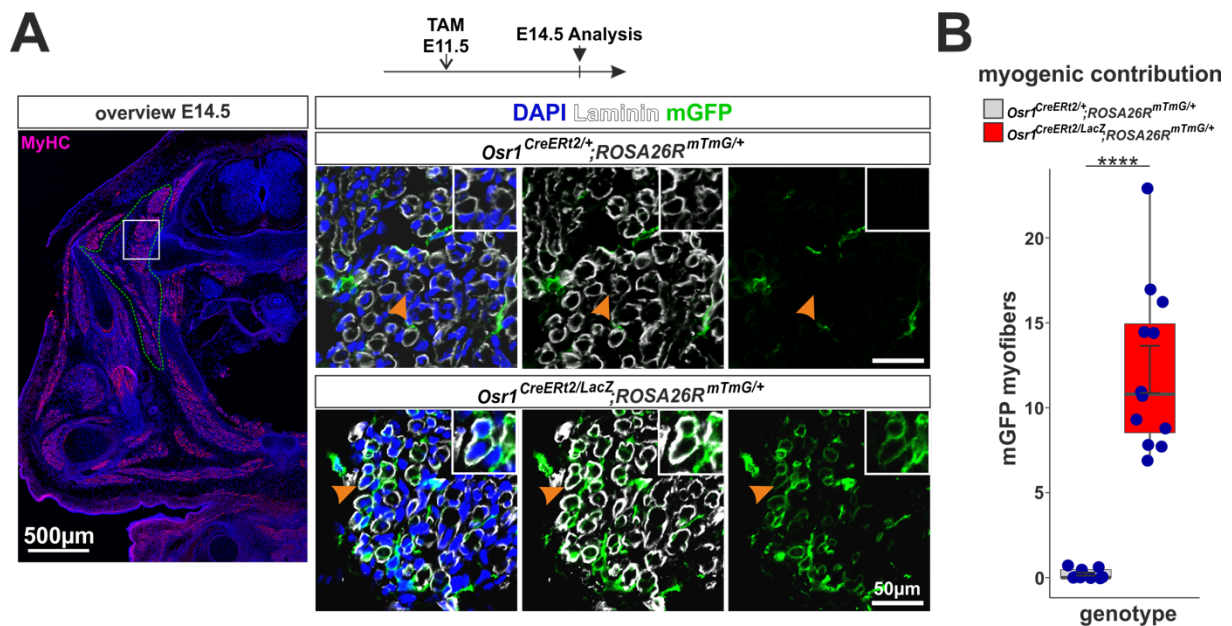
Figure 76: The E11.5 Osr1-lineage becomes myogenic in the absence of Osr1
A) lineage tracing was conducted on Osr1$^{CreERt2/+}$;ROSA$^{mTmG/+}$ and Osr1$^{CreERt2/LacZ}$;ROSA$^{mTmG/+}$ embryos from stage E11.5 till E14.5. The green dashed line in the MyHC (magenta) labeled tissue section of an E14.5 embryo highlights the area of interest. Immunostainings for Laminin (white) to specify the basal lamina of myotubes and mGFP (green) to detect the E11.5 Osr1 lineage were investigated. The bottom of panel A) displays that the mGFP+ Osr1-lineage in the Osr1-mutant embryo contributed to myotubes (orange arrowhead). However, the myogenic potential was not detected in the Osr1-lineage of a heterozygous embryo (orange arrowhead, upper panel in A). B) depicts the quantified myogenic contribution in the three muscle bundles next to the spine. The boxplot demonstrates that the control cohort: Osr1$^{CreERt2/+}$;ROSA$^{mTmG/+}$ (grey) had almost 0% contribution compared to the Osr1$^{CreERt2/LacZ}$;ROSA$^{mTmG/+}$ (red) cohort which reached more than 20%. Data are presented as counts per total myofibers ± SEM (n = 3); statistical analysis was done using two-tailed Student's t tests: * $p<0.05$; ** $p<0.001$, *** $p<0.0001$, **** $p<0.00001$.

4.8.1.2 Osr1 overexpression in C2C12 myoblasts allows adipogenic differentiation

The C2C12 myoblast cell line has been described to not have an adipogenic potential (Rajakumari et al., 2013, Seale et al., 2008). Importantly, qPCR data revealed that C2C12 myoblasts are negative for Osr1 expression (Fig. 77B). Thus, it was tested whether overexpression of *Osr1* in C2C12 could convert the myogenic identity to an adipogenic. Figure 77C and 77D presents that the C2C12 cells which have experienced *Osr1* expression developed significantly more adipocytes upon adipogenic differentiation. That once again proved that Osr1 could be involved in an adipogenic fate priming process.
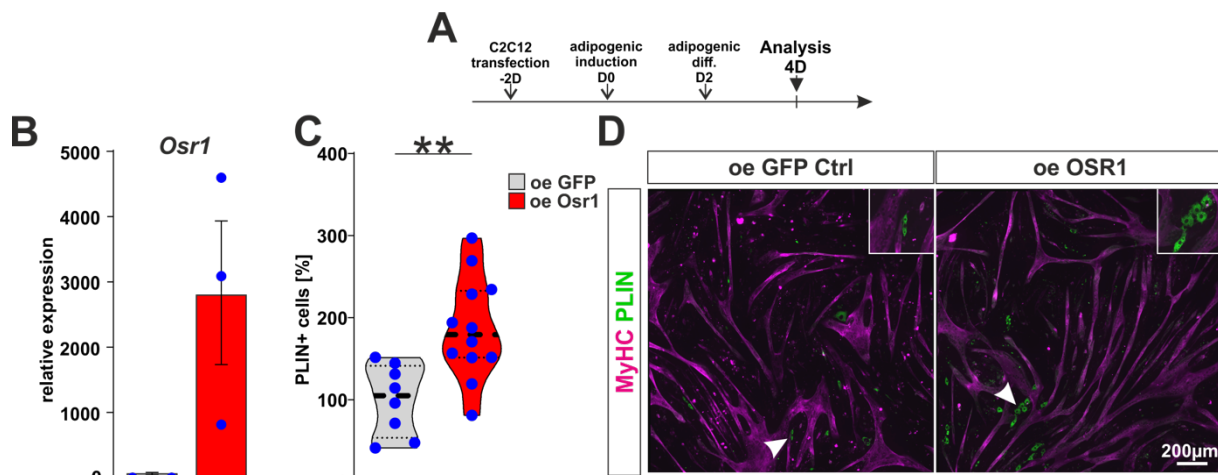
Figure 77: Osr1 overexpression enables the adipogenic program in C2C12 cells
A) depicts the experimental time course of the *Osr1* overexpression in the C2C12 cells that is followed by an adipogenic differentiation assay. B) represents one day after C2C12 transfection the measured *Osr1* expression levels. C) demonstrates that the percentage of PLIN+ cells in the GFP overexpressed group (grey) is lower compared to the *Osr1* overexpressed (red) group. D) shows immunostainings to assess the adipogenic potential in MyHC (magenta) and PLIN (green) stained C2C12 cells after adipogenic differentiation. White arrowheads indicate the presence of PLIN+ adipocytes. Data are presented as counts per image ± SEM (n = 3); statistical analysis was done using two-tailed Student's t tests: * p<0.05; ** p<0.001.

This hypothesis could be further investigated *in vivo* by checking the expression level of myogenic marker genes in the GFP+ cell pool of *Osr1*$^{GCE/+}$ and *Osr1*$^{GCE/GCE}$ embryos.

4.8.1.3 Comparable expression analysis of *Osr1*$^{GCE/+}$ and *Osr1*$^{GCE/GCE}$ cells - highlight distinct changes in the myogenic genes

Osr1$^{GCE/+}$ and *Osr1*$^{GCE/GCE}$ embryos of different stages (E11.5-E13.5) were dissected and GFP+ cells were isolated *via* FACS. RT-qPCR on GFP+ cells was implemented to compare early myogenic gene expression levels between the Osr1 knockout and heterozygous cohort (Fig. 78). Interestingly, *Pax7* was not observed to be enriched in the GFP+ cell population of the *Osr1*$^{GCE/GCE}$ at any embryonic stage. This goes in line with the experimental data from the PAX7$^{CreERt2/+}$;OSR1$^{fl/fl}$ mouse model which did not result in an adipogenic phenotype. However, a significant higher level of *Meox1,* which is important for the somite maturation (Kirilenko et al., 2011, Mankoo et al., 2003) was detected at E11.5 only. Particularly important is that *Myf5* expression was significantly enriched in the Osr1-knockout at E11.5 and E12.5 too. Thus, supporting the observed reduction of the brown adipose tissue in the context of deleting Osr1 from the Myf5-lineage. Apart from that, it was noticed that the myogenic genes were diminished in

the Osr1-knockout cells at E13.5. Interestingly, the work from Vallecillo-Garcia et al. introduced that E13.5 Osr1-knockout cells rather show a more osteogenic identiy instead of a strong connective tissue fibroblasts signature. This could explain the slightly enriched Ebf2 expression level in E13.5 knockout cells (Fig. 59), as Ebf2 was decribed as an pro-osteogenic regulator (Kieslinger et al., 2005). One could speculate that the osteogenic signature goes in line with an even stronger reduction of myogenic genes.

However, the expression analysis revealed a trend of an upregulation of early myogenic marker genes in the Osr1-knockout around stage E11.5. Of note, it should be considered that just a subset of the analyzed GFP+ cells represented the pre-adipogenic progenitor population that experience the myogenic to adipogenic transition.
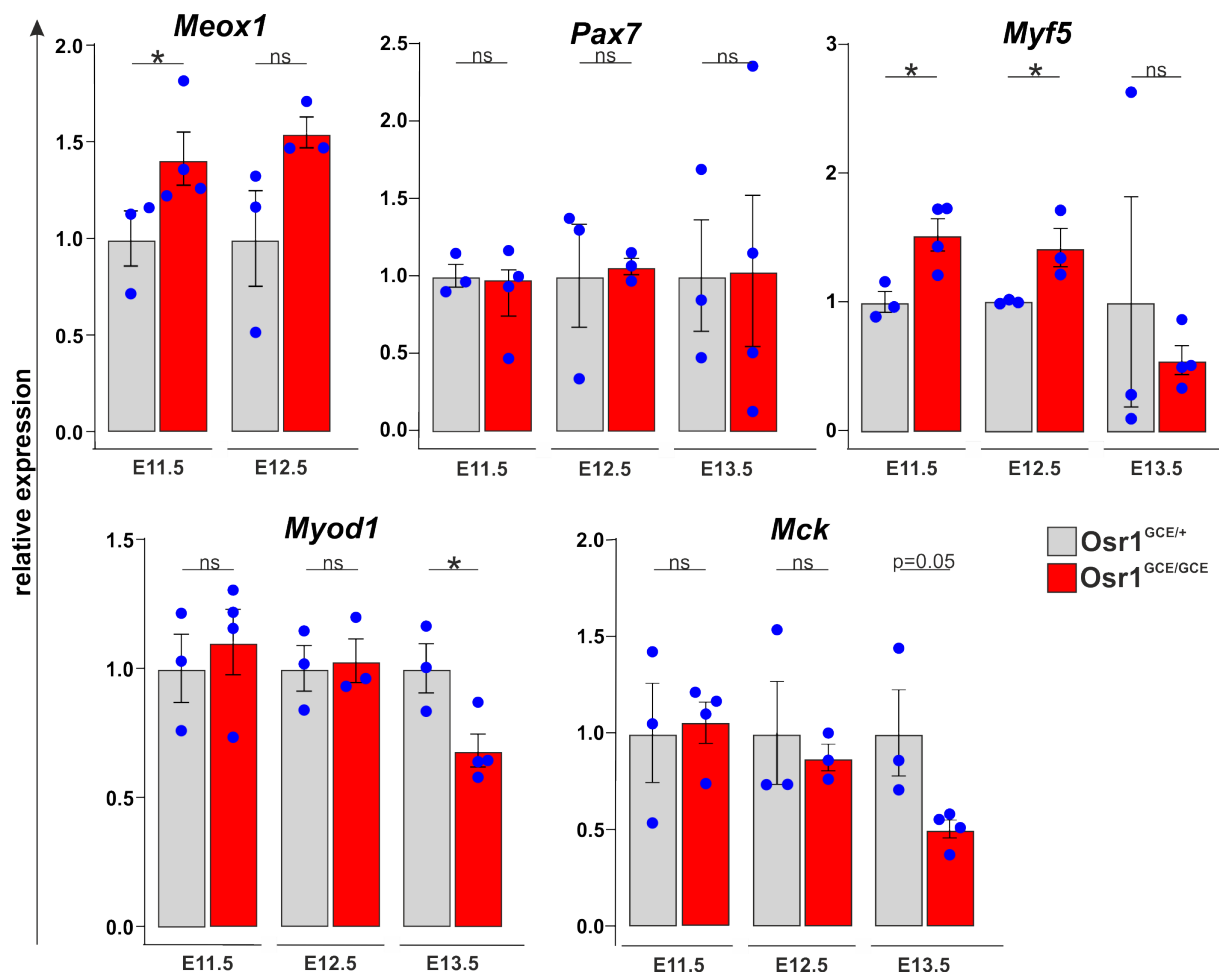
Figure 78: *Osr1^{GCE/GCE}* GFP+ cells are slightly more myogenic at E11.5 to E12.5
FACS sorted GFP+ cells from *Osr1^{GCE/+}* (grey) and *Osr1^{GCE/GCE}* (red) embryos of indicated stages were tested for the expression levels of specific myogenic markers. A) illustrates that *Meox1* was significantly higher in the Osr1-mutant at stage E11.5. *Pax7* expression levels in B) were not affected in the Osr1-knockout. However, C) demonstrates that *Myf5* expression was significantly upregulated in the Osr1-mutant at stage E11.5 and E12.5. D) represents expression levels of *Myod1* and E) of *Mck*. Both show the same trend. There was no difference detected at E11.5 and E12.5 but a significant downregulation at stage E13.5 Data are presented as mean ± SEM (n = 3 or 4); statistical analysis was done using two-tailed Student's t tests: * p<0.05.

Altogether, Osr1 implements the adipogenic fate in a prior myogenic cell. Thus, it seems very clear that Osr1 is integrated in a transcriptional complex that silences the myogenic signature genes to facilitate adipogenic identity.

4.8.2 GLP interacts with Osr1 at an important timepoint of initial adipose tissue development

To date several studies have shown that especially the brown adipogenic program can be featured after silencing of the myogenic progenitor signature genes *via* a transcriptional regulator complex (Seale et al., 2007, Kajimura et al., 2009, Yin et al., 2013). The main protagonist of this complex is the co-regulator PR domain zinc finger

protein 16 (Prdm16) which gathers different co-factors to mediate the reprogramming of myogenic progenitors. The regulator complex also recruits an euchromatic histone-lysine N-methyltransferase 1 (EHMT1, also known as GLP) that is controlling the H3K9 methylation status of the muscle-selective gene promoters (Ohno et al., 2013). Thus, it was tested whether a protein-protein interaction between the main actors of the PRDM16 regulator complex and OSR1 was predicted in the online STRING database (Fig. 79A). The STRING tool calculated with medium confidence an interaction pathway between OSR1 and PPARγ *via* EHMT1 (GLP). This finding once again gave evidence that Osr1 is involved in an epigenetic remodeling process. Since OSR1 was predicted to directly interact with GLP an immunostaining assay on an E11.5 embryo was performed to locate this cell population (Fig. 79B). Remarkably, OSR1+PAX7+ cells which reside in the dermomyotomal derivate are also labeled for GLP+.
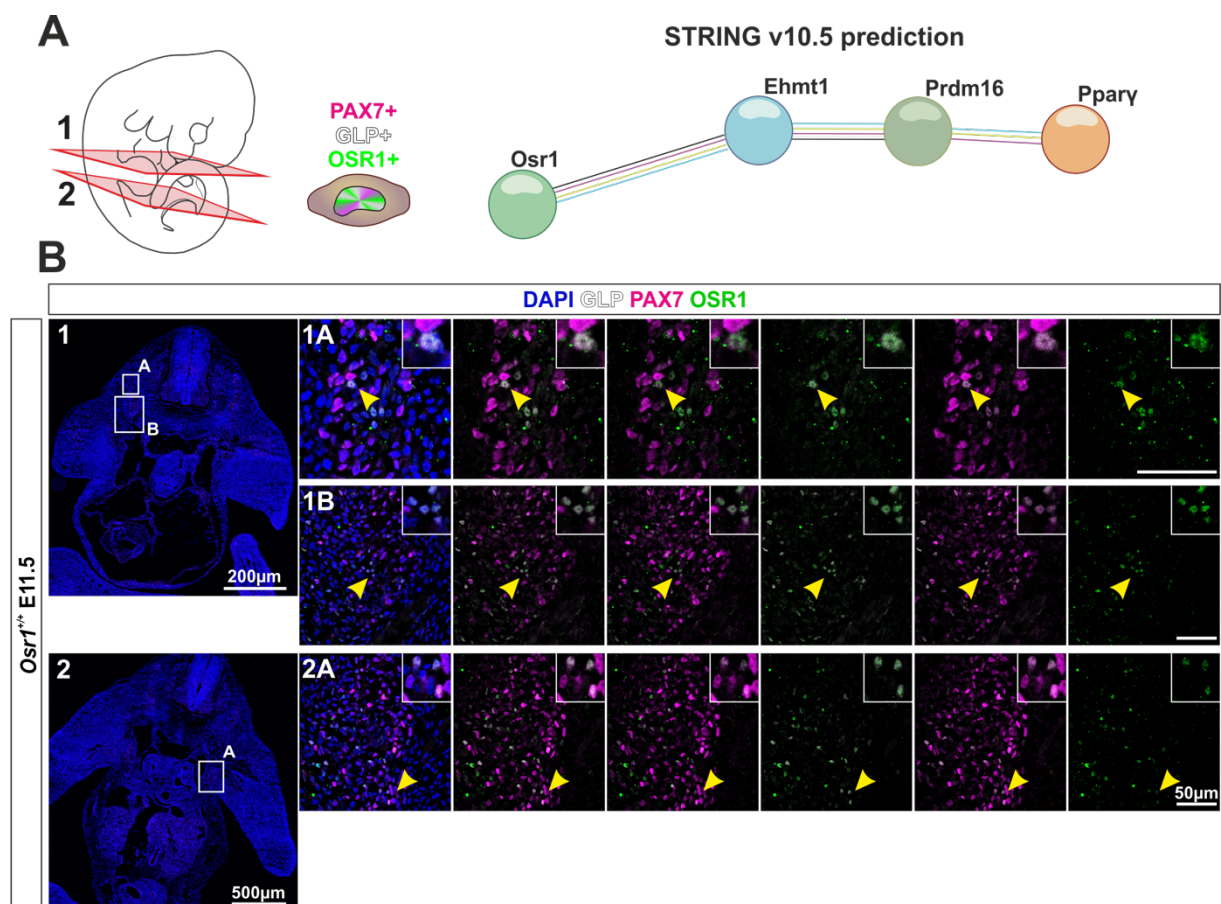
Figure 79: The dermomyotomal derivate harbors PAX7+/OSR1+/GLP+ cells
A) depicts the STRING based prediction of the protein-protein interaction pathway between OSR1 and PPARγ. Cross sections from an E11.5 embryo were investigated whether GLP (also known as EHMT1), PAX7 and OSR1 show co-expression in B). 1 and 2 provide an overview image of where the regions of interest locate. The closeups (1A, 1B and 2A) represent regions of the dermomyotomal derivate. Yellow arrowheads identify cells that show co-labeling of OSR1, PAX7 and GLP.
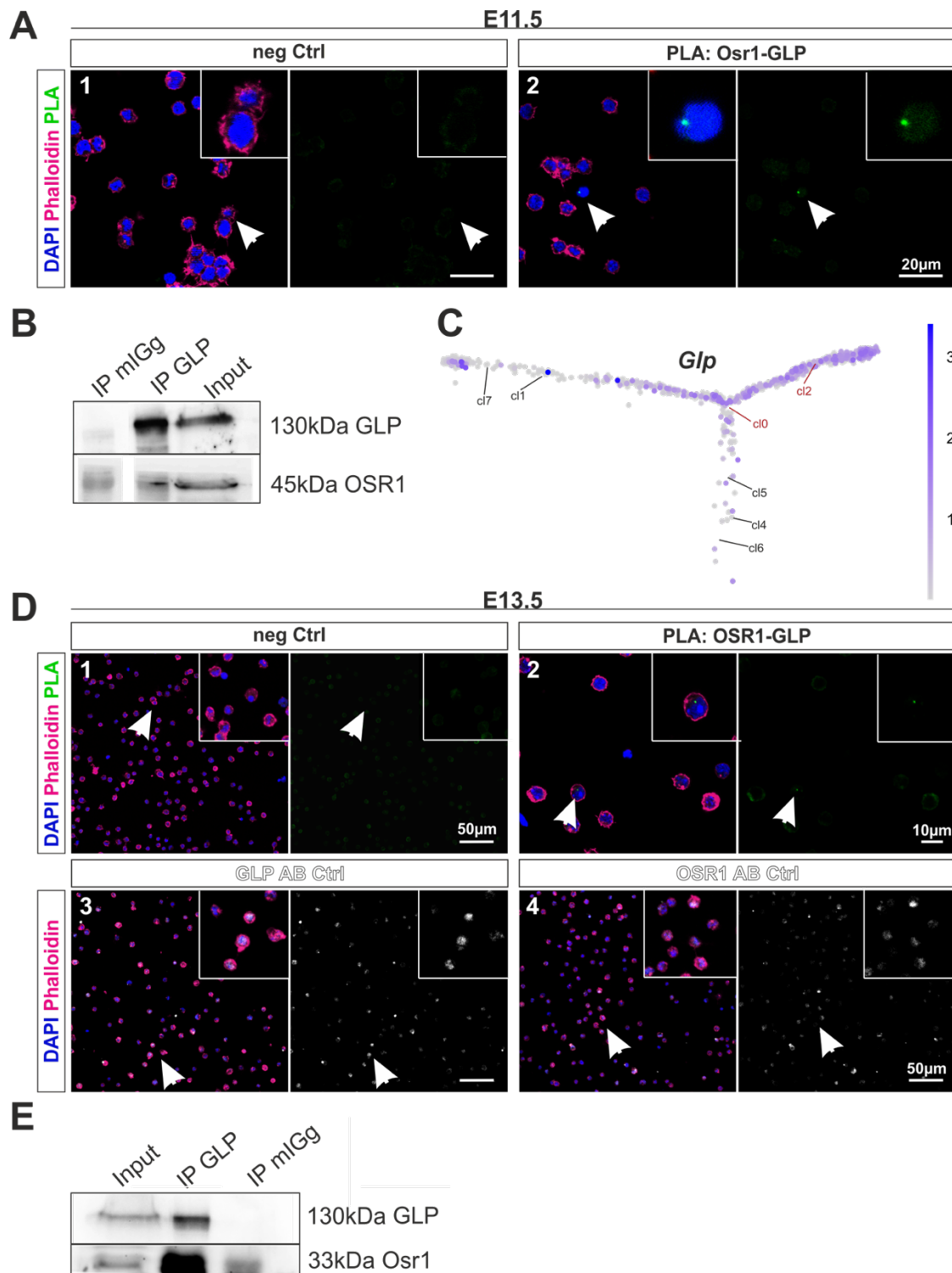
Figure 80: GLP and OSR1 show protein-protein interaction at E11.5 and E13.5
A) Osr1+ cells from the E11.5 Osr1[GCE/+] embryo were FACS sorted and tested for GLP and OSR1 interaction by using the PLA method. The white arrow in A2) displays that OSR1 and GLP show interaction at E11.5. The negative control in A1), on the other hand, did not. Co-immunoprecipitation results *via* GLP on whole E11.5 protein lysate is summarized in B) showing that OSR1 was co-precipitated with GLP. C) illustrates the trajectory tree of the Osr1-opject at E11.5 for *Glp* expression to show its enrichment in cl0 and cl2. The PLA assay was repeated on E13.5 Osr1+ FACS sorted cells in D). D1) clearly demonstrates that no PLA signal was found in the negative control (white arrow). However, D2) confirms that OSR1 and GLP displays interaction in the PLA experiment (white arrow). D3) and D4) represent the antibody control for OSR1 and GLP, both proteins were sufficiently targeted (white arrows). Furthermore, the co-immunoprecipitation on whole E13.5 protein lysate in E) revealed that OSR1 was detectable in the protein pulldown of GLP.

These findings lead to the conclusion that OSR1 and GLP are co-expressed in a PAX7+ cell pool which might just experience an epigenetic reprogramming to allow the shift from a myogenic to an adipogenic state.

To confirm protein-protein interaction between OSR1 and GLP a proximity ligation assay (PLA) was performed on E11.5 FACS sorted Osr1+ primary cells. As expected from the previous results a small Osr1+ population validated interaction with GLP (Fig. 80A). To provide further prove on the possible interaction of GLP and OSR1 a co-immunoprecipitation assay was performed on a dissociated E11.5 embryo. Supportingly, figure 80B depicts that OSR1 was detected *via* western blot in the pulldown after GLP precipitation. Notably, the *Glp* expression was measured in the E11.5 Osr1 single cell object in order to elucidate that the *Glp* pattern (Fig. 80C) overlaps with the Ebf2 pre-BAT signature (Fig. 55A). These findings indicate that indeed the OSR1+GLP+ cells match the brown pre-adipogenic progenitors. Nevertheless, interaction of OSR1 and GLP was also tested at E13.5 when early BAT-depots have formed. Both, the PLA assay and the co-immunoprecipitation *via* GLP on FACS sorted E13.5 Osr1+ cells validated their direct interaction, summarizing that OSR1 through GLP could have a role in epigenetic remodeling processes.

4.8.3 The Osr1-BioID incorporates pre-adipogenic signature candidates

Acquired data from the Osr1-knockout lineage tracing experiments and reprogramming assay of C2C12 becoming adipogenic highlighted the potential of the Osr1 transcription factor to be incorporated into an epigenetic remodeling complex. First evidence is that OSR1 directly interacts with GLP which has been assigned to be epigenetically important in the early process of myogenic to adipogenic determination (Ohno et al., 2013, Kajimura, 2015).

To assess the full spectrum of OSR1 interaction partners an OSR1 interactome screen using Bio-ID was performed on mouse embryonic fibroblasts (MEFs). Biotinylated proteins were precipitated with Streptavidin and digested to conduct a mass spectrometric analysis.

**OSR1 Bio-ID in MEFs
Important candidates**
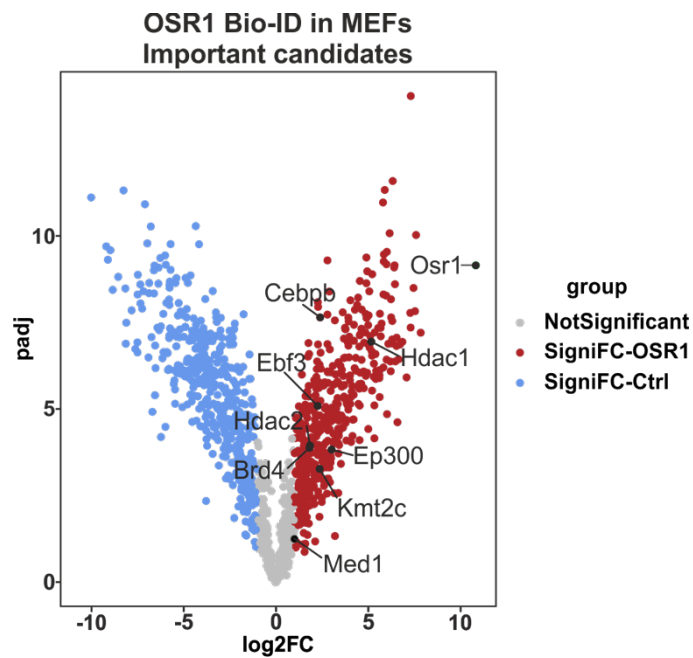
Figure 81: OSR1 Bio-ID identified epigenetic regulators of the adipogenic program
The OSR1 Bio-ID displays specific candidates that determine the adipogenic identity *via* an epigenetic remodeling process. CEBPβ, KMT2C (MLL3), EP300, BRD4 as well as MED1 were detected.

The OSR1 Bio-ID elucidated that OSR1 is in fact interacting with candidates like CEBPβ, histone-lysine n-methyltransferase MLL3 (KMT2C), EP300, BRD4 and MED1 which have been assigned to regulate the adipogenic transcriptional landscape *via* a chromatin remodeling process (Fig. 81) (Lee et al., 2017, Lai et al., 2017, Lee et al., 2013, Lee et al., 2019). A different experimental set up was chosen to validate EP300 and CEBPβ interaction with OSR1 to give more significance to the OSR1 Bio-ID. Here, a PLA assay was conducted on a pre-adipogenic progenitor cell line 3T3-L1 (Fig. 82). Of note, 3T3-L1 cells were labeled for EP300, CEBPβ and OSR1 to visualize their expression pattern. EP300 was ubiquitously expressed and resides in the cytoplasm and nucleus. CEBPβ was observed mainly in the nucleus in approximately 70%-80% of the investigated 3T3-L1 cells. However, OSR1 is found exclusively in the nucleus and in approximately 20% of studied 3T3-L1 cells. The PLA experiment in figure 82 revealed direct interaction for both conditions in the nucleus: OSR1-CEBPβ and OSR1-EP300. In conclusion, Osr1 interacts with epigenetic remodelers which have been assigned to be important to prime and drive the adipogenic potential.
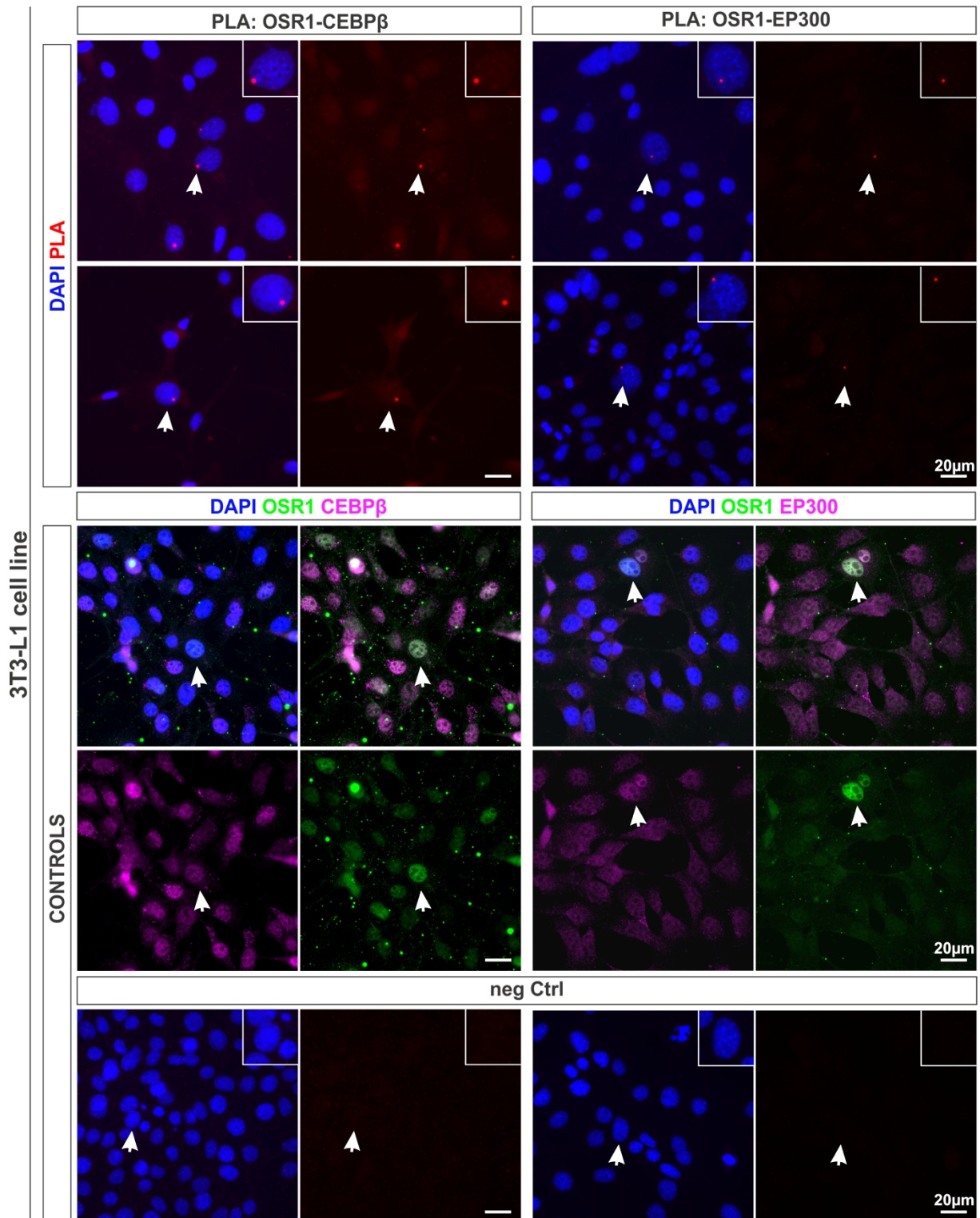
Figure 82: Proximity ligation assay confirmed OSR1-CEBPβ and Osr1-EP300 interaction
It is demonstrated that 3T3-L1 cells show direct protein-protein interaction between OSR1-CEBPβ and OSR1-EP300 by using the PLA method. The white arrows highlight the event of interaction in the top panel. The center part visualizes immunolabeling for EP300, CEBPβ in magenta and OSR1 in green. White arrows point at cells that co-express both candidates inside the nuclear compartment. The negative control of the PLA experiment is displayed on the bottom line. No PLA signal was detectable in the entire negative control experiment - the white arrows point at two representative cells.

Taking the most relevant pro-adipogenic chromatin remodelers from the OSR1 Bio-ID into account and measure their expression in the Osr1 single cell trajectory tree (Fig. 83A) it becomes obvious that the entire set of proteins at E11.5 are enriched in state 1 (a fibroblast-like cell), whereas state 3 (an endothelial / epithelial cell) represents a better match at E9.5. This observation matches with the initial findings that a meso-angioblast of the endothelium at E9.5 and a fibroblast-like cell at E11.5 holds pre-adipogenic features.
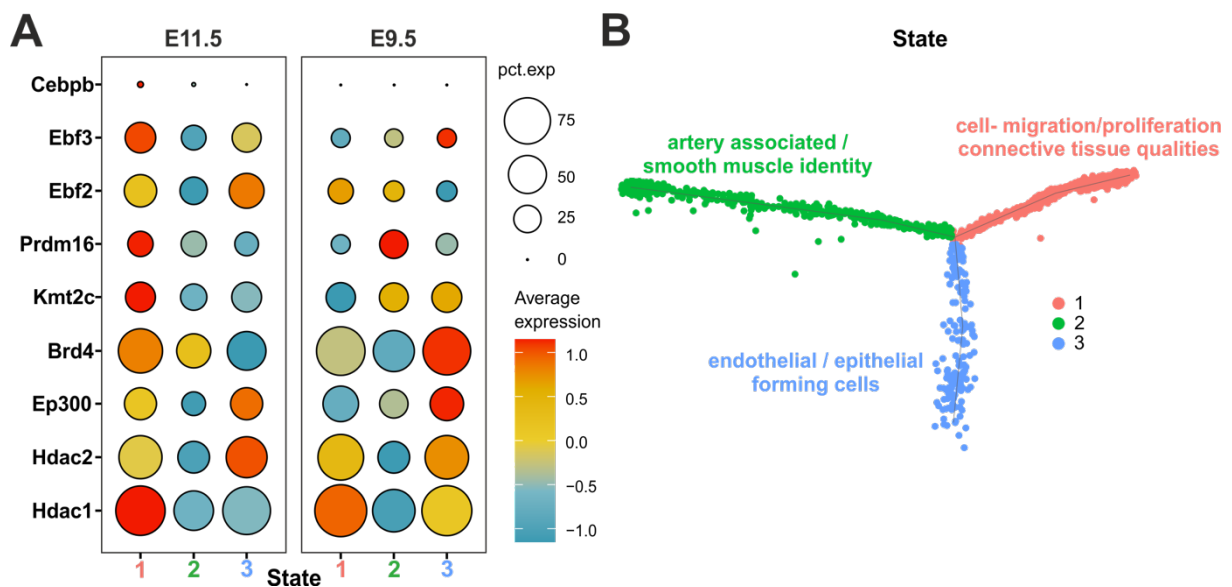
Figure 83: Adipogenic regulators peak in different cell types of the Osr1-object
Candidates who have been stated to be relevant for the priming process of pre-adipogenic progenitors are listed in A). The expression level of them is demonstrated in the three states of the Osr1-trajectory tree at E9.5 and E11.5. Obviously, the best match of all markers holds state 1 at E11.5 and state 3 at E9.5. B) presents the trajectory tree of the Osr1-object and its 3 states which are linked to specific cell characteristics.

To give a synopsis of my results, the generated data go hand in hand and support that OSR1 is establishing a pre-adipogenic identity *via* an epigenetic mechanism that overwrites the myogenic program and enhances the adipogenic transcriptional machinery. Osr1 defines two independent sources of pre-adipogenic progenitors earlier coming from an endothelial - / smooth muscle like cell and later originating from a fibroblast-like cell type.

5 DISCUSSION

5.1 Osr1 lineage maturation during embryogenesis

Data from the Osr1 single cell RNA-Seq introduced important differences between embryonic stage E9.5 and E11.5. First, the Osr1 cell pool from E9.5 revealed a higher grade of diversity compared to E11.5 and second, the cell density plots at E9.5 demonstrated that the highest cell density is recognized in cl1 (smooth muscle like) and cl2 (G2/M mesenchymal stromal cells), whereas cl0 (mesenchymal stromal cells) was strongest amplified at E11.5. Of note, Osr1 lineage tracing experiments demonstrated that the E9.5 Osr1 cells possess a greater differentiation potential than the E11.5 ones. Intriguingly, this is in line with a study from the McMahon group about the role of Osr1+ progenitors of the aorta-mesonephros-gonadal (AGM) region in kidney development (Mugford et al., 2008).

5.1.1 The AGM region, a potent microenvironment

Around E9.5, Osr1 expression is located in the central body axis of the embryo. Here, Osr1+ cells reside in specific organs like the gastrointestinal tube, heart, early lung buds or in microenvironments as the dorsal aorta compartment. Lineage tracing experiments using the Osr1$^{CreERt2/+}$;ROSA$^{mTmG/+}$ mouse model revealed that the E9.5 Osr1 progeny stayed in their originally detected organ, clearly contributing to its organogenesis, whereas E9.5 Osr1 descendants in the dorsal aorta seem to show a different picture. The distribution pattern of Osr1 progeny is concentrated around the dorsal aorta but also in further distant areas, indicating spreading of the Osr1 lineage. This observation raises the question whether Osr1 cells mark a mobile progenitor that contributes to different mesodermal tissues arising from the dorsal aorta compartment, also referred to as aorta-gonadal-mesonephros (AGM) region. Of note, specifically the AGM region was described as such an important microenvironment where potent progenitors get induced to commit to various lineages (De Angelis et al., 1999, Minasi et al., 2002, Mendes et al., 2005, Crosse et al., 2020, Esner et al., 2006).

However, it needs to be discussed which cell populations reside in the AGM region, holding a brown adipogenic as well as a skeletal muscle potential, where the E9.5 Osr1 lineage could also be assigned.

5.1.1.1 Haemato-endothelial specification

As mentioned above, the AGM region generates distinct progenitor populations during early embryogenesis. One of the well described processes in the AGM region is hematopoiesis. The literature defines hematopoiesis as the maturation process of a common blood progenitor in its developmental niche to give rise to the entire set of blood cells (Schmitt et al., 2014). Through an endothelial-to-hematopoietic transition, first definitive hematopoietic stem cells (HSCs) arise from the ventral endothelium of the dorsal aorta (Dzierzak and Medvinsky, 1995, de Bruijn et al., 2000, Mendes et al., 2005, Boisset et al., 2010, Dzierzak and Bigas, 2018). Thus, HSCs gradually emerge from cells integrated in the dorsal aorta endothelial layer, showing endothelial characteristics which identify an hemogenic endothelial cell (HEC), expressing CD34, Flk1 and Kit but lacking mature hematopoietic surface markers (CD41+/CD45+) (Hou et al., 2020, Minasi et al., 2002). Since HECs reside in the dorsal aorta, it needs to be assessed whether the E9.5 Osr1 cell pool marks a subpopulation of HECs. Considering the identified single cell RNA-Seq cluster annotation, cell types of the hematopoietic trajectory such as: dorsal aorta endothelial cells, primitive erythrocytes, macrophages and megakaryocytes, were recognized. Interestingly, these populations decreased in number at stage E11.5, recapitulating the stated time course of hematogenesis between E8.0 to E11.0 (Hou et al., 2020). That in turn implicates that Osr1 possibly is involved in the early process of endothelial-to-hematopoietic transition. Nevertheless, this would require additional testing and investigation of the Osr1 lineage at a later embryonic stage such as E18.5. The identified hematopoietic clusters and the Osr1 expression profile at E9.5 in the dorsal aorta could be assigned to the early process of hematogenesis. However, this does not explain the fact that the E9.5 Osr1 lineage contains skeletal muscle identity, since HSCs or HECs do not provide progenitors to the myogenic cell pool.

5.1.1.2 Mesoangioblast

It needs to be clarified what other cell lineages at E9.5 give rise to skeletal muscle irrespective from the somites. The E9.5 Osr1 expression and lineage pattern, as described above, proposes once again the AGM region as a potential compartment that provides a progenitor type with a myogenic capacity. Different studies have shown

that the dorsal aorta is a source of hematopoietic stem cells, mesodermal stem cells and mesoangioblasts (de Bruijn et al., 2000, Esner et al., 2006, De Angelis et al., 1999). Of note, it was also mentioned that the latter recapitulates an intermediate cell type of endothelial/pericytes, sharing expression of early endothelial markers such as *Flk1, CD34* and upon cell cultivation αSMA (Cossu and Bianco, 2003, Esner et al., 2006, Minasi et al., 2002). Moreover, both have been demonstrated to participate in muscle formation during embryogenesis (Minasi et al., 2002, Dellavalle et al., 2011). Noteworthy, it is conspicuous that apparently the mesoangioblasts, depending on their actual developmental state, transiently recapitulate stem cell signatures of HECs and pericytes, describing a cell signature continuum. However, data from Minasi et al. stated that at E9.5 mesoangioblasts reside in the dorsal aorta endothelium and its perithelial cell layers (Minasi et al., 2002).

The mesoangioblast characteristics highly overlap with the E9.5 Osr1+ cells, residing in the dorsal aorta endothelium, representing cl6 in the E9.5 single cell RNA-seq dataset, expressing *Flk1* (*Kdr*), *Cd34* and *Pecam1* (*Cd31*). Apart from that, a smooth muscle cell like cluster (cl1) was identified, expressing lower levels of *Cd34* and *Flk1* as the endothelium. This particularly could indicate that an Osr1+ cell pool in the endothelium, as well as associated to the dorsal aorta, possibly identifies mesoangioblasts. Nevertheless, most importantly, the mesoangioblasts as well as the Osr1+ cells from E9.5 show a notable contribution to myogenic tissue. Another supporting aspect is that lineage tracing experiments demonstrate that E9.5 Osr1+ cells mark a mobile progenitor in the AGM region. Here, it was detected that a very small population of E9.5 Osr1 progeny is distributed and contributing into various tissues such as brown adipose tissue, early muscle tissue and connective tissue near the vascular network.

In conclusion, these observations highlight for the very first time that an E9.5 Osr1 cell pool in the dorsal aorta compartment labeled a common progenitor, with high similarities to mesoangioblasts, that contributes to brown adipose tissue. With that I introduce the earliest BAT progenitor cell pool that has ever been described before.

5.2 The Osr1 lineage capable to recapitulate the course of embryonic adipogenesis

Generated lineage tracing data using the inducible Osr1$^{CreERt2/+}$;ROSA$^{mTmG/+}$ mouse line, revealed a moderate adipogenic contribution to brown and white adipose tissue at E9.5 and E11.5. Of note, both timepoints demonstrated approximately the same percentual adipocyte contribution per fat depot. Consequently, it could be asked whether a lineage tracing experiment using a constitutive Cre would have pointed out that the entire adipose tissue arise from the Osr1+ progenitor cell pool. This could be a potential scenario, since the single cell RNA-Seq revealed that the Osr1+ pool identified a common mesenchymal progenitor that according to immunostainings resides in distinct locations of an embryo. Moreover, it was reported that multiple lineages together, that are heterogeneously and dynamically distributed during embryogenesis, enable adipose tissue formation (Sanchez-Gurmaches and Guertin, 2014b, Sanchez-Gurmaches and Guertin, 2014a, Cristancho and Lazar, 2011, Sebo and Rodeheffer, 2019). However, a constitutive Osr1 lineage tracing experiment has not yet been carried out. Instead, it was investigated whether other identified pre-adipogenic progeniture markers colocalize with Osr1 during the initial phase of adipogenesis.

5.3 Localization of pre-adipogenic progenitors during embryogenesis

Commonly accepted pre-adipogenic progenitor markers such as Ebf2, Dlk1 and Pparγ in combination with Pax7 were used to detect Osr1+ pre-adipogenic progenitors (Lepper and Fan, 2010, Wang et al., 2014, Rajakumari et al., 2013, Hudak et al., 2014, Hudak and Sul, 2013, Nueda et al., 2007). Immunolabeling specifically demonstrated that three regions in the E11.5 embryo confirmed co-expression of Osr1 and pre-adipogenic markers. First, a cell population of EBF2, DLK1 and OSR1 was detected dorsally, in close proximity to the embryonic heart. Second, a cell cluster in the dermomyotomal derivate (dmd), showing PAX7, EBF2 and OSR1 colocalization and finally, a limited area close to the peritoneal wall revealed OSR1, PPARγ, EBF2 and DLK1 expression.

Lineage tracing experiments revealed that the BAT derives from a myogenic source and Ebf2 was described as an important factor to maintain the brown adipogenic identity (Wang et al., 2014, Rajakumari et al., 2013). Thus, it could be considered that cells in the dmd expressing PAX7, OSR1 and EBf2 cells, right at that moment, transiently experience the fate-switch from a myogenic not yet adipogenic identity. However, cells that actively express Pparγ, the master regulator of adipogenesis, marks a cell that is committed to the adipogenic lineage (Rosen et al., 2002, Rosen et al., 1999, Rosen and Spiegelman, 2014). Hence, cells observed arranging around the peritoneum represent the initial pre-adipogenic progenitors. Dlk1 co-expression was recognized too, a marker which had also been linked to identify pre-adipogenic progenitors that prevents though terminal adipogenic differentiation (Nueda et al., 2007, Hudak et al., 2014, Hudak and Sul, 2013). This in the context of development is conclusive since the founder PPARγ+ cell pool has to multiply and reassembly in their anatomical niche.

Finally, an EBF2, DLK1 and OSR1 expressing cell population, residing dorsally from the embryonic heart, was identified. Here, the interpretation is rather difficult since immunostainings of all three markers showed a very broad distribution pattern. This observation is highlighting the fact that the specificity to label exclusively cells from the adipogenic trajectory is very unlikely. Nevertheless, an adipogenic assignment of the third population lacks further information. For now, neither co-labeling with the myogenic marker PAX7 nor with the adipogenic master regulator PPARγ was observed. In respect thereof, the literature does not provide any further information that described establishment and localization of the initial adipogenic lineage to allow further discrimination of the pre-adipogenic progenitor signature at embryonic stage E11.5. This clearly indicates once again that the developmental process of adipose tissue is not yet fully understood.

5.3.1 The embryonic Osr1 lineage populates the adult SVF

As mentioned above the embryonic Osr1 lineage from E9.5 and E11.5 gave rise to FABP4+ brown and white adipocytes. However, for quite some years now it has been a matter of interest to understand how the SVF establishes (Jiang et al., 2014, Zwierzina et al., 2015, Schwalie et al., 2018, Bourin et al., 2013). Enlighteningly, data from the Graff lab in 2014 stated that the entire embryonic Pparγ expressing cell pool

was required to allow adipose tissue formation. Deletion of Pparγ during embryogenesis led to complete absence of fat depots in postnatal life. Moreover, it was shown that Pparγ+ cells before E10.5 specifically played an important role in the mature SVF to enable proper tissue homeostasis (Jiang et al., 2014). These data indicated that before E10.5, an adipogenic progenitor whose location is unknown, is specifically defined prior to those that enable adipose tissue organogenesis. Furthermore, their study introduced that these progenitors regulate adipose tissue remodeling, providing different cells to overcome external stress stimuli. Interestingly, the Osr1 lineage from E11.5 and E12.5 demonstrated notable contribution to mature adipocytes and αSMA+ mural cells in brown and white fat depots, emphasizing that apparently the Osr1 lineage holds a major role in tissue organogenesis but also in adipose tissue homeostasis. Nevertheless, the adipogenic potential of the identified mGFP+/αSMA+ cells and Lin-:mGFP+/Sca1+ cells need to be further assessed either in an *in vitro* approach or *in vivo,* inducing an pro-adipogenic stress response.

The Osr1 lineage from E9.5 was not able to study in adulthood since delivery problems occurred. However, short time lineage tracing data during embryogenesis uncovered that the E9.5 lineage compared to E11.5 Osr1 descendants contributes to adipose tissue at a later stage of embryogenesis. Thus, it can be assumed that an independent pre-adipogenic source is involved. Moreover, the E9.5 Osr1 pro-adipogenic progeny, most likely throughout clonal expansion, reached the same level of adipogenic contribution as measured in the E11.5 Osr1 lineage at E18.5. This scenario to some extent recapitulates the findings from Jiang et al., as explained above, described an independent pre-adipogenic progenitor pool, specified before E10.5, populates the adipogenic niche at a later stage than those that orchestrate organogenesis (Jiang et al., 2014).

5.3.2 Osr1+ cells reside in the adult SVF

Published single cell RNA-Seq data from P3 and adult thoracic aorta perivascular adipose tissue (PVAT) identified Osr1 as a marker of the αSMA+ compartment and the mesothelium. Most importantly, Osr1 expression was recognized in progenitor, intermediate and preadipocyte fibroblast populations too (Angueira et al., 2021). These findings lead to the hypothesis that Osr1 plays a role in adipose tissue remodeling. Thus, it was tested whether Osr1 expression *in vivo* is affected upon pro-adipogenic

stressors. As expected from the PVAT dataset, the adult Osr1 lineage upon cold exposure gave rise to mature adipocytes in white and brown adipose tissue. Furthermore, expression levels of *Osr1* right after high fat diet were significantly reduced in fat depots. These findings confirmed that the Osr1+ pre-adipogenic progenitor population was involved in adipose tissue remodeling, through activation of the differentiation program, which in turn resulted in a decrease of *Osr1* expression. The latter can be explained by the fact that the Osr1+ pool has been recruited and upon adipogenic differentiation turned off since Osr1 was never detected in mature adipocytes. This is in line with the observation made during embryogenesis, when Osr1 was detectable in developing but not in mature adipocytes.

A study from Schwalie et al. used the single cell RNA-Seq approach on adipogenic stem and precursor cells (ASPCs) of subcutaneous WAT and described an adipogenesis-regulatory cell population named "Aregs" (Schwalie et al., 2018). Most remarkably, Osr1 was described to be enriched in the CD142+ Areg population. However, Aregs exclusively hold a very low adipogenic potential. Mixtures of Aregs with highly potent adipogenic progenitors reduced the final adipogenic potential significantly in a paracrine manner. Depletion of the Areg pool within the adipogenic SVF induced excessive adipocyte formation, highlighting their regulatory function in adipose tissue expansion (Schwalie et al., 2018). If we assume that the Osr1+ cells in the SVF share common features and functions to Aregs it would in turn position Osr1 as a negative regulator of adipogenesis. In support, preliminary data from tamoxifen inducible Osr1 knockout experiments using the CAGG[CreERt2/+];Osr1^{fl/fl} mouse model revealed a trend to adipose tissue expansion. It could also be assumed from Osr1 lineage tracing experiments, that Osr1 expression in the SVF marks a pre-adipogenic cell in a poised state that needs an external stimulus to deactivate Osr1 expression and induce adipogenesis. Another scenario could be that Osr1+ cells secrete regulatory factors, which in a paracrine manner influence action of neighboring cells. However, these possible events need to be further evaluated by investigating the secretome, as well as the epigenetic landscape of an Osr1 expressing cell, to assess their actual function in the adipogenic niche.

Nevertheless, it can be concluded that the Osr1 lineage during embryogenesis enabled adipose tissue organogenesis and SVF completion. In contrast, Osr1 during adulthood labeled cells in the SVF which have adipogenic potential and may possess regulatory function to control adipose tissue expansion or shrinkage.

5.4 Priming the adipogenic fate in the myogenic lineage

A comprehensive expression analysis of GFP+ FACS sorted cells from Osr1$^{GCE/+}$ Osr1$^{GCE/GCE}$ embryos of stage E11.5 to E13.5 was conducted and introduced a gradual reduction of early pre-adipogenic markers such as *Cebpα, Cebpβ, Cebpδ, Dlk1 and Pparγ* between E12.5 and E13.5 in the Osr1-knockout cells. Of note, generated qPCR data from GFP+ cells provided an insight but did not show a very clear pattern of regulated pre-adipogenic markers. This could be explained by the fact that the selected GFP+ cells represent a rather heterogenic cell pool. Consequently, the establishment of the reduced adipogenic potential in Osr1-knockouts is not fully assessed.

In contrast, genes that define the early myogenic lineage such as *Myf5* and *Meox1* were significantly upregulated in E11.5 Osr1-knockout cells. These data indicated that apparently Osr1 at stage E11.5 is needed to suppress myogenic lineage genes. This hypothesis was also tested in a lineage tracing experiment were Osr1-knockout cells from E11.5 were pursued till E14.5. This experiment uncovered that Osr1-knockout cells contribute to myogenic tissue in the anatomical region where brown adipose tissue develops. Moreover, a C2C12 myoblast cell line upon *Osr1* overexpression recorded a significant higher adipogenic potential compared to those that did not experienced *Osr1* before. These observations in summary present that Osr1 regulates to some extant the fate shift from a myogenic to an adipogenic identity.

5.5 Osr1 together with pro-brown pre-adipogenic transcriptional key regulators induce brown fat identity

5.5.1 Ebf2, the identifier of brown fat specific genes

B cell factor-2 (Ebf2) is a well-studied transcription factor that was first identified to be involved in bone formation processes during embryogenesis (Kieslinger et al., 2005). However, in 2013 the Seale lab discovered that Ebf2 is crucial to maintain the brown fat identity during embryogenic BAT organogenesis as well as in mature adipocytes (Rajakumari et al., 2013, Angueira et al., 2020). Ebf2 knockout embryos at E18.5 revealed that not the size of brown adipose tissue was affected but the adipocyte identity was converted into white adipocytes. Most interestingly, overexpression of

Ebf2 in C2C12 myoblasts was sufficient to induce a brown fat-specific differentiation program (Rajakumari et al., 2013). That observation indicated first parallels between Osr1 and Ebf2 since Osr1 was also capable to drive adipogenesis in C2C12 cells upon adipogenic differentiation. However, it was not tested whether brown or white adipogenesis was induced.

In embryogenesis, Ebf2 was used as a marker to establish a brown pre-adipogenic progeniture signature from an E14.5 embryo, comprising genes which have also been recognized to be enriched in the brown adipogenic Myf5-PDGFRα lineage (Wang et al., 2014). Importantly, the identified Ebf2 brown pre-adipogenic progeniture signature was found to be expressed in the E11.5 Osr1 single cell RNA-seq dataset which suggests that apparently Osr1 recognizes Ebf2-pre-BAT-progenitors too. Thus, conducted immunostainings that revealed colocalization of OSR1 and EBF2 at E11.5 identifies pre-brown adipogenic progenitors even before stage E14.5. In (Wang et al., 2014) it was stated that EBF2 was not detectable earlier than E11.5 which again was in line with very low *Ebf2* expression levels in the E9.5 Osr1 single cell RNA-Seq object. That leads to the assumption that most possibly the described Ebf2+ brown pre-adipogenic progenitors have not specified at E9.5. Thus, we could conclude that Osr1 at E9.5 identifies a novel Ebf2 independent BAT-progenitor.

However, so far it was reported that Ebf2 functions as one of the pioneer identifiers of the brown fat specific genes and enhancers to therewith enable binding of other transcriptional regulators such as PPARγ and PRDM16 to promote brown adipogenesis (Lai et al., 2017, Rajakumari et al., 2013, Seale, 2015). Thus, Ebf2 as pioneer identifier of BAT genes allows the identification of pre-BAT progenitors in the E11.5 Osr1 single cell RNA-Seq dataset as well as on E11.5 embryonic tissue sections. However, it should be considered that the E9.5 Osr1+ pre-adipogenic progenitor pool might activate Ebf2 expression at a later stage of embryogenesis.

5.5.2 Prdm16 modulates connectivity between transcriptional co-factors and enhancers

Several studies from the Speigelmann, Seale and Kajimura labs demonstrated that the acquirement of the brown adipogenic fate in the Myf5 lineage is dependent on a transcriptional complex with its transcriptional key regulator PRDM16 (PR domain containing 16). Their research showed that in the absence of PRDM16, brown adipose

tissue stayed uneffaced, whereas its phenotypical look and its functionality shifted from brown to white adipose tissue. (Harms et al., 2014, Seale et al., 2008, Rajakumari et al., 2013).

So far, Prdm16 at E11.5 has never been labeled together with early myogenic markers, such as Pax7 and Myf5, to discriminate cells that experience a fate shift. Apart from the fact that both PRDM16 and OSR1 are zinc finger transcription factors, more parallels were discovered. Most pivotal, as mentioned for Ebf2 before, was that C2C12 myoblasts upon Osr1 overexpression facilitated adipogenesis, whereas a loss of both demonstrated an enrichment of the myogenic capacity in pre-adipogenic progenitors (Seale et al., 2008, Seale et al., 2007). In consequence, it could be concluded that both arrange in the same pathway to enable brown adipogenesis.

5.5.2.1 Osr1 and Prdm16 share the same interaction partners

However, Prdm16 was reported to interact with important co-factors such as Cebpβ and Med1 which together have been demonstrated to be important in regulating BAT specific gene transcription (Harms et al., 2015, Kajimura et al., 2009). In particular, the CCAAT enhancer binding protein beta (Cebpβ), a basic leucine zipper TF, was identified as a pioneer TF in the initial phase of adipogenesis. ChIP-Seq data recognized CEBPβ binding to adipogenic enhancer regions and thus, recruitment of other pro-adipogenic TFs to form activated adipogenic enhancers to finally drive expression of late acting TFs such as $Ppar\gamma$ and $Cebp\alpha$ (Siersbæk et al., 2011, Siersbæk et al., 2012). Of note, overexpression of Prdm16 and Cebpβ in mouse embryonic fibroblasts (MEFs) or primary skin fibroblasts was sufficient to induce brown like adipocyte formation (Kajimura et al., 2009).

Moreover, Prdm16 was identified to not only physically bind but also to recruit Med1 (Mediator of RNA polymerase II transcription subunit 1). Med1, on the other hand, represents a sub-component of the mediator complex and arranges connectivity to brown fat-selective super-enhancers. A mediator complex was observed to be an important bridging-element to enable higher interconnectivity of TF-bound enhancer regions with the general transcriptional machinery as well as RNA Pol II at specific gene promoters (Malik and Roeder, 2010). Deficiency of PRDM16 showed reduced Med1 binding at PRDM16 target sites and major changes in the chromatin architecture in BAT-selective genes (Harms et al., 2015). Thus, the gained knowledge indicates

that PRDM16 together with CEBPβ and MED1 facilitates chromatin remodeling and enhancer activation to drive transcription of brown adipogenic identity genes. It is of interest whether OSR1 is found to interact with the same candidates. For this purpose, an OSR1 protein-protein interaction dataset (OSR1-Bio-ID) was investigated, and the results revealed a significant, physical-binding of the same candidates that haven been introduced for PRDM16. In summary, these findings underline once more the idea that PRDM16 and OSR1 operate in the same transcriptional machinery.

5.5.2.2 Suppression of the myogenic potential

Euchromatic histone-lysine *N*-methyltransferase 1 (EHMT1) also referred to as GLP was recognized as a BAT enriched enzyme which was found to integrate in the PRDM16 transcriptional complex to promote the BAT-selective thermogenic program (Ohno et al., 2013). Glp was recognized to have a distinctive role and position in controlling the brown adipose cell fate commitment. Investigations of E18.5 Myf5$^{Cre/+}$;Ehmt1$^{fl/fl}$ embryos revealed a significant reduction of BAT mass and BAT-specific genes. In contrast, a phenotypical as well as a transcriptional shift towards a myogenic identity was detected. That introduced Glp to function already during embryogenesis. The deficiency of Glp causes muscle differentiation instead of brown adipogenesis through demethylation events of histone 3 lysine 9 (H3K9me2 and 3) of muscle selective gene promoters in brown adipocytes (Ohno et al., 2013). Since Glp was confirmed to be required during development, to control the brown adipose cell fate shift by repressing the myogenic genes, it is reasonable to assume that Osr1 is involved in the process. Remarkedly, at E11.5, OSR1, GLP and PAX7 together were found in the dermomyotomal derivate (dmd) where EBF2+ cells also reside. In consequence, it is most likely that those cells in the dmd represent the myogenic cells that experience a fate shift towards the adipogenic lineage. It is important to highlight that PPARγ+ cells appeared more ventrally to those about the same time. Furthermore, the interaction of OSR1 and GLP was tested by applying a co-immunoprecipitation (Co-IP) assay and proximity ligation assay (PLA) and both approaches disclosed that GLP and OSR1 at E11.5 as well as at E13.5 physically interact. These data indicate that GLP, PRDM16 and OSR1 act among a similar interactome to control brown adipose cell fate determination.

5.6 Chromatin architecture and epigenetic signatures regulate the transcriptional adipogenic landscape

5.6.1 3D Chromatin architecture describes the state of interconnectivity

Since many similarities between Prdm16 and Osr1 were found it needs to be discussed whether the functionality of Osr1 is linked to a specific 3D chromatin architecture too. The PLA assays with OSR1 in combination with either GLP, CEBPβ or EP300 demonstrated that protein interaction was recognized in one single region in the nucleus. This observation could be firstly, interpreted as an experimental artifact or secondly, as a meaningful readout, introducing protein-interaction-hotspots in the genome. The latter introduces the relevance of highly interconnected genomic organizing structural domains also called 3D hubs, which design a regulatory hotspot. This was observed in "highly interconnected enhancer communities" (HICEs) that are highly enriched of CTCF motifs which on the other hand enable chromatin looping (Phillips and Corces, 2009, Guelen et al., 2008, Hou et al., 2008, Madsen et al., 2020). HICEs empowers much higher interconnectivity between regular- and super-enhancer communities as well as an enrichment of the total and dynamic enhancer-promoter connections (Madsen et al., 2020). Thus, regulatory hotspots, stabilized through HICEs, define indicators of cell fate regulating machineries (Madsen et al., 2020, Rauch and Mandrup, 2021) that could possibly incorporate OSR1 and its identified pro-adipogenic interaction partners such as Ep300 and CEBPβ to facilitate the adipogenic fate shift.

5.6.1.1 Epigenetic remodelers interact with Osr1 to drive the adipogenic program

It was shown that epigenetic modulators are required to enable enhancer activation, whereas mediator complexes facilitated TF-bound enhancers to interconnect with the general transcriptional machinery including RNA Pol II on specific gene promoters (Malik and Roeder, 2010). Activated enhancer regions have been described to carry H3K4me1 and H3K27ac marks which were established from epigenomic writers such

as histone H3K4me1/2 methyltransferases MLL3/4 and H3K27 acetyltransferases CBP/p300 (Lee et al., 2019, Lee et al., 2013). Experiments revealed that MLL4 together with EBF2 and CEBPβ pre-mark a subset of super-enhancer constituents (SECs) prior to adipogenesis, introducing an enhancer-priming role of the three candidates (Lai et al., 2017, Lee et al., 2019).

However, animal work revealed that Mll4 was essential for both adipogenesis and myogenesis since Myf5$^{cre/+}$;Mll4$^{fl/fl}$ embryos at E18.5 displayed strong decreases of embryonic BAT and muscle mass. These data in first place indicated that Mll4 plays a super ordinate role in development (Lee et al., 2013). Moreover, deletion of Mll4 from Mll3 knockout preadipocytes (Mll3$^{-/-}$;Mll4$^{f/f}$) as well as a double knockout of Mll3/Mll4 demonstrated commonly a substantially reduced binding of CBP/p300 on MLL4+ active enhancers and loci of adipogenic master regulators such as the Pparγ, Cebpα and brown adipocyte markers like Prdm16 and Ucp1. These findings and the overall decreases of H3K4me1and H3K4me2 marks results in a reduced adipogenic potential (Lai et al., 2017, Lee et al., 2013). Thus, MLL3/MLL4 were identified to function as enhancer-priming enzymes to facilitate CBP/p300 binding and therewith activation of adipogenic lineage enhancers (Lai et al., 2017).

The epigenomic reader bromodomain and extra terminal domain (BET) protein BRD4 identifies H3K4me1 and H3K27ac marks and recruits the transcription coactivator mediator and Pol II to induce Pparγ and Cebpα expression (Lee et al., 2019, Brown et al., 2018, Lee et al., 2017, Lee et al., 2013, Lai et al., 2017). Interestingly, loss of Brd4 in the Myf5 lineage (Myf5$^{cre/+}$;Brd4$^{f/f}$) demonstrated the same muscle and fat phenotype, as described before, from the Myf5$^{cre/+}$;Mll4$^{f/f}$ embryos at E18.5. Thus, demonstrating a downstream position of the Mll4 enhancer activation pathway (Lai et al., 2017, Lee et al., 2013). In conclusion, research from the Ge group revealed sequential actions of epigenomic factors on enhancers in adipogenesis (Lee et al., 2017, Lee et al., 2019). However, the obtained muscle phenotype can be in part a consequence of impaired myogenesis, since Myf5 is expressed in the early dermomyotome too. So far, this fact was not addressed and investigated. Experiments using conditional knockouts in specific cell types such as pre-adipogenic cells (Osr1^{CreERt}, Pdgfra^{CreERt}) and muscle cells (MyoD^{Cre}) would allow to distinguish tissue specific effects.

The OSR1 protein-protein interaction dataset confirmed that CEBPβ, MLL3, EP300, BRD4 as well as MED1 are binding partners of OSR1. All of them have been

mentioned to drive the enhancer activation pathway to promote the adipogenic fate. Thus, it could be assumed that OSR1 indeed cooperates with epigenomic remodelers to overwrite the myogenic identity and thus prime the adipogenic signature instead. However, the striking Osr1 knockout adipogenic phenotype at E14.5 recapitulated just in part the phenotype of the Myf5$^{cre/+}$;Mll4$^{f/f}$ and Myf5$^{cre/+}$;Brd4$^{f/f}$ assuming that Mll4, which acts most upstream of the enhancer activation pathway, plays a more super ordinated role, since Mll4 is not restricted to the adipogenic differentiation pathway (Lee et al., 2013). Nevertheless, it remains unknown what in the epigenetic signature of the adipogenic transcriptional landscape induced the Osr1-knockout fat phenotype. Thus, a ChIP-Seq experiment of Osr1-knockout cells would elucidate discrimination of one specific deregulated event in the process of Osr1 mediated adipogenesis.

6 SUMMARY

This work demonstrated that Osr1 during embryogenesis as well as in postnatal life represents a reliable marker for pre-adipogenic progenitors. Since Osr1 and already defined pre-adipogenic markers, such as Ebf2 and Dlk1, show a wide expression pattern during embryogenesis, a combinatory signature should be used to discriminate pre-adipogenic progenitors in the embryo. However, generated single cell RNA-Seq data from E9.5 and E11.5 Osr1+ cells supported the hypothesis that two independent sources of adipose tissue progenitors exist in development.

At E11.5, co-immunostainings of common pre-adipogenic markers such as DLK1 and PPARγ as well as EBF2, which instead marks brown pre-adipogenic progenitors, worked sufficiently to co-localize them with OSR1+ in distinct regions. These potent regions recapitulate different stages of adipogenic commitment. First, EBF2+ / OSR1+ / PAX7+ cells were recognized in the dermomyotomal derivate that most probably describe the cell pool, which experiences in that moment a shift from a myogenic identity to a future brown adipogenic fate. Second, the PPARγ+ / DLK1+ / OSR1+ cell pool, on the other hand, was located more ventrally, proximal to the peritoneum which was assumed to represent the fully committed pre-adipogenic founder population. Thus, these findings demonstrate single steps of a dynamical process to determine the adipogenic fate (Lepper and Fan, 2010, Wang et al., 2014, Rajakumari et al., 2013, Hudak et al., 2014, Hudak and Sul, 2013, Nueda et al., 2007).

However, at E9.5, OSR1+ labeled cells specifically in organs, such as the lung, esophagus and the gastrointestinal systems, cells that are already in the process of organogenesis and committed to a certain fate. Most importantly, Osr1 was also detected in the dorsal aorta compartment also referred to as the aorta-gonadal-mesonephros region, which was described as a potent microenvironment that harbors progenitor cells, which can commit to various lineages (De Angelis et al., 1999, Minasi et al., 2002, Mendes et al., 2005, Crosse et al., 2020, Esner et al., 2006). Here, it was observed that Osr1 labeled CD31+/FLK1+/CD34+ cells that have been revealed to either be HECs, that experience an endothelial-to-hematopoietic transition to form hematopoietic stem cells (HSCs) or mesoangioblasts that contribute to diverse mesodermal lineages (de Bruijn et al., 2000, Esner et al., 2006, De Angelis et al., 1999, Hou et al., 2020, Minasi et al., 2002). Both cell identities fit, since first, the hematopoietic trajectory was identified in the single cell RNA-Seq of E9.5 and second,

that E9.5 Osr1-lineage tracing studies unmasked a myogenic differentiation potential exclusively.

However, additional indications highlight that two independent brown pre-adipogenic progenitor sources in the Osr1-lineage exist. First, a non dermomyotomal derived and Ebf2 negative E9.5 Osr1+ brown adipogenic progenitor pool residing in the dorsal aorta compartment was observed. Second, time resolved lineage tracing investigations disclosed that the E11.5 Osr1 lineage contributed to brown adipose tissue before the E9.5 Osr1 progeny did, highlighting that TAM induced tracing was very specific and that there was no spill-over from a shot at day 9.5 to the 11.5 pool. In consequence, these findings indicate that restricted to stage E9.5, the Osr1 cell pool harbors a multipotent progenitor which drives differentiation of more mesodermal lineages such as myogenic and brown adipose tissue.

However, tracing the E11.5/12.5 Osr1+ cells into adulthood, it was observed that the Osr1 lineage contributes not only to the process of adipose tissue organogenesis but also into the SVF cell pool, labeling the αSMA+ and Sca1+ compartment, which mediates tissue homeostasis. Apart from that, Osr1+ cells in the SVF of mature adipose tissue can upon external stimuli form adipocytes to allow adipose tissue remodeling.

Nevertheless, depletion of Osr1 from the Myf5 lineage (Myf5$^{Cre/+}$;Osr1$^{fl/fl}$) caused a stable and significant decrease of sBAT and cBAT which perfectly recapitulated the brown adipose tissue phenotype of the Osr1 knockout. This finding validated the fact that Osr1 is important in the myogenic lineage to promote brown adipose tissue development. That was further investigated in a lineage tracing experiment where E11.5 Osr1-knockout cells were traced till E14.5 and confirmed upon immunostaining muscle fiber formation in the anatomical region of sBAT and cBAT.

Finally, Osr1 protein-protein interaction data introduced that Osr1 is in involved in the process of epigenetic remodeling. OSR1 interaction partners such as MLL3, EP300, BRD4 and MED1 have been recognized to activate super-enhancers by placing H3K4me1 and H3K27ac marks and in turn to recruit a mediator complex to bridge activated enhancers to the general transcriptional machinery to induce Pparγ and Cebpα expression (Lee et al., 2019, Brown et al., 2018, Lee et al., 2017, Lee et al., 2013, Lai et al., 2017).
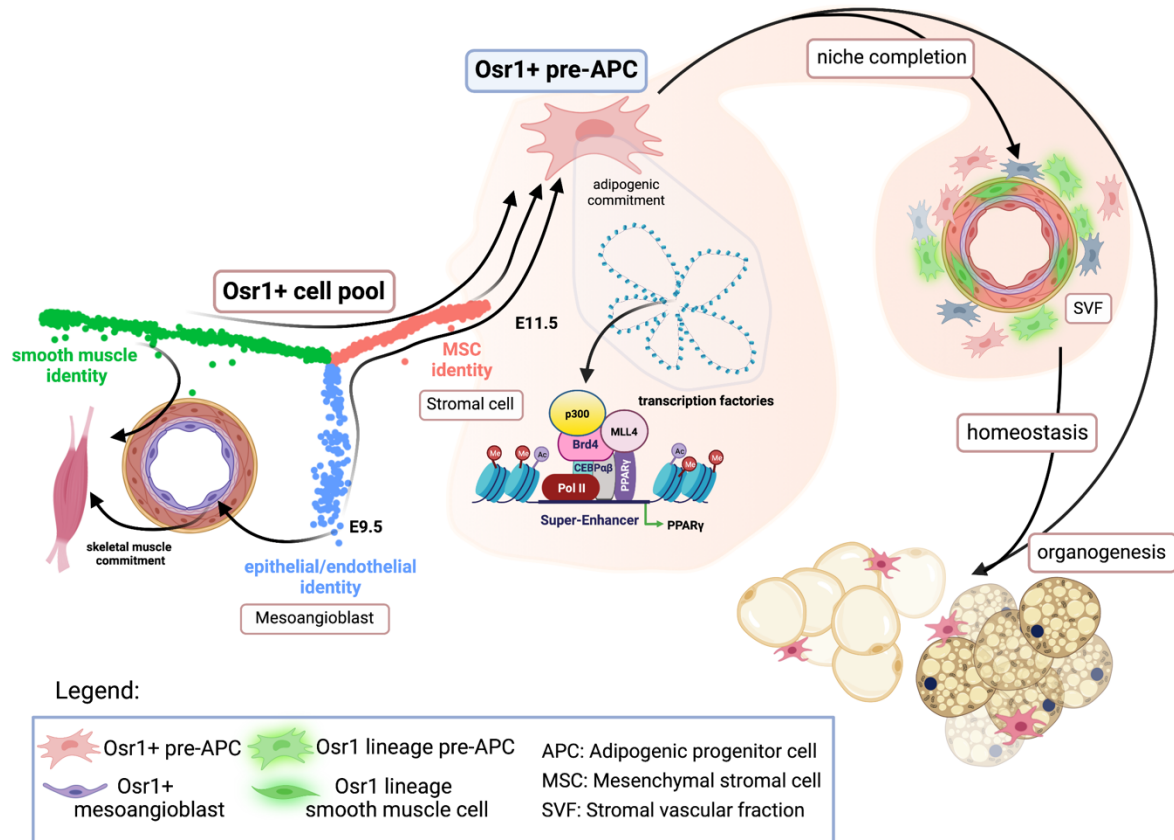
Figure 84: The assignment of the Osr1 lineage to the adipogenic fate
A multipotent endothelial cell at E9.5 and a mesenchymal stromal cell at E11.5 has the potential to directly contribute to adipose tissue organogenesis or/and to populate the stromal vascular fraction (SVF) of mature adipose tissue. Osr1+ cells in the adipogenic niche, upon external stimulation feed in the adipocyte pool to promote tissue remodulating. Interaction of OSR1 with epigenomic factors introduce a powerful machinery that primes and activates super-enhancers of the adipogenic program. MSC: mesenchymal stromal cells; SVF: stromal vascular fraction. Created with BioRender.com.

7 FUTURE PERSPECTIVE

This work introduced Osr1 as common marker of distinct pre-adipogenic progenitor subsets during embryogenesis and postnatal life. The analysis of Osr1+ cells in different phases of prenatal and postnatal life offered new insights and a better understanding of how the adipogenic lineage is established. Thus, extraction of Osr1 cells from different stages and anatomical regions together, specifically help to identify the signature transitions on a single cell level that recapitulates mesenchymal lineage specification processes. These data would provide further conclusion and knowledge of intermediate steps of a gradual fate decision making process in a time resolved manner.

Osr1 can be implemented to identify new pre-adipogenic microenvironments to in turn develop an understanding of a niche assembly and its cell type composition since Osr1 labeled intermediate states of a fate commitment action. A novel technique called spot-based spatial cell-type analysis by multidimensional mRNA density estimation (SSAM) would offer a starting point to investigate cell type interaction and crosstalk in a 2D and 3D.

In this study it was emphasized that Osr1 interacts with epigenetic remodelers that have been described to be crucial to promote the adipogenic identity. Thus, investigation of the epigenetic marks in the adipogenic landscape in Osr1 knockout cells compared to its respective controls would demonstrate whether activating histone marks or chromatin architecture changed and thus caused miss-regulation of the adipogenic program in the Osr1 knockout cells. Besides that, proximity ligation assays revealed that the interaction with pre-adipogenic epigenetic remodelers specifically takes place in a discrete location in the nucleus. Here, the investigation of that distinct transcriptional regulator complex, its functional units, 3D chromatin architecture as well as gene targets and involved enhancer communities, is potent to shed some light on the strategy of how Osr1 introduces the pre-adipogenic signature. Conclusions would enable to target the Osr1 mediated pre-adipogenic pathway with specific drugs to modulate the process in any direction.

The myogenic potential was recognized to be suppressed in the Osr1+ cells. Here, the aim would be to first understand the mechanism by identifying the collaborators of Osr1 to be able to titrate or control the process of skeletal muscle and adipose tissue formation to fight health problems of our society. Furthermore, the Osr1+ population of

mature adipose tissue was confirmed to have an adipogenic potential but also to be potentially in charge to inhibit or control the adipose tissue expansion by a non-cell autonomous mechanism. That indication opens a new chapter and question how Osr1+ cells can be implemented in therapies to overcome obesity and consequently asks how to identify stimuli that can be used to support and maintain the state of health.

8 REFERENCES

ACCILI, D. & TAYLOR, S. I. 1991. Targeted inactivation of the insulin receptor gene in mouse 3T3-L1 fibroblasts via homologous recombination. *Proc Natl Acad Sci U S A,* 88**,** 4708-12.

AKUNE, T., OHBA, S., KAMEKURA, S., YAMAGUCHI, M., CHUNG, U. I., KUBOTA, N., TERAUCHI, Y., HARADA, Y., AZUMA, Y., NAKAMURA, K., KADOWAKI, T. & KAWAGUCHI, H. 2004. PPARgamma insufficiency enhances osteogenesis through osteoblast formation from bone marrow progenitors. *J Clin Invest,* 113**,** 846-55.

ANGUEIRA, A. R., SAKERS, A. P., HOLMAN, C. D., CHENG, L., ARBOCCO, M. N., SHAMSI, F., LYNES, M. D., SHRESTHA, R., OKADA, C., BATMANOV, K., SUSZTAK, K., TSENG, Y. H., LIAW, L. & SEALE, P. 2021. Defining the lineage of thermogenic perivascular adipose tissue. *Nat Metab,* 3**,** 469-484.

ATIT, R., SGAIER, S. K., MOHAMED, O. A., TAKETO, M. M., DUFORT, D., JOYNER, A. L., NISWANDER, L. & CONLON, R. A. 2006. Beta-catenin activation is necessary and sufficient to specify the dorsal dermal fate in the mouse. *Dev Biol,* 296**,** 164-76.

BARAK, Y., NELSON, M. C., ONG, E. S., JONES, Y. Z., RUIZ-LOZANO, P., CHIEN, K. R., KODER, A. & EVANS, R. M. 1999. PPAR gamma is required for placental, cardiac, and adipose tissue development. *Mol Cell,* 4**,** 585-95.

BEN-YAIR, R., KAHANE, N. & KALCHEIM, C. 2003. Coherent development of dermomyotome and dermis from the entire mediolateral extent of the dorsal somite. *Development,* 130**,** 4325-36.

BERGERS, G., BREKKEN, R., MCMAHON, G., VU, T. H., ITOH, T., TAMAKI, K., TANZAWA, K., THORPE, P., ITOHARA, S., WERB, Z. & HANAHAN, D. 2000. Matrix metalloproteinase-9 triggers the angiogenic switch during carcinogenesis. *Nat Cell Biol,* 2**,** 737-44.

BERNSTEIN, B. E., MIKKELSEN, T. S., XIE, X., KAMAL, M., HUEBERT, D. J., CUFF, J., FRY, B., MEISSNER, A., WERNIG, M., PLATH, K., JAENISCH, R., WAGSCHAL, A., FEIL, R., SCHREIBER, S. L. & LANDER, E. S. 2006. A bivalent chromatin structure marks key developmental genes in embryonic stem cells. *Cell,* 125**,** 315-26.

BILLON, N., IANNARELLI, P., MONTEIRO, M. C., GLAVIEUX-PARDANAUD, C., RICHARDSON, W. D., KESSARIS, N., DANI, C. & DUPIN, E. 2007. The generation of adipocytes by the neural crest. *Development,* 134**,** 2283-92.

BISWAS, S. & RAO, C. M. 2018. Epigenetic tools (The Writers, The Readers and The Erasers) and their implications in cancer therapy. *Eur J Pharmacol,* 837**,** 8-24.

BLÜHER, M., MICHAEL, M. D., PERONI, O. D., UEKI, K., CARTER, N., KAHN, B. B. & KAHN, C. R. 2002. Adipose tissue selective insulin receptor knockout protects against obesity and obesity-related glucose intolerance. *Dev Cell,* 3**,** 25-38.

BOULOUMIÉ, A., SENGENÈS, C., PORTOLAN, G., GALITZKY, J. & LAFONTAN, M. 2001. Adipocyte Produces Matrix Metalloproteinases 2 and 9. *Diabetes,* 50**,** 2080.

BOURIN, P., BUNNELL, B. A., CASTEILLA, L., DOMINICI, M., KATZ, A. J., MARCH, K. L., REDL, H., RUBIN, J. P., YOSHIMURA, K. & GIMBLE, J. M. 2013. Stromal cells from the adipose tissue-derived stromal vascular fraction and culture expanded adipose tissue-derived stromal/stem cells: a joint statement of the International Federation for Adipose Therapeutics and Science (IFATS) and the International Society for Cellular Therapy (ISCT). *Cytotherapy,* 15**,** 641-8.

BOWERS, R. R., KIM, J. W., OTTO, T. C. & LANE, M. D. 2006. Stable stem cell commitment to the adipocyte lineage by inhibition of DNA methylation: role of the BMP-4 gene. *Proc Natl Acad Sci U S A,* 103**,** 13022-7.

BRAKENHIELM, E., VEITONMAKI, N., CAO, R., KIHARA, S., MATSUZAWA, Y., ZHIVOTOVSKY, B., FUNAHASHI, T. & CAO, Y. 2004. Adiponectin-induced antiangiogenesis and antitumor activity involve caspase-mediated endothelial cell apoptosis. *Proc Natl Acad Sci U S A,* 101**,** 2476-81.

BROWN, J. D., FELDMAN, Z. B., DOHERTY, S. P., REYES, J. M., RAHL, P. B., LIN, C. Y., SHENG, Q., DUAN, Q., FEDERATION, A. J., KUNG, A. L., HALDAR, S. M., YOUNG, R. A., PLUTZKY, J. & BRADNER, J. E. 2018. BET bromodomain proteins regulate enhancer function during adipogenesis. *Proc Natl Acad Sci U S A,* 115**,** 2144-2149.

BRYAN, B. A., MITCHELL, D. C., ZHAO, L., MA, W., STAFFORD, L. J., TENG, B. B. & LIU, M. 2005. Modulation of muscle regeneration, myogenesis, and adipogenesis by the Rho family guanine nucleotide exchange factor GEFT. *Mol Cell Biol,* 25**,** 11089-101.

CAMELL, C. D., SANDER, J., SPADARO, O., LEE, A., NGUYEN, K. Y., WING, A., GOLDBERG, E. L., YOUM, Y. H., BROWN, C. W., ELSWORTH, J., RODEHEFFER, M. S., SCHULTZE, J. L. & DIXIT, V. D. 2017. Inflammasome-driven catecholamine catabolism in macrophages blunts lipolysis during ageing. *Nature,* 550**,** 119-123.

CAO, J., SPIELMANN, M., QIU, X., HUANG, X., IBRAHIM, D. M., HILL, A. J., ZHANG, F., MUNDLOS, S., CHRISTIANSEN, L., STEEMERS, F. J., TRAPNELL, C. & SHENDURE, J. 2019. The single-cell transcriptional landscape of mammalian organogenesis. *Nature,* 566**,** 496-502.

CAO, R., BRAKENHIELM, E., WAHLESTEDT, C., THYBERG, J. & CAO, Y. 2001. Leptin induces vascular permeability and synergistically stimulates angiogenesis with FGF-2 and VEGF. *Proc Natl Acad Sci U S A,* 98**,** 6390-5.

CAO, Y. 2007. Angiogenesis modulates adipogenesis and obesity. *J Clin Invest,* 117**,** 2362-8.

CAO, Y. 2010. Adipose tissue angiogenesis as a therapeutic target for obesity and metabolic diseases. *Nat Rev Drug Discov,* 9**,** 107-15.

CAO, Z., UMEK, R. M. & MCKNIGHT, S. L. 1991. Regulated expression of three C/EBP isoforms during adipose conversion of 3T3-L1 cells. *Genes Dev,* 5**,** 1538-52.

CAWTHORN, W. P., BREE, A. J., YAO, Y., DU, B., HEMATI, N., MARTINEZ-SANTIBAÑEZ, G. & MACDOUGALD, O. A. 2012. Wnt6, Wnt10a and Wnt10b inhibit adipogenesis and stimulate osteoblastogenesis through a β-catenin-dependent mechanism. *Bone,* 50**,** 477-89.

CHAU, Y. Y., BANDIERA, R., SERRELS, A., MARTINEZ-ESTRADA, O. M., QING, W., LEE, M., SLIGHT, J., THORNBURN, A., BERRY, R., MCHAFFIE, S., STIMSON, R. H., WALKER, B. R., CHAPULI, R. M., SCHEDL, A. & HASTIE, N. 2014. Visceral and subcutaneous fat have different origins and evidence supports a mesothelial source. *Nat Cell Biol,* 16**,** 367-75.

CHAWLA, A., NGUYEN, K. D. & GOH, Y. P. 2011. Macrophage-mediated inflammation in metabolic disease. *Nat Rev Immunol,* 11**,** 738-49.

CHEN, E. Y., TAN, C. M., KOU, Y., DUAN, Q., WANG, Z., MEIRELLES, G. V., CLARK, N. R. & MA'AYAN, A. 2013. Enrichr: interactive and collaborative HTML5 gene list enrichment analysis tool. *BMC Bioinformatics,* 14**,** 128.

CHEN, T. & DENT, S. Y. 2014. Chromatin modifiers and remodellers: regulators of cellular differentiation. *Nat Rev Genet,* 15**,** 93-106.

CHO, D. S., LEE, B. & DOLES, J. D. 2019. Refining the adipose progenitor cell landscape in healthy and obese visceral adipose tissue using single-cell gene expression profiling. *Life Sci Alliance,* 2.

CHO, Y. W., HONG, S., JIN, Q., WANG, L., LEE, J. E., GAVRILOVA, O. & GE, K. 2009. Histone methylation regulator PTIP is required for PPARgamma and C/EBPalpha expression and adipogenesis. *Cell Metab,* 10**,** 27-39.

CHOI, Y. H., PARK, S., HOCKMAN, S., ZMUDA-TRZEBIATOWSKA, E., SVENNELID, F., HALUZIK, M., GAVRILOVA, O., AHMAD, F., PEPIN, L., NAPOLITANO, M., TAIRA, M., SUNDLER, F., STENSON HOLST, L., DEGERMAN, E. & MANGANIELLO, V. C. 2006. Alterations in regulation of energy homeostasis in cyclic nucleotide phosphodiesterase 3B-null mice. *J Clin Invest,* 116**,** 3240-51.

CHRISTIAENS, V. & LIJNEN, H. R. 2006. Role of the fibrinolytic and matrix metalloproteinase systems in development of adipose tissue. *Arch Physiol Biochem,* 112**,** 254-9.

CÎMPEAN, A. M., RAICA, M. & SUCIU, C. 2007. CD105/smooth muscle actin double immunostaining discriminate between immature and mature tumor blood vessels. *Rom J Morphol Embryol,* 48**,** 41-5.

CINTI, S. 2009. Transdifferentiation properties of adipocytes in the adipose organ. *Am J Physiol Endocrinol Metab,* 297**,** E977-86.

CINTI, S. 2012. The adipose organ at a glance. *Dis Model Mech,* 5**,** 588-94.

CLARKE, S. L., ROBINSON, C. E. & GIMBLE, J. M. 1997. CAAT/enhancer binding proteins directly modulate transcription from the peroxisome proliferator-activated receptor gamma 2 promoter. *Biochem Biophys Res Commun,* 240**,** 99-103.

CORNIER, M. A., DABELEA, D., HERNANDEZ, T. L., LINDSTROM, R. C., STEIG, A. J., STOB, N. R., VAN PELT, R. E., WANG, H. & ECKEL, R. H. 2008. The metabolic syndrome. *Endocr Rev,* 29**,** 777-822.

COULTER, D. E., SWAYKUS, E. A., BERAN-KOEHN, M. A., GOLDBERG, D., WIESCHAUS, E. & SCHEDL, P. 1990. Molecular analysis of odd-skipped, a zinc finger encoding segmentation gene with a novel pair-rule expression pattern. *The EMBO Journal,* 9**,** 3795-3804.

COULTER, D. E. & WIESCHAUS, E. 1988. Gene activities and segmental patterning in Drosophila: analysis of odd-skipped and pair-rule double mutants. *Genes Dev,* 2**,** 1812-23.

CRANDALL, D. L., HAUSMAN, G. J. & KRAL, J. G. 1997. A review of the microcirculation of adipose tissue: anatomic, metabolic, and angiogenic perspectives. *Microcirculation,* 4**,** 211-32.

CRISTANCHO, A. G. & LAZAR, M. A. 2011. Forming functional fat: a growing understanding of adipocyte differentiation. *Nat Rev Mol Cell Biol,* 12**,** 722-34.

DE FRAIPONT, F., NICHOLSON, A. C., FEIGE, J.-J. & VAN MEIR, E. G. 2001. Thrombospondins and tumor angiogenesis. *Trends in Molecular Medicine,* 7**,** 401-407.

DEBEER, P., DE RAVEL, T. J. L., DEVRIENDT, K., FRYNS, J.-P., HUYSMANS, C. & VAN DE VEN, W. J. M. 2002. Human homologues of Osr1 and Osr2 are not involved in a syndrome with distal limb deficiencies, oral abnormalities, and renal defects. *American Journal of Medical Genetics,* 111**,** 455-456.

DUPONT, C., ARMANT, D. R. & BRENNER, C. A. 2009. Epigenetics: definition, mechanisms and clinical perspective. *Semin Reprod Med,* 27**,** 351-7.

ENGLEKA, K. A., GITLER, A. D., ZHANG, M., ZHOU, D. D., HIGH, F. A. & EPSTEIN, J. A. 2005. Insertion of Cre into the Pax3 locus creates a new allele of Splotch and identifies unexpected Pax3 derivatives. *Dev Biol,* 280**,** 396-406.

FANTUZZI, G. & FAGGIONI, R. 2000. Leptin in the regulation of immunity, inflammation, and hematopoiesis. *J Leukoc Biol,* 68**,** 437-46.

FARAHANI, R. M. & XAYMARDAN, M. 2015. Platelet-Derived Growth Factor Receptor Alpha as a Marker of Mesenchymal Stem Cells in Development and Stem Cell Biology. *Stem Cells Int,* 2015**,** 362753.

FARMER, S. R. 2006. Transcriptional control of adipocyte formation. *Cell Metab,* 4**,** 263-73.

FEINGOLD, K. R., DOERRLER, W., DINARELLO, C. A., FIERS, W. & GRUNFELD, C. 1992. Stimulation of lipolysis in cultured fat cells by tumor necrosis factor, interleukin-1, and the interferons is blocked by inhibition of prostaglandin synthesis. *Endocrinology,* 130**,** 10-6.

FLATT, J. P. & BALL, E. G. 1964. Studies on the Metabolism of Adipose Tissue. *Journal of Biological Chemistry,* 239**,** 675-685.

FOLKMAN, J. 1995. Angiogenesis in cancer, vascular, rheumatoid and other disease. *Nat Med,* 1**,** 27-31.

FONTAINE, C., COUSIN, W., PLAISANT, M., DANI, C. & PERALDI, P. 2008. Hedgehog signaling alters adipocyte maturation of human mesenchymal stem cells. *Stem Cells,* 26**,** 1037-46.

FREESE, J., KLEMENT, R. J., RUIZ-NUNEZ, B., SCHWARZ, S. & LOTZERICH, H. 2017. The sedentary (r)evolution: Have we lost our metabolic flexibility? *F1000Res,* 6**,** 1787.

GABELLA, G. 1989. Development of smooth muscle: ultrastructural study of the chick embryo gizzard. *Anatomy and Embryology,* 180**,** 213-226.

GALLO, M. A. & KAUFMAN, D. 1997. Antagonistic and agonistic effects of tamoxifen: significance in human cancer. *Semin Oncol,* 24**,** S1-71-s1-80.

GESTA, S., TSENG, Y. H. & KAHN, C. R. 2007. Developmental origin of fat: tracking obesity to its source. *Cell,* 131**,** 242-56.

GHABEN, A. L. & SCHERER, P. E. 2019. Adipogenesis and metabolic health. *Nat Rev Mol Cell Biol,* 20**,** 242-258.

GOLDSTEIN, R. E., COOK, O., DINUR, T., PISANTE, A., KARANDIKAR, U. C., BIDWAI, A. & PAROUSH, Z. 2005. An eh1-like motif in odd-skipped mediates recruitment of Groucho and repression in vivo. *Mol Cell Biol,* 25**,** 10711-20.

GRANNEMAN, J. G., LI, P., ZHU, Z. & LU, Y. 2005. Metabolic and cellular plasticity in white adipose tissue I: effects of beta3-adrenergic receptor activation. *Am J Physiol Endocrinol Metab,* 289**,** E608-16.

GRENIER, G., SCIMÈ, A., LE GRAND, F., ASAKURA, A., PEREZ-IRATXETA, C., ANDRADE-NAVARRO, M. A., LABOSKY, P. A. & RUDNICKI, M. A. 2007. Resident endothelial precursors in muscle, adipose, and dermis contribute to postnatal vasculogenesis. *Stem Cells,* 25**,** 3101-10.

GROS, J., SCAAL, M. & MARCELLE, C. 2004. A two-step mechanism for myotome formation in chick. *Dev Cell,* 6**,** 875-82.

GUELEN, L., PAGIE, L., BRASSET, E., MEULEMAN, W., FAZA, M. B., TALHOUT, W., EUSSEN, B. H., DE KLEIN, A., WESSELS, L., DE LAAT, W. & VAN STEENSEL, B. 2008. Domain organization of human chromosomes revealed by mapping of nuclear lamina interactions. *Nature,* 453**,** 948-51.

GUENTHER, M. G., LEVINE, S. S., BOYER, L. A., JAENISCH, R. & YOUNG, R. A. 2007. A chromatin landmark and transcription initiation at most promoters in human cells. *Cell,* 130**,** 77-88.

HAEUSLER, R. A., MCGRAW, T. E. & ACCILI, D. 2018. Biochemical and cellular properties of insulin receptor signalling. *Nat Rev Mol Cell Biol,* 19**,** 31-44.

HARMS, M. & SEALE, P. 2013. Brown and beige fat: development, function and therapeutic potential. *Nat Med,* 19**,** 1252-63.

HARVEY, I., BOUDREAU, A. & STEPHENS, J. M. 2020. Adipose tissue in health and disease. *Open Biol,* 10**,** 200291.

HAYASHI, S. & MCMAHON, A. P. 2002. Efficient recombination in diverse tissues by a tamoxifen-inducible form of Cre: a tool for temporally regulated gene activation/inactivation in the mouse. *Dev Biol,* 244**,** 305-18.

HNISZ, D., ABRAHAM, B. J., LEE, T. I., LAU, A., SAINT-ANDRE, V., SIGOVA, A. A., HOKE, H. A. & YOUNG, R. A. 2013. Super-enhancers in the control of cell identity and disease. *Cell,* 155**,** 934-47.

HOOPER, J. E. & SCOTT, M. P. 2005. Communicating with Hedgehogs. *Nat Rev Mol Cell Biol,* 6**,** 306-17.

HOSOGAI, N., FUKUHARA, A., OSHIMA, K., MIYATA, Y., TANAKA, S., SEGAWA, K., FURUKAWA, S., TOCHINO, Y., KOMURO, R., MATSUDA, M. & SHIMOMURA, I. 2007. Adipose tissue hypoxia in obesity and its impact on adipocytokine dysregulation. *Diabetes,* 56**,** 901-11.

HOTAMISLIGIL, G. S. 2006. Inflammation and metabolic disorders. *Nature,* 444**,** 860-7.

HOU, C., ZHAO, H., TANIMOTO, K. & DEAN, A. 2008. CTCF-dependent enhancer-blocking by alternative chromatin loop formation. *Proc Natl Acad Sci U S A,* 105**,** 20398-403.

HUANG, H., SONG, T. J., LI, X., HU, L., HE, Q., LIU, M., LANE, M. D. & TANG, Q. Q. 2009. BMP signaling pathway is required for commitment of C3H10T1/2 pluripotent stem cells to the adipocyte lineage. *Proc Natl Acad Sci U S A,* 106**,** 12670-5.

HUDAK, C. S., GULYAEVA, O., WANG, Y., PARK, S. M., LEE, L., KANG, C. & SUL, H. S. 2014. Pref-1 marks very early mesenchymal precursors required for adipose tissue development and expansion. *Cell Rep,* 8**,** 678-87.

INAGAKI, T., SAKAI, J. & KAJIMURA, S. 2016. Transcriptional and epigenetic control of brown and beige adipose cell fate and function. *Nat Rev Mol Cell Biol,* 17**,** 480-95.

JAMES, R. G., KAMEI, C. N., WANG, Q., JIANG, R. & SCHULTHEISS, T. M. 2006. Odd-skipped related 1 is required for development of the metanephric kidney and regulates formation and differentiation of kidney precursor cells. *Development,* 133**,** 2995-3004.

JAMES, R. G. & SCHULTHEISS, T. M. 2005. Bmp signaling promotes intermediate mesoderm gene expression in a dose-dependent, cell-autonomous and translation-dependent manner. *Dev Biol,* 288**,** 113-25.

JEON, M. J., KIM, J. A., KWON, S. H., KIM, S. W., PARK, K. S., PARK, S. W., KIM, S. Y. & SHIN, C. S. 2003. Activation of peroxisome proliferator-activated receptor-gamma inhibits the Runx2-mediated transcription of osteocalcin in osteoblasts. *J Biol Chem,* 278**,** 23270-7.

JIANG, Y., BERRY, D. C. & GRAFF, J. M. 2017. Distinct cellular and molecular mechanisms for beta3 adrenergic receptor-induced beige adipocyte formation. *Elife,* 6.

JIANG, Y., BERRY, D. C., TANG, W. & GRAFF, J. M. 2014. Independent stem cell lineages regulate adipose organogenesis and adipose homeostasis. *Cell Rep,* 9**,** 1007-22.

JOE, A. W., YI, L., EVEN, Y., VOGL, A. W. & ROSSI, F. M. 2009. Depot-specific differences in adipogenic progenitor abundance and proliferative response to high-fat diet. *Stem Cells,* 27**,** 2563-70.

KATAGIRI, T. & WATABE, T. 2016. Bone Morphogenetic Proteins. *Cold Spring Harb Perspect Biol,* 8.

KATOH, M. 2002. Molecular cloning and characterization of OSR1 on human chromosome 2p24. *Int J Mol Med,* 10**,** 221-5.

KAWAGUCHI, N., XU, X., TAJIMA, R., KRONQVIST, P., SUNDBERG, C., LOECHEL, F., ALBRECHTSEN, R. & WEWER, U. M. 2002. ADAM 12 Protease Induces Adipogenesis in Transgenic Mice. *The American Journal of Pathology,* 160**,** 1895-1903.

KELLER, C., HANSEN, M. S., COFFIN, C. M. & CAPECCHI, M. R. 2004. Pax3:Fkhr interferes with embryonic Pax3 and Pax7 function: implications for alveolar rhabdomyosarcoma cell of origin. *Genes Dev,* 18**,** 2608-13.

KINAMERI, E., INOUE, T., ARUGA, J., IMAYOSHI, I., KAGEYAMA, R., SHIMOGORI, T. & MOORE, A. W. 2008. Prdm proto-oncogene transcription factor family expression and interaction with the Notch-Hes pathway in mouse neurogenesis. *PLoS One,* 3**,** e3859.

KLEMM, D. J., LEITNER, J. W., WATSON, P., NESTEROVA, A., REUSCH, J. E., GOALSTONE, M. L. & DRAZNIN, B. 2001. Insulin-induced adipocyte differentiation. Activation of CREB rescues adipogenesis from the arrest caused by inhibition of prenylation. *J Biol Chem,* 276**,** 28430-5.

KOZAK, L. P. 2011. The genetics of brown adipocyte induction in white fat depots. *Front Endocrinol (Lausanne),* 2**,** 64.

KOZAK, L. P. & ANUNCIADO-KOZA, R. 2008. UCP1: its involvement and utility in obesity. *Int J Obes (Lond),* 32 Suppl 7**,** S32-8.

KULESHOV, M. V., JONES, M. R., ROUILLARD, A. D., FERNANDEZ, N. F., DUAN, Q., WANG, Z., KOPLEV, S., JENKINS, S. L., JAGODNIK, K. M., LACHMANN, A., MCDERMOTT, M. G., MONTEIRO, C. D., GUNDERSEN, G. W. & MA'AYAN, A. 2016. Enrichr: a comprehensive gene set enrichment analysis web server 2016 update. *Nucleic Acids Res,* 44**,** W90-7.

KUZNETSOV, A. V., HERMANN, M., SAKS, V., HENGSTER, P. & MARGREITER, R. 2009. The cell-type specificity of mitochondrial dynamics. *Int J Biochem Cell Biol,* 41**,** 1928-39.

LAEMMLI, U. K. 1970. Cleavage of Structural Proteins during the Assembly of the Head of Bacteriophage T4. *Nature,* 227**,** 680-685.

LAN, Y., LIU, H., OVITT, C. E. & JIANG, R. 2011. Generation of Osr1 conditional mutant mice. *Genesis,* 49**,** 419-22.

LANDSCHULZ, W. H., JOHNSON, P. F. & MCKNIGHT, S. L. 1989. The DNA binding domain of the rat liver nuclear protein C/EBP is bipartite. *Science,* 243**,** 1681-8.

LANE, M. D., TANG, Q.-Q. & JIANG, M.-S. 1999. Role of the CCAAT Enhancer Binding Proteins (C/EBPs) in Adipocyte Differentiation. *Biochemical and Biophysical Research Communications,* 266**,** 677-683.

LANG, D., LU, M. M., HUANG, L., ENGLEKA, K. A., ZHANG, M., CHU, E. Y., LIPNER, S., SKOULTCHI, A., MILLAR, S. E. & EPSTEIN, J. A. 2005. Pax3 functions at a nodal point in melanocyte stem cell differentiation. *Nature,* 433**,** 884-887.

LAWSON, K. A., MENESES, J. J. & PEDERSEN, R. A. 1991. Clonal analysis of epiblast fate during germ layer formation in the mouse embryo. *Development,* 113**,** 891-911.

LAZAR, M. A. 2005. How obesity causes diabetes: not a tall tale. *Science,* 307**,** 373-5.

LEE, J. E. & GE, K. 2014. Transcriptional and epigenetic regulation of PPARgamma expression during adipogenesis. *Cell Biosci,* 4**,** 29.

LEE, J. E., SCHMIDT, H., LAI, B. & GE, K. 2019. Transcriptional and Epigenomic Regulation of Adipogenesis. *Mol Cell Biol,* 39.

LEE, J. E., WANG, C., XU, S., CHO, Y. W., WANG, L., FENG, X., BALDRIDGE, A., SARTORELLI, V., ZHUANG, L., PENG, W. & GE, K. 2013a. H3K4 mono- and di-methyltransferase MLL4 is required for enhancer activation during cell differentiation. *Elife,* 2**,** e01503.

LEE, Y. H., PETKOVA, A. P. & GRANNEMAN, J. G. 2013b. Identification of an adipogenic niche for adipose tissue remodeling and restoration. *Cell Metab,* 18**,** 355-67.

LEE, Y. H., PETKOVA, A. P., MOTTILLO, E. P. & GRANNEMAN, J. G. 2012. In vivo identification of bipotential adipocyte progenitors recruited by beta3-adrenoceptor activation and high-fat feeding. *Cell Metab,* 15**,** 480-91.

LEE, Y. H., THACKER, R. I., HALL, B. E., KONG, R. & GRANNEMAN, J. G. 2014. Exploring the activated adipogenic niche: interactions of macrophages and adipocyte progenitors. *Cell Cycle,* 13**,** 184-90.

LEHRKE, M. & LAZAR, M. A. 2005. The many faces of PPARgamma. *Cell,* 123**,** 993-9.

LEPPER, C., CONWAY, S. J. & FAN, C. M. 2009. Adult satellite cells and embryonic muscle progenitors have distinct genetic requirements. *Nature,* 460**,** 627-31.

LEPPER, C. & FAN, C. M. 2010. Inducible lineage tracing of Pax7-descendant cells reveals embryonic origin of adult satellite cells. *Genesis,* 48**,** 424-36.

LIJNEN, H. R. 2008. Angiogenesis and obesity. *Cardiovasc Res,* 78**,** 286-93.

LIN, H., TANG, Y., LOZITO, T. P., OYSTER, N., WANG, B. & TUAN, R. S. 2019. Efficient in vivo bone formation by BMP-2 engineered human mesenchymal stem cells encapsulated in a projection stereolithographically fabricated hydrogel scaffold. *Stem Cell Res Ther,* 10**,** 254.

LOGAN, C. Y. & NUSSE, R. 2004. The Wnt signaling pathway in development and disease. *Annu Rev Cell Dev Biol,* 20**,** 781-810.

LV, X. J., ZHOU, G. D., LIU, Y., LIU, X., CHEN, J. N., LUO, X. S. & CAO, Y. L. 2012. In vitro proliferation and differentiation of adipose-derived stem cells isolated using anti-CD105 magnetic beads. *Int J Mol Med,* 30**,** 826-34.

MADSEN, J. G. S., MADSEN, M. S., RAUCH, A., TRAYNOR, S., VAN HAUWAERT, E. L., HAAKONSSON, A. K., JAVIERRE, B. M., HYLDAHL, M., FRASER, P. & MANDRUP, S. 2020. Highly interconnected enhancer communities control lineage-determining genes in human mesenchymal stem cells. *Nat Genet,* 52**,** 1227-1238.

MAHADEV, K., WU, X., DONNELLY, S., OUEDRAOGO, R., ECKHART, A. D. & GOLDSTEIN, B. J. 2008. Adiponectin inhibits vascular endothelial growth factor-induced migration of human coronary artery endothelial cells. *Cardiovasc Res,* 78**,** 376-84.

MAKKI, K., FROGUEL, P. & WOLOWCZUK, I. 2013. Adipose tissue in obesity-related inflammation and insulin resistance: cells, cytokines, and chemokines. *ISRN Inflamm,* 2013**,** 139239.

MARCHETTI, P., BUGLIANI, M., DE TATA, V., SULEIMAN, M. & MARSELLI, L. 2017. Pancreatic Beta Cell Identity in Humans and the Role of Type 2 Diabetes. *Front Cell Dev Biol,* 5**,** 55.

MARTIN, S. K., FITTER, S., DUTTA, A. K., MATTHEWS, M. P., WALKLEY, C. R., HALL, M. N., RUEGG, M. A., GRONTHOS, S. & ZANNETTINO, A. C. 2015. Brief report: the differential roles of mTORC1 and mTORC2 in mesenchymal stem cell differentiation. *Stem Cells,* 33**,** 1359-65.

MARTINEZ-SANTIBANEZ, G. Insights on Adipose Tissue Extracellular Matrix Remodeling: Models of Diet-Induced Obesity and Weight Loss. 2015.

MATHARU, N. & AHITUV, N. 2015. Minor Loops in Major Folds: Enhancer-Promoter Looping, Chromatin Restructuring, and Their Association with Transcriptional Regulation and Disease. *PLoS Genet,* 11**,** e1005640.

MATSUOKA, T., AHLBERG, P. E., KESSARIS, N., IANNARELLI, P., DENNEHY, U., RICHARDSON, W. D., MCMAHON, A. P. & KOENTGES, G. 2005. Neural crest origins of the neck and shoulder. *Nature,* 436**,** 347-55.

MAYEUF-LOUCHART, A., LANCEL, S., SEBTI, Y., POURCET, B., LOYENS, A., DELHAYE, S., DUHEM, C., BEAUCHAMP, J., FERRI, L., THOREL, Q., BOULINGUIEZ, A., ZECCHIN, M., DUBOIS-CHEVALIER, J., EECKHOUTE, J., VAUGHN, L. T., ROACH, P. J., DANI, C., PEDERSON, B. A., VINCENT, S. D., STAELS, B. & DUEZ, H. 2019. Glycogen Dynamics Drives Lipid Droplet Biogenesis during Brown Adipocyte Differentiation. *Cell Rep,* 29**,** 1410-1418 e6.

MEISSNER, A., MIKKELSEN, T. S., GU, H., WERNIG, M., HANNA, J., SIVACHENKO, A., ZHANG, X., BERNSTEIN, B. E., NUSBAUM, C., JAFFE, D. B., GNIRKE, A., JAENISCH, R. & LANDER, E. S. 2008. Genome-scale DNA methylation maps of pluripotent and differentiated cells. *Nature,* 454**,** 766-70.

MELIGA, E., STREM, B. M., DUCKERS, H. J. & SERRUYS, P. W. 2007. Adipose-Derived Cells. *Cell Transplantation,* 16**,** 963-970.

MIKKELSEN, T. S., KU, M., JAFFE, D. B., ISSAC, B., LIEBERMAN, E., GIANNOUKOS, G., ALVAREZ, P., BROCKMAN, W., KIM, T. K., KOCHE, R. P., LEE, W., MENDENHALL, E., O'DONOVAN, A., PRESSER, A., RUSS, C., XIE, X., MEISSNER, A., WERNIG, M., JAENISCH, R., NUSBAUM, C., LANDER, E. S. & BERNSTEIN, B. E. 2007. Genome-wide maps of chromatin state in pluripotent and lineage-committed cells. *Nature,* 448**,** 553-60.

MIYAZONO, K., KAMIYA, Y. & MORIKAWA, M. 2010. Bone morphogenetic protein receptors and signal transduction. *J Biochem,* 147**,** 35-51.

MODICA, S., STRAUB, L. G., BALAZ, M., SUN, W., VARGA, L., STEFANICKA, P., PROFANT, M., SIMON, E., NEUBAUER, H., UKROPCOVA, B., UKROPEC, J. & WOLFRUM, C. 2016. Bmp4 Promotes a Brown to White-like Adipocyte Shift. *Cell Rep,* 16**,** 2243-2258.

MUECKLER, M. & THORENS, B. 2013. The SLC2 (GLUT) family of membrane transporters. *Mol Aspects Med,* 34**,** 121-38.

MUGFORD, J. W., SIPILA, P., MCMAHON, J. A. & MCMAHON, A. P. 2008. Osr1 expression demarcates a multi-potent population of intermediate mesoderm that undergoes progressive restriction to an Osr1-dependent nephron progenitor compartment within the mammalian kidney. *Dev Biol,* 324**,** 88-98.

MURPHY, M. M., LAWSON, J. A., MATHEW, S. J., HUTCHESON, D. A. & KARDON, G. 2011. Satellite cells, connective tissue fibroblasts and their interactions are crucial for muscle regeneration. *Development,* 138**,** 3625-37.

MUZUMDAR, M. D., TASIC, B., MIYAMICHI, K., LI, L. & LUO, L. 2007. A global double-fluorescent Cre reporter mouse. *Genesis,* 45**,** 593-605.

NAKAE, J., KITAMURA, T., KITAMURA, Y., BIGGS, W. H., 3RD, ARDEN, K. C. & ACCILI, D. 2003. The forkhead transcription factor Foxo1 regulates adipocyte differentiation. *Dev Cell,* 4**,** 119-29.

NAKAGAMI, H., MORISHITA, R., MAEDA, K., KIKUCHI, Y., OGIHARA, T. & KANEDA, Y. 2006. Adipose tissue-derived stromal cells as a novel option for regenerative cell therapy. *J Atheroscler Thromb,* 13**,** 77-81.

NAKAMURA, E., NGUYEN, M. T. & MACKEM, S. 2006. Kinetics of tamoxifen-regulated Cre activity in mice using a cartilage-specific CreER(T) to assay temporal activity windows along the proximodistal limb skeleton. *Dev Dyn,* 235**,** 2603-12.

NGUYEN, M. T., ZHU, J., NAKAMURA, E., BAO, X. & MACKEM, S. 2009. Tamoxifen-dependent, inducible Hoxb6CreERT recombinase function in lateral plate and limb mesoderm, CNS isthmic organizer, posterior trunk neural crest, hindgut, and tailbud. *Dev Dyn,* 238**,** 467-74.

NUEDA, M. L., BALADRON, V., SANCHEZ-SOLANA, B., BALLESTEROS, M. A. & LABORDA, J. 2007. The EGF-like protein dlk1 inhibits notch signaling and potentiates adipogenesis of mesenchymal cells. *J Mol Biol,* 367**,** 1281-93.

NÜSSLEIN-VOLHARD, C. & WIESCHAUS, E. 1980. Mutations affecting segment number and polarity in Drosophila. *Nature,* 287**,** 795-801.

OLIVERA-MARTINEZ, I., THÉLU, J. & DHOUAILLY, D. 2004. Molecular mechanisms controlling dorsal dermis generation from the somitic dermomyotome. *Int J Dev Biol,* 48**,** 93-101.

ONG, C. T. & CORCES, V. G. 2011. Enhancer function: new insights into the regulation of tissue-specific gene expression. *Nat Rev Genet,* 12**,** 283-93.

PANG, D. & THOMPSON, D. N. 2011. Embryology and bony malformations of the craniovertebral junction. *Childs Nerv Syst,* 27**,** 523-64.

PARK, H. Y., KWON, H. M., LIM, H. J., HONG, B. K., LEE, J. Y., PARK, B. E., JANG, Y., CHO, S. Y. & KIM, H. S. 2001. Potential role of leptin in angiogenesis: leptin induces endothelial cell proliferation and expression of matrix metalloproteinases in vivo and in vitro. *Exp Mol Med,* 33**,** 95-102.

PATEL, S. R. & DRESSLER, G. R. 2013. The genetics and epigenetics of kidney development. *Semin Nephrol,* 33**,** 314-26.

PHILLIPS, J. E. & CORCES, V. G. 2009. CTCF: master weaver of the genome. *Cell,* 137**,** 1194-211.

PIAO, M. & TOKUNAGA, O. 2006. Significant expression of endoglin (CD105), TGFbeta-1 and TGFbeta R-2 in the atherosclerotic aorta: an immunohistological study. *J Atheroscler Thromb,* 13**,** 82-9.

POMBO, A. & DILLON, N. 2015. Three-dimensional genome architecture: players and mechanisms. *Nat Rev Mol Cell Biol,* 16**,** 245-57.

POWELL, K. 2007. Obesity: the two faces of fat. *Nature,* 447**,** 525-7.

PRUMMEL, K. D., HESS, C., NIEUWENHUIZE, S., PARKER, H. J., ROGERS, K. W., KOZMIKOVA, I., RACIOPPI, C., BROMBACHER, E. C., CZARKWIANI, A., KNAPP, D., BURGER, S., CHIAVACCI, E., SHAH, G., BURGER, A., HUISKEN, J., YUN, M. H., CHRISTIAEN, L., KOZMIK, Z., MULLER, P., BRONNER, M., KRUMLAUF, R. & MOSIMANN, C. 2019. A conserved regulatory program initiates lateral plate mesoderm emergence across chordates. *Nat Commun,* 10**,** 3857.

PU, Q., ABDUELMULA, A., MASYUK, M., THEISS, C., SCHWANDULLA, D., HANS, M., PATEL, K., BRAND-SABERI, B. & HUANG, R. 2013. The dermomyotome ventrolateral lip is essential for the hypaxial myotome formation. *BMC Developmental Biology,* 13**,** 37.

RAJAKUMARI, S., WU, J., ISHIBASHI, J., LIM, H. W., GIANG, A. H., WON, K. J., REED, R. R. & SEALE, P. 2013. EBF2 determines and maintains brown adipocyte identity. *Cell Metab,* 17**,** 562-74.

RAJASHEKHAR, G., TRAKTUEV, D. O., ROELL, W. C., JOHNSTONE, B. H., MERFELD-CLAUSS, S., VAN NATTA, B., ROSEN, E. D., MARCH, K. L. & CLAUSS, M. 2008. IFATS collection: Adipose stromal cell differentiation is reduced by endothelial cell contact and paracrine communication: role of canonical Wnt signaling. *Stem Cells,* 26**,** 2674-81.

RAUCH, A. & MANDRUP, S. 2021. Transcriptional networks controlling stromal cell differentiation. *Nat Rev Mol Cell Biol,* 22**,** 465-482.

REIK, W. 2007. Stability and flexibility of epigenetic gene regulation in mammalian development. *Nature,* 447**,** 425-32.

RODEHEFFER, M. S., BIRSOY, K. & FRIEDMAN, J. M. 2008. Identification of white adipocyte progenitor cells in vivo. *Cell,* 135**,** 240-9.

RODRÍGUEZ, C. I., BUCHHOLZ, F., GALLOWAY, J., SEQUERRA, R., KASPER, J., AYALA, R., STEWART, A. F. & DYMECKI, S. M. 2000. High-efficiency deleter mice show that FLPe is an alternative to Cre-loxP. *Nature Genetics,* 25**,** 139-140.

ROSEN, E. D., HSU, C. H., WANG, X., SAKAI, S., FREEMAN, M. W., GONZALEZ, F. J. & SPIEGELMAN, B. M. 2002. C/EBPalpha induces adipogenesis through PPARgamma: a unified pathway. *Genes Dev,* 16**,** 22-6.

ROSEN, E. D. & MACDOUGALD, O. A. 2006. Adipocyte differentiation from the inside out. *Nat Rev Mol Cell Biol,* 7**,** 885-96.

ROSS, S. E., HEMATI, N., LONGO, K. A., BENNETT, C. N., LUCAS, P. C., ERICKSON, R. L. & MACDOUGALD, O. A. 2000. Inhibition of adipogenesis by Wnt signaling. *Science,* 289**,** 950-3.

SACCO, A., DOYONNAS, R., KRAFT, P., VITOROVIC, S. & BLAU, H. M. 2008. Self-renewal and expansion of single transplanted muscle stem cells. *Nature,* 456**,** 502-6.

SAITO, D. & TAKAHASHI, Y. 2015. Sympatho-adrenal morphogenesis regulated by the dorsal aorta. *Mech Dev,* 138 Pt 1**,** 2-7.

SALMA, N., XIAO, H. & IMBALZANO, A. N. 2006. Temporal recruitment of CCAAT/enhancer-binding proteins to early and late adipogenic promoters in vivo. *J Mol Endocrinol,* 36**,** 139-51.

SANCHEZ-GURMACHES, J. & GUERTIN, D. A. 2014a. Adipocyte lineages: tracing back the origins of fat. *Biochim Biophys Acta,* 1842**,** 340-51.

SANCHEZ-GURMACHES, J. & GUERTIN, D. A. 2014b. Adipocytes arise from multiple lineages that are heterogeneously and dynamically distributed. *Nat Commun,* 5**,** 4099.

SANCHEZ-GURMACHES, J., HSIAO, W. Y. & GUERTIN, D. A. 2015. Highly selective in vivo labeling of subcutaneous white adipocyte precursors with Prx1-Cre. *Stem Cell Reports,* 4**,** 541-50.

SANTORO, A., MCGRAW, T. E. & KAHN, B. B. 2021. Insulin action in adipocytes, adipose remodeling, and systemic effects. *Cell Metab,* 33**,** 748-757.

SARANTOPOULOS, C. N., BANYARD, D. A., ZIEGLER, M. E., SUN, B., SHATERIAN, A. & WIDGEROW, A. D. 2018. Elucidating the Preadipocyte and Its Role in Adipocyte Formation: a Comprehensive Review. *Stem Cell Rev Rep,* 14**,** 27-42.

SAULIER-LE DREAN, B., NASIADKA, A., DONG, J. & KRAUSE, H. M. 1998. Dynamic changes in the functions of Odd-skipped during early Drosophila embryogenesis. *Development,* 125**,** 4851-4861.

SCHULZ, T. J., HUANG, P., HUANG, T. L., XUE, R., MCDOUGALL, L. E., TOWNSEND, K. L., CYPESS, A. M., MISHINA, Y., GUSSONI, E. & TSENG, Y. H. 2013. Brown-fat paucity due to impaired BMP signalling induces compensatory browning of white fat. *Nature,* 495**,** 379-83.

SCHULZ, T. J., HUANG, T. L., TRAN, T. T., ZHANG, H., TOWNSEND, K. L., SHADRACH, J. L., CERLETTI, M., MCDOUGALL, L. E., GIORGADZE, N., TCHKONIA, T., SCHRIER, D., FALB, D., KIRKLAND, J. L., WAGERS, A. J. & TSENG, Y. H. 2011. Identification of inducible brown adipocyte progenitors residing in skeletal muscle and white fat. *Proc Natl Acad Sci U S A,* 108**,** 143-8.

SCHULZ, T. J. & TSENG, Y. H. 2009. Emerging role of bone morphogenetic proteins in adipogenesis and energy metabolism. *Cytokine Growth Factor Rev,* 20**,** 523-31.

SEALE, P., BJORK, B., YANG, W., KAJIMURA, S., CHIN, S., KUANG, S., SCIME, A., DEVARAKONDA, S., CONROE, H. M., ERDJUMENT-BROMAGE, H., TEMPST, P., RUDNICKI, M. A., BEIER, D. R. & SPIEGELMAN, B. M. 2008. PRDM16 controls a brown fat/skeletal muscle switch. *Nature,* 454**,** 961-7.

SEBO, Z. L., JEFFERY, E., HOLTRUP, B. & RODEHEFFER, M. S. 2018. A mesodermal fate map for adipose tissue. *Development,* 145.

SEBO, Z. L. & RODEHEFFER, M. S. 2019. Assembling the adipose organ: adipocyte lineage segregation and adipogenesis in vivo. *Development,* 146.

SGAIER, S. K., MILLET, S., VILLANUEVA, M. P., BERENSHTEYN, F., SONG, C. & JOYNER, A. L. 2005. Morphogenetic and cellular movements that shape the mouse cerebellum; insights from genetic fate mapping. *Neuron,* 45**,** 27-40.

SHACKLETON, M., VAILLANT, F., SIMPSON, K. J., STINGL, J., SMYTH, G. K., ASSELIN-LABAT, M. L., WU, L., LINDEMAN, G. J. & VISVADER, J. E. 2006. Generation of a functional mammary gland from a single stem cell. *Nature,* 439**,** 84-8.

SIDNEY, L. E., BRANCH, M. J., DUNPHY, S. E., DUA, H. S. & HOPKINSON, A. 2014. Concise review: evidence for CD34 as a common marker for diverse progenitors. *Stem Cells,* 32**,** 1380-9.

SIEBER, C., KOPF, J., HIEPEN, C. & KNAUS, P. 2009. Recent advances in BMP receptor signaling. *Cytokine Growth Factor Rev,* 20**,** 343-55.

SIERSBÆK, R., NIELSEN, R., JOHN, S., SUNG, M. H., BAEK, S., LOFT, A., HAGER, G. L. & MANDRUP, S. 2011. Extensive chromatin remodelling and establishment of transcription factor 'hotspots' during early adipogenesis. *Embo j,* 30**,** 1459-72.

SIERSBÆK, R., NIELSEN, R. & MANDRUP, S. 2012. Transcriptional networks and chromatin remodeling controlling adipogenesis. *Trends in Endocrinology & Metabolism,* 23**,** 56-64.

SMITH, S. R., LOVEJOY, J. C., GREENWAY, F., RYAN, D., DEJONGE, L., DE LA BRETONNE, J., VOLAFOVA, J. & BRAY, G. A. 2001. Contributions of total body fat, abdominal subcutaneous adipose tissue compartments, and visceral adipose tissue to the metabolic complications of obesity. *Metabolism,* 50**,** 425-35.

SO, P. L. & DANIELIAN, P. S. 1999. Cloning and expression analysis of a mouse gene related to Drosophila odd-skipped. *Mech Dev,* 84**,** 157-60.

SORDELLA, R., JIANG, W., CHEN, G. C., CURTO, M. & SETTLEMAN, J. 2003. Modulation of Rho GTPase signaling regulates a switch between adipogenesis and myogenesis. *Cell,* 113**,** 147-58.

STEINBRING, J., GRAJA, A., JANK, A. M. & SCHULZ, T. J. 2017. Flow Cytometric Isolation and Differentiation of Adipogenic Progenitor Cells into Brown and Brite/Beige Adipocytes. *Methods Mol Biol,* 1566**,** 25-36.

STRICKER, S., BRIESKE, N., HAUPT, J. & MUNDLOS, S. 2006. Comparative expression pattern of Odd-skipped related genes Osr1 and Osr2 in chick embryonic development. *Gene Expr Patterns,* 6**,** 826-34.

STRICKER, S., MATHIA, S., HAUPT, J., SEEMANN, P., MEIER, J. & MUNDLOS, S. 2012. Odd-skipped related genes regulate differentiation of embryonic limb mesenchyme and bone marrow mesenchymal stromal cells. *Stem Cells Dev,* 21**,** 623-33.

STUMM, J., VALLECILLO-GARCIA, P., VOM HOFE-SCHNEIDER, S., OLLITRAULT, D., SCHREWE, H., ECONOMIDES, A. N., MARAZZI, G., SASSOON, D. A. & STRICKER, S. 2018. Odd skipped-related 1 (Osr1) identifies muscle-interstitial fibro-adipogenic progenitors (FAPs) activated by acute injury. *Stem Cell Res,* 32**,** 8-16.

SUGIMOTO, K., ICHIKAWA-TOMIKAWA, N., SATOHISA, S., AKASHI, Y., KANAI, R., SAITO, T., SAWADA, N. & CHIBA, H. 2013. The tight-junction protein claudin-6 induces epithelial differentiation from mouse F9 and embryonic stem cells. *PLoS One,* 8**,** e75106.

SUH, J. M., GAO, X., MCKAY, J., MCKAY, R., SALO, Z. & GRAFF, J. M. 2006. Hedgehog signaling plays a conserved role in inhibiting fat formation. *Cell Metab,* 3**,** 25-34.

SUN, C., SAKASHITA, H., KIM, J., TANG, Z., UPCHURCH, G. M., YAO, L., BERRY, W. L., GRIFFIN, T. M. & OLSON, L. E. 2020. Mosaic Mutant Analysis Identifies PDGFRalpha/PDGFRbeta as Negative Regulators of Adipogenesis. *Cell Stem Cell,* 26**,** 707-721 e5.

TAJBAKHSH, S. & SPÖRLE, R. 1998. Somite Development: Constructing the Vertebrate Body. *Cell,* 92**,** 9-16.

TALLQUIST, M. D., WEISMANN, K. E., HELLSTROM, M. & SORIANO, P. 2000a. Early myotome specification regulates PDGFA expression and axial skeleton development. *Development,* 127**,** 5059-5070.

TALLQUIST, M. D., WEISMANN, K. E., HELLSTRÖM, M. & SORIANO, P. 2000b. Early myotome specification regulates PDGFA expression and axial skeleton development. *Development,* 127**,** 5059-70.

TANAKA, T., YOSHIDA, N., KISHIMOTO, T. & AKIRA, S. 1997. Defective adipocyte differentiation in mice lacking the C/EBPbeta and/or C/EBPdelta gene. *Embo j,* 16**,** 7432-43.

TANG, Q. Q., GRONBORG, M., HUANG, H., KIM, J. W., OTTO, T. C., PANDEY, A. & LANE, M. D. 2005. Sequential phosphorylation of CCAAT enhancer-binding protein beta by MAPK and glycogen synthase kinase 3beta is required for adipogenesis. *Proc Natl Acad Sci U S A,* 102**,** 9766-71.

TANG, Q. Q., OTTO, T. C. & LANE, M. D. 2004. Commitment of C3H10T1/2 pluripotent stem cells to the adipocyte lineage. *Proc Natl Acad Sci U S A,* 101**,** 9607-11.

TANG, W., ZEVE, D., SUH, J. M., BOSNAKOVSKI, D., KYBA, M., HAMMER, R. E., TALLQUIST, M. D. & GRAFF, J. M. 2008. White fat progenitor cells reside in the adipose vasculature. *Science,* 322**,** 583-6.

TEN DIJKE, P., YAMASHITA, H., SAMPATH, T. K., REDDI, A. H., ESTEVEZ, M., RIDDLE, D. L., ICHIJO, H., HELDIN, C. H. & MIYAZONO, K. 1994. Identification of type I receptors for osteogenic protein-1 and bone morphogenetic protein-4. *J Biol Chem,* 269**,** 16985-8.

TENA, J. J., NETO, A., DE LA CALLE-MUSTIENES, E., BRAS-PEREIRA, C., CASARES, F. & GOMEZ-SKARMETA, J. L. 2007. Odd-skipped genes encode repressors that control kidney development. *Dev Biol,* 301**,** 518-31.

THOONEN, R., HINDLE, A. G. & SCHERRER-CROSBIE, M. 2016. Brown adipose tissue: The heat is on the heart. *Am J Physiol Heart Circ Physiol,* 310**,** H1592-605.

THUL PJ, Å. L., WIKING M, MAHDESSIAN D, GELADAKI A, AIT BLAL H, ALM T, ASPLUND A, BJÖRK L, BRECKELS LM, BÄCKSTRÖM A, DANIELSSON F, FAGERBERG L, FALL J, GATTO L, GNANN C, HOBER S, HJELMARE M, JOHANSSON F, LEE S, LINDSKOG C, MULDER J, MULVEY CM, NILSSON P, OKSVOLD P, ROCKBERG J, SCHUTTEN R, SCHWENK JM, SIVERTSSON Å, SJÖSTEDT E, SKOGS M, STADLER C, SULLIVAN DP, TEGEL H, WINSNES C, ZHANG C, ZWAHLEN M, MARDINOGLU A, PONTÉN F, VON FEILITZEN K, LILLEY KS, UHLÉN M, LUNDBERG E. 2017. *THE HUMAN PROTEIN ATLAS*

A subcellular map of the human proteome. [Online]. Science. Available: https://www.proteinatlas.org/ENSG00000198888-MT-ND1/celltype [Accessed 18 September 2021 2021].

TOMLINSON, J. J., BOUDREAU, A., WU, D., ABDOU SALEM, H., CARRIGAN, A., GAGNON, A., MEARS, A. J., SORISKY, A., ATLAS, E. & HACHÉ, R. J. 2010. Insulin sensitization of human preadipocytes through glucocorticoid hormone induction of forkhead transcription factors. *Mol Endocrinol,* 24**,** 104-13.

TRAYHURN, P., WANG, B. & WOOD, I. S. 2008. Hypoxia in adipose tissue: a basis for the dysregulation of tissue function in obesity? *Br J Nutr,* 100**,** 227-35.
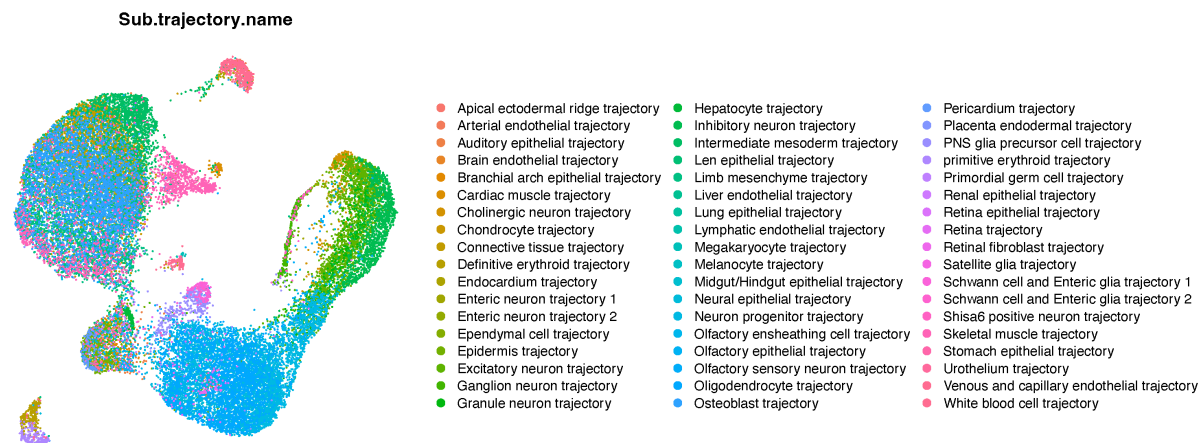
TREVOR, L. V., RICHES-SUMAN, K., MAHAJAN, A. L. & THORNTON, M. J. 2020. Adipose Tissue: A Source of Stem Cells with Potential for Regenerative Therapies for Wound Healing. *J Clin Med,* 9.

TSENG, Y. H., BUTTE, A. J., KOKKOTOU, E., YECHOOR, V. K., TANIGUCHI, C. M., KRIAUCIUNAS, K. M., CYPESS, A. M., NIINOBE, M., YOSHIKAWA, K., PATTI, M. E. & KAHN, C. R. 2005. Prediction of preadipocyte differentiation by gene expression reveals role of insulin receptor substrates and necdin. *Nat Cell Biol,* 7**,** 601-11.

TSENG, Y. H., KOKKOTOU, E., SCHULZ, T. J., HUANG, T. L., WINNAY, J. N., TANIGUCHI, C. M., TRAN, T. T., SUZUKI, R., ESPINOZA, D. O., YAMAMOTO, Y., AHRENS, M. J., DUDLEY, A. T., NORRIS, A. W., KULKARNI, R. N. & KAHN, C. R. 2008. New role of bone morphogenetic protein 7 in brown adipogenesis and energy expenditure. *Nature,* 454**,** 1000-4.

TSENG, Y. H., KRIAUCIUNAS, K. M., KOKKOTOU, E. & KAHN, C. R. 2004. Differential roles of insulin receptor substrates in brown adipocyte differentiation. *Mol Cell Biol,* 24**,** 1918-29.

VALLECILLO-GARCIA, P., ORGEUR, M., VOM HOFE-SCHNEIDER, S., STUMM, J., KAPPERT, V., IBRAHIM, D. M., BORNO, S. T., HAYASHI, S., RELAIX, F., HILDEBRANDT, K., SENGLE, G., KOCH, M., TIMMERMANN, B., MARAZZI, G., SASSOON, D. A., DUPREZ, D. & STRICKER, S. 2017. Odd skipped-related 1 identifies a population of embryonic fibro-adipogenic progenitors regulating myogenesis during limb development. *Nat Commun,* 8**,** 1218.

VITALI, A., MURANO, I., ZINGARETTI, M. C., FRONTINI, A., RICQUIER, D. & CINTI, S. 2012. The adipose organ of obesity-prone C57BL/6J mice is composed of mixed white and brown adipocytes. *J Lipid Res,* 53**,** 619-29.

VOIGT, P., LEROY, G., DRURY, W. J., 3RD, ZEE, B. M., SON, J., BECK, D. B., YOUNG, N. L., GARCIA, B. A. & REINBERG, D. 2012. Asymmetrically modified nucleosomes. *Cell,* 151**,** 181-93.

WANG, L., YU, P., ZHOU, B., SONG, J., LI, Z., ZHANG, M., GUO, G., WANG, Y., CHEN, X., HAN, L. & HU, S. 2020. Single-cell reconstruction of the adult human heart during heart failure and recovery reveals the cellular landscape underlying cardiac function. *Nat Cell Biol,* 22**,** 108-119.

WANG, N. D., FINEGOLD, M. J., BRADLEY, A., OU, C. N., ABDELSAYED, S. V., WILDE, M. D., TAYLOR, L. R., WILSON, D. R. & DARLINGTON, G. J. 1995. Impaired energy homeostasis in C/EBP alpha knockout mice. *Science,* 269**,** 1108-12.

WANG, Q., LAN, Y., CHO, E. S., MALTBY, K. M. & JIANG, R. 2005. Odd-skipped related 1 (Odd 1) is an essential regulator of heart and urogenital development. *Dev Biol,* 288**,** 582-94.

WANG, S. & YANG, X. 2017. Inter-organ regulation of adipose tissue browning. *Cell Mol Life Sci,* 74**,** 1765-1776.

WANG, W., KISSIG, M., RAJAKUMARI, S., HUANG, L., LIM, H. W., WON, K. J. & SEALE, P. 2014. Ebf2 is a selective marker of brown and beige adipogenic precursor cells. *Proc Natl Acad Sci U S A,* 111**,** 14466-71.

WANKHADE, U. D. & RANE, S. G. 2017. Flow Cytometry Assisted Isolation of Adipose Tissue Derived Stem Cells. *Methods Mol Biol,* 1566**,** 17-24.

WEINHOLD, B. 2006. Epigenetics: The Science of Change. *Environmental Health Perspectives,* 114**,** A160-A167.

WHYTE, W. A., ORLANDO, D. A., HNISZ, D., ABRAHAM, B. J., LIN, C. Y., KAGEY, M. H., RAHL, P. B., LEE, T. I. & YOUNG, R. A. 2013. Master transcription factors and mediator establish super-enhancers at key cell identity genes. *Cell,* 153**,** 307-19.

WIPER-BERGERON, N., SALEM, H. A., TOMLINSON, J. J., WU, D. & HACHÉ, R. J. 2007. Glucocorticoid-stimulated preadipocyte differentiation is mediated through acetylation of C/EBPbeta by GCN5. *Proc Natl Acad Sci U S A,* 104**,** 2703-8.

WU, Z., BUCHER, N. L. & FARMER, S. R. 1996. Induction of peroxisome proliferator-activated receptor gamma during the conversion of 3T3 fibroblasts into adipocytes is mediated by C/EBPbeta, C/EBPdelta, and glucocorticoids. *Mol Cell Biol,* 16**,** 4128-36.

WU, Z., ROSEN, E. D., BRUN, R., HAUSER, S., ADELMANT, G., TROY, A. E., MCKEON, C., DARLINGTON, G. J. & SPIEGELMAN, B. M. 1999. Cross-Regulation of C/EBPα and PPARγ Controls the Transcriptional Pathway of Adipogenesis and Insulin Sensitivity. *Molecular Cell,* 3**,** 151-158.

WU, Z., XIE, Y., BUCHER, N. L. & FARMER, S. R. 1995. Conditional ectopic expression of C/EBP beta in NIH-3T3 cells induces PPAR gamma and stimulates adipogenesis. *Genes Dev,* 9**,** 2350-63.

XIE, Z., BAILEY, A., KULESHOV, M. V., CLARKE, D. J. B., EVANGELISTA, J. E., JENKINS, S. L., LACHMANN, A., WOJCIECHOWICZ, M. L., KROPIWNICKI, E., JAGODNIK, K. M., JEON, M. & MA'AYAN, A. 2021. Gene Set Knowledge Discovery with Enrichr. *Curr Protoc,* 1**,** e90.

XU, J. & LIAO, K. 2004. Protein kinase B/AKT 1 plays a pivotal role in insulin-like growth factor-1 receptor signaling induced 3T3-L1 adipocyte differentiation. *J Biol Chem,* 279**,** 35914-22.

XUE, B., RIM, J. S., HOGAN, J. C., COULTER, A. A., KOZA, R. A. & KOZAK, L. P. 2007. Genetic variability affects the development of brown adipocytes in white fat but not in interscapular brown fat. *J Lipid Res,* 48**,** 41-51.

YUSUF, F. & BRAND-SABERI, B. 2006. The eventful somite: patterning, fate determination and cell division in the somite. *Anat Embryol (Berl),* 211 Suppl 1**,** 21-30.

YUSUFZAI, T. M., TAGAMI, H., NAKATANI, Y. & FELSENFELD, G. 2004. CTCF Tethers an Insulator to Subnuclear Sites, Suggesting Shared Insulator Mechanisms across Species. *Molecular Cell,* 13**,** 291-298.

ZEHENTNER, B. K., LESER, U. & BURTSCHER, H. 2000. BMP-2 and sonic hedgehog have contrary effects on adipocyte-like differentiation of C3H10T1/2 cells. *DNA Cell Biol,* 19**,** 275-81.

ZHANG, X., CHEN, J., SUN, L. & XU, Y. 2018. SIRT1 deacetylates KLF4 to activate Claudin-5 transcription in ovarian cancer cells. *J Cell Biochem,* 119**,** 2418-2426.

ZHONG, Z. A., SUN, W., CHEN, H., ZHANG, H., LAY, Y.-A. E., LANE, N. E. & YAO, W. 2015. Optimizing tamoxifen-inducible Cre/loxp system to reduce tamoxifen effect on bone turnover in long bones of young mice. *Bone,* 81**,** 614-619.

ZHOU, L., LIU, J., OLSON, P., ZHANG, K., WYNNE, J. & XIE, L. 2015. Tbx5 and Osr1 interact to regulate posterior second heart field cell cycle progression for cardiac septation. *J Mol Cell Cardiol,* 85**,** 1-12.

ZHU, Y., QI, C., KORENBERG, J. R., CHEN, X. N., NOYA, D., RAO, M. S. & REDDY, J. K. 1995. Structural organization of mouse peroxisome proliferator-activated receptor gamma (mPPAR gamma) gene: alternative promoter use and different splicing yield two mPPAR gamma isoforms. *Proceedings of the National Academy of Sciences,* 92**,** 7921.

ZUO, Y., QIANG, L. & FARMER, S. R. 2006. Activation of CCAAT/enhancer-binding protein (C/EBP) alpha expression by C/EBP beta during adipogenesis requires a peroxisome proliferator-activated receptor-gamma-associated repression of HDAC1 at the C/ebp alpha gene promoter. *J Biol Chem,* 281**,** 7960-7.

9 APPENDIX

9.1 Sub-Trajectories of the Cao et al., 2019 dataset

Sub.trajectory.name

● Apical ectodermal ridge trajectory	● Hepatocyte trajectory	● Pericardium trajectory
● Arterial endothelial trajectory	● Inhibitory neuron trajectory	● Placenta endodermal trajectory
● Auditory epithelial trajectory	● Intermediate mesoderm trajectory	● PNS glia precursor cell trajectory
● Brain endothelial trajectory	● Len epithelial trajectory	● primitive erythroid trajectory
● Branchial arch epithelial trajectory	● Limb mesenchyme trajectory	● Primordial germ cell trajectory
● Cardiac muscle trajectory	● Liver endothelial trajectory	● Renal epithelial trajectory
● Cholinergic neuron trajectory	● Lung epithelial trajectory	● Retina epithelial trajectory
● Chondrocyte trajectory	● Lymphatic endothelial trajectory	● Retina trajectory
● Connective tissue trajectory	● Megakaryocyte trajectory	● Retinal fibroblast trajectory
● Definitive erythroid trajectory	● Melanocyte trajectory	● Satellite glia trajectory
● Endocardium trajectory	● Midgut/Hindgut epithelial trajectory	● Schwann cell and Enteric glia trajectory 1
● Enteric neuron trajectory 1	● Neural epithelial trajectory	● Schwann cell and Enteric glia trajectory 2
● Enteric neuron trajectory 2	● Neuron progenitor trajectory	● Shisa6 positive neuron trajectory
● Ependymal cell trajectory	● Olfactory ensheathing cell trajectory	● Skeletal muscle trajectory
● Epidermis trajectory	● Olfactory epithelial trajectory	● Stomach epithelial trajectory
● Excitatory neuron trajectory	● Olfactory sensory neuron trajectory	● Urothelium trajectory
● Ganglion neuron trajectory	● Oligodendrocyte trajectory	● Venous and capillary endothelial trajectory
● Granule neuron trajectory	● Osteoblast trajectory	● White blood cell trajectory

9.2 Enrichr gene lists

Table 25: Top 50 gene signatures ranked by https://shiny.mdc-berlin.de/sivisca/ tool to perform Enrichr cell type analysis: https://maayanlab.cloud/Enrichr/enrich#

CL0	CL1	CL2
Itm2a	mt-Rnr1	Ube2c
Ptn	mt-Nd2	Nusap1
Dcn	mt-Nd1	Ccnb1
Mfap4	mt-Rnr2	Spc25
Mfap2	mt-Nd4	Ccnb2
Fos	mt-Cytb	Cks2
Lum	mt-Nd6	Pttg1
Lgals1	mt-Co1	Ckap2l
Efemp1	Gm10800	Cdca3
Rnd3	mt-Nd5	Aurka
Id1	Il31ra	Birc5
Glipr2	Map1b	Arl6ip1
Ogn	Gm10801	Kpna2
Igf1	Gm21738	Cdc25c
6330403K07Rik	Ccnd2	Bub3
Tsc22d1	CT010467.1	Shcbp1

Maged2	Trp53inp2	Pbk
Serinc2	Gm26917	Cdk1
Klf6	Gm33838	Bub1
Cxcl12	Fzr1	G2e3
Egr1	Cyb5r3	Tacc3
Capn6	Lars2	Cenpl
Nrep	Uba6	Ska2
Snai2	Slit3	Kif20a
Osr1	Simc1	Cenpa
Gas2	Cacna1c	Ckap2
Rgs2	Abl2	Mis18bp1
Cd63	Zfp397	Kif18a
Shox2	Cep192	Sgo1
Ldhb	mt-Tp	Arrdc3
AW551984	Dnm3os	Psrc1
Anxa2	Ttf2	Aurkb
Tmem263	Gak	Spc24
Dnajb4	Fbxl5	Prrx1
Asb4	Kcnq5	Depdc1a
Zfp36	Vps39	Id2
Sparc	Wdr11	Pclaf
Fblim1	Zfp760	Mfap2
Cmtm3	Nckap5	Lum
Cdo1	Atrnl1	Kif23
Prrx1	Mga	Cdca8
S1pr3	Gm15564	Mfap4
Tmem176b	Tmem186	Prc1
Hbp1	Fbn2	Cenpn
Lpar1	Cblb	Cdo1
Clk1	Knstrn	Cdca4
Ssbp2	Apbb1	Ska3
Id2	Prpf6	Nuf2
Nfib	Smarca4	Ect2
Runx1t1	Spock1	Lgals1

9.3 E11.5 Osr1 cluster gene lists

Table 26: Top 50 gene signatures sorted by average 2FoldChange in the E11.5 Osr1 dataset "find_all_markers" gene list for cluster: 0, 1 and 2 to predict cluster identities using the Angueira et al., 2021 P3 thoracic aorta dataset.

CL0	CL1	CL2
Itm2a	mt-Rnr1	Aurka
Ogn	mt-Nd2	Aurkb
Tpm1	mt-Nd1	Ckap2l
Efemp1	mt-Rnr2	Bub1
Id1	mt-Nd4	Nusap1
Capn6	mt-Cytb	Spc25
Ptn	mt-Nd6	Tacc3
Mest	mt-Co1	Hmmr
Maged2	Gm10800	Kif20a
Mcm4	mt-Nd5	Nuf2
Tcim	Il31ra	Prc1
Glipr2	Map1b	Cdc25c
Id3	Gm10801	Ccnb1
Rcn3	Gm21738	Pimreg
Cmtm3	Ccnd2	Depdc1a
Rnd3	CT010467.1	Tpx2
Ifitm2	Trp53inp2	Mis18bp1
Fos	Gm26917	Plk1
Klf6	Gm33838	Cdk1
Asb4	Fzr1	Cdca3
Serpinh1	Cyb5r3	Kif23
Gpc3	Lars2	Pbk
Igfbp5	Uba6	Birc5
Mcm6	Slit3	Cdca8
Tsc22d1	Simc1	Kif22
Mfap4	Cacna1c	Ube2c
Crabp2	Abl2	Kif11

Fblim1	Zfp397	Sgo1
H19	Cep192	Hmgb2
Gas2	mt-Tp	Cenpe
Dnajb4	Dnm3os	Ect2
Serinc2	Ttf2	Top2a
Mfap2	Gak	Cks2
Snhg18	Fbxl5	Psrc1
Mdk	Kcnq5	Shcbp1
Cdca7	Vps39	Ndc80
Aldh1a2	Wdr11	Ccna2
Cxcl12	Zfp760	Ska1
Id2	Nckap5	Ncapg
Sparc	Atrnl1	Smc4
Tcf7l2	Mga	Ttk
Tmem9	Gm15564	Spc24
Chaf1b	Tmem186	Kif2c
Surf4	Fbn2	Melk
AW551984	Cblb	Mad2l1
Dvl3	Knstrn	Knstrn
Snai2	Apbb1	Kpna2
Osr1	Prpf6	Ska3
Maged1	Smarca4	Oip5
Gsta4	Spock1	Bub3

9.4 Signature lists of the P3 thoracic aorta dataset

Table 27: Top 50 gene signatures of GSE166355: the annotated P3 thoracic aorta cluster: Intermediate cells, Progenitor cells and Preadipocytes were.

INTERMEDIATE CELLS	PROGENITOR CELLS	PREADIPOCYTES
Mfap4	Ly6a	Lpl
Wisp1	Clec3b	Penk
Vstm4	Pi16	Gsn
Mgp	H19	Tnfaip6
Fhl2	Mfap5	Dlk1

Postn	Dlk1	Col15a1
Cygb	Cdkn1c	H19
Epha3	Gpx3	Lum
Mmp14	Cd34	Srpx
Pcolce	Cthrc1	Mgst1
Tmem158	Serpinf1	Igf1
Gm13305	Tppp3	Ldhb
Dpt	Nrk	Adh1
Thbs2	Serping1	Ebf1
Mfap2	Entpd2	Dkk2
Tmem119	Ogn	Cdkn1c
Nap1l1	Mest	Mmp2
Smoc2	Htra3	Clec3b
Fmo2	Dcn	Tshz2
Prss35	Postn	Cxcl1
Fhl1	Gap43	Olfml3
Tspan11	Fbn1	Fbln2
Mdk	Gpc3	Cryab
Fkbp9	Il33	Tm4sf1
Pdgfrl	Sfrp1	Gas1
Gpx7	Pcolce	Mgp
Pam	Col5a2	Cxcl12
Serpinf1	Plagl1	Acta2
Gxylt2	Cd248	Cd9
Plpp1	Tnxb	Mest
Qpct	Tmeff2	Gpx3
Kdelr3	Col14a1	Peg3
Twist2	Dpt	Tpm2
Pid1	Fbln1	Serpinf1
Dkk3	Col6a1	Dpt
Mxra7	Lum	Cnn2
Lhfp	Col5a1	Pcolce
Eva1b	Peg3	
Mfap5	Col6a2	

Mmp23	Olfml3
Pdlim2	Mmp2
Efemp2	Mfap4
Kdelr2	Tshz2
Fkbp7	Igf1
Ntrk2	Tgfbi
Olfml3	C1qtnf2
Fkbp10	Lpl
Lum	Cygb
Fbn1	Tagln
Myl9	Tpm2

9.5 E9.5 Osr1 cluster gene lists

Table 28: Top 50 gene signatures sorted by average 2FoldChange in the E9.5 Osr1 dataset "find_all_markers" gene list for cluster: 0, 1 and 2 to predict cluster identities using the Angueira et al., 2021 P3 thoracic aorta dataset.

CL0	CL1	CL2
Ifitm1	mt-Nd1	Ccnb1
Gm14226	mt-Rnr1	Aurka
Rpa2	mt-Cytb	Nusap1
Ccne2	mt-Nd4	Ccnf
Ifitm2	mt-Rnr2	Kif20a
Hoxc10	mt-Nd2	Kif2c
Rrm2	Il31ra	Prc1
Chaf1b	mt-Co1	Ube2c
Dck	mt-Nd6	Ubb
Snai1	mt-Nd5	Aurkb
Arg1	Ubb	Plk1
Bcat1	Eef1a1	Kif22
Cdc6	Tax1bp1	Psrc1
Mfap2	Rpl32	Knstrn
Mdk	Dpf2	Kif23
Dusp6	Lin7c	Cenpf

Cdc45	Rps9	Cdc25c
Mthfd1	Rpl37a	Hmmr
Isyna1	Ppp5c	Bub1
Klhl22	Rps3	Spc25
Hoxb1	Nxf1	Ckap2l
Pcna	Ppia	Arl6ip1
Ppp1cb	9530068E07Rik	Arhgef39
Mcm7	Dnttip2	Cdc20
Mfap4	Nubp2	Cenpl
Snrpa	Impa1	Kif11
Maged1	Ap1m1	Ect2
Nkd2	Pcid2	Bub1b
Cacybp	Prmt7	Sgo1
Ccn1	Ttc4	Pimreg
Uhrf1	Ythdf2	Tpx2
Dcakd	Kat7	Hjurp
Mcm4	Vps35	Ncapg
Ptma	Gm8186	Bub3
Mcm6	Phf6	Il31ra
Ppa1	Seh1l	mt-Rnr1
Cdca4	Dnajb1	mt-Cytb
Umps	Gm15564	mt-Nd1
Exo1	Atg4b	mt-Nd4
Dhfr	Serinc1	Spdl1
Sf3a3	Tug1	Racgap1
Cdk2	Rpl4	Nde1
Impdh2	Far1	mt-Co1
Hoxb5os	Tpd52l2	Ttk
Cct8	Suv39h1	Gtse1
Cdx4	Abcf2	Cip2a
Car14	Bckdk	Fgfr1op
Psmc2	Sf3a1	Tex10
Frzb	Mtfr1l	Ska3
Hspe1	Nup62	Naa35

9.6 List of figures

9.7 Abbreviations

αSMA	Alpha smooth muscle actin
ADRB3	β3-adrenergic receptor
ADSCs	Adipo-derived stromal cells
AGM	Aorta-gonadal-mesonephros
APs	Pre-adipogenic progenitors
APs	Pre-adipogenic progenitors
ASPCs	Adipogenic stem and precursor cells
asWAT	Anterior subcutaneous white adipose depot
ATGL	Adipose triglyceride lipase
aw	Abdominal wall
axiWAT	Axillary white adipose tissue
BAT	Brown adipose tissue
bidest	Bidistillated
BMPs	Bone morphogenic proteins
bp	Base pair
Brd4	Bromodomain and extra terminal domain (BET) protein
BSA	Bovine serum albumin
cBAT	Cervical brown adipose tissue
Cebpα	CCAAT enhancer binding protein alpha
Chip-Seq	Chromatin immune precipitation DNA-Sequencing
cl	Cluster
Cldn5	Claudin-5
CLSs	Crown-like structures
Co-IP	Co-immunoprecipitation
CREB	Camp response element-binding protein
CTCFs	CCCTC binding factors
cv	Cardinal vein
da	Dorsal aorta
Dex	Dexamethasone
dmd	Dermomyotomal derivate

DNA	Deoxyribonucleic acid
dpi	Days post injury
E	Embryonic stage
e.g.	For example
Ebf2	Early B cell factor-2
ECM	Extracellular matrix
Ehmt1 or Glp	Euchromatic histone-lysine N-methyltransferase 1
En1	Engrailed homeobox 1
ERAAs	Estrogen receptor agonist/antagonist
ESC	Embryonic stem cell
Fabp4	Fatty acid binding protein 4
FACS	Fluorescence-activated cell sorting
FFA	Free fatty acid
Fig.	Figure
fl	Floxed
FOXOs	Forkhead proteins
GCE	Egfp-Cre-ert2 cassette
GCRs	Glucocorticoid receptors
GCs	Glucocorticoids
GFP	Green fluorescent protein
GM	Growth medium
h	Hour
HEC	Hemogenic endothelial cell
HICEs	Highly interconnected enhancer communities
HIF1	Hypoxia-inducible transcription factor 1
hMSCs	Human mesenchymal stem cells
HoxB6	Homeobox B6
HSCs	Hematopoietic stem cells
HSL	Hormone-sensitive lipase
i.e.	that is
iBAT / inscBAT	Interscapular brown adipose tissue
IBMX	Isobutylmethylxanthine

IF	Immunofluorescence
IGF1	Insulin growth factor 1
IL-6	Interleukin-6
IM	Intermediate mesoderm
ingWAT	Inguinal white adipose tissue
inscWAT	Interscapular white adipose depot
KDR / FLK1	Vascular endothelial growth factor receptor 2
KO	Knockout
latBAT	Lateral brown adipose tissue
Lhx1	Lim-type homeobox 1 gene
Lin	Lineage
LPM	Lateral plate mesoderm
Ly6a / Sca1	Stem cell antigen 1
MEFs	Mouse embryonic fibroblasts
Meox1	Mesenchyme homeobox 1
MMP	Metalloproteinases
MSCs	Mesenchymal stem cells
mTmG	Membrane tomato membrane GFP
mWAT	Mesenteric white adipose tissue
Myf5	Myogenic factor 5
MyHC	Myosin heavy chain
o/n	Overnight
Odd	Odd-skipped
ORO	Oil red o
Osr1	Odd skipped related gene 1
paBAT	Peri-aortal brown adipose tissue
Pax2	Paired-box genes 2
Pax3	Paired-box 3
Pax7	Paired-box 7
Pax8	Paired-box genes 8
PCR	Polymerase chain reaction
PDGFRα	Platelet derived growth factor receptor alpha

pgWAT	Perigonadal white adipose tissue
PI3K	Phosphatidylinositol-3 kinase
PLA	Proximity ligation assay
Plin	Perilipin
Pol II	RNA polymerase II
Pparγ	Peroxisome proliferator-activated receptor γ
prBAT	Perirenal brown adipose tissue
Prdm16	PR domain zinc finger protein 16
Prx1	Paired related homeobox 1
PTC	Patched
PVAT	Perivascular adipose tissue
PVDF	Polyvinylidene fluoride membrane
qPCR	Quantitative polymerase chain reaction
RFP	Red fluorescent protein
ROCK	RHO-associated kinase
RUNX2	Runt-related transcription factor 2
rWAT	Retroperitoneal white adipose tissue
savWAT / submanWAT	Salivary gland - or submandibular gland white adipose tissue
sBAT / subscBAT	Subscapular brown adipose tissue
sc	Single cell
SDS-PAGE	Sodium dodecyl sulfate-polyacrylamide gel electrophoresis
SEM	Standard error of mean
Seq	Sequencing
SEs	Super-enhancers
SMCs	Smooth muscle cells
SMO	Smoothened
Sox10	Sry-related hmg-Box gene 10
subWAT	Subcutaneous white adipose tissue
SVF	Stroma vascular fraction
TAD	Topologically associated domain

TAG	Triacyl glycerides
TAM	Tamoxifen
TFs	Transcription factors
TGFβ	Transforming growth factor-β
TNF	Tumor necrosis factor
Tubb3	Beta 3 class III
UCP1	Uncoupling protein 1
v	Vessel
VEGFA	Vascular endothelial growth factor A
vWAT	Visceral white adipose tissue
WAT	White adipose tissue
wks	Weeks
WT	Wildtype
Wt1	Wilms tumor 1 suppressor gene
X-Gal	5-bromo- 4-chloro-3-indolyl-β-D-galactopyranoside